ECMWF COPERNICUS REPORT

Copernicus Atmosphere Monitoring Service

Validation report of the CAMS near-real time global atmospheric composition service

March – May 2019

Issued by: KNMI

Date: 27 September 2019

Ref: CAMS84_2018SC1_D1.1.1_MAM2019_v1

IMPLEMENTED BY ECMWF

This document has been produced in the context of the Copernicus Atmosphere Monitoring Service (CAMS).
The activities leading to these results have been contracted by the European Centre for Medium-Range Weather Forecasts, operator of CAMS on behalf of the European Union (Delegation Agreement signed on 11/11/2014). All information in this document is provided "as is" and no guarantee or warranty is given that the information is fit for any particular purpose. The user thereof uses the information at its sole risk and liability. For the avoidance of all doubts, the European Commission and the European Centre for Medium-Range Weather Forecasts has no liability in respect of this document, which is merely representing the authors view.

Validation report of the CAMS near-real-time global atmospheric composition service. Period March - May 2019

EDITORS:
Y. Christophe (BIRA-IASB), M. Ramonet (LSCE), A. Wagner (MPG),
M. Schulz (MetNo), H.J. Eskes (KNMI)

AUTHORS:
S. Basart (BSC), A. Benedictow (MetNo), Y. Bennouna (CNRS-LA),
A.-M. Blechschmidt (IUP-UB), S. Chabrillat (BIRA-IASB), E. Cuevas (AEMET),
A. El-Yazidi (LSCE), H. Flentje (DWD), K. M. Hansen (AU), U. Im (AU),
J. Kapsomenakis (AA), B. Langerock (BIRA-IASB), A. Richter (IUP-UB),
N. Sudarchikova (MPG), V. Thouret (CNRS-LA), T. Warneke (UBC),
C. Zerefos (AA)

REPORT OF THE COPERNICUS ATMOSPHERE MONITORING SERVICE, VALIDATION SUBPROJECT.

AVAILABLE AT:
http://atmosphere.copernicus.eu/quarterly_validation_reports

CITATION:
Christophe, Y., M. Ramonet, A. Wagner, M. Schulz, H. J. Eskes, S. Basart, A. Benedictow, Y. Bennouna, A.-M. Blechschmidt, S. Chabrillat, E. Cuevas, A. El-Yazidi, H. Flentje, K.M. Hansen, U. Im, J. Kapsomenakis, B. Langerock, A. Richter, N. Sudarchikova, V. Thouret, T. Warneke, C. Zerefos, Validation report of the CAMS near-real-time global atmospheric composition service: Period March - May 2019, Copernicus Atmosphere Monitoring Service (CAMS) report, CAMS84_2018SC1_D1.1.1_MAM2019_v1.pdf, September 2019, doi:10.24380/1t4q-1h53.

STATUS:
Version 1.0, Final

DATE:
27 September 2019

Executive Summary

The Copernicus Atmosphere Monitoring Service (http://atmosphere.copernicus.eu, CAMS) is a component of the European Earth Observation programme Copernicus. The CAMS global near-real time (NRT) service provides daily analyses and forecasts of reactive trace gases, greenhouse gases and aerosol concentrations. This document presents the validation statistics and system evolution of the CAMS NRT service for the period up to 1 June 2019. Updates of this document appear every 3 months. The previous report for DJF-2019 is Schulz et al. (2019).

This summary is split according to service themes as introduced on the CAMS website: air quality & atmospheric composition, climate forcing, ozone layer and UV. Specific attention is given to the ability of the CAMS system to capture recent events. We focus on the 'o-suite' composition fields, which are the daily analyses and forecasts produced by the IFS (Integrated Forecast System) modelling system at ECMWF, using the available meteorological and atmospheric composition observations which are ingested in the ECMWF 4D-Var assimilation system. The model and assimilation configurations are summarised in section 2. We furthermore assess the impact of the composition observations by comparing the validation results from the 'o-suite' to a 'control' configuration without assimilation. Also, the pre-operational delayed-mode analyses and high-resolution forecasts of CO_2 and CH_4 are assessed in this report.

The o-suite data delivery for the period March-May 2019 (DJF-2019) was excellent, with an availability of 100% at 10 and 22 UTC (two forecasts per day).

Air quality and atmospheric composition

Tropospheric ozone (O_3)

CAMS o-suite ozone is validated with surface and free tropospheric ozone observations from the GAW and ESRL networks, IAGOS airborne data, ozone sondes and IASI tropospheric ozone retrievals. For free tropospheric ozone against ozone sondes the o-suite modified normalized mean biases (MNMBs) are on average small, ±10% over the Northern Hemisphere (NH), between ±30% for stations in the Tropics, and ±15% for the Arctic in more recent years (Fig. S.1). Over Antarctica o-suite biases are observed between 0% and +20% for recent years, whereas the control run shows negative biases. For MAM 2019 good agreement is found over the NH mid latitudes in the free troposphere.

In the first half of the MAM period, a good agreement with IAGOS is found over Frankfurt from the surface to the free troposphere. However, starting from mid-April, the o-suite bias appears to increase with an overestimation of ozone, a behaviour not observed in the control run. This difference may be attributed to the CAMS model or IAGOS observations. The comparison with IAGOS Level 2 data (not available yet) may answer this question. In the UTLS region, ozone is generally overestimated by the o-suite and partly better represented by the control run. Good agreement with the IAGOS free troposphere ozone profiles is also found over the other regions of the world, with often large differences in the UTLS region in particular over North America and the Middle East.

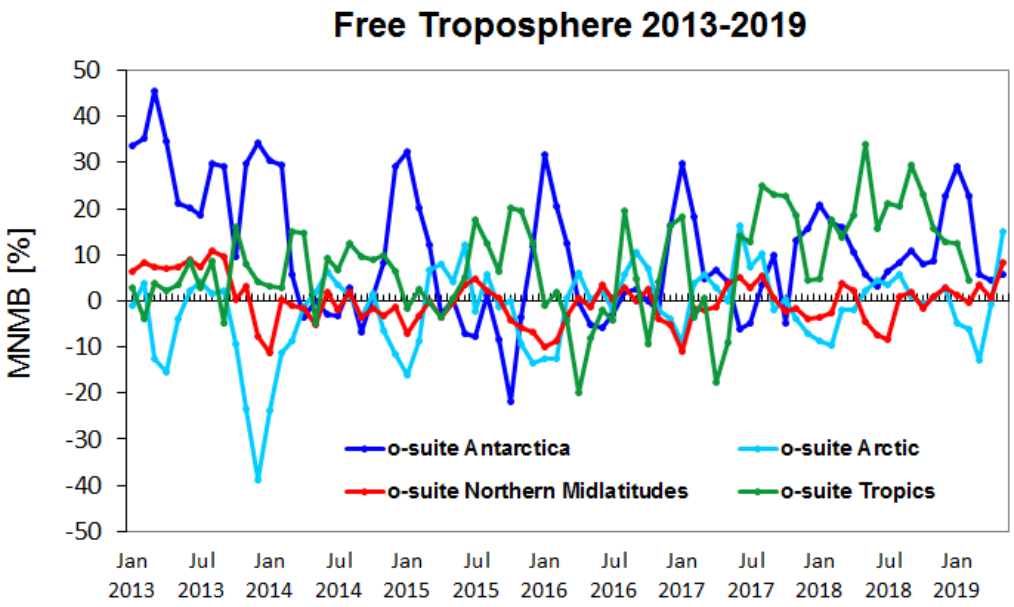

Figure S.1: Time series of MNMB of ozone in the o-suite, compared against ozone sondes, averaged over different latitude bands. The free troposphere is defined here as the layer between 750 and 300 hPa.

In comparison with surface observations we find a steady improvement of the o-suite over the past 5 years over European GAW stations. Biases are generally around ±10%, and within ±20% (the Arctic is discussed below). The o-suite has biases close to zero for surface ozone for Europe during March to May 2019. Both runs overestimate O_3 minimum observations for Asia with MNMBs up to 19% for the o-suite and up to 16% for the control run. For the tropics, surface ozone is overestimated with MNMBs within 15%. Both runs can reproduce Antarctic surface observations with MNMBs within -10%.

Tropospheric Nitrogen dioxide (NO_2)

Model validation, with respect to SCIAMACHY/Envisat NO_2 data before April 2012 and GOME-2/MetOp-A NO_2 data afterwards, shows that tropospheric NO_2 columns are well reproduced by the NRT model runs, indicating that emission patterns and NO_x photochemistry are generally well represented, although modelled shipping signals are more pronounced than in the satellite retrievals. Tropospheric NO_2 columns over some local emission hotspots (e.g. Moscow, and Red Basin in China) are overestimated, while wintertime and springtime values over Europe around Benelux are underestimated. Since December 2014, the agreement between satellite retrievals and model results for time series over East-Asia and Europe is better than for previous years (Fig. S.2), as observed columns of NO_2 decreased in 2014, likely associated with reduced emissions, and (in contrast to the observations) simulated values show an increase over the whole timeseries available. Between spring and autumn, the models regularly show an overestimation over several regions with boreal forest fire activity (Canada, Alaska, Siberia).

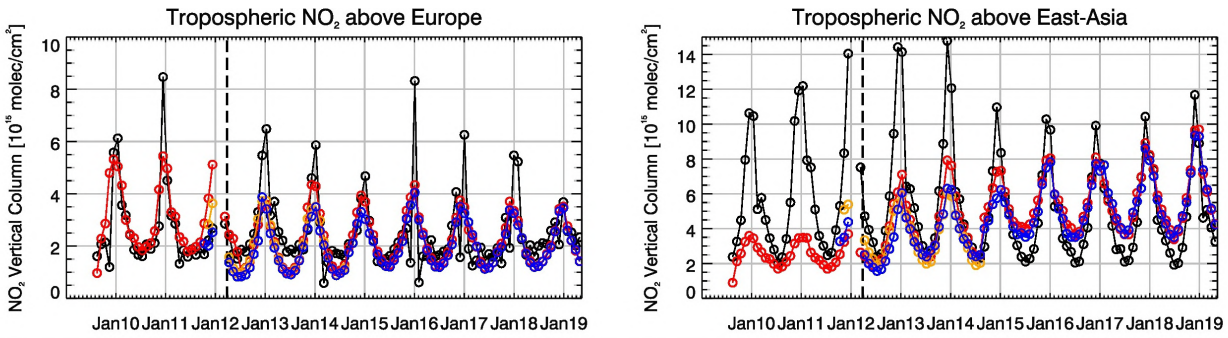

Figure S.2: Time series of tropospheric NO_2 columns from SCIAMACHY (up to March 2012) and GOME-2 (from April 2012 onwards) compared to model results for Europe and East-Asia. The o-suite is in red, control is in blue (the model run without data assimilation is termed control since Sep 2014).

Tropospheric Carbon Monoxide (CO)

Model validation with respect to GAW network surface observations, IAGOS airborne data, FTIR observations (NDACC and TCCON) and MOPITT / IASI satellite retrievals reveals that the absolute values, latitude dependence and seasonality, as well as day-to-day variability of CO can be reproduced well by the CAMS-global analyses and forecasts. Biases are between 4% and -17% for European GAW stations, and up to ±4% in Asia.

For stations in the southern hemisphere the comparison with NDACC (Fig. S.3) and GAW, measurements show that data assimilation efficiently reduces the large positive MNMBs observed in the control run. The o-suite compared with the TCCON CO observations shows basically no latitude dependence. Overall, there seems to be a small positive bias of < 5% with TCCON. Similar results are obtained when comparing to the NDACC FTIR measurements, but now with a small negative bias of a few % for the tropospheric CO column. A small seasonal cycle is observed in the biases, but this stays within 5%.

According to IAGOS aircraft observations CO is mostly underestimated over Frankfurt by both the o-suite and control run without assimilation and the largest bias is found in the lowest layers. The performance is similar in the lowest layers, but the o-suite performs slightly better than the control run in the free troposphere. For most other regions of the world the results of the two CAMS configurations are similar, as for Europe. However, over Eastern Asia the impact of assimilation is clear with often much better agreement with observations for the o-suite than for the control run.

The comparisons with MOPITT and IASI confirm these findings. The day 0 o-suite forecast shows differences within 10% regionally compared to MOPITT, with little latitude dependence of the bias. Regionally these biases increase during the 4-day forecast. A general reduction of CO emissions from the year 2015 to the year 2018 can be seen over Europe, the US and East Asian regions. Due to the stability of the (small) bias this trend is well reproduced by the o-suite.

Formaldehyde

Model validation, with respect to SCIAMACHY/Envisat HCHO data before April 2012 and GOME-2/MetOp-A HCHO data afterwards (Fig. S.4), shows that modelled monthly HCHO columns represent well the magnitude of oceanic and continental background values and the overall spatial distribution in comparison with mean satellite HCHO columns. Compared to GOME-2 satellite retrie-

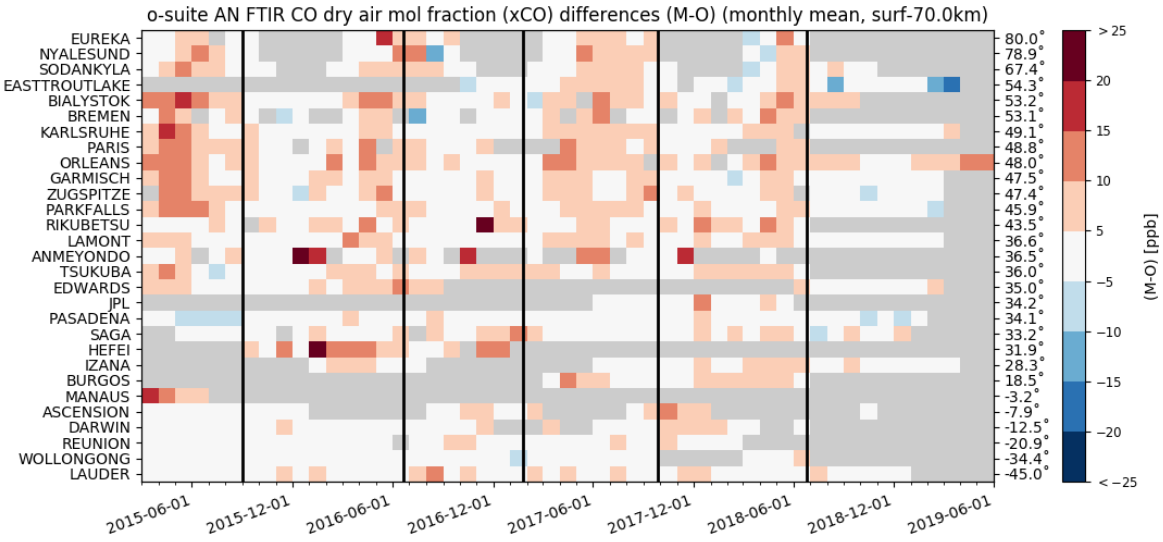

Figure S.3: Monthly mean relative CO bias (o-suite – observation)/observation for the last 4 years. Comparisons are made against TCCON FTIR CO remote sensing observations. Model upgrades are indicated with the black lines. The stations are sorted with decreasing latitude (northern to southern hemisphere). A similar plot for the control run shows biases up to 40% in the southern hemisphere.

vals, an overestimation of values regularly occurs over Australia and Central Africa, which could be both related to biogenic emissions and fire emissions. For time series over East-Asia and the Eastern US, both regions where HCHO columns are probably dominated by biogenic emissions, models and retrievals agree rather well, but the yearly cycle over East-Asia is underestimated by the models.

Aerosol

We estimate that the o-suite aerosol optical depth showed an average positive bias in the latest three months of +18%, measured as modified normalized mean bias against daily Aeronet (V3 level 1.5) sun photometer data. The 3-day forecasted aerosol distribution shows 19% less aerosol optical depth (AOD) than that from the initial forecast day, as shown in Fig. S.5-a. The spatiotemporal correlation, shown in Fig. S.5-b, shows month-to-month variation in MAM 2019 similar to spring 2018, indicating the simulation reproduces approximately 60% of the day to day AOD variability across all Aeronet stations. We find a high AOD bias in Southern Latitudes. The o-suite forecast at +3 days shows slightly lower correlation, as a consequence of imperfect forecasted meteorology and fading impact of the initial assimilation of MODIS AOD and MODIS fire info on model performance. The o-suite forecast running each day at 12UTC shows almost identical performance as the forecast starting at 00UTC.

The AOD performance of the o-suite with respect to the AERONET data exhibits no pronounced seasonal cycle but somewhat less correlation in late summer. Since October 2017, the largest contributions to global AOD come from organics and sea salt. Sea salt AOD increased further due to the latest model upgrade in June 2018 with the new sea salt emission scheme activated, while dust AOD became lower compared to earlier years.

The aerosol Ångström exponent (AE) contains information about the size distribution of the aerosol, and implicitly about composition. In the last year the o-suite AE became more positive indicating a change to slightly more fine particles since the latest model upgrade to version 45R1 in June 2018.

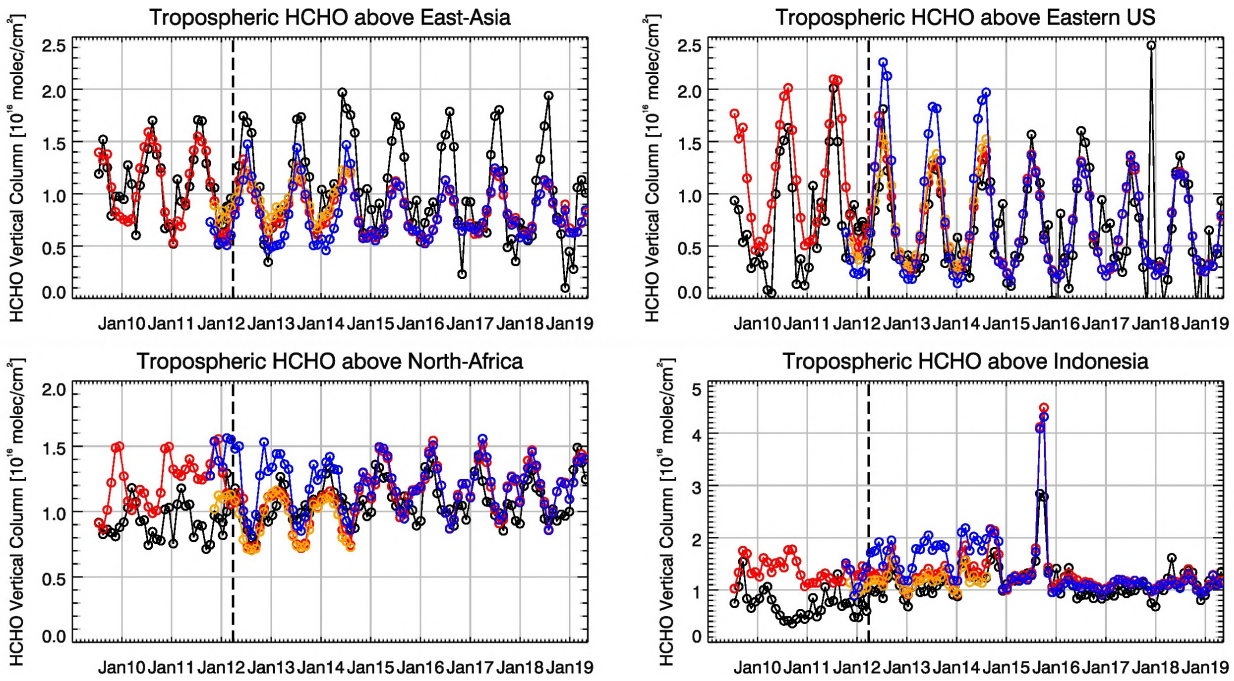

Figure S.4: Time series of average tropospheric HCHO columns [10^{16} molec cm^{-2}] from SCIAMACHY (up to March 2012) and GOME-2 (from April 2012 onwards) compared to model results for different regions. The blue line shows CAMS control results including older configurations from the MACC project before September 2014. The regions are: East-Asia (25-40°N, 110-125°E), Eastern US (30-40°N, 75-90°W), Northern Africa (0-15°N, 15°W-25°E) and Indonesia (5°S-5°N, 100-120°E). Vertical dashed black lines mark the change from SCIAMACHY to GOME-2 based comparisons in April 2012.

PM10 and PM25, as defined by the IFS aerosol model, are evaluated against an average from rural and background site data in the period 2000-2009 at 160 sites in North America and Europe. This indicates that PM10 concentrations exhibit on average in the latest period an underestimation with MNMB bias of -42% in Europe and overestimation of 9% in North America. PM25 concentrations are underestimated -17% in Europe and overestimated 54% in North America. Consistent with this finding a higher positive bias is also found for AOD in North America than in Europe. The fraction of PM simulated data within a factor 2 of observed values stayed similar since September 2017 for both PM10 and PM25. PM25 seems to have deteriorated compared to periods before mid 2017, while PM10 shows an improvement.

For spring, both CAMS experiments simulate well the main areas of dust activity in the North Africa in comparison with MODIS although both overestimate AOD seasonal values in the Eastern Sahara and northern Arabian Peninsula. The o-suite and control run show generally lower season values (seasonal DOD up to 0.5). CAMS o-suite presents lower season values (seasonal DOD up to 0.5) than control (seasonal DOD up to 0.7) which are in general higher than the SDS-WAS multi-median product. Otherwise, dust transport over the North Atlantic region and the Red Sea appears underestimated in comparison with the satellites (particularly in the o-suite). For March to May, the o-suite reproduces the daily variability of AERONET observations with a correlation coefficient of 0.84, averaged over all the AERONET sites (as in the case of the SDS-WAS multi-model that achieves values of 0.85), this is close to the control experiment that shows a correlation coefficient of 0.82.

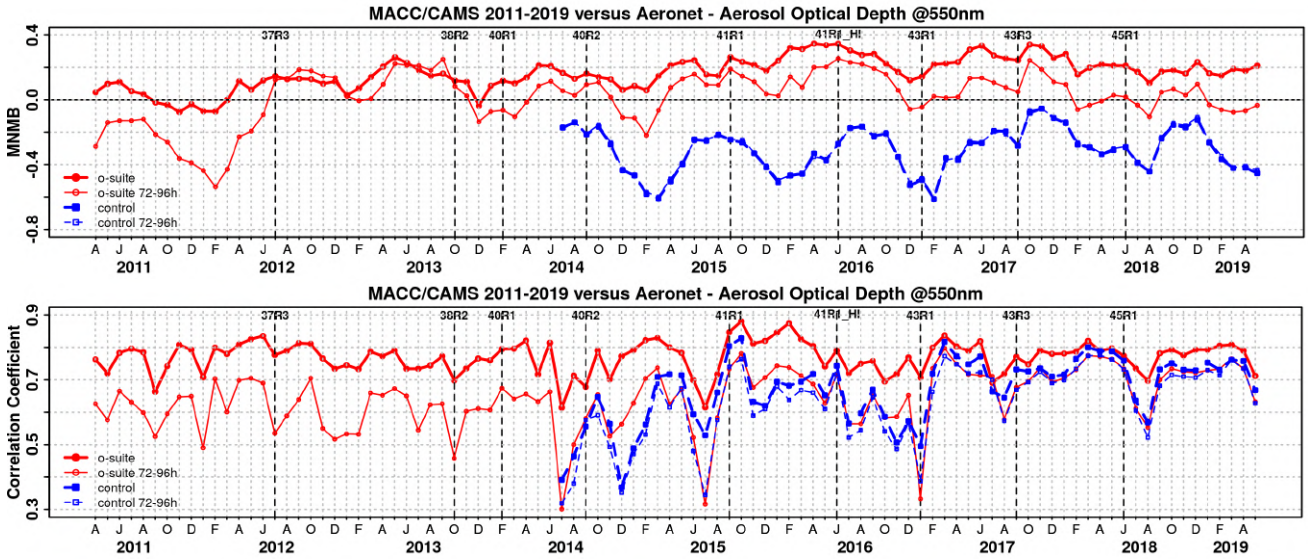

Figure S.5. Aerosol optical depth at 550nm in IFS 00Z model simulations for April 2011 – May 2019 against daily matching Aeronet Version3 level 1.5 data. a) Modified normalized mean bias (MNMB); o-suite (thick red curve); o-suite at last forecast day (light red curve); Control (blue dashed); Control at last forecast day (light blue dashed); b) Corresponding correlation coefficient. Model version changes are marked as vertical bars.

Regarding mean bias (MB), both CAMS o-suite and control, as well as the SDS-WAS Multi-model, underestimate the AERONET observations, resulting in an MB of 0 for control, -0.02 for o-suite and the SDS-WAS multi-model.

Over the Sahara both CAMS products show good agreement, with a correlation coefficient of 0.82 for control and 0.84 for o-suite, although o-suite shows a slightly higher overestimation (mean bias MB of 0.05) than the control run. On the contrary, in the Sahel, the o-suite shows strong underestimations (MB of -0.12, slightly higher than control with MB of -0.06). The o-suite better reproduces the observed daily variability, with a correlation value of 0.53 for the o-suite in comparison to 0.45 for the control run. The underestimations observed in o-suite in the Sahel are also spread to the Tropical North Atlantic. In the Middle East, the o-suite better reproduces the daily variability than control, with a correlation coefficient of 0.73 for o-suite and 0.71 for control. The SDS-WAS Multi-model median shows lower correlations here (0.63). Overestimations are observed in both CAMS products (MB of 0.14 for control and 0.17 for o-suite). For long-range transport regions over the Iberian Peninsula and the Mediterranean, both CAMS o-suite and control present high correlations (between 0.75 and 0.90) and slight underestimations (MB between -0.03 and -0.01).

The forecast is stable during the 3-days forecasts with correlation coefficients of 0.84 (0.82), 0.82 (0.81), and 0.79 (0.79) respectively for 24, 48 and 72h forecasts, for all the sites, for o-suite (control) with mean biases of -0.02 (0), -0.02 (0) and -0.01 (0) respectively for 24, 48 and 72h forecasts.

Backscatter coefficients (BSC) are biased low in the planetary boundary layer (PBL). As before, possible reasons are missing of ammonia and nitrate in the model (foreseen to be activated soon), assumption of too high particle densities (for pure compact materials) in the mass to backscatter conversion, and the lack of vertical transport barrier at the top of the PBL, causing dilution with free

troposphere air. Against this, free troposphere (FT) background backscatter coefficients are biased high, probably due to the assimilation re-distributing between PBL and FT. The BSC bias on a specific level thus depends on its relative position to the boundary layer top. Generally, monthly average vertical backscatter profiles to some extent follow the annual cycle of the observations, but they are smoother. The reason for the discrepancy between results with two different forward operators is yet not resolved. Monthly Taylor plots over 21 German stations indicate that daily averages of Pearson correlation coefficients cluster around 0.4-0.6, too large variability in winter, often due to overestimated layers of sea-salt and that this causes a less consistent day-to-day performance in winter as compared to summer.

System performance in the Arctic

The CAMS model runs are validated using surface ozone measurements from the ESRL-GMD and the IASOA networks (5 sites) and ozone concentrations in the free troposphere and the stratosphere are evaluated using balloon sonde measurement data.

Both runs strongly overestimate surface ozone values at most of the Arctic stations with MNMB ranging from +21% to +84% for the o-suite and from +28% to +92% for the control run in March - May. This large positive model offset is related to the chemistry scheme in the CAMS global system, which does not contain the halogen reactions to capture the ozone depletion events (ODE) that occur in spring. An exception from this pattern are the results from Svalbard (MNMB = 7% for the o-suite and 18% for the control run), where ODE are only rarely recorded due to the position of the station on a mountaintop, and Summit (MNMB = 10% for the o-suite and 12% for the control run), at the centre of the Greenland ice sheet, where ODE does not occur. In other seasons, the CAMS ozone simulations are generally in good agreement with the observations.

Ozone concentrations in the free troposphere are in fair agreement with observations with low relative bias. In the stratosphere, the o-suite has a bias of -13-+15% for the Arctic sites, whereas the bias for the control run is -8-+1%. In the UTLS, the o-suite overestimates with between 8% and 12%.

Comparison with FTIR observations from the NDACC network shows that the CO tropospheric columns are in good agreements at the arctic sites with bias between -5% and +1% for both the o-suite and the control run. Comparison with MOPITT versions 7 shows that modelled CO total columns are in good agreement with the satellite retrievals with low bias in the Arctic (±10%).

System performance in the Mediterranean

The model is compared to surface O_3 observations from the AirBase network. Our analysis shows that model MNMBs vary between -15% and 20% depending on the station. Temporal correlation coefficients between simulated and observed surface ozone for both the o-suite and control runs are highly significant over the entire Mediterranean from Gibraltar to Cyprus.

The CAMS o-suite reproduces the daily variability of AERONET observations (with correlation coefficients of 0.53, 0.83 and 0.72, respectively for Western, Central and Eastern Mediterranean).

The CAMS o-suite tends to overestimate the observed AOD values at AERONET sites, resulting in a mean bias (MB) of 0.08, 0.11 and 0.09, for the Western, Central and Eastern Mediterranean respectively. The highest peaks on CAMS AOD simulations are linked to desert dust intrusions. The CAMS o-suite and control reproduce the timing of the arrival of the dust plume correctly, although the o-suite better captures the intensity of the most intense events, reducing the overestimations observed in the control run. At surface levels, PM10 and PM2.5 results are close to the observations with an annual MB in average for all the sites of 27.01 (26.31) and 11.47 (13.43) $\mu g/m^3$, respectively for PM10 and PM2.5 for o-suite (control). Aerosol events (PM > 50 $\mu g/m^3$) in the Mediterranean sites observed in control are corrected in o-suite, reducing the observed PM peaks by about 50%.

Climate forcing

Greenhouse gases

CO_2 and CH_4 surface concentrations from ICOS network, and total or partial columns from TCCON and NDACC stations have been used to validate the analysis and high-resolution forecast experiments.

According to ICOS stations, the bias on CH_4 surface measurements is clearly dependent on latitude. We observe a positive bias (20 to 50 ppb) at high latitude, and a negative one in Southern Europe (-10 to -30 ppb). Column measurements (TCCON and NDACC) indicate negative biases, but also appear to be dependent on altitude since NDACC measurements in the stratosphere show a slight overestimation compared to the measurement uncertainty.

The surface and total column measurements indicate an overestimation of the amplitude of the CO_2 seasonal cycle in the northern hemisphere by ±1%. The drought anomaly in spring/summer 2018 has an additional effect on the comparison with surface sites from May to July 2018, with an overestimated impact of the drought on the CO_2 concentrations. The comparison at TCCON/Orleans shows that the overestimation is significantly higher than in previous years and reached up to 5-6 ppm.

Ozone layer and UV

Ozone partial columns and vertical profiles

Ozone columns and profiles have been compared with the following observations: vertical profiles from balloon-borne ozone sondes; ground-based remote-sensing observations from the NDACC (Network for the Detection of Atmospheric Composition Change, http://www.ndacc.org); and satellite observations by two instrument (OMPS-LP, ACE-FTS). Furthermore, the o-suite analyses are compared with those delivered by the independent assimilation system BASCOE.

Compared to ozone sondes the model O_3 partial pressures are slightly overestimated in all latitude bands (MNMB between 4 and +12%) except above the Antarctic.

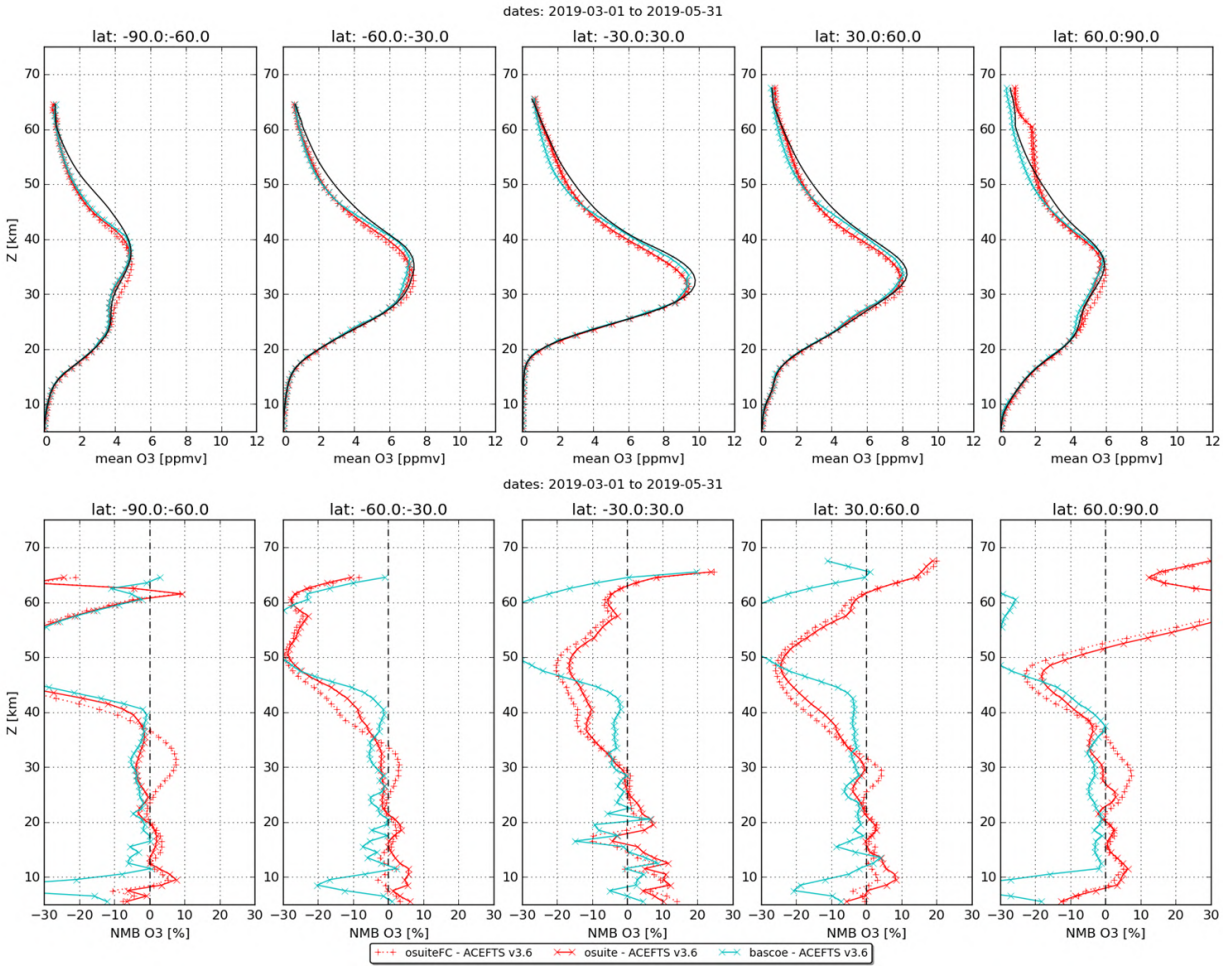

Figure S.7: Mean value (top) and normalized mean bias (bottom) of the ozone profile between o-suite analyses (red, solid), o-suite forecasts 4th day (red, dotted) and BASCOE (cyan line) with ACE-FTS observations for the period March 2019 to May 2019.

Comparisons with the NDACC network include 15 stations for UVVIS and FTIR stratospheric columns, microwave profiles for Ny Alesund (78.9°N) and Bern (47°N) and LIDAR profiles at Hohenpeissenberg (47.8°N) and Observatoire Haute Provence (OHP), France (43°N). The comparison with the UVVIS stations is generally in agreement with the o-suite, while it indicates a latitudinal dependence of the biases for the control run. The result from MWR and LIDAR comparisons for the current period are in line with those of previous reports.

The comparison with independent satellite observations is generally in good agreement for the considered period: for ACE-FTS (Fig. S.7), the NMB is mainly within 10% between 5km and 40km, and mostly within 5% between 15km and 35km except in the tropics. OMPS-LP has less regular profiles, but the NMB still remain within 15% for most parts of the 20-40 km range.

Other stratospheric trace gases

Due to the lack of stratospheric chemistry in the C-IFS-CB05 scheme, the only useful product in the stratosphere is ozone. Other species, like NO_2, have also been evaluated but the results are only indicative.

Events

There was a **fire event in the south-west of China** in the beginning of April 2019. IASI data does not show the exact location of the fire due to missing data pixels, but it clearly shows an eastward transport of a pollution plume on April 2nd. Both model runs captured the geographical location and extent of the plume. There is a clear underestimation of the CO values in the plume up to 40% in the o-suite run and up to 50% in the control run. The values located close to the source of the fire seems to be overestimated.

In **second half of April 2019**, the MODIS satellite detected an **intense outbreak of dust over the Mediterranean Basin**. The event was associated with the presence of clouds. Because of this, the quantitative comparison with the MODIS AOD products is limited. The CAMS AOD o-suite did timely reproduce the spatial distribution of the two dust plumes as shown by the comparison with MODIS/Terra. However, the comparison with AERONET and EIONET shows that the CAMS o-suite overestimated the aerosol concentrations during this event, with AOD values over 1.5 over the Mediterranean and PM10 over 300 $\mu g/m^3$ for some European sites.

Table of Contents

1. Introduction

The Copernicus Atmosphere Monitoring Service (CAMS, http://atmosphere.copernicus.eu/) is a component of the European Earth Observation programme Copernicus. The CAMS global near-real time (NRT) service provides daily analyses and forecasts of trace gas and aerosol concentrations. The CAMS near-real time services consist of daily analysis and forecasts with the ECMWF IFS system with data assimilation of trace gas concentrations and aerosol properties. This document presents the system evolution and the validation statistics of the CAMS NRT global atmospheric composition analyses and forecasts. The validation methodology and measurement datasets are discussed in Eskes et al. (2015).

In this report the performance of the system is assessed in two ways: both the longer-term mean performance (seasonality) as well as its ability to capture recent events are documented. Table 1.1 provides an overview of the trace gas species and aerosol aspects discussed in this CAMS near-real time validation report. This document is updated every 3 months to report the recent status of the near-real time service. The report covers results for a period of at least one year to document the seasonality of the biases. Sometimes reference is made to other model versions or the reanalysis to highlight aspects of the near-real time products.

This validation report is accompanied by the "Observations characterization and validation methods" report, Eskes et al. (2018a), which describes the observations used in the comparisons, and the validation methodology. This report can also be found on the global validation page, http://atmosphere.copernicus.eu/user-support/validation/verification-global-services.

Key CAMS NRT products and their users are: Boundary conditions for regional air quality models (e.g. AQMEII, air quality models not participating in CAMS); Long range transport of air pollution (e.g. LRTAP); Stratospheric ozone column and UV (e.g. WMO, DWD); 3D ozone fields (e.g. SPARC). As outlined in the MACC-II Atmospheric Service Validation Protocol (2013) and MACC O-INT document (2011), relevant user requirements are quick looks of validation scores, and quality flags and uncertainty information along with the actual data. This is further stimulated by QA4EO (Quality Assurance Framework for Earth Observation, http://www.qa4eo.org) who write that “all earth observation data and derived products is associated with it a documented and fully traceable quality indicator (QI)”. It is our long-term aim to provide such background information. The user is seen as the driver for any specific quality requirements and should assess if any supplied information, as characterised by its associated QI, are "fit for purpose" (QA4EO task team, 2010).

CAMS data are made available to users as data products (grib or netcdf files) and graphical products from ECMWF, accessible through the catalogue on http://atmosphere.copernicus.eu/.

A summary of the system and its recent changes is given in section 2. Subsequent sections gives an overview of the performance of the system for various species, and during recent events. Routine validation results can be found online via regularly updated verification pages, http://atmosphere.copernicus.eu/user-support/validation/verification-global-services. Table 1.2 lists all specific validation websites that can also be found through this link.

Table 1.1: Overview of the trace gas species and aerosol aspects discussed in this CAMS near-real time validation report. Shown are the datasets assimilated in the CAMS analysis (second column) and the datasets used for validation, as shown in this report (third column). Green colours indicate that substantial data is available to either constrain the species in the analysis, or substantial data is available to assess the quality of the analysis. Yellow boxes indicate that measurements are available, but that the impact on the analysis is not very strong or indirect (second column), or that only certain aspects are validated (third column).

Species, vertical range	Assimilation	Validation
Aerosol, optical properties	MODIS Aqua/Terra AOD PMAp AOD	AOD, Ångström: AERONET, GAW, Skynet, MISR, OMI, lidar, ceilometer
Aerosol mass (PM10, PM2.5)	MODIS Aqua/Terra	European AirBase stations
O_3, stratosphere	MLS, GOME-2A, GOME-2B, OMI, SBUV-2, OMPS, TROPOMI	Sonde, lidar, MWR, FTIR, OMPS, ACE-FTS, OSIRIS, BASCOE and MSR analyses
O_3, UT/LS	MLS	IAGOS, ozone sonde
O_3, free troposphere	Indirectly constrained by limb and nadir sounders	IAGOS, ozone sonde, IASI
O_3, PBL / surface		Surface ozone: WMO/GAW, NOAA/ESRL-GMD, AIRBASE
CO, UT/LS	IASI, MOPITT	IAGOS
CO, free troposphere	IASI, MOPITT	IAGOS, MOPITT, IASI, TCCON
CO, PBL / surface	IASI, MOPITT	Surface CO: WMO/GAW, NOAA/ESRL
NO_2, troposphere	OMI, GOME-2, partially constrained due to short lifetime	SCIAMACHY, GOME-2, MAX-DOAS
HCHO		GOME-2, MAX-DOAS
SO_2	GOME-2A, GOME-2B (Volcanic eruptions)	
Stratosphere, other than O_3		NO_2 column only: SCIAMACHY, GOME-2
CO_2, surface, PBL		ICOS
CO_2, column	GOSAT	TCCON
CH_4, surface, PBL		ICOS
CH_4, column	GOSAT, IASI	TCCON

Table 1.2: Overview of quick-look validation websites of the CAMS system.

Reactive gases – Troposphere
IAGOS tropospheric ozone and carbon monoxide: http://www.iagos.fr/cams/ Surface ozone from EMEP (Europe) and NOAA-ESRL (USA): http://www.academyofathens.gr/cams Tropospheric nitrogen dioxide and formaldehyde columns against satellite retrievals: http://www.doas-bremen.de/macc/macc_veri_iup_home.html Tropospheric CO columns against satellite retrievals: http://www.mpimet-cams.de GAW surface ozone and carbon monoxide: https://atmosphere.copernicus.eu/charts/cams_gaw_ver/v0d_gaw_oper_operfc_nrt_sites?facets=undefined&time=2018060100,0,2018060100&fieldpair=CO&site=cmn644n00
Reactive gases - Stratosphere
Stratospheric composition: http://www.copernicus-stratosphere.eu NDACC evaluation in stratosphere and troposphere (the NORS server) http://nors-server.aeronomie.be
Aerosol
Evaluation against Aeronet stations: http://aerocom.met.no/cams-aerocom-evaluation/ More in-depth evaluations are available from the Aerocom website. WMO Sand and Dust Storm Warning Advisory and Assessment System (SDS-WAS) model intercomparison and evaluation: http://sds-was.aemet.es/forecast-products/models Aeronet verification of CAMS NRT forecasts: https://atmosphere.copernicus.eu/charts/cams_aeronet_ver/?facets=undefined&time=2019020100,0,2019020100&site=ARM_Graciosa
Satellite data monitoring
Monitoring of satellite data usage in the Near-Real-Time production: https://atmosphere.copernicus.eu/charts/cams/cams_satmon?facets=undefined&time=2016071800&Parameter=AURA_MLS_profile_Ozone_1_GLOBE

Naming and color-coding conventions in this report follow the scheme as given in Table 1.3.

Table 1.3. Naming and colour conventions as adopted in this report.

Name in figs	experiment	Colour
{obs name}	{obs}	black
o-suite D+0 FC	0001	red
control	gsyg	blue
GHG high-resolution run	gqpe / ghqy	orange
GHG global analysis	gqiq	green

2. System summary and model background information

The specifics of the different CAMS model versions are given below (section 2.1) including an overview of model changes. Other systems used in CAMS are listed in section 2.2. An overview of products derived from this system is given in section 2.3. Timeliness and availability of the CAMS products is given in section 2.4.

2.1 System based on the ECMWF IFS model (the o-suite and control run)

Key model information is given on the CAMS data-assimilation and forecast run o-suite and its control experiment, used to assess the performance of the assimilation. The forecast products are listed in Table 2.1. Table 2.2 provides information on the satellite data used in the o-suite. Further details on the different model runs and their data usage can be found at http://atmosphere.copernicus.eu/documentation-global-systems.

Table 2.1: Overview of model runs assessed in this validation report.

Forecast system	Exp. ID	Brief description	Upgrades (e-suite ID)
o-suite	0001	Operational CAMS DA/FC run	20180626-present 20170926-20180625 20170124-20170926 20160621-20170124 20150903-20160620 20140918-20150902
Control	gzhy gsyg gnhb gjjh geuh g4o2	control FC run without DA	20180626-present (gzhy) 20170926-20180625 (gsyg) 20170124-20170926 (gnhb) 20160621-20170124 (gjjh) 20150901-20160620 (geuh) 20140701-20150902 (g4o2)
GHG run	ghqy gf39	High resolution T1279, NRT CO_2 and CH_4 without DA	20160301-20170621 (ghqy) 20150101-20160229 (gf39)
	gqpe	High resolution Tco1279 (~9km) NRT CO_2, CH_4 and linCO forecast, initialized from GHG analysis gqiq and CAMS operational CO analysis	20170101-present
	gqiq	GHG analysis Tco399 (~25km)	20170101-present

Table 2.2: Satellite retrievals of reactive gases and aerosol optical depth that are actively assimilated in the o-suite.

Instrument	Satellite	Provider	Version	Type	Status
MLS	AURA	NASA	V4	O3 Profiles	20130107 -
OMI	AURA	NASA	V883	O3 Total column	20090901 -
GOME-2A	Metop-A	Eumetsat	GDP 4.8	O3 Total column	20131007 - 20181231
GOME-2B	Metop-B	Eumetsat	GDP 4.8	O3 Total column	20140512 -
SBUV-2	NOAA-19	NOAA	V8	O3 21 layer profiles	20121007 -
OMPS	Suomi-NPP	NOAA / EUMETSAT		O3 Profiles	20170124 - 20190409
TROPOMI	Sentinel-5P	ESA		O3 column	20181204-
IASI	MetOp-A	LATMOS/ULB Eumetsat	-	CO Total column	20090901 - 20180621 20180622 -
IASI	MetOp-B	LATMOS/ULB Eumetsat	-	CO Total column	20140918 - 20180621 20180622 -
MOPITT	TERRA	NCAR	V5-TIR V7-TIR V7-TIR Lance	CO Total column	20130129 - 20160124 - 20180626 20180626
OMI	AURA	KNMI	DOMINO V2.0	NO2 Tropospheric column	20120705 -
GOME-2A/2B	METOP A/B	Eumetsat	GDP 4.8	NO2 Tropospheric column	20180626 -
OMI	AURA	NASA	v003	SO2 Tropospheric column	20120705-20150901
GOME-2A/2B	METOP A/B	Eumetsat	GDP 4.8	SO2 Tropospheric column	20150902 -
MODIS	AQUA / TERRA	NASA	Col. 5 Deep Blue Col. 6, 6.1	Aerosol total optical depth, fire radiative power	20090901 - 20150902 - 20170124 -
PMAp	METOP-A METOP-B	EUMETSAT		AOD	20170124 - 20170926 -

2.1.1 o-suite

The o-suite consists of the IFS-CB05 chemistry combined with the CAMS bulk aerosol model. The chemistry is described in Flemming et al. (2015) and Flemming et al. (2017), aerosol is described in Morcrette et al. (2009). The forecast length is 120 h. The o-suite data is stored under **expver '0001'** of **class 'MC'**. On 21 June 2016 the model resolution has seen an upgrade from T255 to T511, and forecasts are produced twice per day. The latest upgrade of the system is based on IFS version cy45r1_CAMS (https://confluence.ecmwf.int/display/COPSRV/Current+global+production+suites)

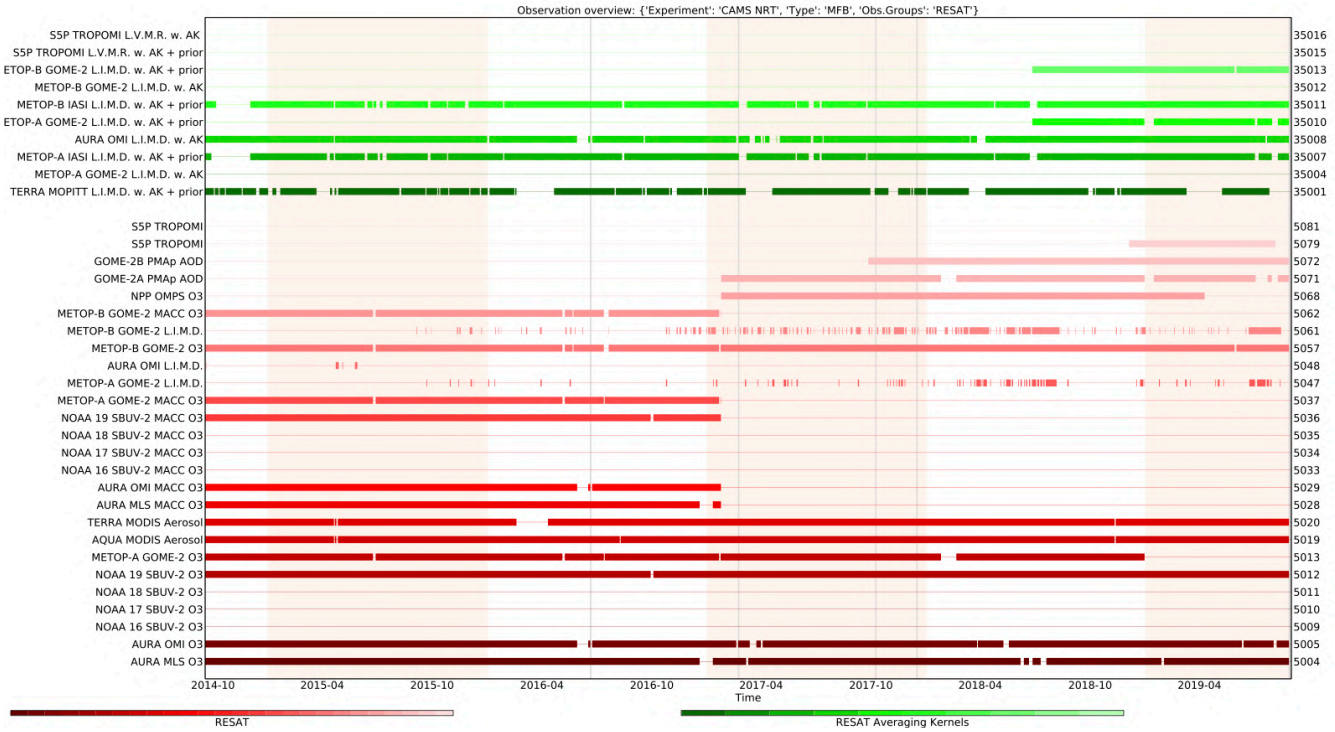

Figure 2.1: Satellite observation usage in the real-time analysis, for ozone, CO, aerosol AOD, from October 2014 onwards. Top eight rows: products assimilated using averaging kernels. New assimilated products since the 24 January 2017 upgrade are the PMaP AOD including GOME-2B and OMPS ozone profile observations. Sentinel-5P TROPOMI ozone is assimilated since Dec. 2018 (5079=O_3) and other products are monitored (35016=NO_2, 35015=CO, 5081=SO_2). Note that the lines mentioning "MACC O3" should be discarded.

and took place on 26 June 2018. The validation for this upgrade is described in Eskes et al., 2018b/2018c. The update relevant for this report (for SON-2018) is this 26 June 2018 upgrade. A short summary of the main specifications:

- The modified CB05 tropospheric chemistry is used (Williams et al., 2013), originally taken from the TM5 chemistry transport model (Huijnen et al., 2010)
- Stratospheric ozone during the forecast is computed from the Cariolle scheme (Cariolle and Teyssèdre, 2007) as already available in IFS, while stratospheric NOx is constrained through a climatological ratio of HNO_3/O_3 at 10 hPa.
- Monthly mean dry deposition velocities are based on the SUMO model provided by the MOCAGE team.
- Data assimilation is described in Inness et al. (2015) and Benedetti et al. (2009) for chemical trace gases and aerosol, respectively. Satellite data assimilated is listed in Table 2.2 and Fig. 2.1.
- Anthropogenic and biogenic emissions are based on MACCity (Granier et al., 2011) and a climatology of the MEGAN-MACC emission inventories (Sindelarova et al., 2014)
- NRT fire emissions are taken from GFASv1.2 (Kaiser et al. 2012).

The aerosol model includes 12 prognostic variables, which are 3 bins for sea salt and desert dust, hydrophobic and hydrophilic organic matter and black carbon, sulphate aerosols and its precursor trace gas SO_2 (Morcrette et al., 2009). Aerosol total mass is constrained by the assimilation of

MODIS AOD (Benedetti et al. 2009). A variational bias correction for the MODIS AOD is in place based on the approach used also elsewhere in the IFS (Dee and Uppala, 2009).

New source scheme for Secondary Organic Aerosols (part of the Organic Matter), based on scaled CO emissions. This is a change from the current AEROCOM-based emissions. The impact is an increase of organic matter aerosol concentrations. The upgrade of 24 January 2017 introduced the following adjustments: 1. Reduced dust emissions over Taklamakan desert and India. 2. Dust emissions adjusted towards more larger particles. 3. Reduction in sulphate aerosol. 4. Mass fixer for aerosols.

A history of updates of the o-suite is given in Table 2.4, and is documented in earlier MACC-VAL reports: https://atmosphere.copernicus.eu/node/326. This includes a list with changes concerning the assimilation system.

The CAMS o-suite system is upgraded regularly, following updates to the ECMWF meteorological model as well as CAMS-specific updates such as changes in chemical data assimilation. These changes are documented in e-suite validation reports, as can be found from the link above. Essential model upgrades are also documented in Table 2.4.

On 26 June 2018 the system has been upgraded to cy45r1. A validation report for this upgrade (Eskes et al., 2018b) is available: https://atmosphere.copernicus.eu/sites/default/files/2018-06/CAMS84_2015SC2_D84.3.1.5_201802_esuite_v1_0.pdf The addendum to this document is called CAMS84_2015SC3_D84.3.1.5_201802_esuite_addendum.pdf (Eskes et al., 2018c).

2.1.2 Control

The control run (relevant expver = **gzhy,** since 26/06/2018) applies the same settings as the respective o-suites, based on the coupled IFS-CB05 system with CAMS aerosol for cy54r1, except that data assimilation is not switched on. The only two exceptions with regard to this setup are:

- at the start of every forecast the ECMWF operational system is used to initialise *stratospheric* ozone, considering that stratospheric ozone, as well as other stratospheric species are not considered to be a useful product of this run. The reason for doing so is that this ensures reasonable stratospheric ozone as boundary conditions necessary for the tropospheric chemistry.
- The full meteorology in the control run is also initialized from the ECMWF operational NWP analyses. Note that this is different from the o-suite, which uses its own data assimilation setup for meteorology. This can cause slight differences in meteorological fields between o-suite and control, e.g. as seen in evaluations of upper stratospheric temperatures.

2.1.3 High-resolution CO_2 and CH_4 forecasts and delayed-mode analyses

The pre-operational forecasts of CO_2 and CH_4 use an independent setup of the IFS at a resolution of TL1279, i.e. ~16 km horizontal, and with 137 levels. This system runs in real time, and does not apply data assimilation for the greenhouse gases.

The land vegetation fluxes for CO_2 are modelled on-line by the CTESSEL carbon module (Boussetta et al., 2013). A biogenic flux adjustment scheme is used in order to reduce large-scale biases in the net ecosystem fluxes (Agusti-Panareda, 2015). The anthropogenic fluxes are based on the annual

Table 2.4: Long-term o-suite system updates.

Date	o-suite update
2009.08.01	Start of first NRT experiment f7kn with coupled MOZART chemistry, without aerosol. Also without data assimilation.
2009.09.01	Start of first MACC NRT experiment f93i, based on meteo cy36r1, MOZART v3.0 chemistry, MACC aerosol model, RETRO/REAS and GFEDv2 climatological emissions, T159L60 (IFS) and 1.875°×1.875° (MOZART) resolution.
2012.07.05	Update to experiment fnyp: based on meteo cy37r3, MOZART v3.5 chemistry, where changes mostly affect the stratosphere, MACCity (gas-phase), GFASv1 emissions (gas phase and aerosol), T255L60 (IFS) and 1.125°×1.125° (MOZART) resolution. Rebalancing aerosol model, affecting dust.
2013.10.07	Update of experiment fnyp from e-suite experiment fwu0: based on meteo cy38r2, no changes to chemistry, but significant rebalancing aerosol model. Assimilation of 21 layer SBUV/2 ozone product
2014.02.24	Update of experiment fnyp from e-suite experiment fzpr: based on meteo cy40r1. No significant changes to chemistry and aerosol models.
2014.09.18	Update to experiment g4e2: based on meteo cy40r2. In this model version IFS-CB05 is introduced to model atmospheric chemistry.
2015.09.03	Update to experiment g9rr: based on meteo cy41r1.
2016.06.21	Update to experiment 0067: based on meteo cy41r1, but a resolution increase from T255 to T511, and two production runs per day
2017.01.24	Update to cycle 43R1_CAMS, T511L60
2017.09.26	Update to cycle 43R3_CAMS, T511L60
2018.06.26	Update to cycle 45R1_CAMS, T511L60

mean EDGARv4.2 inventory using the most recent year available (i.e. 2008) with estimated and climatological trends to extrapolate to the current year. The fire fluxes are from GFAS (Kaiser et al., 2012). Methane fluxes are prescribed in the IFS using inventory and climatological data sets, consistent with those used as prior information in the CH_4 flux inversions from Bergamaschi et al. (2009). The anthropogenic fluxes are from the EDGAR 4.2 database (Janssens-Maenhout et al, 2012) valid for the year 2008. The biomass burning emissions are from GFAS v1.2 (Kaiser et al., 2012). The high-resolution forecast experiments also included a linear CO scheme (Massart et al., 2015).

The experiments analysed in this report are:

- "**ghqy**" from March 2016. The initial conditions used in ghqy on 1st of March 2016 are from the GHG analysis (experiment gg5m). Furthermore, the meteorological analysis used to initialize the ghqy forecast changed resolution and model grid in March 2016. Note that the CO_2, CH_4 and linear CO tracers are free-running.

- "**gqpe**" from January 2017 to present. It runs with a TCO1279 Gaussian cubic octahedral grid (equivalent to approximately 9km horizontal resolution). Note that the CO_2, CH_4 and linear CO tracers are initialized with the GHG analysis (gqiq) for CO_2 and CH_4 and the CAMS operational analysis for CO.
- The greenhouse gas analysis experiment "**gqiq**" runs on a TCO399 grid (equivalent to around 25km) and 137 vertical levels and is available from January 2017. This experiment runs in delayed mode (4 days behind real time) and makes use of observations from TANSO-GOSAT (methane and CO_2) and MetOp-IASI (methane).

2.2 Other systems

2.2.1 BASCOE

The NRT analyses and forecasts of ozone and related species for the stratosphere, as delivered by the Belgian Assimilation System for Chemical ObsErvations (BASCOE) of BIRA-IASB (Lefever et al., 2014; Errera et al., 2008), are used as an independent model evaluation of the CAMS products. The NRT BASCOE product is the ozone analysis of Aura/MLS-SCI level 2 standard products, run in the following configuration (version 05.07):

- The following species are assimilated: O_3, H_2O, HNO_3, HCl, HOCl, N_2O and ClO.
- It lags by typically 4 days, due to latency time of 4 days for arrival of non-ozone data from Aura/MLS-SCI (i.e. the scientific offline Aura/MLS dataset).
- Global horizontal grid with a 3.75° longitude by 2.5° latitude resolution.
- Vertical grid is hybrid-pressure and consists in 86 levels extending from 0.01 hPa to the surface.
- Winds, temperature and surface pressure are interpolated in the ECMWF operational 6-hourly analyses.
- Time steps of 20 minutes, output every 3 hours

See the stratospheric ozone service at http://www.copernicus-stratosphere.eu/. It delivers graphical products dedicated to stratospheric composition and allows easy comparison between the results of o-suite, BASCOE and TM3DAM. The BASCOE data products (HDF4 files) are also distributed from this webpage. Other details and bibliographic references on BASCOE can be found at http://bascoe.oma.be/. A detailed change log for BASCOE can be found at http://www.copernicus-stratosphere.eu/4_NRT_products/3_Models_changelogs/BASCOE.php.

2.2.2 TM3DAM and the multi-sensor reanalysis

One of the MACC products was a 30-year reanalysis, near-real time analysis and 10-day forecast of ozone column amounts performed with the KNMI TM3DAM data assimilation system, the Multi-Sensor Reanalysis (MSR) system (van der A et al., 2010, 2013),
http://www.temis.nl/macc/index.php?link=o3_msr_intro.html.
The corresponding validation report can be found at
http://www.copernicus-atmosphere.eu/services/gac/global_verification/validation_reports/.

The NRT TM3DAM product used for the validation of the CAMS NRT streams is the ozone analysis of Envisat/SCIAMACHY (until April 2012), AURA/OMI, and MetOp-A/GOME-2, run in the following configuration:

- total O_3 columns are assimilated

- Global horizontal grid with a 3° longitude by 2° latitude resolution.
- Vertical grid is hybrid-pressure and consists in 44 levels extending from 0.1 hPa to 100 hPa.
- Dynamical fields from ECMWF operational 6-hourly analysis.

An update of the MSR (MSR-2) was presented in van der A et al. (2015), which extended the record to 43 years based on ERA-interim reanalysis meteo and with an improved resolution of 1x1 degree.

2.2.3 SDS-WAS multimodel ensemble

The World Meteorological Organization's Sand and Dust Storm Warning Advisory and Assessment System (WMO SDS-WAS) for Northern Africa, Middle East and Europe (NAMEE) Regional Center (http://sds-was.aemet.es/) has established a protocol to routinely exchange products from dust forecast models as the basis for both near-real-time and delayed common model evaluation. Currently, twelve regional and global models (see the complete list in the following link https://sds-was.aemet.es/forecast-products/forecast-evaluation/model-inter-comparison-and-forecast-evaluation/at_download/file) provides daily operational dust forecasts (i.e. dust optical depth, DOD, and dust surface concentration).

Different multi-model products are generated from the different prediction models. Two products describing centrality (multi-model median and mean) and two products describing spread (standard deviation and range of variation) are daily computed. In order to generate them, the model outputs are bi-linearly interpolated to a common grid mesh of 0.5º x 0.5º. The multimodel DOD (at 550 nm) Median from nine dust prediction models participating in the SDS-WAS Regional Center is used for the validation of the CAMS NRT streams.

2.3 CAMS products

An extended list of output products from the NRT stream o-suite are available as 3-hourly instantaneous values up to five forecast days. These are available from ECMWF (through ftp in grib2 and netcdf format, https://atmosphere.copernicus.eu/data).

2.4 Availability and timing of CAMS products

The availability statistics provided in Table 2.6 are computed for the end of the 5-day forecast run. The CAMS production KPI is defined as the percentage of cycles in which all the general data dissemination tasks are completed before the deadlines: 10 UTC for the 00:00 and 22 UTC for the 12:00 UTC run. This was in part based on requirements from the regional models. We note that at present most regional models can still provide their forecasts even if the global forecast is available a bit later. Note that since 21 June 2016 two CAMS forecasts are produced each day.

For the period March - May 2019, 100% of the forecasts were delivered on time.

Table 2.6: Timeliness of the o-suite from December 2014. From June 2016 onwards CAMS has produced two forecasts per day.

Months	**On time, 10 & 22 utc**	**80th perc**	**90th perc**	**95th perc**
Dec-Feb '14-'15	97%	D+0, 19:43	D+0, 20:28	D+0, 21:13
Mar-May 2015	96%	D+0, 19:38	D+0, 21:03	D+0, 21:40
Jun-Aug 2015	95%	D+0, 20:24	D+0, 20:53	D+0, 21:54
Sept-Nov 2015	95%	D+0, 19:44	D+0, 20:55	D+0, 21:51
Dec-Feb '15-'16	100%	D+0, 18:39	D+0, 18:57	D+0, 19:43
Mar-May 2016	98%	D+0, 19:32	D+0, 19:47	D+0, 20:00
Jun-Aug 2016 (00 and 12 cycle)	100%	D+0, 08:53 D+0, 20:55	D+0, 09:04 D+0, 21:01	D+0, 09:18 D+0, 21:18
Sep-Nov 2016	98.9%	D+0, 08:44 D+0, 20:44	D+0, 08:51 D+0, 20:48	D+0, 08:52 D+0, 20:51
Dec 2016 - Feb 2017	99.4%	D+0, 09:02 D+0, 21:01	D+0, 09:11 D+0, 21:02	D+0, 09:18 D+0, 21:04
Mar-May 2017	100%	D+0, 09:08 D+0, 21:07	D+0, 09:14 D+0, 21:09	D+0, 09:19 D+0, 21:11
Jun-Aug 2017	100%	D+0, 09:05 D+0, 21:05	D+0, 09:07 D+0, 21:08	D+0, 9:09 D+0, 21:10
Sep-Nov 2017	100%	D+0, 09:02 D+0, 21:00	D+0, 09:05 D+0, 21:04	D+0, 9:09 D+0, 21:07
Dec 2017 - Feb 2018	98.33%	D+0, 08:55 D+0, 20:54	D+0, 08:59 D+0, 20:59	D+0, 09:01 D+0, 21:02
Mar-May 2018	98.9%	D+0, 09:00 D+0, 21:00	D+0, 09:06 D+0, 21:03	D+0, 09:08 D+0, 21:06
Jun-Aug 2018	100%	D+0, 09:11 D+0, 21:07	D+0, 09:14 D+0, 21:09	D+0, 09:20 D+0, 21:11
Sep-Nov 2018	100%	D+0, 09:05 D+0, 21:03	D+0, 09:09 D+0, 21:07	D+0, 09:13 D+0, 21:10
Dec 2018 - Feb 2019	98.85%	D+0, 09:03 D+0, 21:04	D+0, 09:06 D+0, 21:06	D+0, 09:08 D+0, 21:10
Mar-May 2019	100%	D+0, 09:07 D+0, 21:05	D+0, 09:10 D+0, 21:09	D+0, 09:12 D+0, 21:11

3. Tropospheric Ozone

3.1 Validation with sonde data in the free troposphere

Model profiles of the CAMS runs were compared to free tropospheric balloon sonde measurement data of 38 stations taken from the NDACC, WOUDC, NILU and SHADOZ databases for January 2013 to May 2019 (see Fig. 3.1.1 - 3.1.2). Towards the end of the period, the number of available soundings decreases, which implies that the evaluation results may become less representative. The figures contain the number of profiles in each month that are available for the evaluation. The methodology for model comparison against the observations is described in Douros et al., 2017. The free troposphere is defined as the altitude range between 750 and 200hPa in the tropics and between 750 and 300hPa elsewhere.

MNMBs for the o-suite are mostly within the range ±20%, for all months, in all zonal bands, except for the Tropics and Antarctica, where larger positive MNMBs up to ±45% appear, see Fig. 3.1.4. During the last year (May 2018 to May 2019) MNMBs are ±15% over the Arctic and Northern Midlatitudes and up to 35% for Antarctica and the Tropics, see Fig. 3.1.1.-3.1.4.

Over the Arctic, the o-suite mostly shows slightly positive MNMBs during summer and spring (MNMBs up to 10%), while during the winter season the MNMBs get negative (within -10%) see, Fig. 3.1.1.

Over the NH mid-latitudes MNMBs for the o-suite are on average close to zero all year round (maxima are -8% to +8%), which is generally a clear improvement compared to the control run, which shows larger MNMBs during the respective period.

Over the Tropics and over Antarctica, ozone mixing ratios are mostly overestimated by the o-suite (up to 34%) by the o-suite, see Fig. 3.1.2. The control run shows large negative MNMBs for Antarctica.

In the UTLS, ozone is overestimated by the o-suite over all regions. MNMBs range mostly within ±20%.

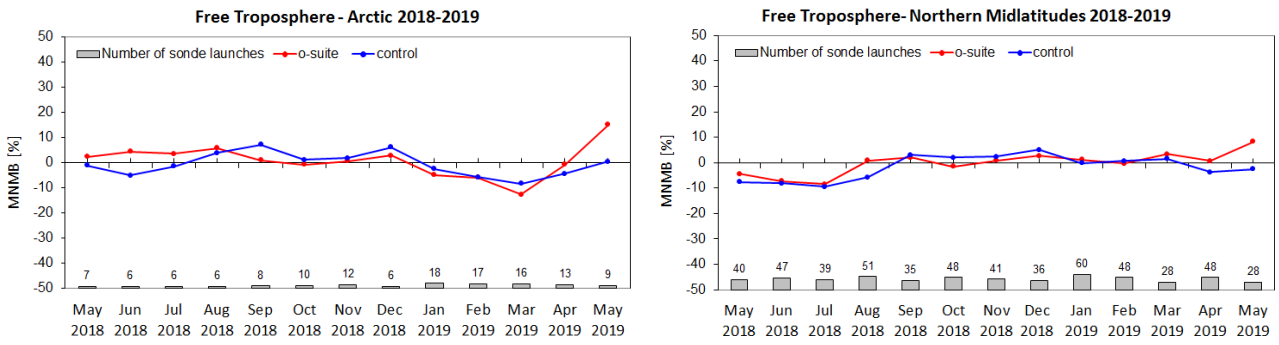

Figure 3.1.1: MNMBs (%) of ozone in the free troposphere (between 750 and 300 hPa) from the IFS model runs against aggregated sonde data over the Arctic (left) and the Northern mid latitudes (right). The numbers indicate the amount of individual number of sondes.

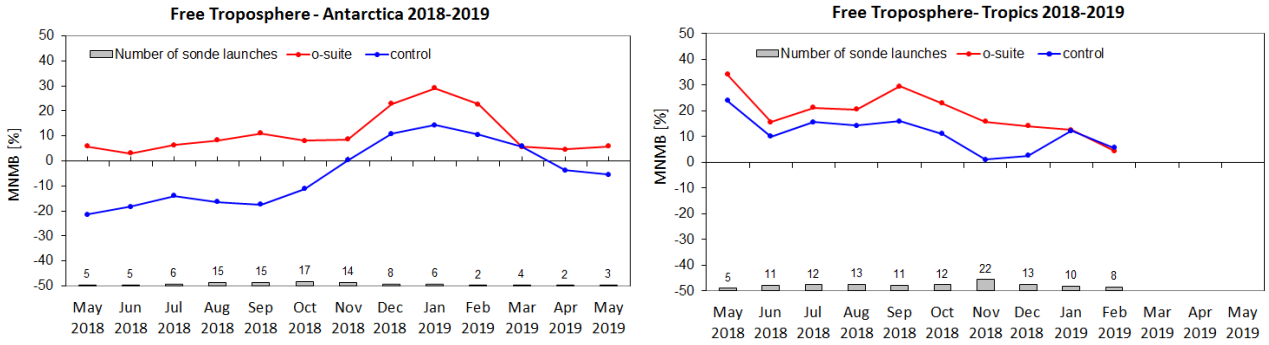

Figure 3.1.2: MNMBs (%) of ozone in the free troposphere (between 750 and 200hPa (Tropics) / 300hPa) from the IFS model runs against aggregated sonde data over the Tropics (left) and Antarctica (right). The numbers indicate the amount of individual number of sondes.

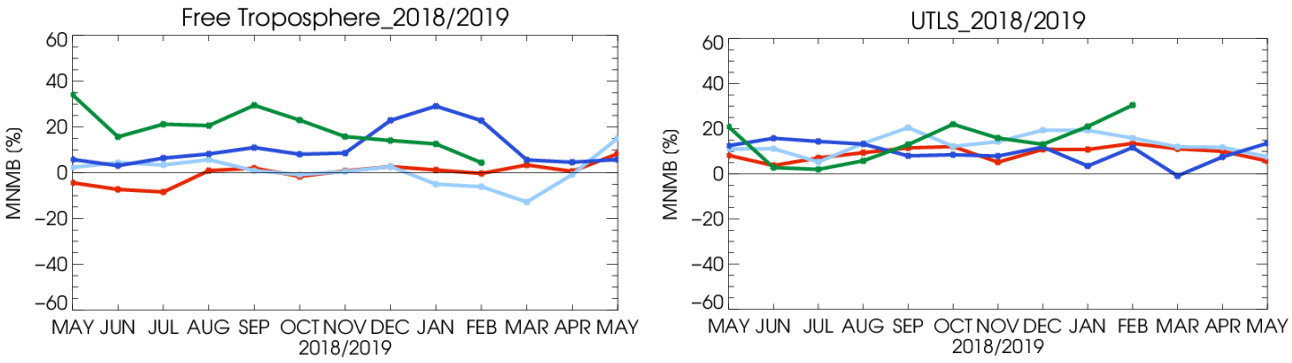

Figure 3.1.3: MNMBs (%) of ozone in the free troposphere (left, between 750 and 200hPa (Tropics) / 300hPa) and UTLS (right, between 300 and 100hPa (Tropics) / 60hPa) from the IFS model runs against aggregated sonde data over the Tropics (green) and Antarctica (blue), Arctic (light blue) and Northern Midlatitudes (red).

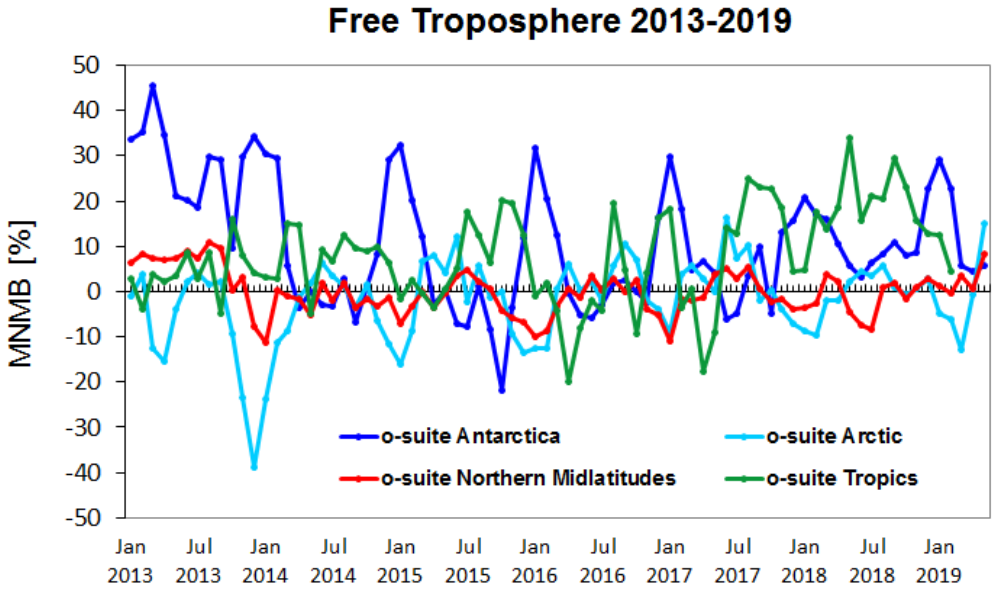

Figure 3.1.4: Time series of MNMB of ozone in the o-suite, compared against ozone sondes, averaged over different latitude bands. The free troposphere is defined here as the layer between 750 and 300 hPa.

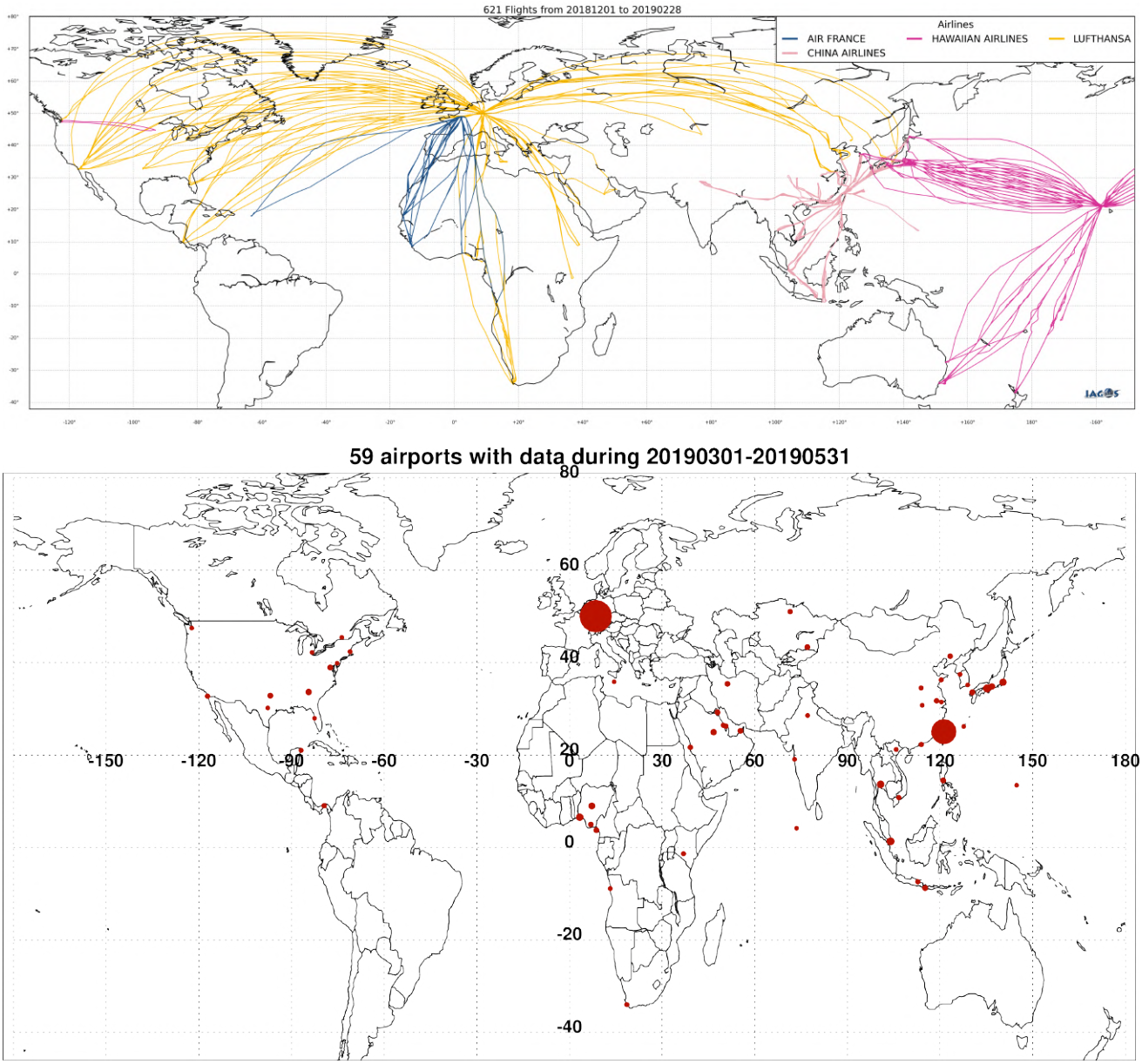

Figure 3.2.1. Map of the flights (top) and the visited airports (bottom) during the period March - May 2019, by the IAGOS-equipped aircraft. The size of the plotting circle represents the number of profiles available.

3.2 Ozone validation with IAGOS data

The daily profiles of ozone measured at airports around the world are shown on the CAMS website at http://www.iagos.fr/macc/nrt_day_profiles.php. For the period from March - May 2019, the data displayed on the web pages and in this report include only the data as validated by the instrument PI. The available flights and available airports are shown in Fig. 3.2.1 top and bottom respectively. Performance indicators have been calculated for different parts of the IAGOS operations.

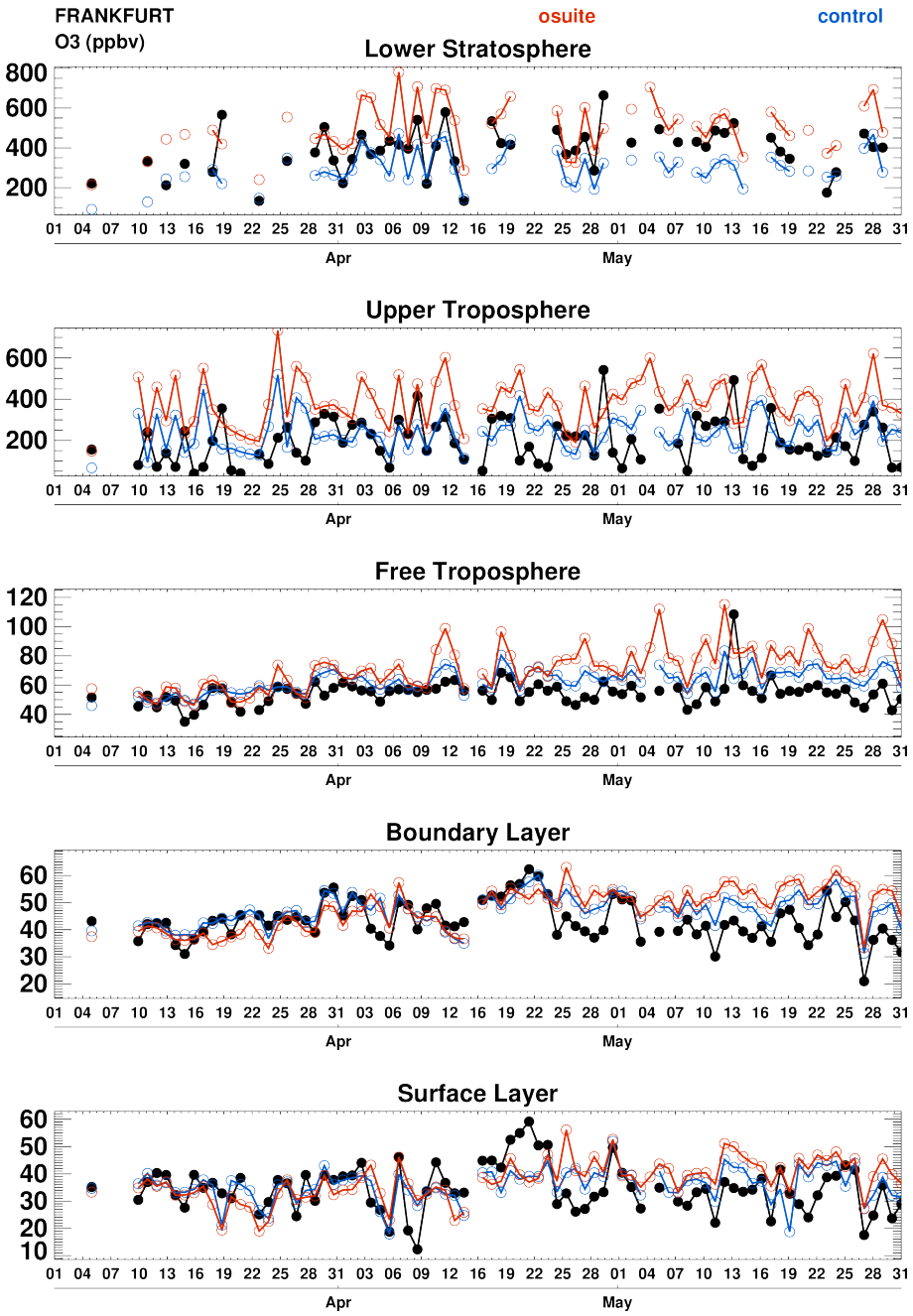

Figure 3.2.2. Time series of daily mean ozone over Frankfurt during MAM 2019 for 5 layers: Surface Layer, Boundary Layer, Free Troposphere, Upper Troposphere and Lower Stratosphere. The o-suite is shown in red and associated control run in blue.

Six aircraft were operating during this period. With these aircrafts, operating fully over the three-month period, we can expect a total of about 1260 flights. The actual number of flights within the period was 621 (1242 profiles) giving a performance of 49 %. These flights are shown in Fig. 3.2.1 (top). Nine percent (41%) of the operational flights had usable measurements of ozone and 56% of the flights had usable CO. Delivering these O_3 and CO data were two aircraft from Lufthansa operating from Frankfurt, one aircraft operated by Air France based in Paris, two from China Airlines

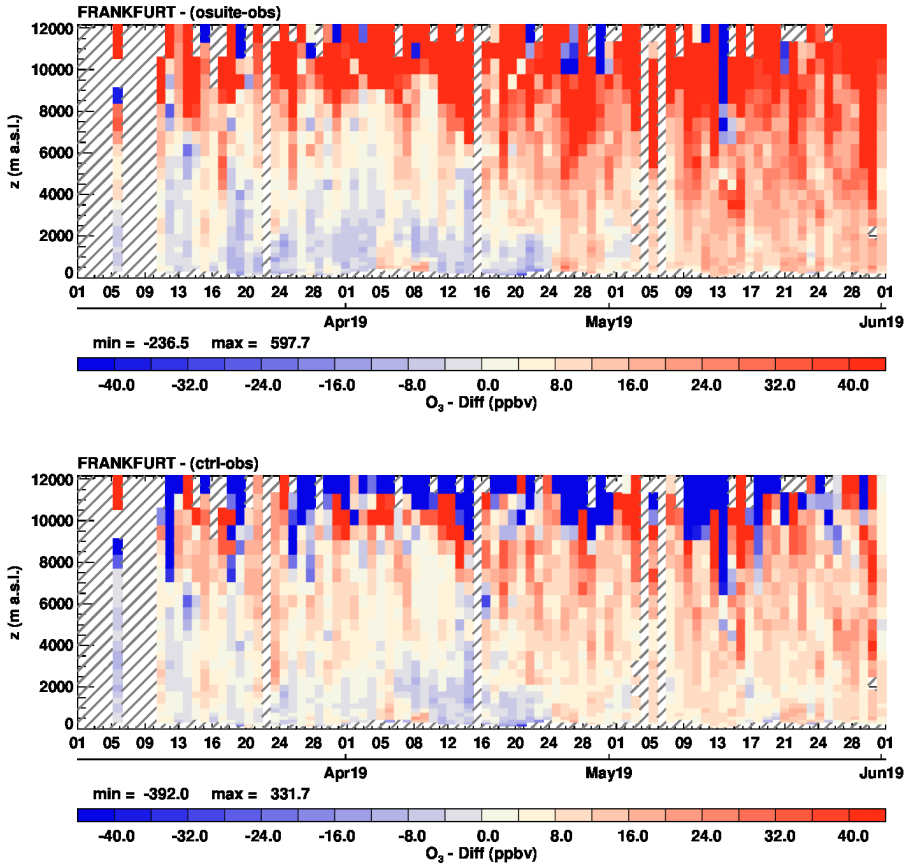

Figure 3.2.3 Time series of the absolute differences (model - observations) in daily profiles for ozone over Frankfurt during MAM 2019. Top panel corresponds to o-suite and low panel to control run.

based in Taipei and one from Hawaiian Airlines with flight operations from Honolulu. Fig. 3.2.1 (bottom) shows the available airports, with a plotting circle scaled to the highest number of flights at an airport.

Europe

Fig. 3.2.2 presents ozone time series at Frankfurt during March – May 2019. In the first half of the period, ozone is in general well represented from the surface to the free troposphere by both runs. However, starting around mid-April the model biases appear to increase with an overestimation of ozone. Note that the OMPS data format changed from 12L to 21L, and this data was blacklisted as precaution after 10 April. It is not clear if the bias increase is linked to this change. This can also be seen clearly in the time series of the differences in fig. 3.2.3. In the UTLS region is mostly overestimated by the o-suite while the performance of control run is better with smaller overestimations in the UT layer and underestimations in the LS layer. Some examples of individual profiles are presented in Fig. 3.2.4.

As compared to the two previous reports, the availability of IAGOS data is better during this period, however several of the issues mentioned in SON 2018 and DJF 2019 reports remain. This explains that for example for Taipei although many flights are departing/arriving from this airport no data are available for these flights.

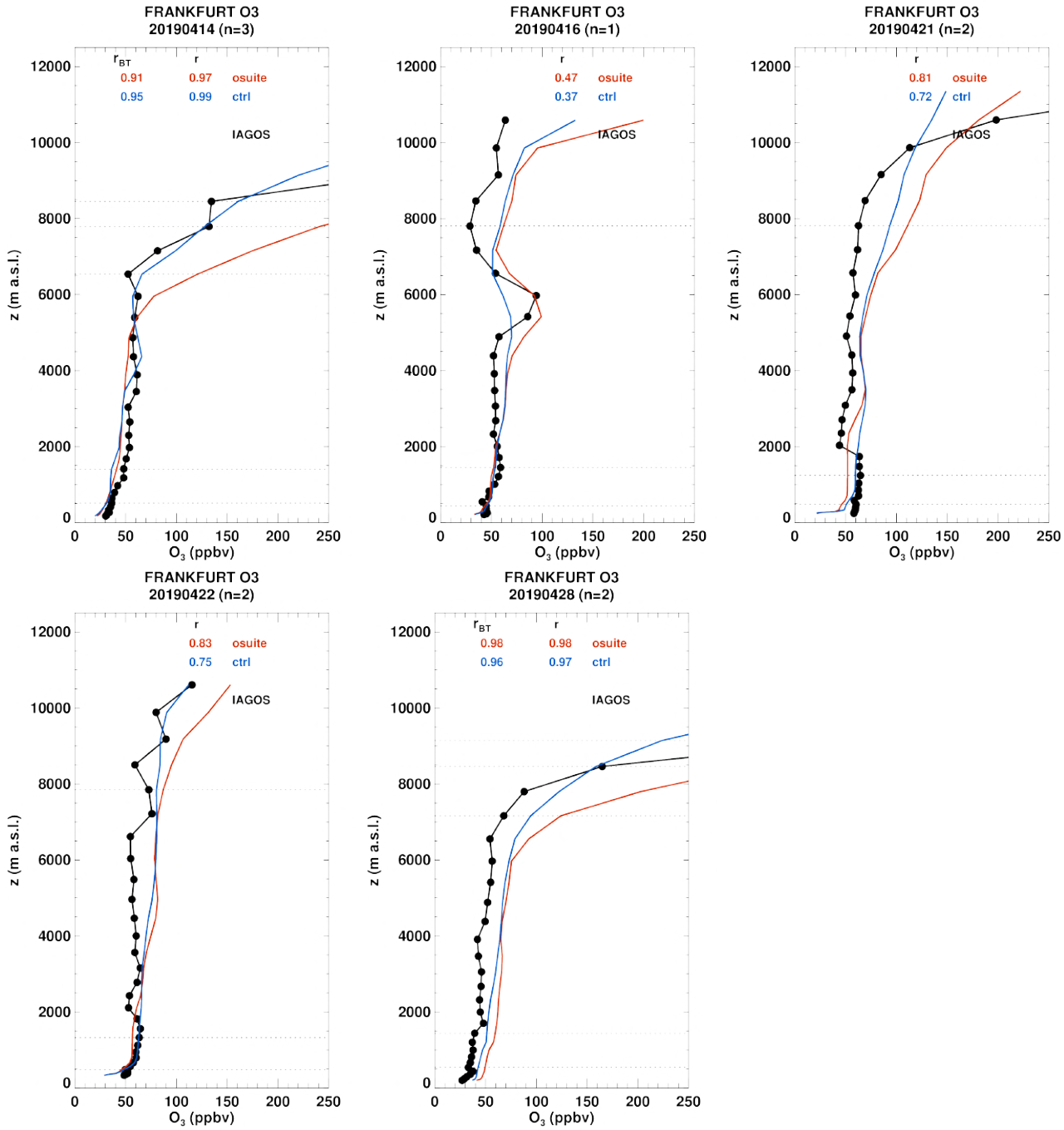

Figure 3.2.4.a Daily profiles for ozone from IAGOS (black) and the two NRT runs (o-suite: red, control: blue) over Europe during MAM 2019.

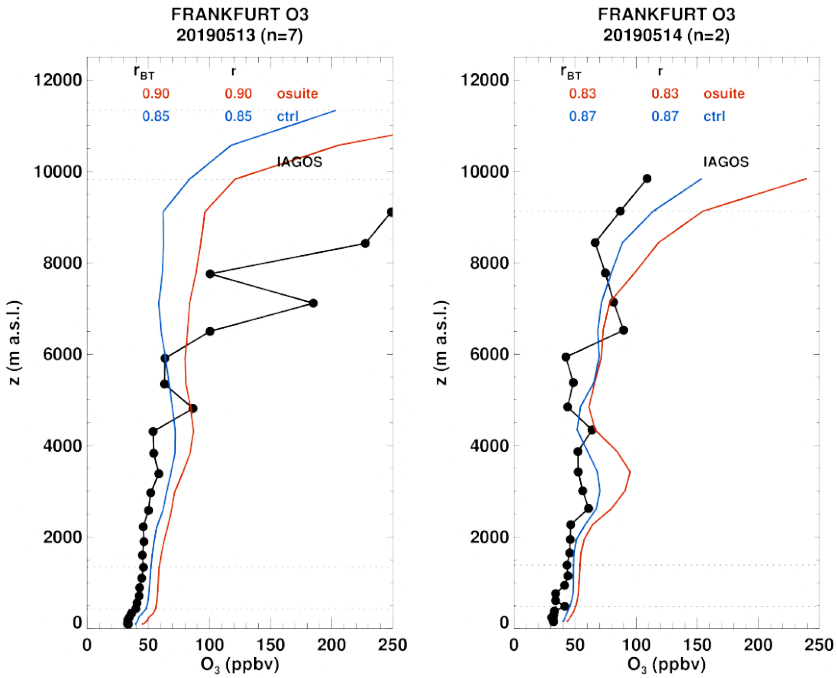

Figure 3.2.4.b Daily profiles for ozone from IAGOS (black) and the two NRT runs (o-suite: red, control: blue) over Europe during MAM 2019.

A selection of profiles at Frankfurt are presented in Fig. 3.2.4.a-b. During this period, the maximum of ozone in the surface and boundary layer is found around the 21 of April as shown on the time series and profiles with about 60 ppbv from the surface to the lower part of the free troposphere (Fig. 3.2.2 and 3.2.4.a). The profiles of day 21 and 22 April are well represented by the models with the exception of the UTLS especially for the o-suite which overestimates.

On the profile of the 16 April a peak in ozone is observed near 6000 m. This is likely due to a stratospheric intrusion given the profiles of the previous day with a very low tropopause (Fig. 3.2.4.a).

On the time series a sharp peak in ozone values is observed in the free troposphere around mid-May. On day 14 the shape of the profile is complex with two maxima of ozone in the free troposphere, the largest reaching 90 ppbv in the upper part of the free troposphere. The models reproduce only the first maximum at the correct altitude near of about 3000 m and the agreement with observations is better for control run than the o-suite which overestimates.

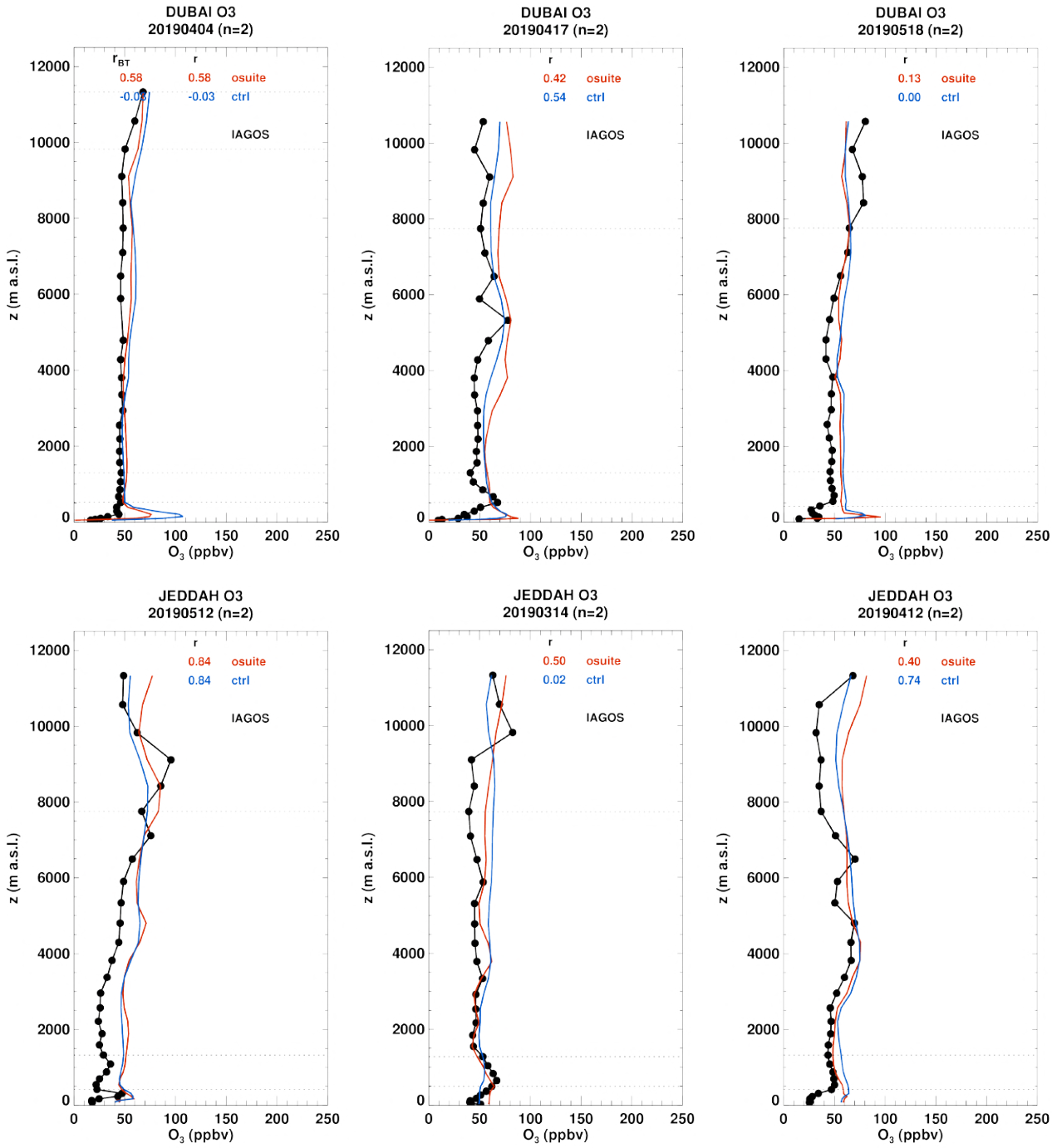

Figure 3.2.5.a Daily profile for ozone from IAGOS (black) and the two NRT runs (o-suite: red, control: blue) over the Middle East during MAM 2019.

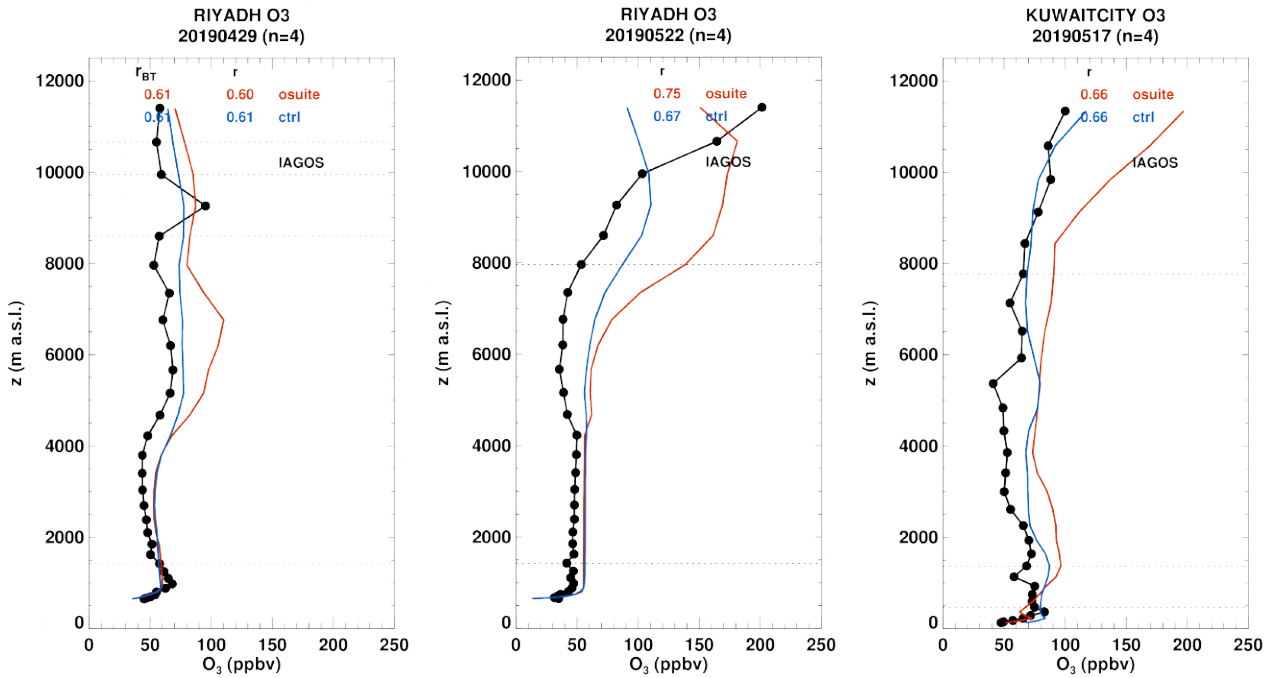

Figure 3.2.5.b Daily profile for ozone from IAGOS (black) and the two NRT runs (o-suite: red, control: blue) over the Middle East during MAM 2019.

Middle East

Several profiles are available over the Middle East at the airports of Dubai, Riyadh, Jeddah and Kuwait City (Fig. 3.2.5.a-b). For these profiles, ozone is in general below 50 ppbv in the surface and boundary layer. Both runs provide good results in the low troposphere with a rather good agreement in the boundary layer. However, some overestimations are often found near the surface. From the mid-troposphere to the UTLS ozone values are overestimated with a better agreement from control run. The small maximum of about 80 ppbv observed in the mid-troposphere are well reproduced by the models as it is the case on 12 and 17 April at Jeddah and Dubai respectively.

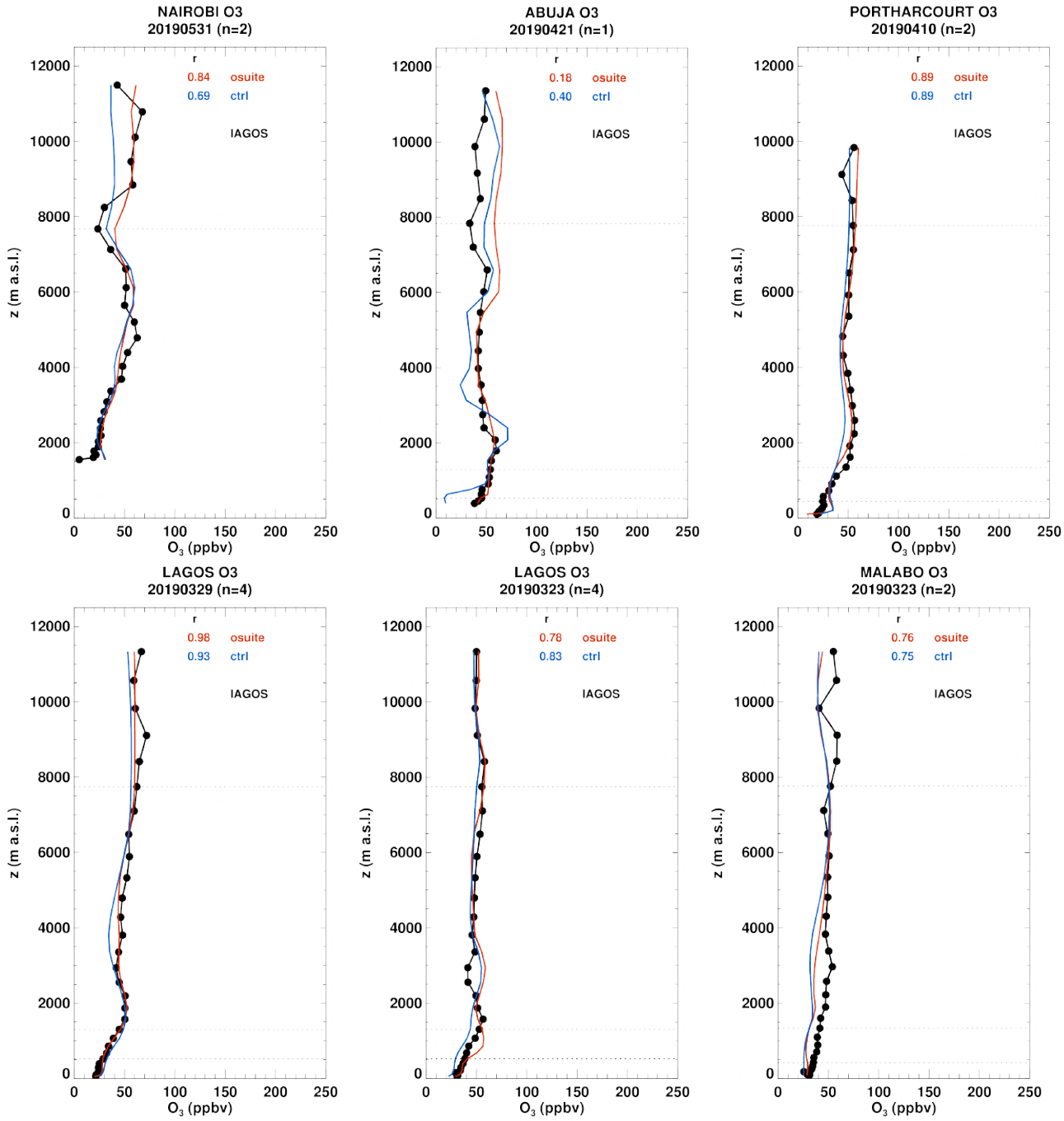

Figure 3.2.6 Daily profiles for ozone from IAGOS (black) and the two NRT runs (o-suite: red, control: blue) over West Africa during MAM 2019.

Africa

IAGOS profiles are available at Nigerian airports of Abuja and Port Harcourt, in the gulf of Guinea at Lagos and Malabo, as well as at the Kenyan airport of Nairobi (Fig. 3.2.6). Most of these profiles are nearly constant with very low ozone of about 30 ppbv in the lowest layers. The two runs present similar performance with a good agreement in the low troposphere and slightly worse performance in the UTLS for some profiles with both overestimations and underestimations depending on cases.

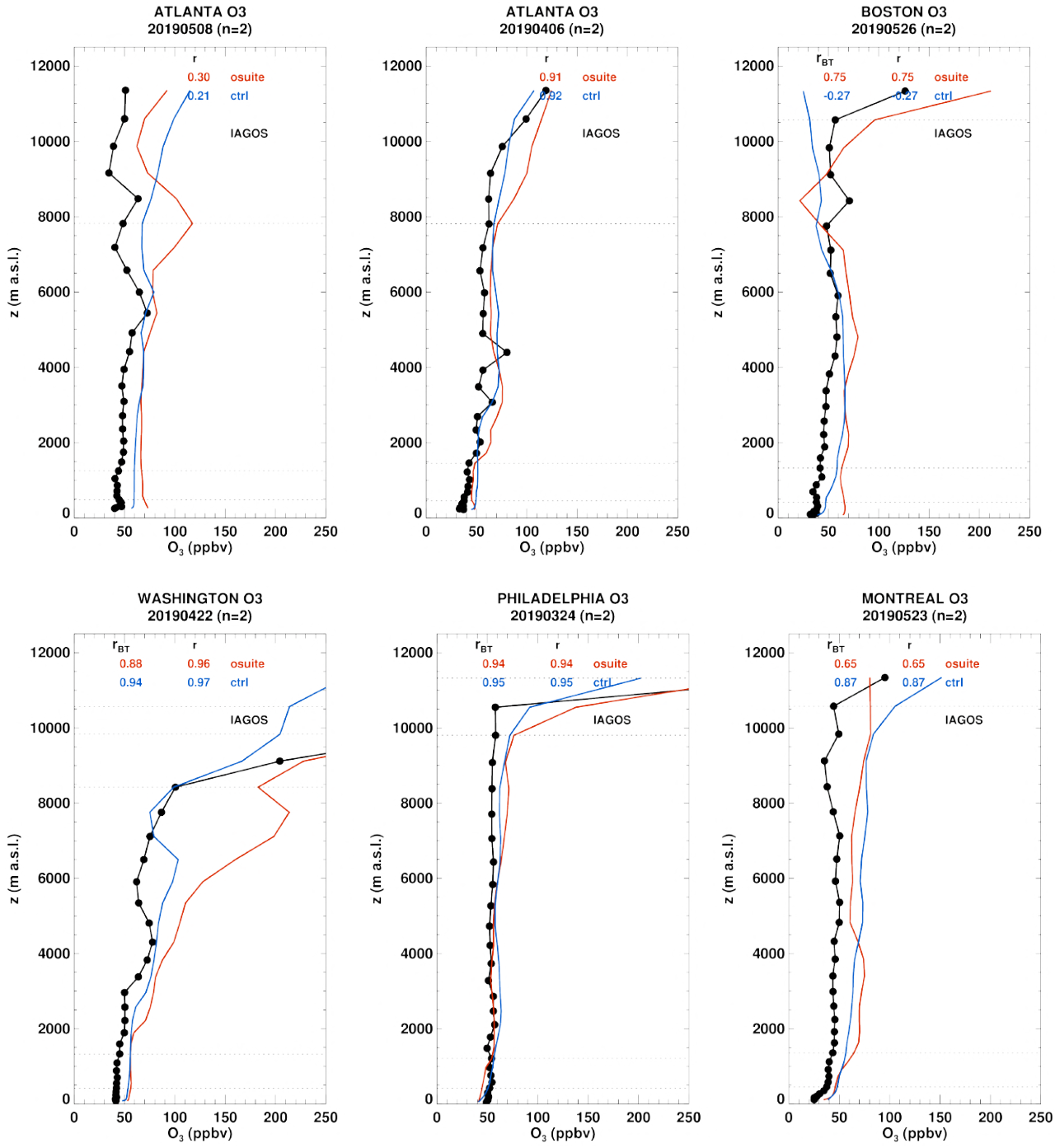

Figure 3.2.7.a Daily profiles for ozone from IAGOS (black) and the two NRT runs (o-suite: red, control: blue) over North America during MAM 2019.

North America

Many North American airports are visited during MAM 2019: Montreal, Detroit, Boston, Washington, Philadelphia, Atlanta, Dallas, San Diego and Tampa. For all profiles, ozone values are generally near or below 50 ppbv from the surface to the free troposphere (Fig. 3.2.7a-b).

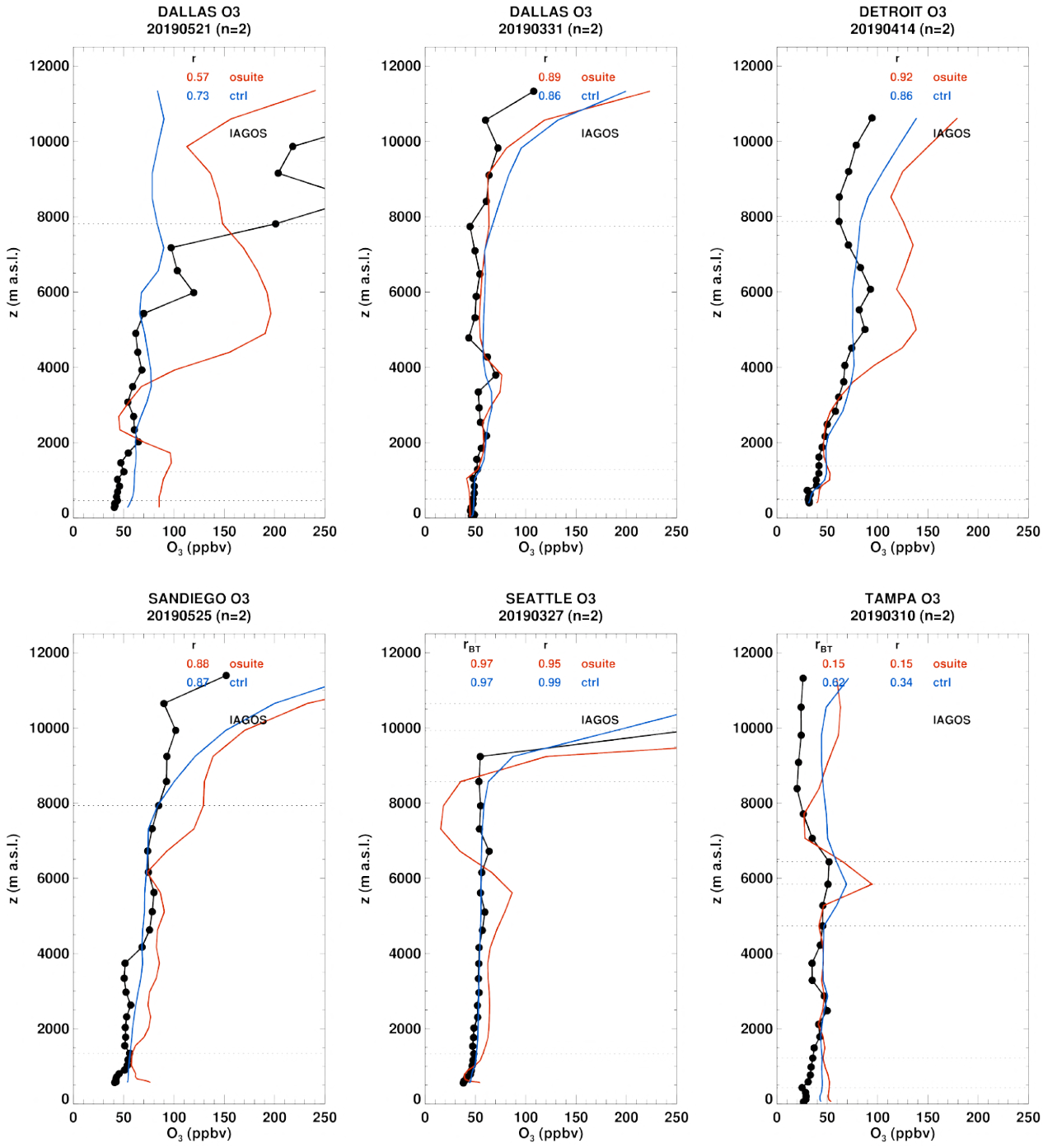

Figure 3.2.7.b Daily profiles for ozone from IAGOS (black) and the two NRT runs (o-suite: red, control: blue) over North America during MAM 2019.

Both o-suite and control overestimate ozone in the lowest layers and in the free troposphere with a slightly better performance from control run. The bias is the largest in the UTLS for both runs with slightly better performance from control run. The o-suite presents mostly overestimations in the UTLS, while both overestimations and underestimations are found for control run.

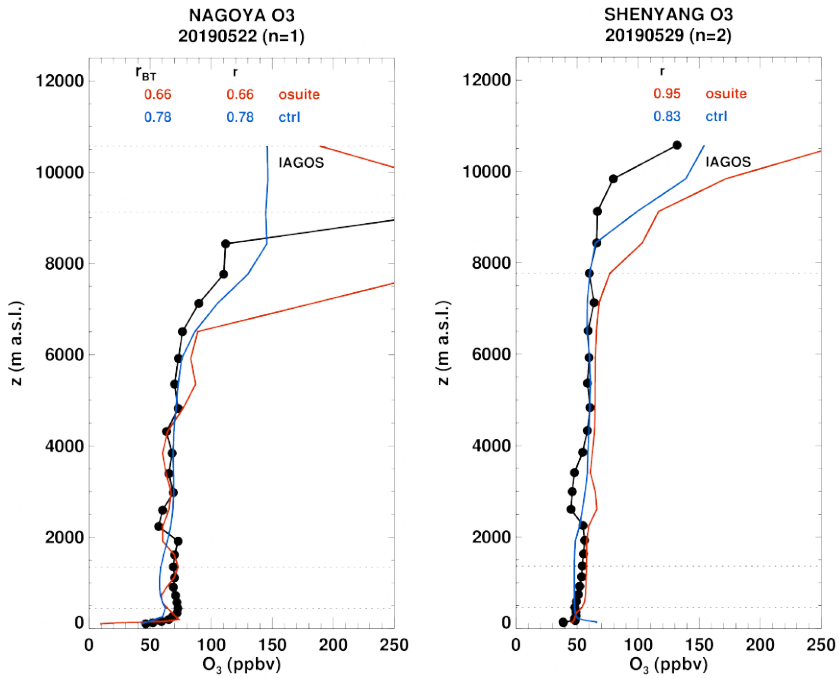

Figure 3.2.8.a Daily profiles for ozone from IAGOS (black) and the two NRT runs (o-suite: red, control: blue) over East Asia during MAM 2019.

On the profile at Tampa on 10 March, a peak in ozone is produced by the o-suite near 6000 m, which is not present so clearly neither in the observations and nor in control run results. This maximum might be related to the maximum of CO at the same altitude, which is possibly attributed to the long-range transport of forest fire plumes from Eastern Asia (see section 4.2).

East Asia

Over East Asia ozone profiles are available only at Nagoya and Shenyang and for two days on 22 and 29 May respectively. These two profiles are nearly constant up to 7000 m and both runs agree well with observations from the surface up to this altitude. At higher altitudes, the results of the models are worse and differ between the two runs with a better agreement from the control run.

3.3 Validation with GAW and ESRL-GMD surface observations

For the Near Real Time (NRT) validation, 13 GAW stations and 14 ESRL stations are currently delivering O_3 surface concentrations in NRT, and the data are compared to model results. In the following, a seasonal evaluation of model performance for the 2 NRT runs (o-suite and control) has been carried out for the period from March to May 2019. The latest validation results based on GAW stations and based on ESRL observations can be found on the CAMS website, see section 1, table 1.2.

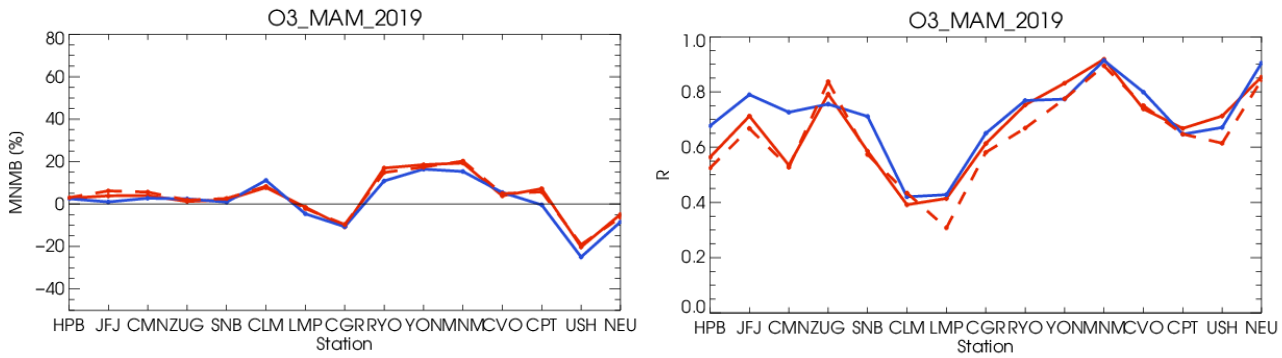

Figure 3.3.1: Modified normalized mean bias in % (left) and correlation coefficient (right) of the NRT model runs compared to observational GAW data in the period March 2019 to May 2019 (o-suite: solid red, D+2: red-dashed, and control: blue).

Modified normalized mean biases in % (left panel) and correlation coefficients (right panel) for different forecasts days (D+2, red-dashed and D+4, red- pointed) with respect to GAW and ESRL observations are shown in Figs. 3.3.1 and 3.3.2. It indicates that MNMBs for both o-suite and control run mostly remain stable up to D+4 (forecast run from 96h to 120h). Correlations between simulated and observed surface ozone values remain almost stable up to D+2 (forecast run from 48h to 72h), but then drop (correlations for D+4 are lower than correlations for D+2 and D+0), see Fig. 3.3.1 and 3.3.2, right graph).

A comparison of the seasonal-mean MNMB over Europe (Fig. 3.3.3) from December 2012 to present shows minimal MNMBs during the winter season and larger biases in other months. Also, on average the MNMB for the o-suite and control shows an improvement over the years. The temporal correlation is consistently better for the control run than for the o-suite, but the o-suite shows strong improvements recently. The GAW results are summarized in Figs 3.3.1 and 3.3.3.

Looking at different regions, for European stations (HPB, JFJ, ZUG, SNB, CMN, LMP, CLM, CGR), observed O_3 surface mixing ratios are very close to the observations. MNMBs are between -10% and 7% for the o-suite and between -10% and 11% for the control run, see Fig. 3.3.1. Correlations for European stations are between 0.39 and 0.79 for the o-suite and between 0.42 and 0.79 for the control run, see Fig. 3.3.1.

Over Point Barrow (BRW) Arctic station, due to ozone depletion events from March to May the model simulations overestimate measured concentrations, except for the few days without depletion events, where the predicted model levels are in a fair agreement with observations. This results in large positive bias ($MNMB_{o\text{-}suite}\approx30\%$, $MNMB_{control}\approx40\%$) and poor correlation coefficients ($r\approx0$ for both the o-suite and the control run). These events are related to halogen chemistry reactions that are not represented in the model simulations. On the other hand over Summit station in Greenland, due to the position of the station in the center of Greenland in elevation higher than 3000 m, depletion events are only rarely recorded and the predicted levels are generally in good agreement with the measurements ($MNMB_{o\text{-}suite}\approx10\%$, $MNMB_{control}\approx12\%$; $r_{o\text{-}suite}\approx0.70$, $r_{control}\approx0.75$)

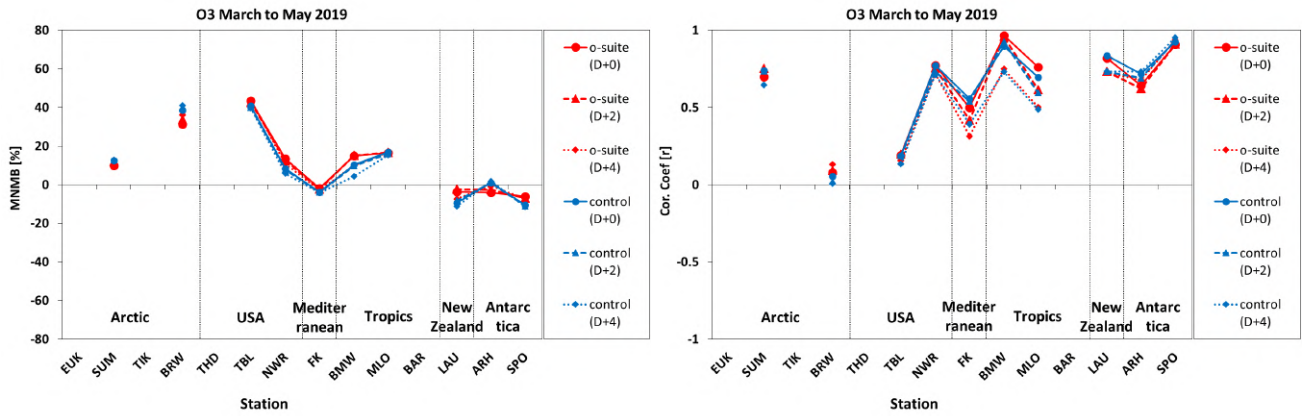

Figure 3.3.2: Modified normalized mean bias in % (left) and correlation coefficient (right) of the NRT forecast runs compared to observational ESRL data in the period March to May 2019. Circles correspond to D+0, triangles to D+2 and rhombs to D+4 metrics respectively.

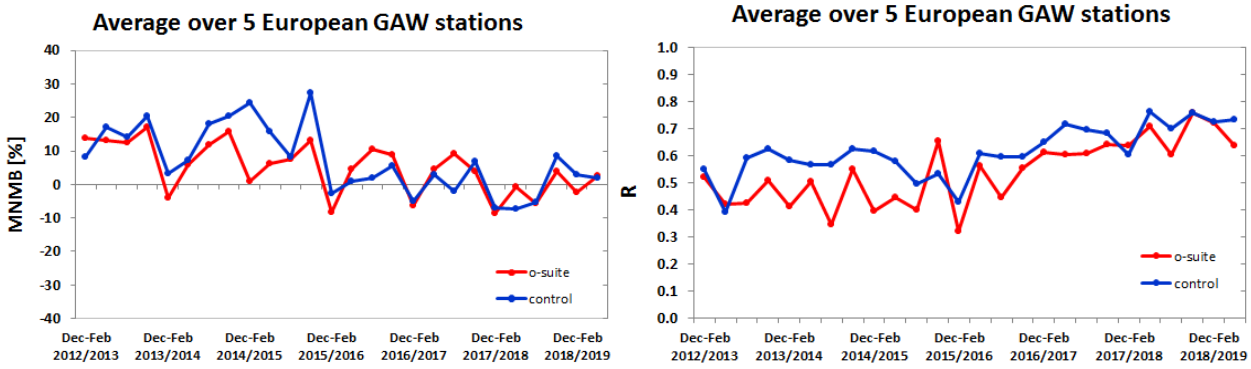

Figure 3.3.3: Long term (Dec. 2012 – May 2019) evolution of seasonal mean MNMB (left) and correlation (right), as averaged over 5 GAW stations in Europe, for o-suite (red) and control (blue).

For stations located in Asia (RYO, YON, MNM) both runs strongly overestimate O_3 mixing ratios with MNMBs between 16% and 19% for the o-suite and between 10% and 16% for the control run, see Fig 3.3.6. Correlation coefficients range between 0.76 and 0.91.

For the TBL USA station, the observed ozone mixing ratios are strongly overestimated (MNMB≈40%) by both the o-suite and the control run. Ozone mixing ratios are also overestimated over NWR by about 10%. Correlations between modelled and observed surface ozone values are weak over TBL ($r_{o\text{-}suite}=r_{control}=0.18$) and high over NWR ($r_{o\text{-}suite}=r_{control}=0.77$).

The observed ozone mixing ratios are overestimated by both runs over Bermuda (BMW) and Mauna Loa (MLO) stations in the Tropics (MNMB≈15%). Correlations between simulated and observed surface ozone are high for both the o-suite and the control run over MLO stations (r>0.7) and even higher over BMW (r>0.9).

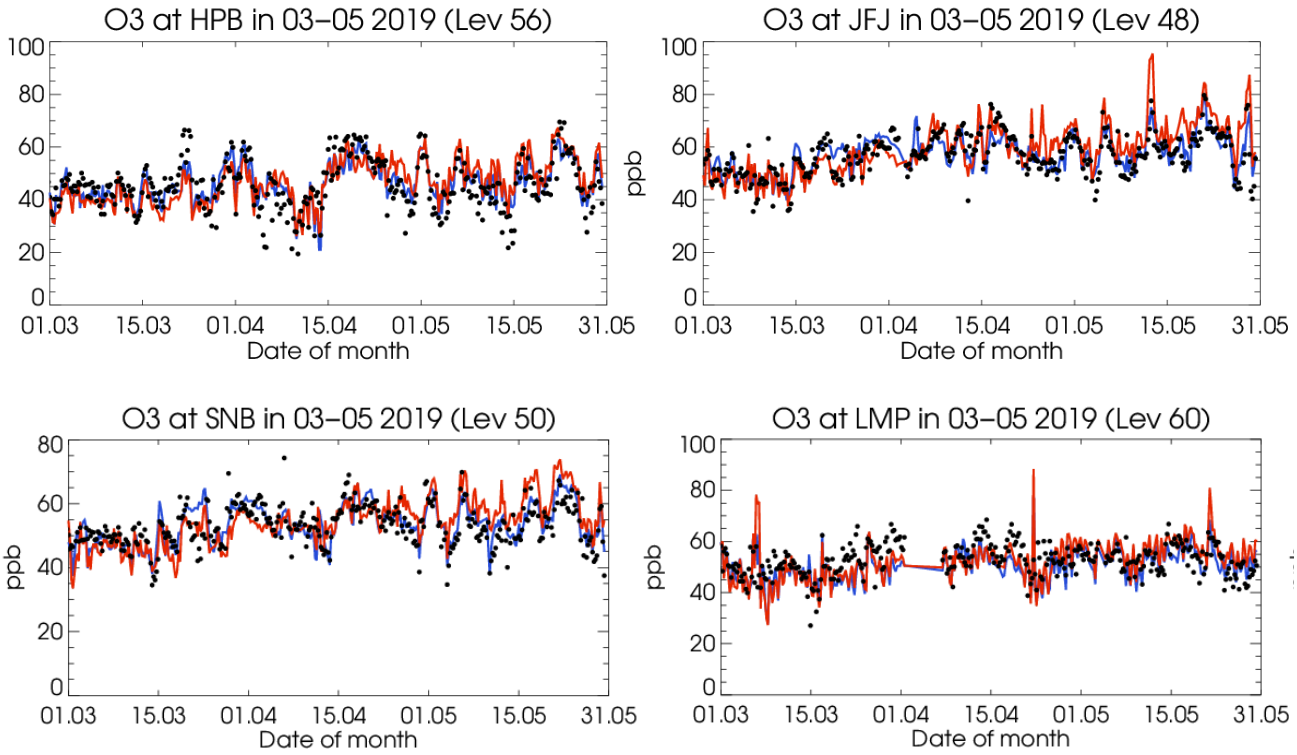

Figure 3.3.4: Time series for the o-suite (red) and control (blue) compared to GAW observations for Hohenpeissenberg (47.8°N, 11.02°E) and Jungfraujoch (46.55°N, 7.99°E) (upper panel). Sonnblick (47.05°N, 12.96°E) and Lampedusa (35.52°N, 12.63°E) (lower panel).

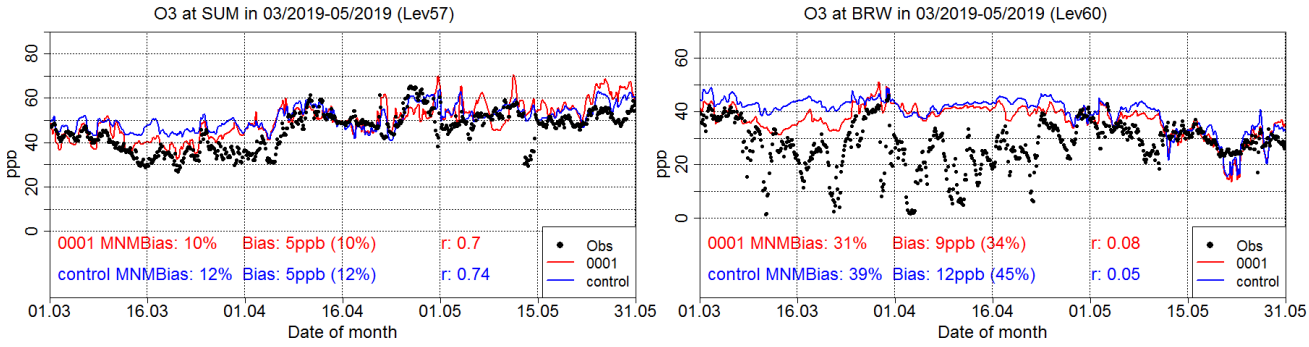

Figure 3.3.5: Time series for the o-suite (red) and control (blue) compared to ESRL observations at Summit, Greenland station (72.57°N, 38.48°W, left) and at Point Barrow, Alaska station (71.32°N, 156.51°W, right)

The O_3 mixing ratios of the southern hemispheric stations (CPT, USH) show MNMBs between 7 and -20% for the o-suite. The control run shows larger underestimations for USH up to -24%, see Fig 3.3.8. Correlation coefficients range around 0.66 and 0.71. At Lauder (LDR) station in New Zealand the o-suite underestimates O_3 mixing ratios by -4%. The control run shows larger underestimation (MNMB=-9%). Correlations between simulated and observed surface ozone values are >0.8 for both runs.

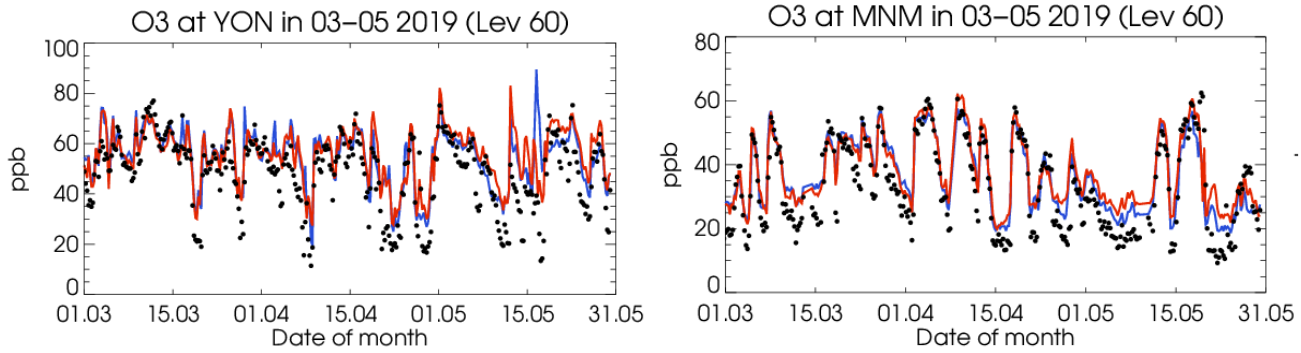

Figure 3.3.6: Time series for the o-suite (red) and control (blue) compared to GAW observations for Yonagunijima (24.47°N, 123.02°E) and Minamitorishima (24.29°N, 153.98°E).

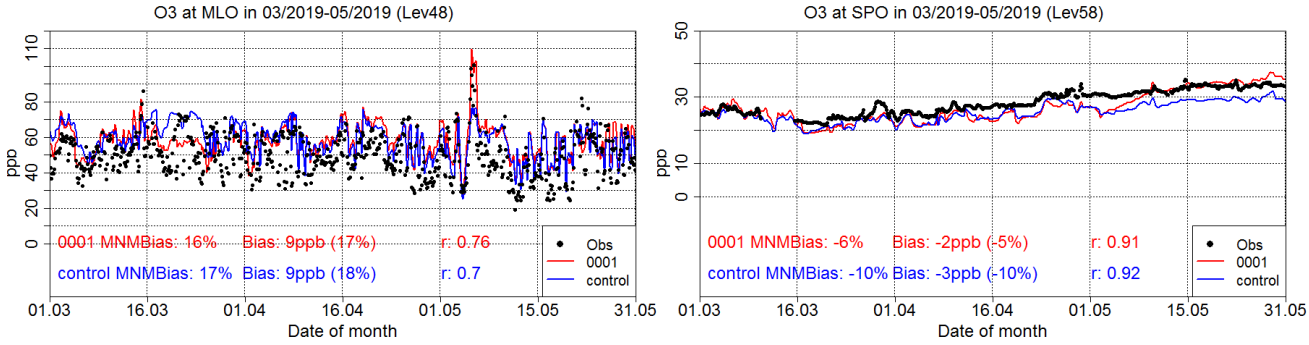

Figure 3.3.7: Time series for the o-suite (red) and control (blue) compared to ESRL observations (black dots) at Maouna Loa, Hawaii station (19.54°N, 155.58°W) and at South Pole, Antarctica station (90.00°S, 24.80°W).

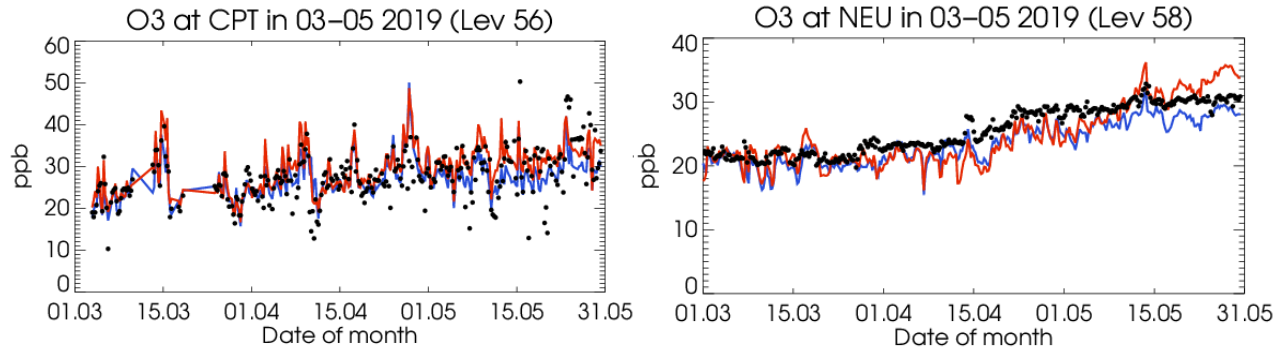

Figure 3.3.8: Time series for the o-suite (red) and control (blue) compared to GAW observations (black dots) at Cape Point (34.55°S, 18.48°W) and GAW observations at Neumayer (70.65°S, 8.25°W).

At Arrival Height (ARH) station in Antarctica the control run has almost zero bias while the o-suite underestimates O_3 mixing ratios by -4%. Finally, for South Pole station in Antarctica (SPO), the MNMB is -6% for the o-suite and -10% for the control run. Correlation coefficients are for both runs 0.7 at ARH and 0.95 at SPO.

For Neumayer station (NEU) the MNMB is -4% for the o-suite and -8% for the control run. Correlation coefficients are 0.91 for the o-suite and 0.85 for the control run, Fig. 3.3.8.

3.4 Validation with AirBase observations in Mediterranean

The surface ozone validation analysis over the Mediterranean is based on an evaluation against station observations from the Airbase Network (http://acm.eionet.europa.eu/databases/airbase/). In addition, 1 station from the Department of Labour Inspection - Ministry of Labour and Social Insurance, of Cyprus (http://www.airquality.dli.mlsi.gov.cy/) is used in the validation analysis. For the validation analysis, stations in the Mediterranean located within about 100 km from the shoreline of the Mediterranean shore are used. Table 3.4.1 shows the names, coordinates, elevation and the MNMBs and correlations obtained with the 2 forecast runs (o-suite and control). It indicates that the variance explained by each station of both the o-suite and control is high and correlations are highly significant over Western, Central and Eastern Mediterranean. It should be noted that the control run reproduces slightly better than the o-suite run the surface ozone day to day variability over almost all the Mediterranean stations (see Table 3.4.1, exception is the Agia marina Cyprus station).

In terms of biases, o-suite MNMBs vary between -15% and 20% depending on the stations over the Mediterranean shore of Spain. The Control MNMBs are on average 2.5% lower than o-suite MNMBs. Over the stations Plan Aups/Ste Baume in France the o-suite overestimate surface ozone concentrations by 8% while over Gharb station in Malta underestimate it by -8%. Again the Control MNMBs are slightly lower by about 2.5% than o-suite MNMBs. Over Finokalia station in Crete the o-suite underestimate surface ozone by -2% while the control run underestimate it by -4%. Finally over Agia Marina in Cyprus both the o-suite and the control run overestimate surface ozone values by 9.2% and 8.2% respectively.

Table 3.4.1: Coordinates, elevation, corresponding model level (level 60 is the surface level), as well as validation scores (MNMBs and correlations for the period MAM 2019) obtained with the 2 forecast runs (o-suite and control), for each one of the selected Mediterranean stations. MNMBs and correlations with blue denote stations where control run performs better while with red are denoted stations where o-suite performs better.

						Distance from the	MNMB		Cor. Coef	
Station Name	Stat_ID	Lon	Lat	Alt (m)	Level	shore (km)	o-suite	control	o-suite	control
Al Cornocales	ES1648A	-5.66	36.23	189	57	16	22.0	18.5	0.51	0.56
Caravaka	ES1882A	-1.87	38.12	1	60	73	13.8	11.2	0.52	0.64
Zarra	ES0012R	-1.10	39.08	885	56	70	0.6	-2.4	0.61	0.82
VIillar Del Arzobispo	ES1671A	-0.83	39.71	430	60	48	2.0	-0.8	0.27	0.49
Cirat	ES1689A	-0.47	40.05	466	60	37	-4.5	-6.8	0.43	0.55
Bujaraloz	ES1400A	-0.15	41.51	327	60	60	-2.7	-4.4	0.49	0.57
Morella	ES1441A	-0.09	40.64	1150	53	51	NA	NA	NA	NA
Bc-La Senia	ES1754A	0.29	40.64	428	59	21	-6.4	-8.8	0.49	0.64
Ay-Gandesa	ES1379A	0.44	41.06	368	58	15	7.8	5.5	0.49	0.69
Ak-Pardines	ES1310A	2.21	42.31	1226	57	81	15.0	12.6	0.35	0.59
Hospital Joan March	ES1827A	2.69	39.68	172	57	3	8.8	3.6	0.43	0.57
Al-Agullana	ES1201A	2.84	42.39	214	60	25	-15.4	-16.2	0.46	0.55
Av-Begur	ES1311A	3.21	41.96	200	56	9	5.5	4.0	0.30	0.47
Plan Aups/Ste Baume	FR03027	5.73	43.34	675	54	21	7.9	5.0	0.44	0.65
Gharb	MT00007	14.20	36.07	114	57	31	-8.0	-10.2	0.40	0.43
Aliartos	GR0001R	23.11	38.37	110	59	18	NA	NA	NA	NA
NEO	-	21.67	37.00	50	60	2	NA	NA	NA	NA
Finokalia	GR0002R	25.67	35.32	250	57	4	-1.9	-3.9	0.50	0.56
Agia Marina	CY0002R	33.06	35.04	532	55	14	9.2	8.2	0.84	0.80

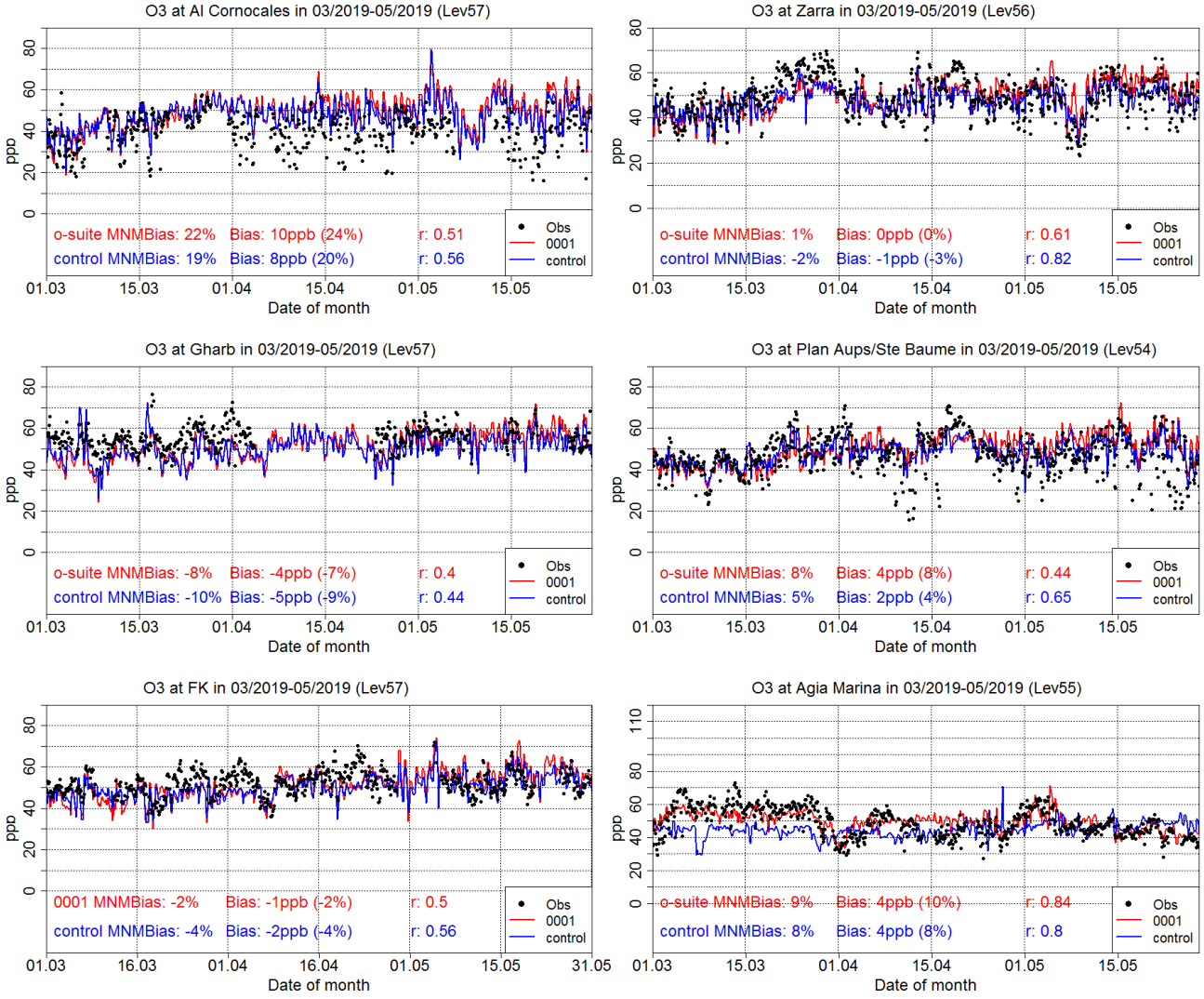

Figure 3.4.1: Time series for the o-suite (red) and Control (blue) compared to Airbase observations at Al Cornocales, Spain station (36.23°N, 5.66 °W, top left), at Zarra, Spain station (39.08°N, 1.10°W, top right), at Plan Aups/Ste Baume, France station (43.34°N, 5.73°E, center left), at Gharb, Malta station (36.07°N, 14.20°E, center right at Finokalia, Crete Greece station (35.32°N, 25.67°E, bottom left) and compared to observations provided by the Department of Labour Inspection - Ministry of Labour and Social Insurance of Cyprus) at Agia Marina, Cyprus station (35.04°N, 33.06 °E, low right).

The spatial distribution of MNMBs and the correlation coefficients of the o-suite over the Mediterranean are shown in 3.1.4.2, where it is evident that correlations over the entire Mediterranean from Gibraltar to Cyprus are highly significant. It is also evident that the CAMS NRT runs have a better performance over Central and eastern Mediterranean compared to the Mediterranean shore of Spain in terms of biases.

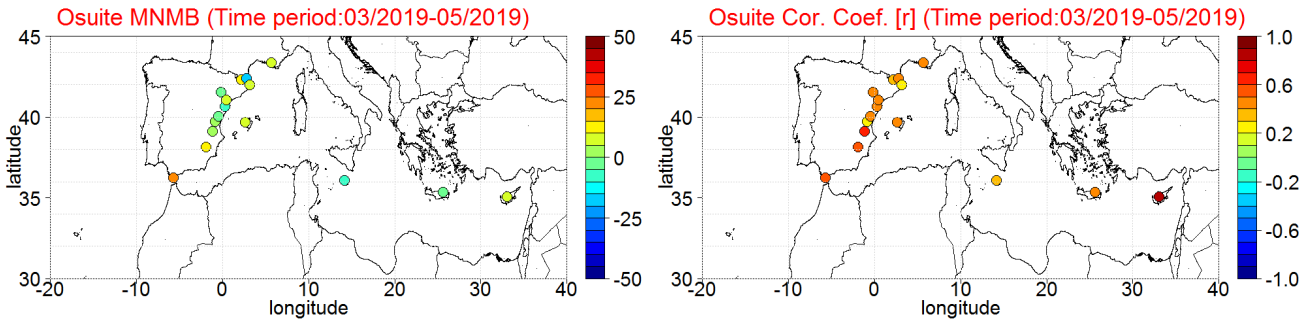

Figure 3.4.2: Spatial distribution of MNMB in % (left) and correlation coefficient (right) of the o-suite run compared to observational data during the period from 1 March 2019 to 31 May 2019.

3.5 Validation with IASOA surface observations

Model results were compared to surface O_3 observations from the Villum Research Station, Station Nord in north Greenland (81.6°N 16.7°W), Eureka, Nunavut, Canada (80.1°N 86.4°W), and Zeppelin Mountain, Svalbard (78.9°N 11.9°E) from the IASOA network (Fig. 3.5.1).

The data from Svalbard and VRS are covering the period from December 2014 to May 2019. Data from Eureka covers the period August 2016 – May 2019. The model simulations do not capture ozone depletion events in March – June in 2015 – 2019 during spring at any of the sites. These events are related to halogen chemistry reactions that are not represented in the model simulations. The simulations are on average in good agreement with the observations apart from the spring depletion events.

For the period March – May 2019 the measurements are not quality controlled. Due to the ozone depletion events the model simulations overestimate measured concentrations, except for the few days without depletion events, where the predicted model levels are in a fair agreement with observations at the sites. This results in large positive bias and low correlation coefficients for the period (Table 3.5.1). One exception from this pattern is the results from Svalbard. Due to the position of the station on a mountaintop depletion events are only rarely recorded, and the predicted levels are generally in good agreement with the measurements.

Table 3.5.1. Modified Normalised Mean Bias (MNMB) and correlation coefficient (r) of the O-suite and the Control simulations for the sites Eureka, Svalbard, and Villum Research Station (VRS) for the period March – May 2019.

		MNMB	R
Eureka	o-suite	0.84	-0.24
	control	0.92	-0.17
Svalbard	o-suite	0.07	-0.02
	control	0.18	0.43
VRS	o-suite	0.21	0.26
	control	0.28	0.40

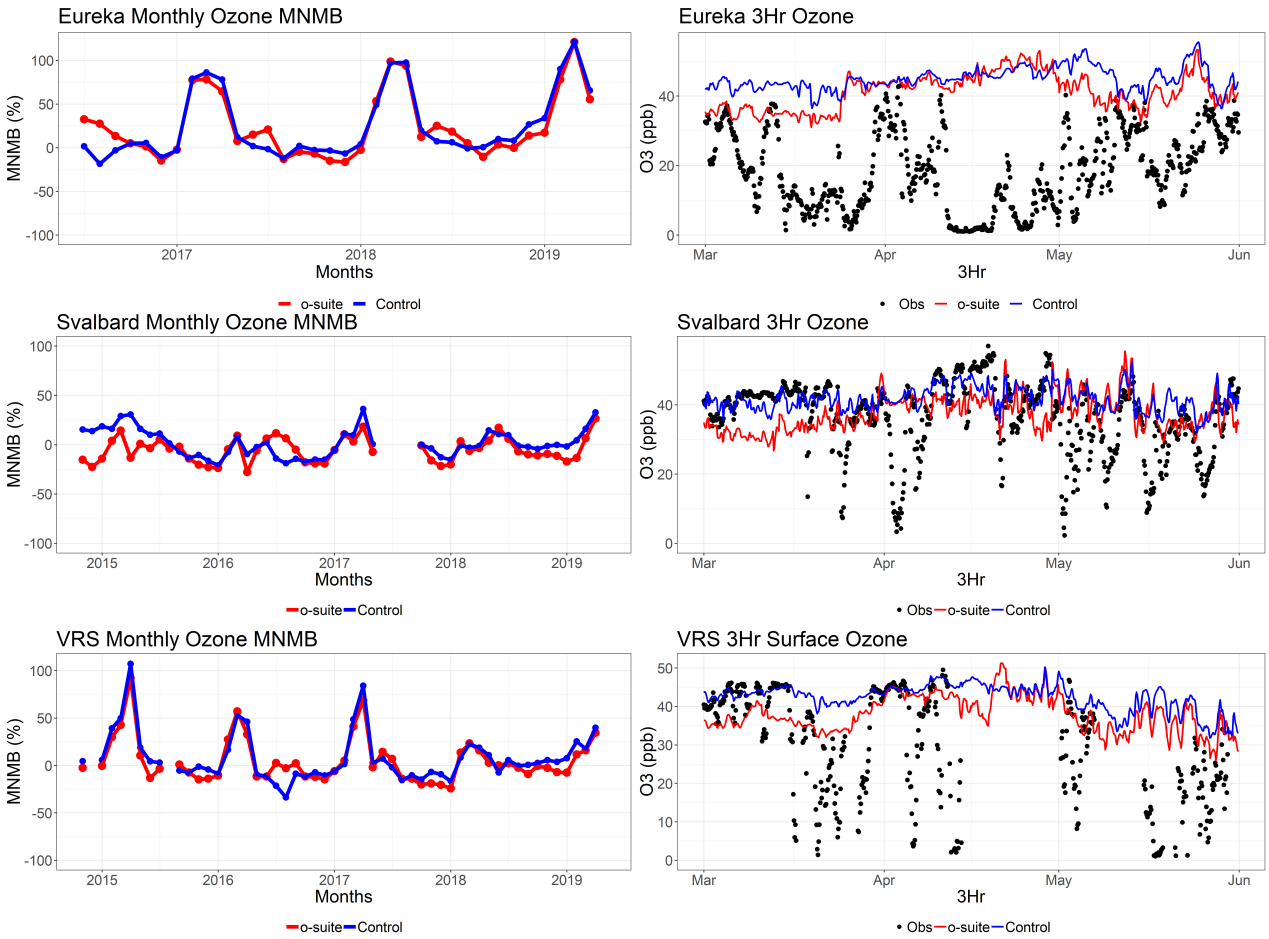

Figure 3.5.1: Time series for o-suite (red) and Control (blue) compared to observations (black dots) at Eureka, Nunavut, Canada (top row), Svalbard (middle row), and the Villum Research Station, Station Nord, Greenland (bottom row) MNMB for the full period (left) and concentrations for March-May (right).

3.6 Validation with IASI data

Ozone total columns from the o-suite and control run are compared with IASI Metop-A version v20151001 daytime only satellite observations (Clerbaux et al., 2009). For the comparison with the IASI data, the vertically integrated model O_3 data were transformed using IASI averaging kernels (Rodgers, 2000).

The global distribution of the O_3 total column obtained from IASI, as well as the relative difference between the model runs and IASI, are shown in Fig. 3.6.1 for April 2019. Satellite data shows high O_3 over the northern high- and mid-latitudes and relatively low values over the Northern Hemisphere low latitudes. The o-suite run captures the high as well as low O_3 values relatively well and is in good agreement with the observations, showing MNMBs within 5%. The control run is mainly negatively biased (up to 20% over the biomass burning area in Africa). Over the high northern latitudes, ozone is overestimated by up to 20%. The forecast day 4 is almost similar to the forecast day 0 (not shown). Note that the IASI sensitivity is the lowest over the cold surfaces of Antarctica and Greenland (especially during March-April-May season) where IASI O_3 values are positively biased by up to 20%.

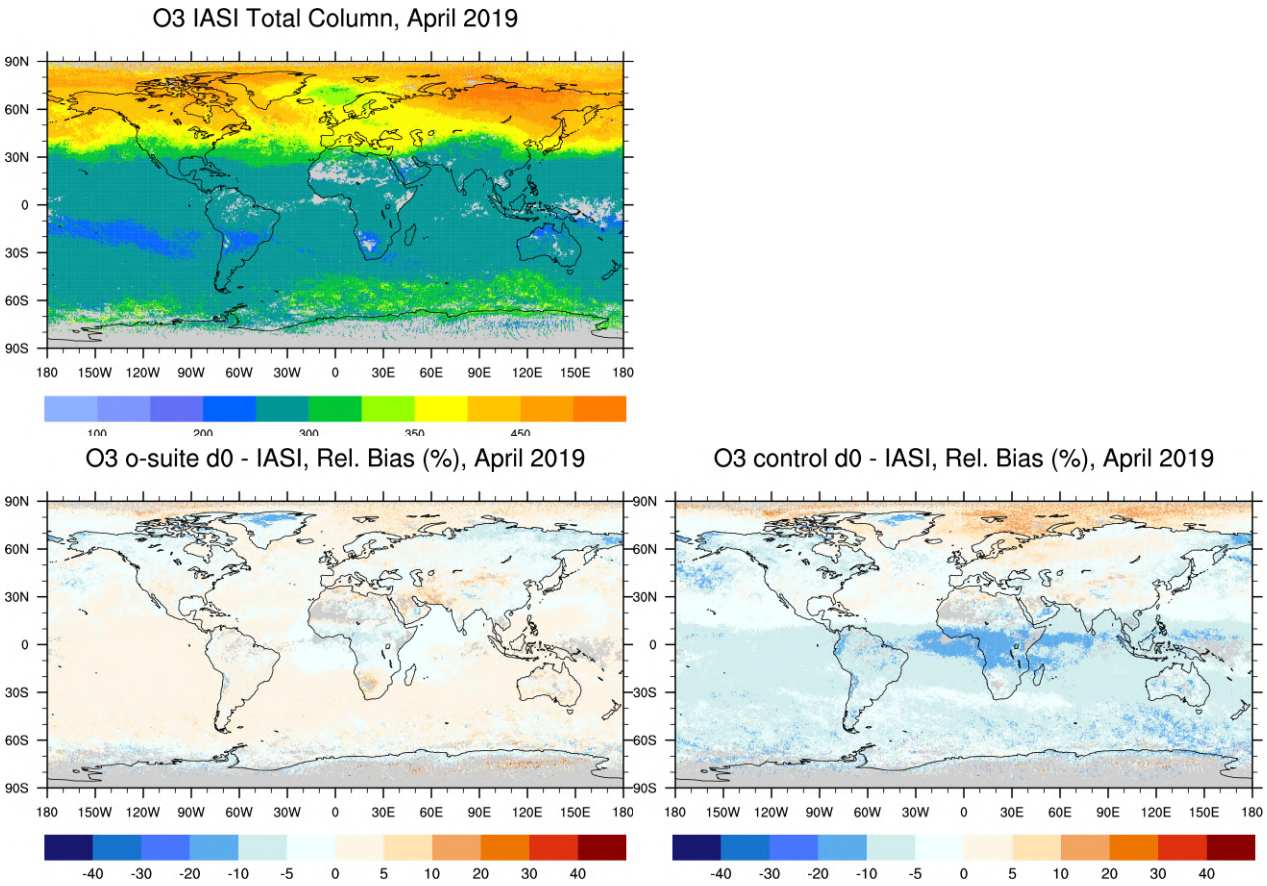

Figure 3.6.1: O_3 total column for IASI satellite observations (top) and relative difference between the model runs and IASI for April 2019: o-suite (bottom left), control run (bottom right). Grey colour indicates missing values.

4. Carbon monoxide

4.1 Validation with Global Atmosphere Watch (GAW) Surface Observations

For the Near-Real-Time (NRT) validation, 10 GAW stations have delivered CO surface mixing ratios in NRT and data is compared to model results as described in Eskes et al. (2018) and is used for CAMS model evaluation for March 2019 to May 2019. The latest validation results can be found on the CAMS website, see section 1.

For stations in the Northern Hemisphere, both runs mostly show slightly negative MNMBs. For CPT station in the Southern Hemisphere, especially the control run shows a slight positive offset.

For most stations, the MNMBs and correlation coefficients indicate that the forecast remains stable for the D+2.

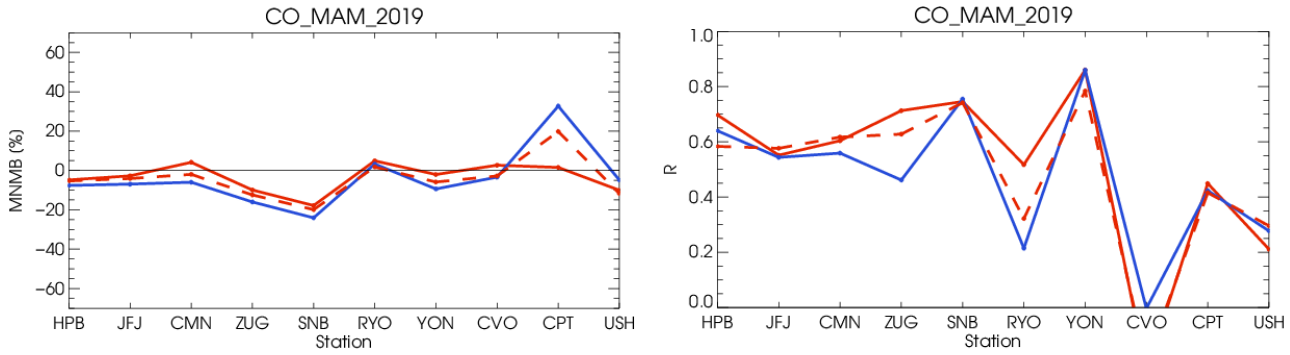

Figure 4.1.1: Modified normalized mean bias in % (left) and correlation coefficient (bottom right) of the NRT model runs compared to observational GAW data in the period March 2019 to May 2019 (o-suite: solid red, D+2: red-dashed, and control: blue).

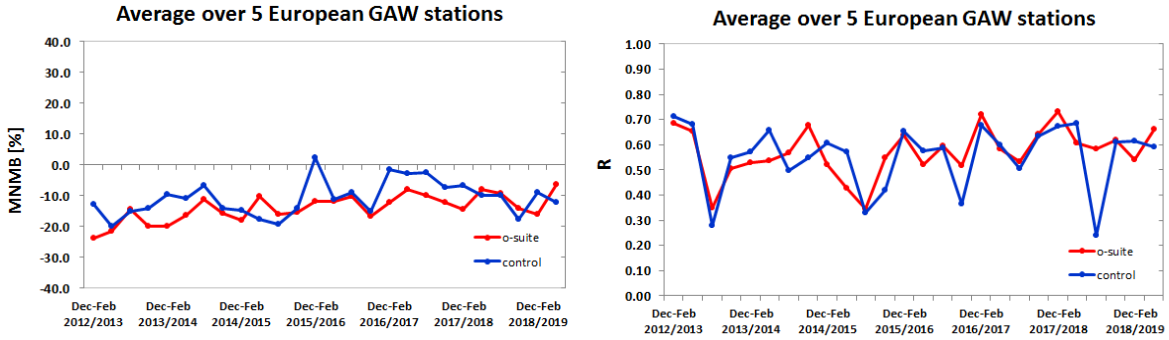

Figure 4.1.2: Long term (Dec. 2012 – May 2019) evolution of seasonal mean MNMB (left) and correlation (right), as averaged over 5 GAW stations in Europe, for o-suite (red) and control (blue).

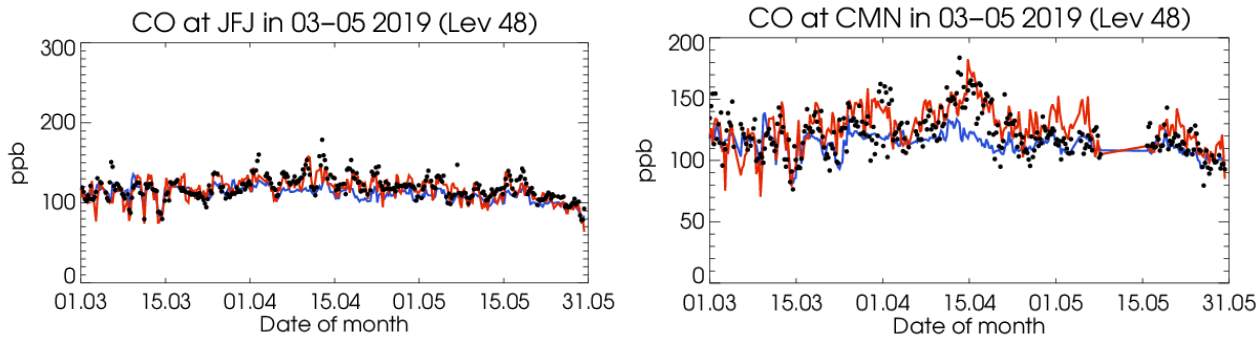

Figure 4.1.3: Time series for the o-suite (red) and control (blue) compared to GAW observations at Jungfraujoch (46.55°N, 7.99°E) and Monte Cimone (44.18°N, 10.7°E)

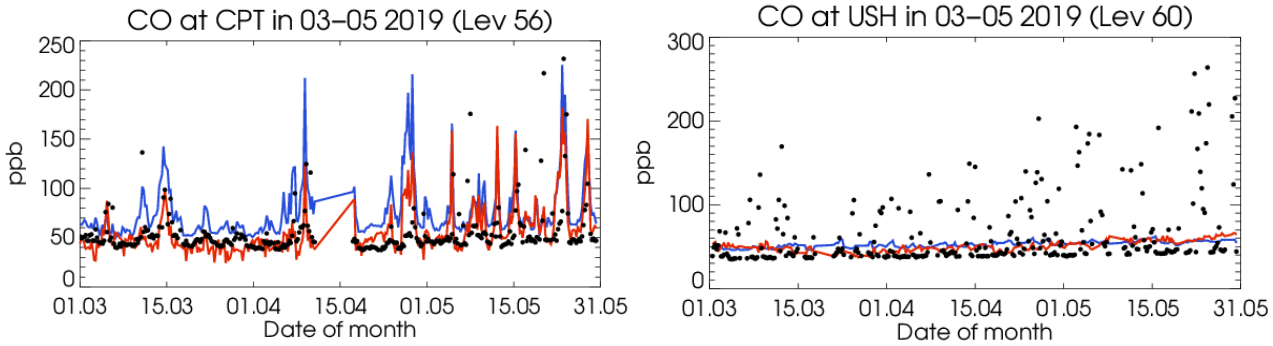

Figure 4.1.4: Time series for the o-suite (red) and control (blue) compared to GAW observations at Ushuaia (-54.85°N, -68.32°W) and Cape Point (34.35°S, 18.5°E).

A comparison of the seasonal-mean MNMB over Europe (Fig. 4.1.2) from December 2012 to present shows a slowly improving MNMB from about -20% in 2013 to about -10% for more recent periods. Temporal correlation remains relatively constant at r=0.6 on average, except for the quarter JJA in 2018, where the correlation of the control run drops to 0.24.

For European stations, the o-suite shows an underestimation of observed CO mixing ratios, with MNMBs between 4% and -17%. The control shows slightly higher MNMBs between -5% and -24%. Around mid-April there is an episode, where the control run does not capture larger CO mixing ratios, while the o-suite remains close to the observations (Fig. 4.1.3. right). Data assimilation thus clearly improves the results here.

Correlation coefficients are between 0.55 and 0.74 for the o-suite and between 0.46 and 0.75 for the control run.

For the two stations in the Southern Mid-latitudes (CPT and USH) the control partly shows an overestimation of CO with and (control) with MNMBs up to 32%, (Fig.4.1.4.) MNMBs of the o-suite are smaller amounting between 3% and -10%.

For stations in Asia (RYO, YON) both runs mostly show a good correspondence with the observations with MNMBs between 4 and -9%, see Fig. 4.1.5. For Ryo station, several positive peaks in the model do not correspond to the observations. Correlation coefficients are better for the o-suite (RYO 0.51, YON 0.86) than for the control run (RYO 0.21, YON 0.85).

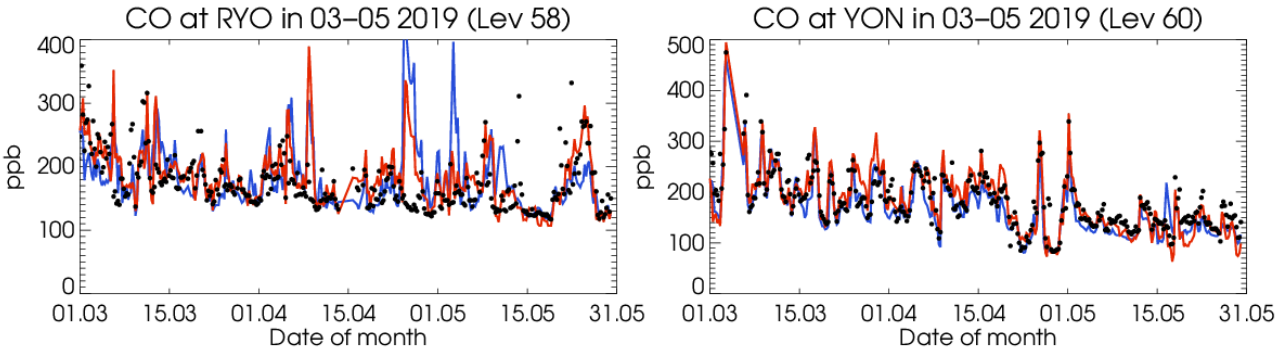

Figure 4.1.5: Time series for the o-suite (red) and control (blue) compared to GAW observations for Ryori (39.03°N, 141.82°E)and Yonagunijima (24.47°N, 132.02°E)

4.2 Validation with IAGOS Data

Like for ozone, time series of CO are only available at Frankfurt during MAM 2019 (Fig. 4.2.1 and 4.2.2). CO is mostly underestimated by both o-suite and associated control run and the largest bias is found in the lowest layers. While the performances of the two runs are similar in the lowest layers, the o-suite performs slightly better than control run in the free troposphere.

Around 22 March a peak in CO is observed in the surface layer as shown on the time series at Frankfurt (Fig. 4.2.1). The individual profiles around this date are presented in Fig. 4.2.2.a. The mixing ratio of CO reaches a value slightly above 300 ppbv in the surface layer on day 23 (Fig. 4.2.1 and 4.2.2.a). On the profiles of day 21 and 24, surface values are lower with about 200 ppbv and CO values are almost constant between the surface and the boundary layer. An increase is detected by both runs although it is very weak as shown on the time series. On the profiles of the 21 and 24 April the shape of the profiles from the model present an increase in the boundary layer but the magnitude of this increase is much smaller than for observations, with the largest underestimations in the surface layer (Fig. 4.2.2.a). The performances of the models are very similar for all the profiles during this episode.

Another increase in CO is observed in the low troposphere at the beginning of the second week of April (Fig. 4.2.1 and 4.2.2.b). On the profiles, the maximum value in the surface layer is found on 9 April with nearly 300 ppbv and in the boundary layer on 10 April with 200 ppbv (Fig. 4.2.2.b). On day 10, this CO mixing ratio is almost constant from the surface up to 4000 m. For the three days of this episode 7, 8 an 9 April, the profiles from the models are nearly constant. Both models do not reproduce the increase although the bias is slightly smaller for the o-suite than for control run.

On day 14 of April, a maximum of CO is observed between 5500 m and 7500 m, with about 180 ppbv near 6000 m. According to satellite images (https://worldview.earthdata.nasa.gov), this maximum is probably due to the long range transport of pollution from forest fires in China which occured at the beginning of April in the Sichuan province, but still has to be confirmed. This maximum is not reproduced at all by the two runs.

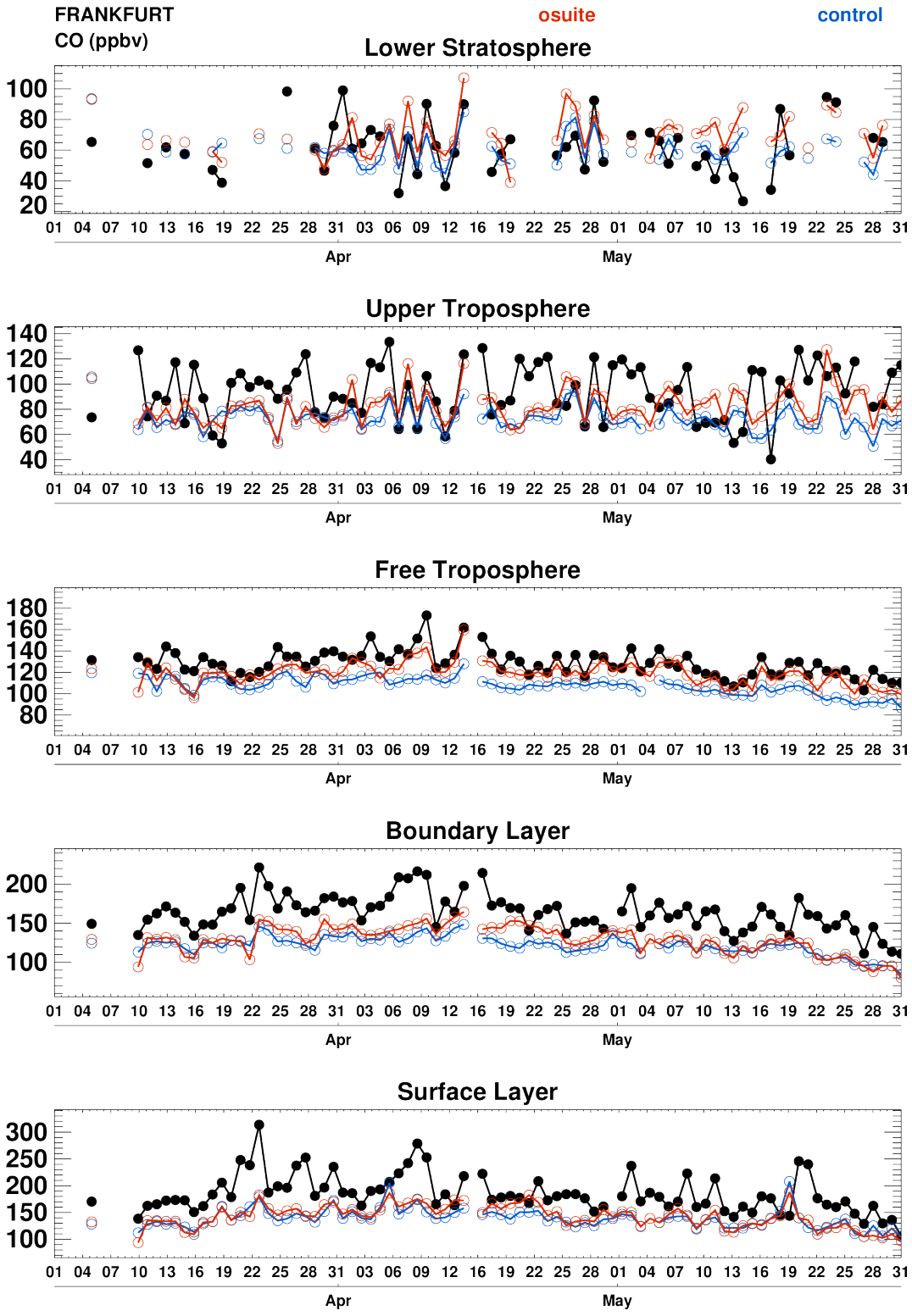

Figure 4.2.1 Time series of daily mean CO over Frankfurt during MAM 2019 for 5 layers: Surface Layer, Boundary Layer, Free Troposphere, Upper Troposphere and Lower Stratosphere. The o-suite is shown in red and associated control run in blue.

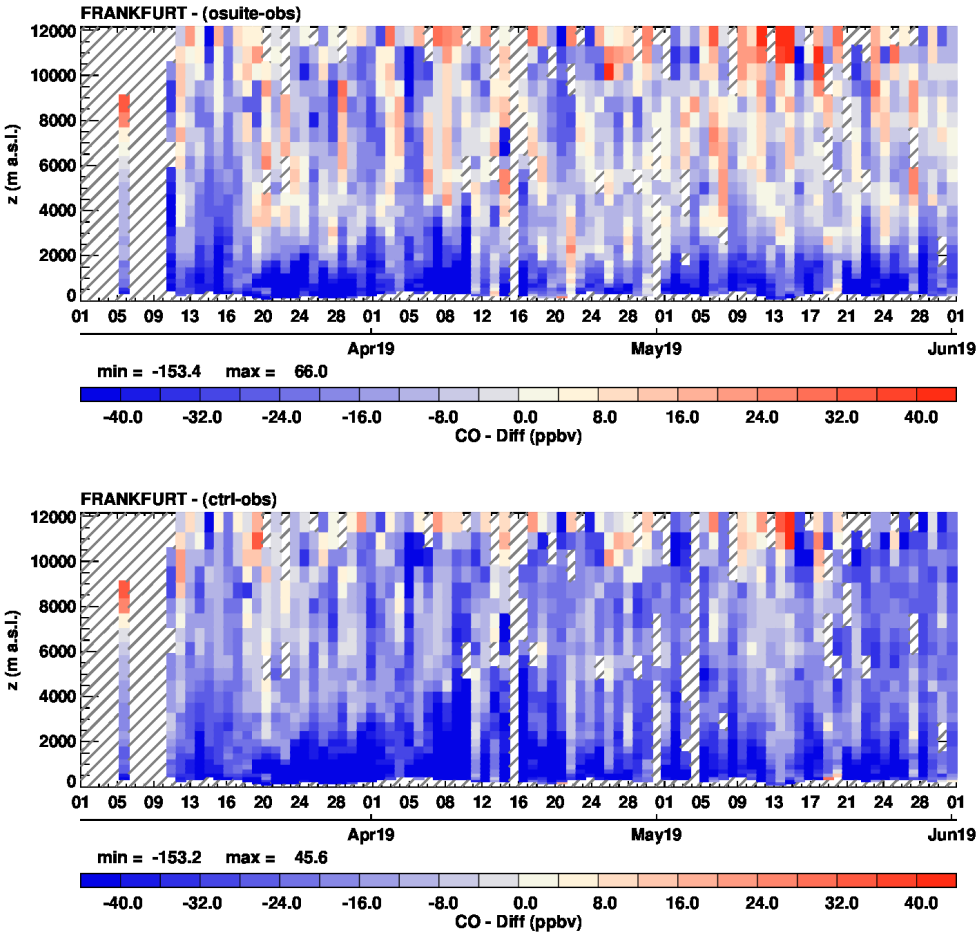

Figure 4.2.2 Time series of the absolute differences (model - observations) in daily profiles for CO over Frankfurt during MAM 2019. Left panel correspond to o-suite and right panel to control run.

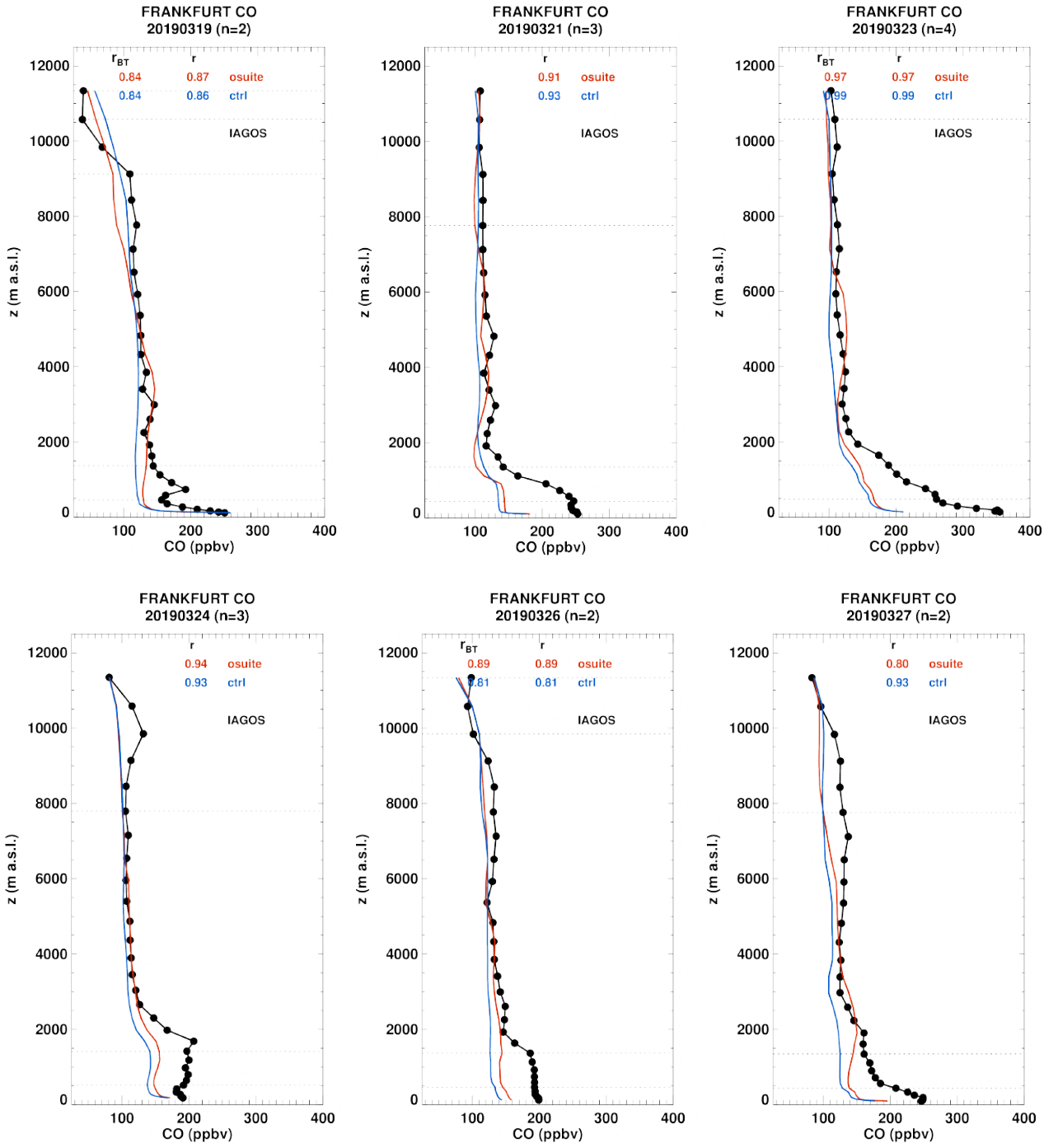

Figure 4.2.3.a Daily profile for CO from IAGOS (black) and the two NRT runs (o-suite: red, control: blue) over the Europe during MAM 2019.

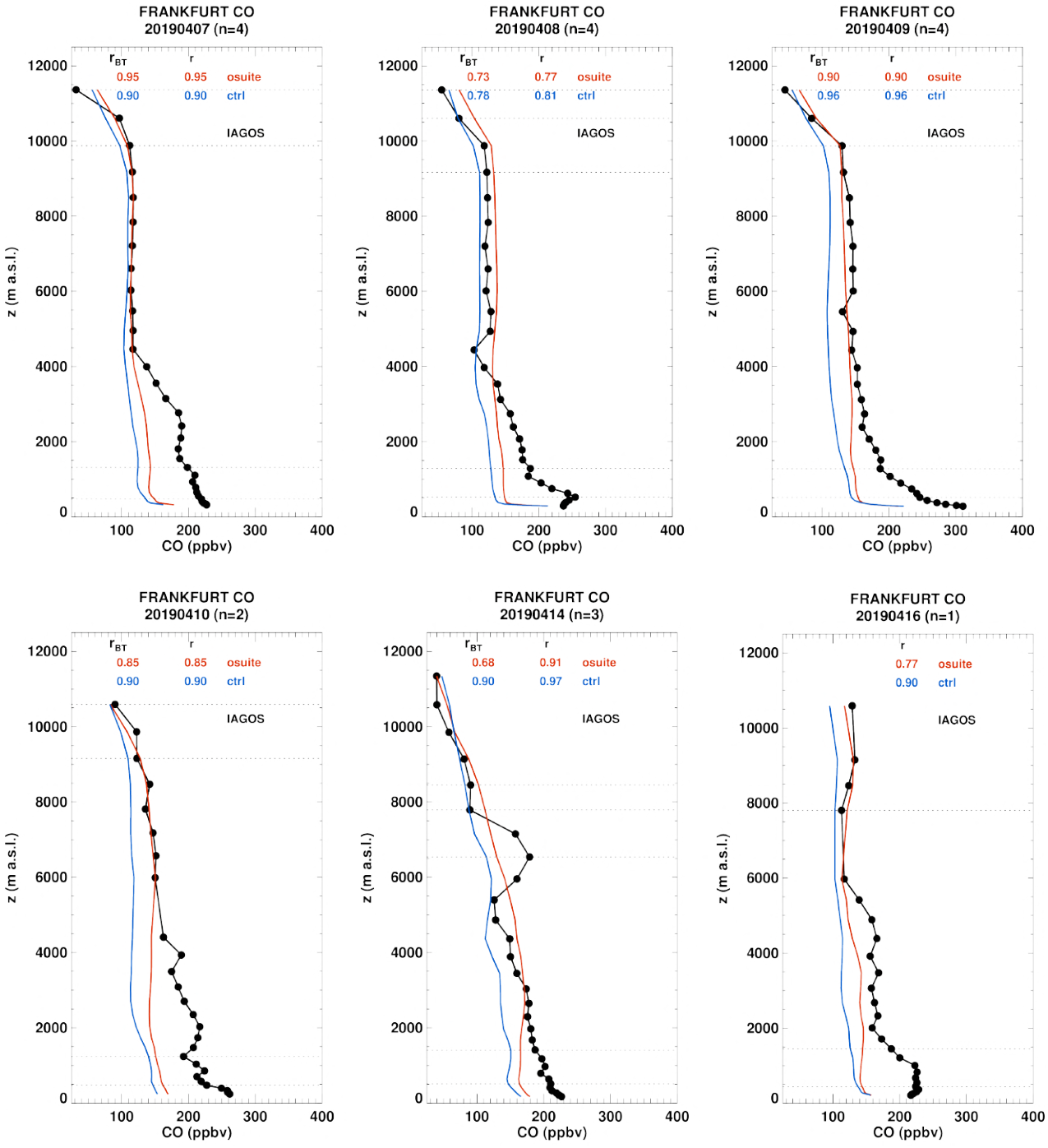

Figure 4.2.3.b Daily profile for CO from IAGOS (black) and the two NRT runs (o-suite: red, control: blue) over the Europe during MAM 2019.

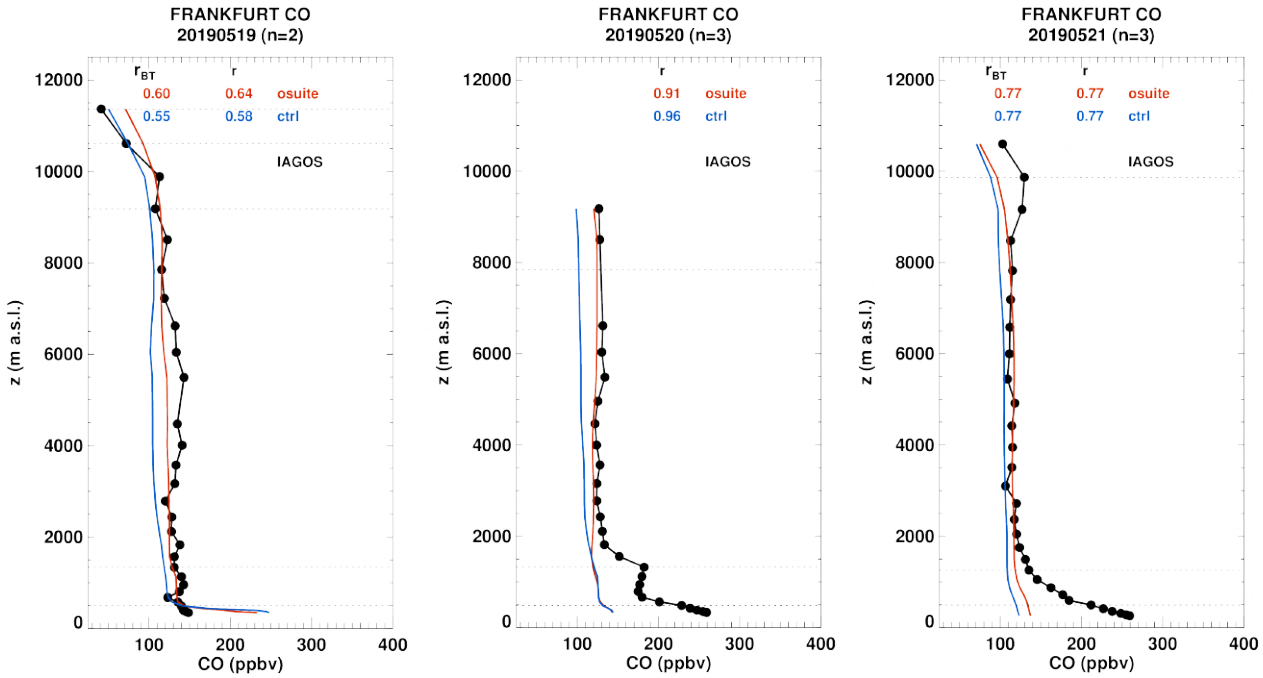

Figure 4.2.3.c Daily profile for CO from IAGOS (black) and the two NRT runs (o-suite: red, control: blue) over the Europe during MAM 2019.

Around 20 May, an increase is observed by IAGOS in the surface layer as shown on the time series and individual profiles (Fig. 4.2.1 and 4.2.3.c). This increase is not reproduced by the models in the profiles of the related days 20 an 21 April. However, from the time series it seems that this increase is detected by the models earlier as shown by the peak found for both o-suite and control run on day 19 (Fig. 4.2.1). This is also confirmed by the individual profile of day 19 which indeed shows that model mixing ratios are larger than those of observations near the surface (Fig. 4.2.3.c).

Middle East

Like for ozone, several profiles are available over the Middle East at the airports of Dubai, Riyadh, Jeddah and Kuwait City (Fig. 4.2.4). High mixing ratios of CO reaching 400 ppbv in the surface layer are observed for some profiles. These values are well reproduced by the models behaving similarly. It is the case at Dubai on day 4 and 5 April as well as at Kuwait City on 3 April. Most profiles are nearly constant from the boundary layer to the UTLS with CO values of about 100 ppbv. Both runs are closed to observations for these layers as well. The only profile which presents a maximum of CO in the free troposphere is that at Jeddah on 14 March. This maximum of CO reaching nearly 150 ppbv is well detected and slightly underestimated by the o-suite, whereas the profile from control run remains constant.

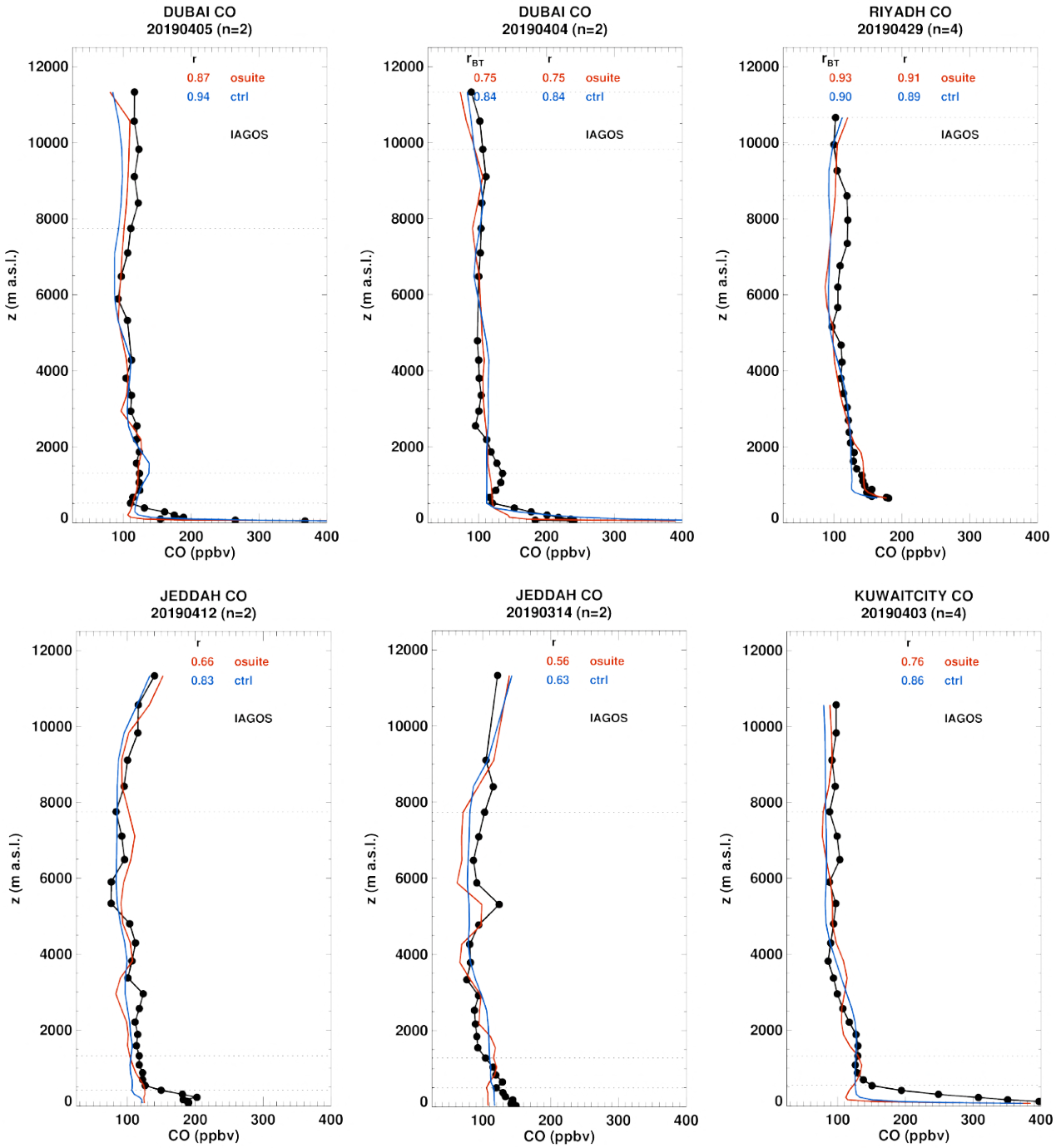

Figure 4.2.4 Daily profile for CO from IAGOS (black) and the two NRT runs (o-suite: red, control: blue) over the Middle East during MAM 2019.

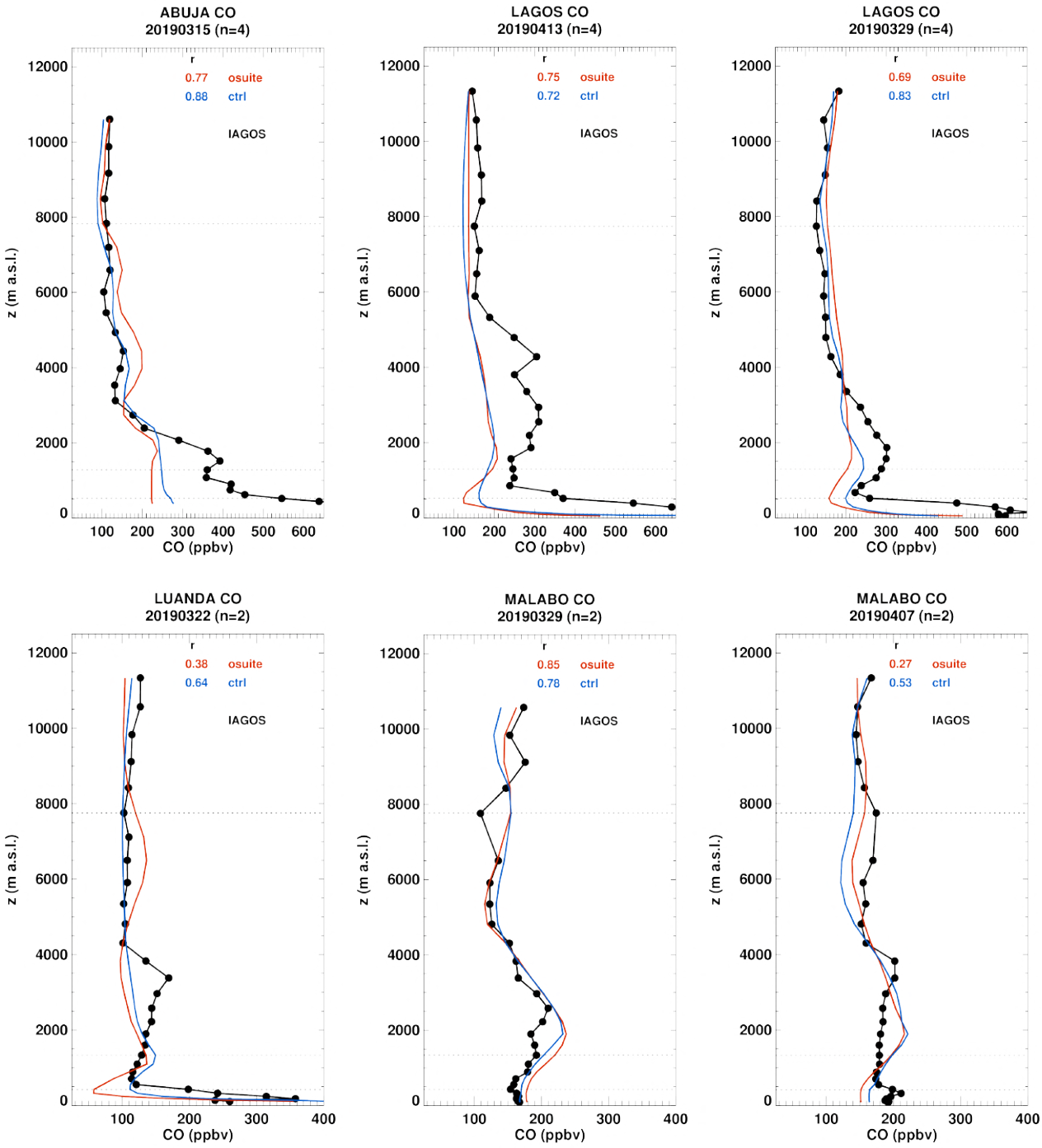

Figure 4.2.5.a Daily profile for CO from IAGOS (black) and the two NRT runs (o-suite: red, control: blue) over Western Africa during MAM 2019.

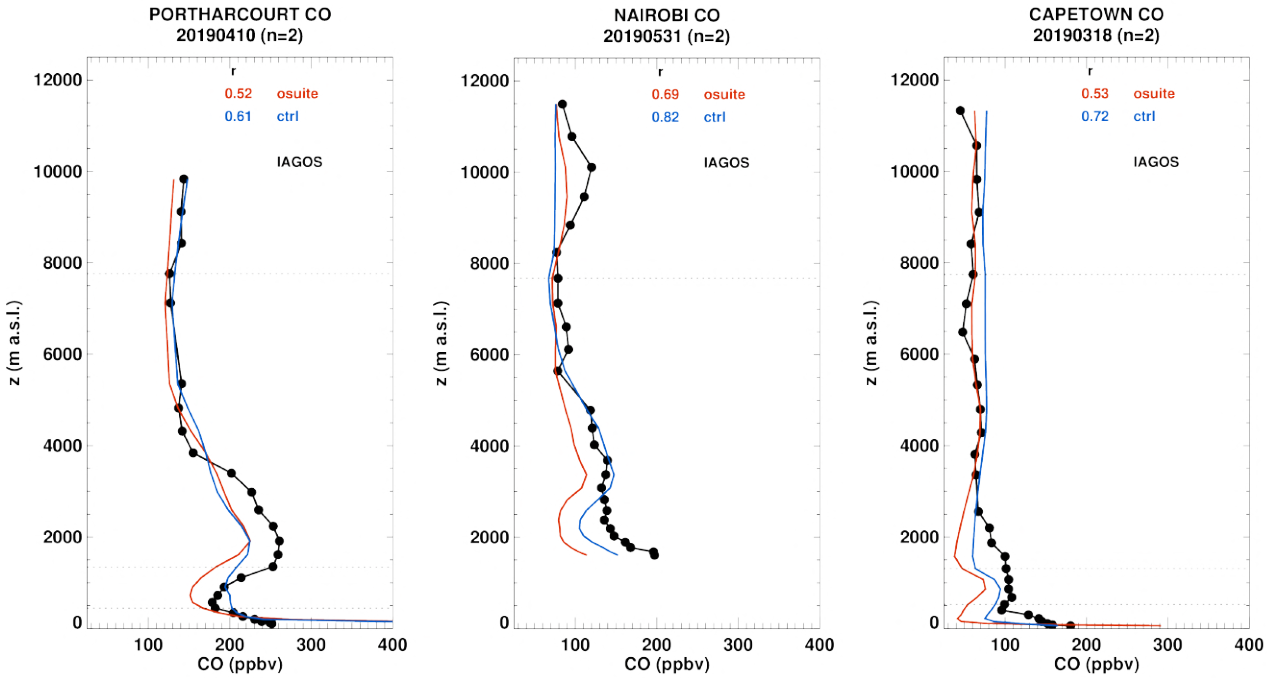

Figure 4.2.5.b Daily profile for CO from IAGOS (black) and the two NRT runs (o-suite: red, control: blue) over Western Africa during MAM 2019.

Africa

During MAM 2019, CO profiles are available over different regions of Africa (Fig. 4.5.a-b). over Western Africa as for previous reports (Lagos, Malabo, Luanda) but also over Eastern Africa (Nairobi) and South Africa (Cape Town). High mixing ratios of CO near the surface above 600 ppbv are in general well reproduced by the models (Lagos 29 March and 13 April, Luanda 22 March) except in the case of Abuja on 15 March. At Nairobi and Cape Town surface values near 200 ppbv are overestimated by the models while the same magnitude is well represented by the models at Malabo. In the boundary layer to the mid-troposphere CO is often underestimated at all locations with similar results from the two runs. However, the shape of the profiles with the occurrences of maxima in the mid-troposphere, are well reproduced by the models (Lagos 29 March and 13 April, Luanda 22 March, Malabo 29 March). The best agreement is found in the UTLS for both o-suite and control run at all locations.

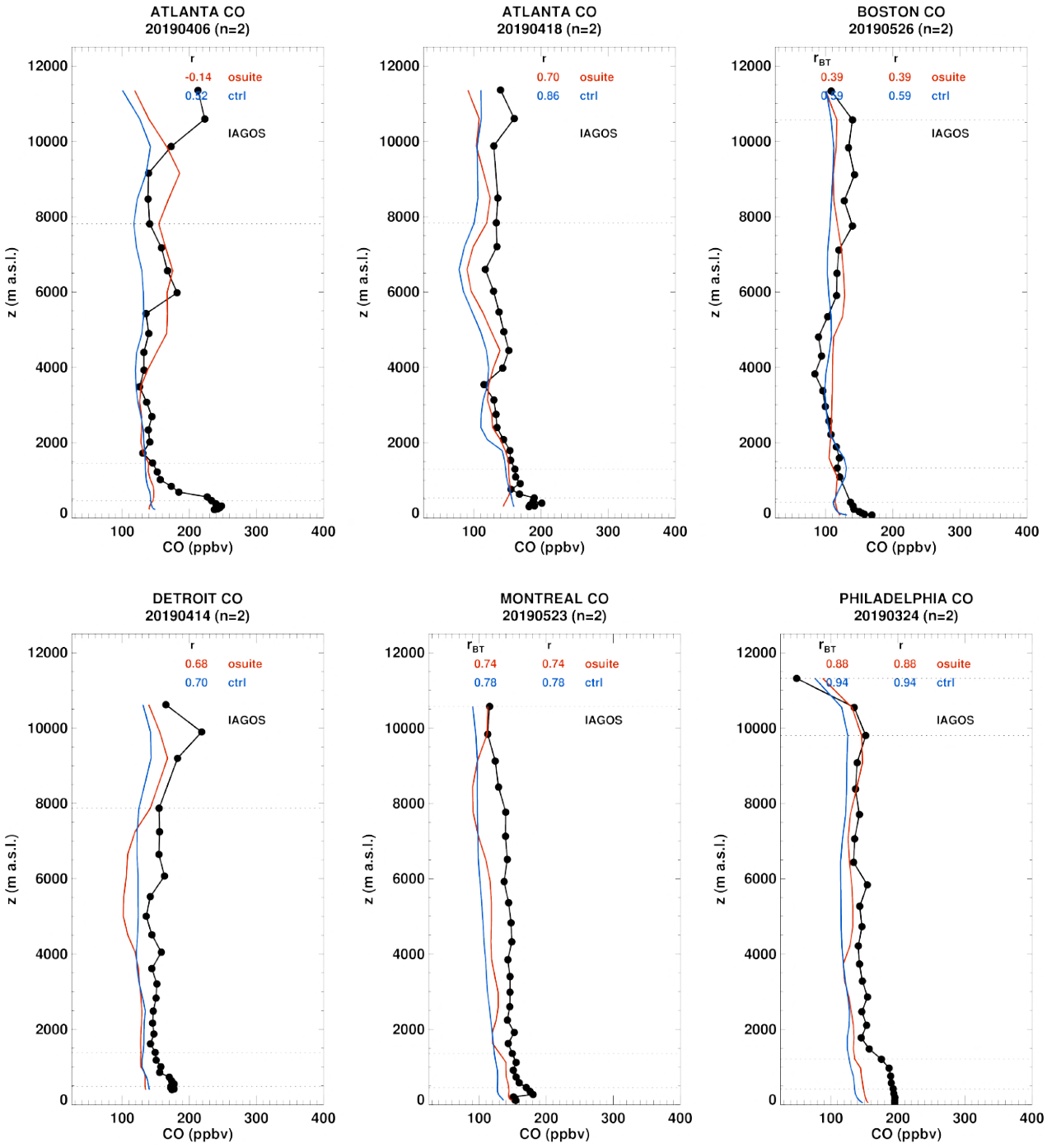

Figure 4.2.6.a Daily profile for CO from IAGOS (black) and the two NRT runs (o-suite: red, control: blue) over North America during MAM 2019.

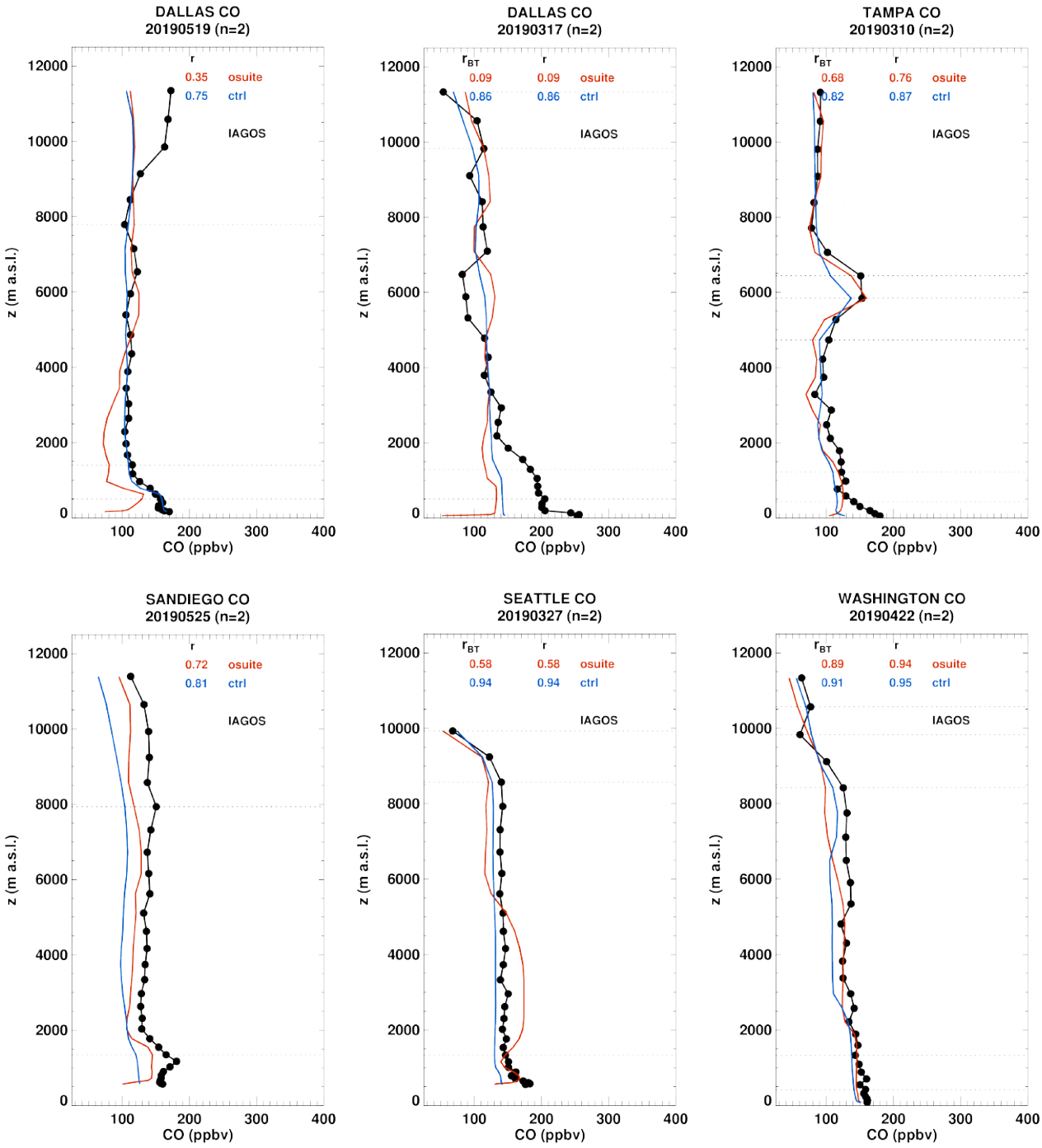

Figure 4.2.6.b Daily profile for CO from IAGOS (black) and the two NRT runs (o-suite: red, control: blue) over North America during MAM 2019.

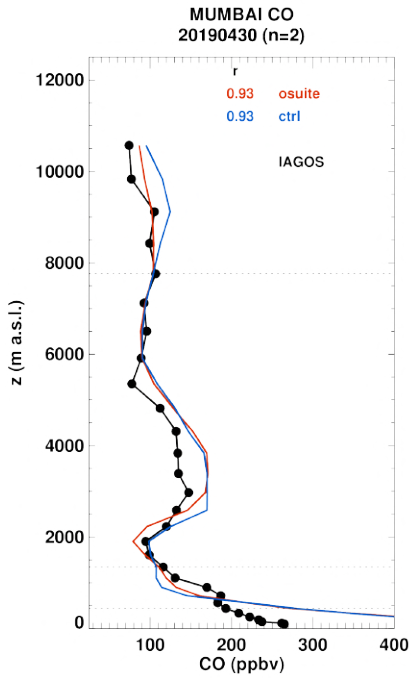

Figure 4.2.7 Daily profile for CO from IAGOS (black) and the two NRT runs (o-suite: red, control: blue) over India during MAM 2019.

North America

Like for ozone, CO profiles are available at many different locations over North America (Fig. 4.2.6.a-b). For all locations values in the surface layer are close to 200 ppbv in all examples of Fig. 4.2.6.a-b, and the models in general agree well with observations or present some underestimations. In most cases the o-suite and control run behave similarly in the surface and boundary layers but sometimes the performances can be slightly different such as at Dallas on 19 May or at San Diego on 25 May where the control runprovides slightly better results in the first case, and conversely the best performance is from the o-suite in the second case. At Tampa on 10 March a sharp peak of CO is observed near 6000 m with a value of about 150 ppbv. According to satellite images (https://worldview.earthdata.nasa.gov), this peak of CO is likely related to the transport of plumes from forest fires in Eastern Asia. As shown before, the profile of ozone at Tampa on the same day is also showing although not so clearly a small maximum at the same altitude which is more pronounced for the o-suite as compared to observations (see section 3.2). The agreement with the models is very good for this profile, although the performance from the o-suite is slightly better than that control run.

India

Over India only one daily profile of CO is available at Mumbai on 30 April (Fig. 4.2.7). This profile presents surface mixing ratio of CO of about 270 ppbv and a maximum of CO between 3000 and 5000 m altitude with values reaching 150 ppbv. The shape of the profile is well reproduced by the models which behave similarly. With the exception of the large overestimations in the surface layer, the models provide values close to observations from the boundary layer to the UTLS, with small overestimations in the range of altitudes where the maximum is found.

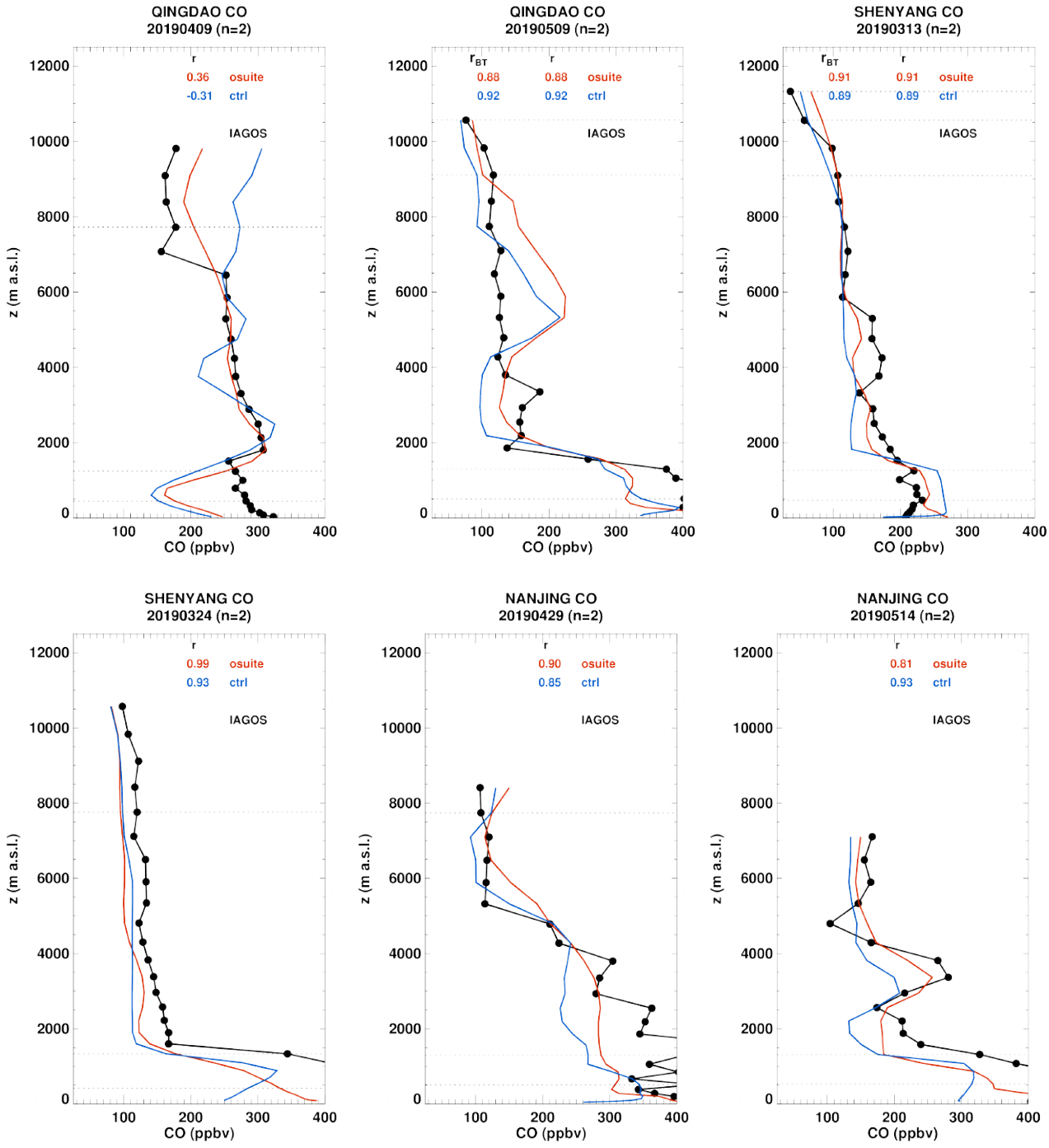

Figure 4.2.8.a Daily profile for CO from IAGOS (black) and the two NRT runs (o-suite: red, control: blue) over East Asia during MAM 2019.

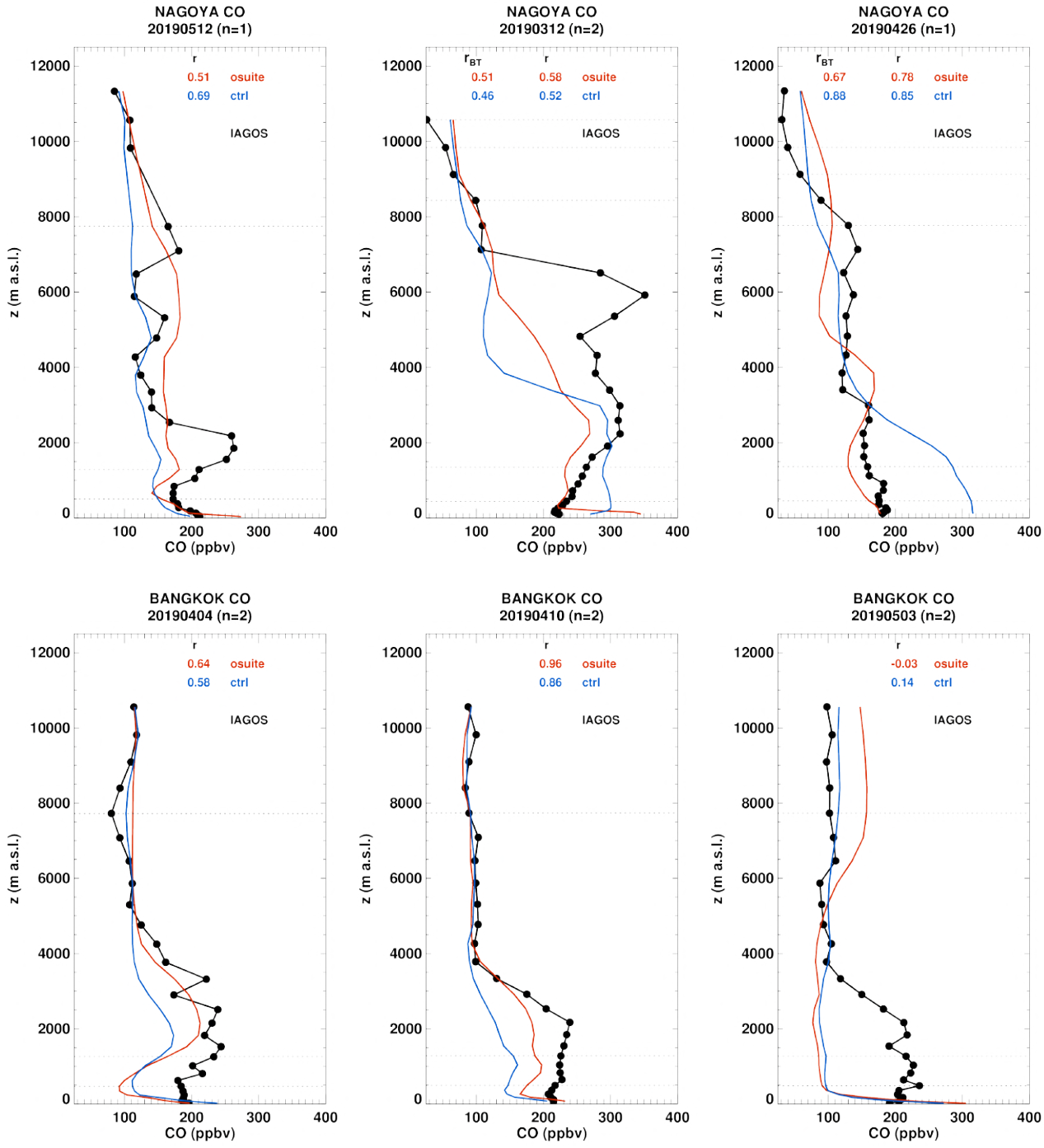

Figure 4.2.8.b Daily profile for CO from IAGOS (black) and the two NRT runs (o-suite: red, control: blue) over East Asia during MAM 2019.

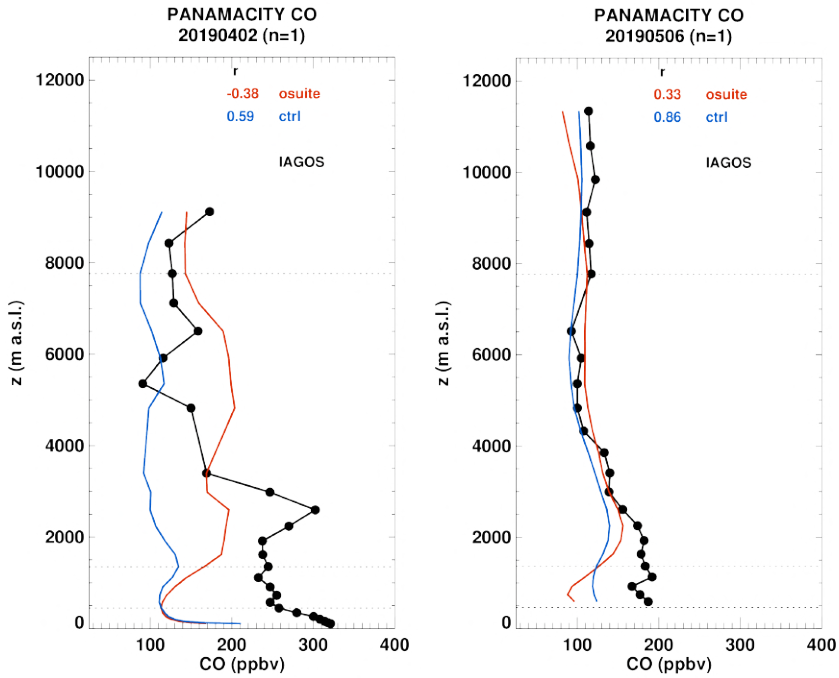

Figure 3.2.9 Daily profile for CO from IAGOS (black) and the two NRT runs (o-suite: red, control: blue) over South America during MAM 2019.

Eastern Asia

CO profiles are available at the Asian airports of: Qingdao, Shenyang, Nanjing, Nagoya, and Bangkok. Many profiles presented in Fig. 4.2.8.a-b present complex shapes which are well reproduced by the two runs with a better performance from the o-suite compared to control run. In the lowest layers up to the mid-troposphere CO is in general underestimated while the agreement with observarions is better in the UTLS.

Central America

Among the new airports that are visited there is the airport of Panama City. Only two profiles of CO are available at this airport (Fig. 3.2.9). The shapes of these two profiles are rather different. In the first case on 6 May, CO mixing ratios are of 180 ppbv up to 2000 m altitude. Above this altitude the profile is nearly constant with a value of 100 ppbv. In this case the two runs provide similar results with underestimations in the lowest layers and a good agreement from the free troposphere to the UTLS. On 2 April the shape of the profile is complex, with CO values from the surface up to 3000 m between 250 and 300 ppbv (sharp maximum near 3000 m). Above CO values decrease to roughly 150 ppbv. The profile obtained with o-suite also present a maximum in the lower part of the free troposphere, but much smoother and with large underestimations from the surface to about 3000 m. In the upper part of the free troposphere CO is overestimated then a good agreement is found in the UTLS. The results from control run are very different with a much worse performance regarding both shape and magnitude with much larger underestimation up to 5000 m.

4.3 Validation against FTIR observations from the NDACC network

In this section, we compare the CO profiles of the CAMS products with FTIR measurements at different FTIR stations within the NDACC network. These ground-based, remote-sensing instruments are sensitive to the CO abundance in the troposphere and lower stratosphere, i.e. between the surface and up to 20 km altitude. Tropospheric CO columns are validated. A description of the instruments and applied methodologies can be found at http://nors.aeronomie.be.

Figure 4.3.1 show that the o-suite tropospheric columns of CO agree well. The overall biases for the o-suite AN and 1d FC are within the measurements uncertainty. For the NH high latitude stations the bias reduced to -4% in MAM 2019 compared to the same period -10% in MAM 2018. For the tropical sites in the NH the reverse is seen: the bias increased to -4%. For the SH, the bias remains within the +-3% range.

For all stations in the southern hemisphere, the control run overestimates the CO with MBs up to 20%.

Fig. 4.3.2 shows a trend in the tropospheric CO column at Jungfraujoch (4km – TP) of about 1.5% per year. A similar trend is observed at Zugspitze (3km asl), but not at other non-mountain sites like St Petersburg. The trend at the o-suite 1dFC at both mountain stations is much lower (around -0.5%/y), which suggests the trend is located in the upper tropospheric column and is related to the assimilation.

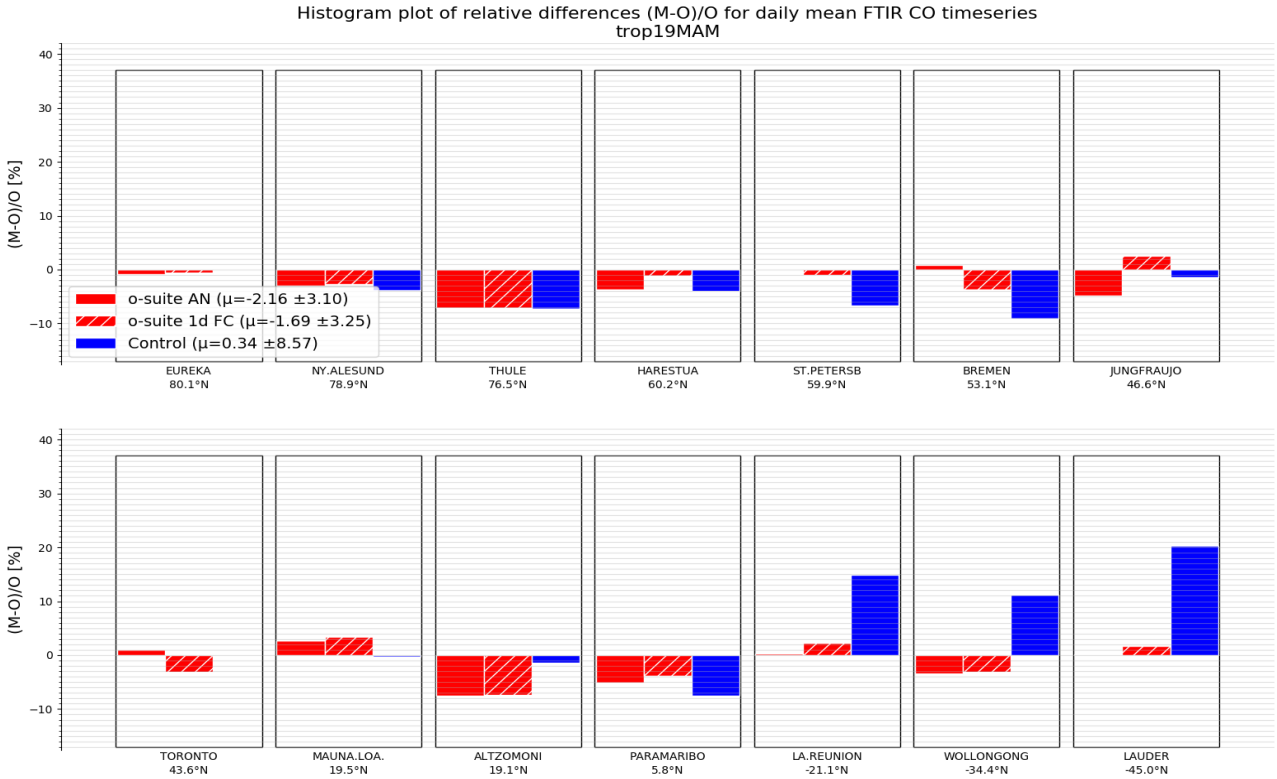

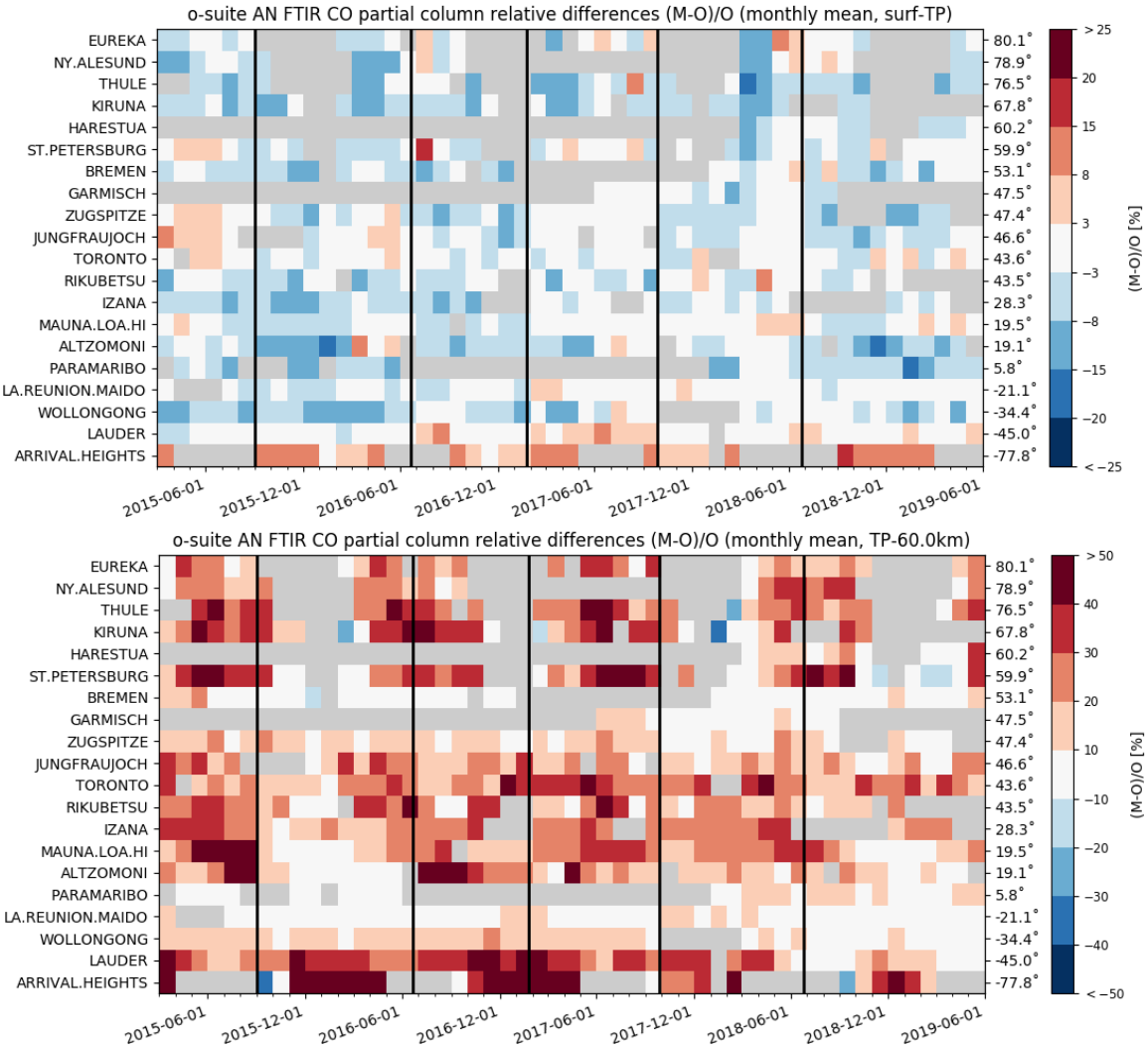

Figure 4.3.1: Seasonal relative mean bias for tropospheric CO columns (MB, %) for the considered period 2019 MAM (top) and monthly mean biases for a longer time period for the tropospheric CO columns (middle) and stratospheric CO columns (bottom) (model upgrades are indicated in black vertical lines).The overall uncertainty for the CO measurements is approximately 3% on the tropospheric columns and 10% for the stratospheric columns. The o-suite AN averaged bias in tropospheric columns for all stations is -2.2% for MAM 2019 and +18% for the stratospheric columns. Stations are sorted with decreasing latitude (northern to southern hemisphere).

The Taylor diagrams in Figure 4.3.3 provide information on the correlation of all three CAMS products under consideration with the FTIR time series. Leaving out the sites with few measurements, the assimilation has a positive effect on the correlation coefficient. Looking at the correlation values for the period 2018 DJF, the o-suite 1d FC (averaged correlation for all sites is 0.82) is comparable to the o-suite AN (averaged correlation for all sites is 0.84).

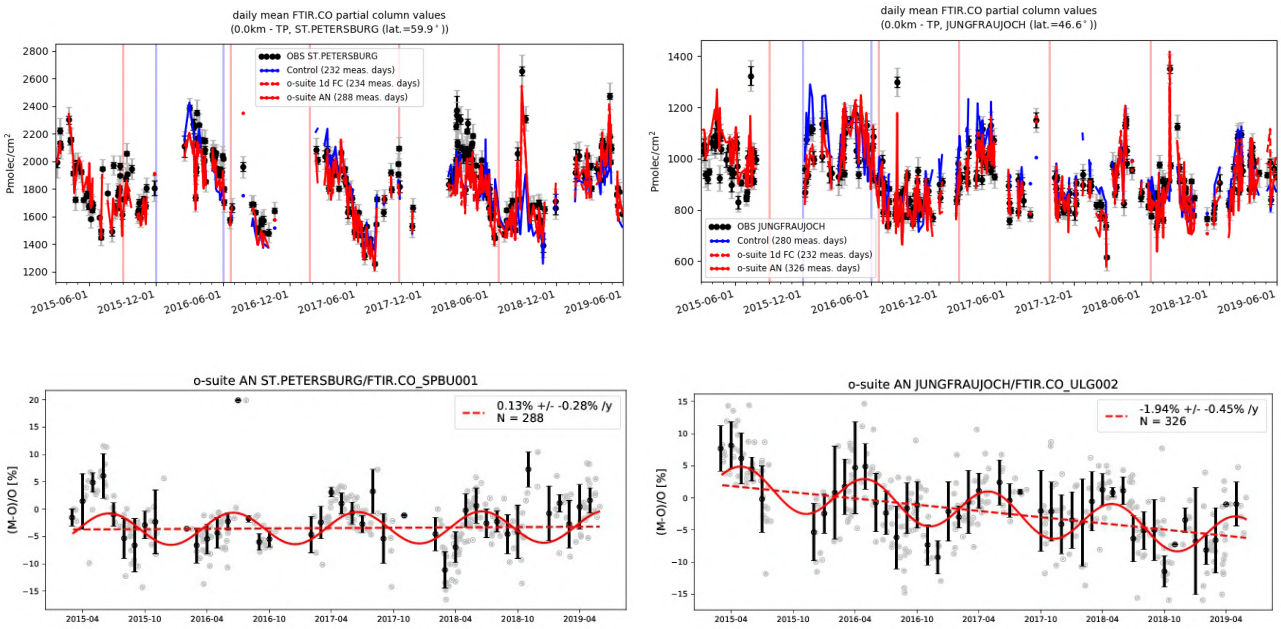

Figure 4.3.2: Top: daily mean values of tropospheric CO columns by the o-suite (AN and 1d FC, red) and the Control run (blue) compared to NDACC FTIR data at St Petersburg and Jungfraujoch for the period March 2015-June 2019. During March 2018 the o-suite underestimated the CO columns at St. Petersburg. Bottom row contains a linear fit and seasonal cycle fit through the relative differences for the o-suite AN. An underestimation is observed during the local autumn/winter months. The trend at Jungfraujoch is not seen in the o-suite 1dFC.

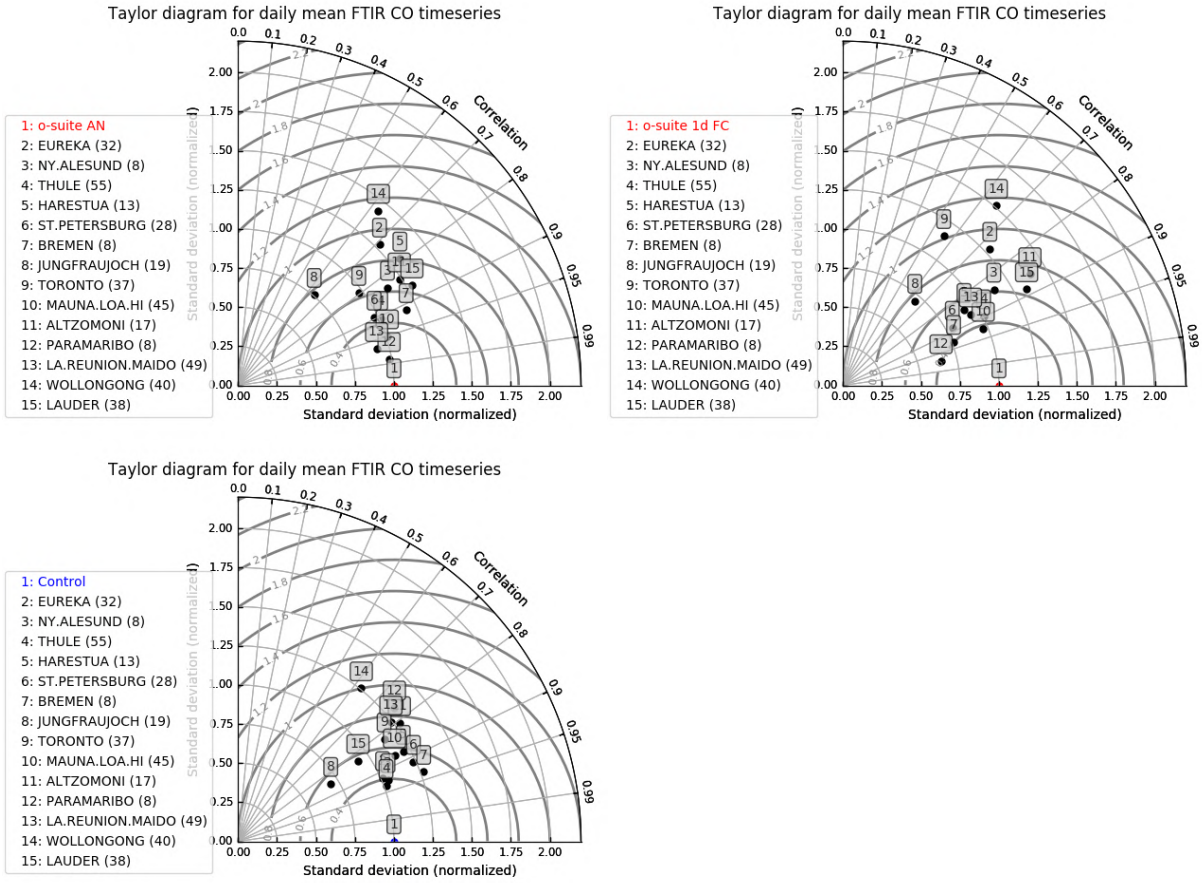

Figure 4.3.3: Taylor diagrams relating the standard deviations for the model /GB time series of tropospheric CO column data and their correlation. Panels are for the o-suite analysis, o-suite 1-day forecast and control run. All time-series are normalized such that the std of the model is 1. The variability of the CO columns in the o-suite 1dFC deviates more from the variability in the FTIR columns compared to the o-suite AN.

4.4 Validation against FTIR observations from the TCCON network

CO column averaged mole fractions of the CAMS models are compared with data from the Total Carbon Column Observing Network (TCCON). For the validation column averaged mole fractions of CO (denoted as XCO) are used. Column averaged mole fractions provide different information content than the in-situ measurements and are therefore complementary to the in-situ data.

In this section, we compare column averaged mole fractions of CO of the CAMS models with TCCON retrievals. Data from the following TCCON sites has been used:

Izana (Blumenstock et al., 2017), Reunion (De Mazière et al., 2017), Bialystok (Deutscher et al., 2017), Manaus (Dubey et al., 2017), Four Corners (Dubey et al., 2017), Ascension (Feist et al., 2017), Anmeyondo (Goo et al., 2017), Darwin (Griffith et al., 2017), Wollongong (Griffith et al., 2017), Karlsruhe (Hase et al., 2017), Edwards (Iraci et al., 2017), Indianapolis (Iraci et al., 2017), Saga (Kawakami et al., 2017), Sodankyla (Kivi et al., 2017), Hefei (Liu et al., 2018), Tsukuba (Morino et al., 2017), Burgos (Morino et al., 2018), Rikubetsu (Morino et al., 2017), Bremen (Notholt et al., 2017), Spitsbergen (Notholt et al., 2017), Lauder (Sherlock et al., 2017, Pollard et al., 2019), Eureka (Strong et al., 2018), Garmisch (Sussmann et al., 2017), Zugspitze (Sussmann et al., 2018), Paris (Te et al.,

2017), Orleans (Warneke et al., 2017), Park Falls (Wennberg et al., 2017), Caltech (Wennberg et al., 2017), Lamont (Wennberg et al., 2017), Jet Propulsion Laboratory (Wennberg et al., 2017), East Trout Lake (Wunch et al., 2017)

For the validation of the models in March-May, only Orleans is available for the three months. Data for Karlsruhe and Izana is only available for March.

The reason for the changing availability of TCCON data is the following: The requirement for TCCON data to become public is 1 year after the measurement. Some TCCON groups make their data earlier available. In the previous CAMS84 project only data from Bialystok, Orleans and Reunion was timely available for the validation of the CAMS models. The Bialystok site has stopped operation and the instrument is currently being transported to Cyprus. Reunion had technical problems and is therefore not operational. It is likely that for future reports fast data will become available again for these three sites. During the first year of the current CAMS84 project data was timely available from several TCCON sites. The reason was that during the first year after the launch of the Sentinel 5 precursor (S5p) several sites received funding to make TCCON data timely available for the validation of the S5p CH4 and CO retrievals. Several non-European TCCON partners contributed to this effort. It is very likely that for future reports only data from Cyprus, Orleans and Reunion will be available.

The comparisons (Fig 4.4.2 - 4.4.3) show that all models capture the seasonality well. The differences during the reporting period (March – May 2019) rely on 3 stations. Out of these three stations only Orleans covers the whole 3 months. Karlsruhe and Izana cover only March. The differences between model and observations are less than 15 ppb at all sites. For the whole reporting period the comparison is only possible for Orleans and for this site the control model shows the best agreement among the 3 model runs.

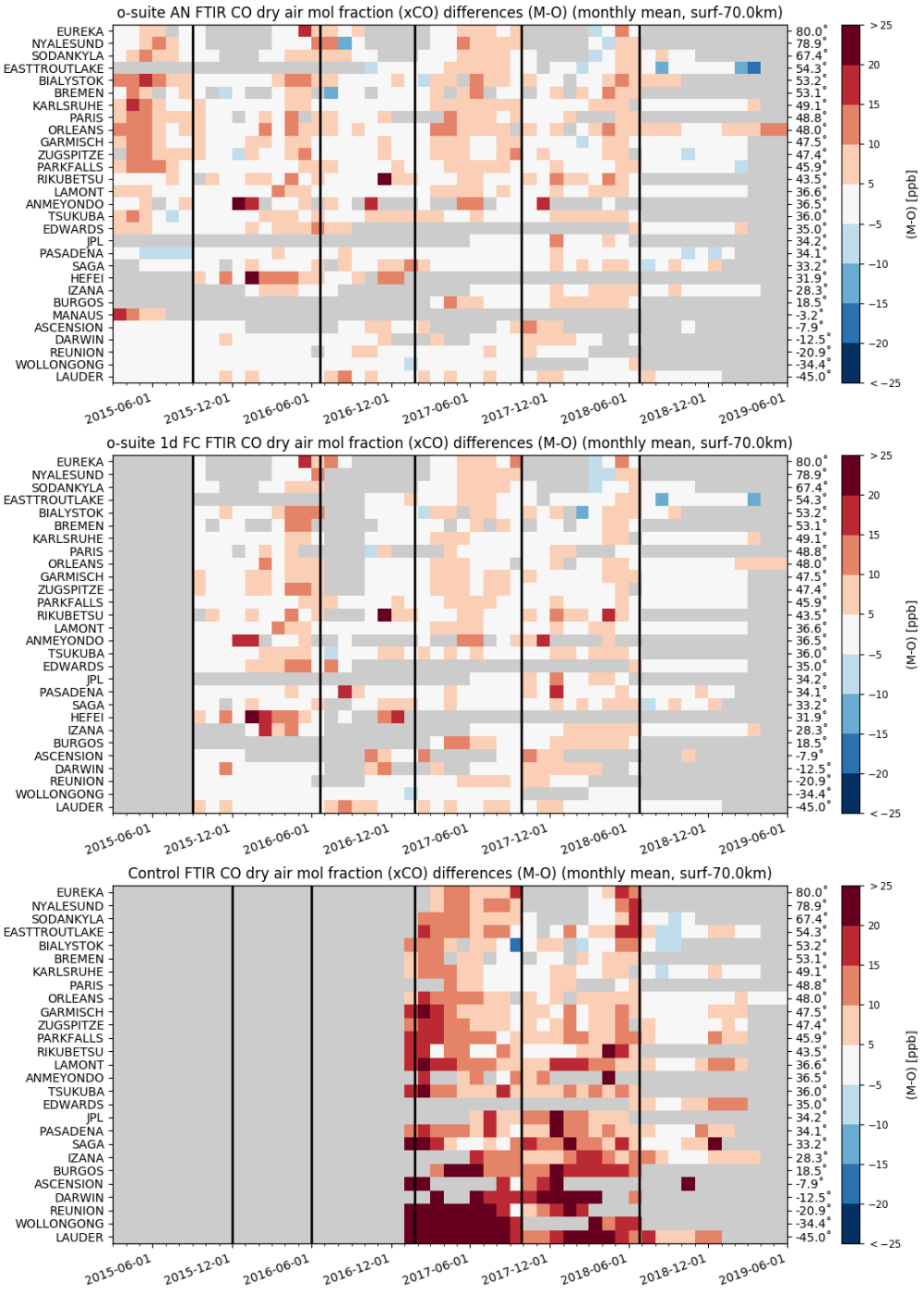

Figure 4.4.1: Monthly differences for the last 4 years. The stations are sorted by latitude (northern to southern hemisphere).

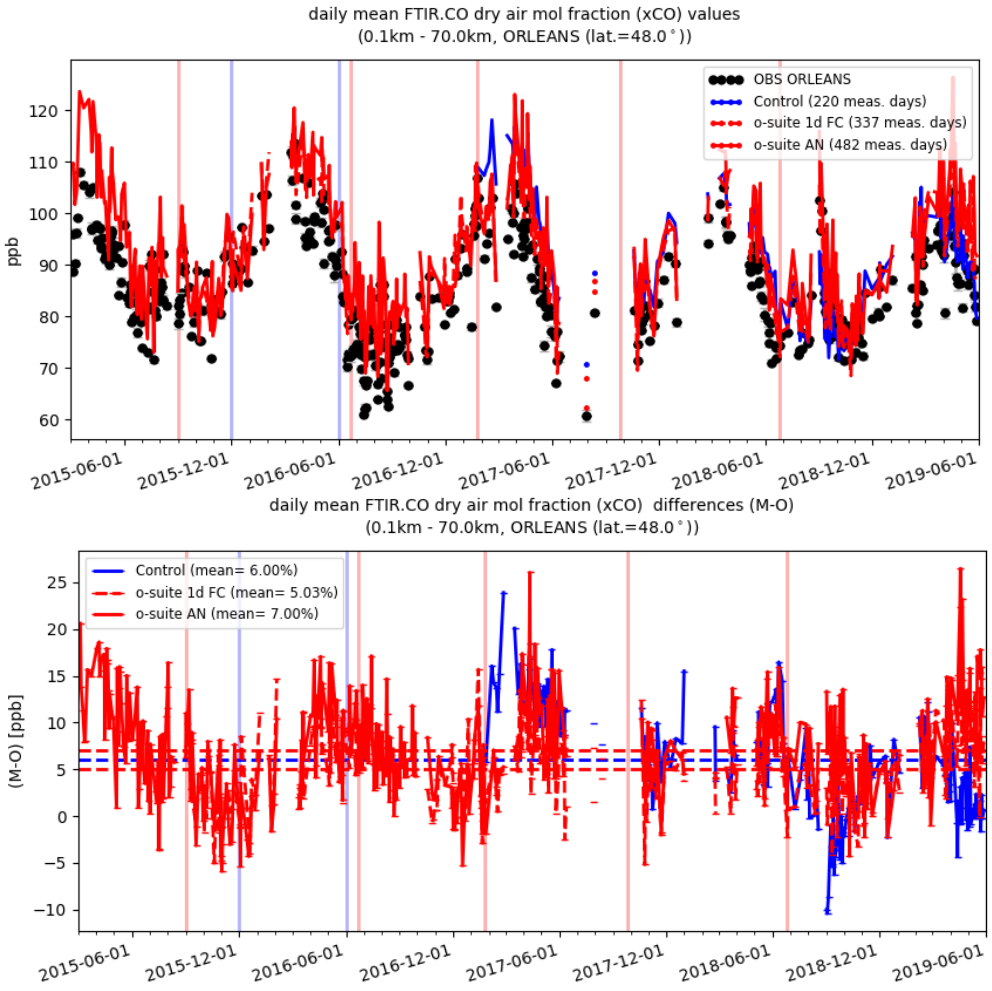

Figure 4.4.2: Comparison of the CO model data with TCCON CO at Orleans.

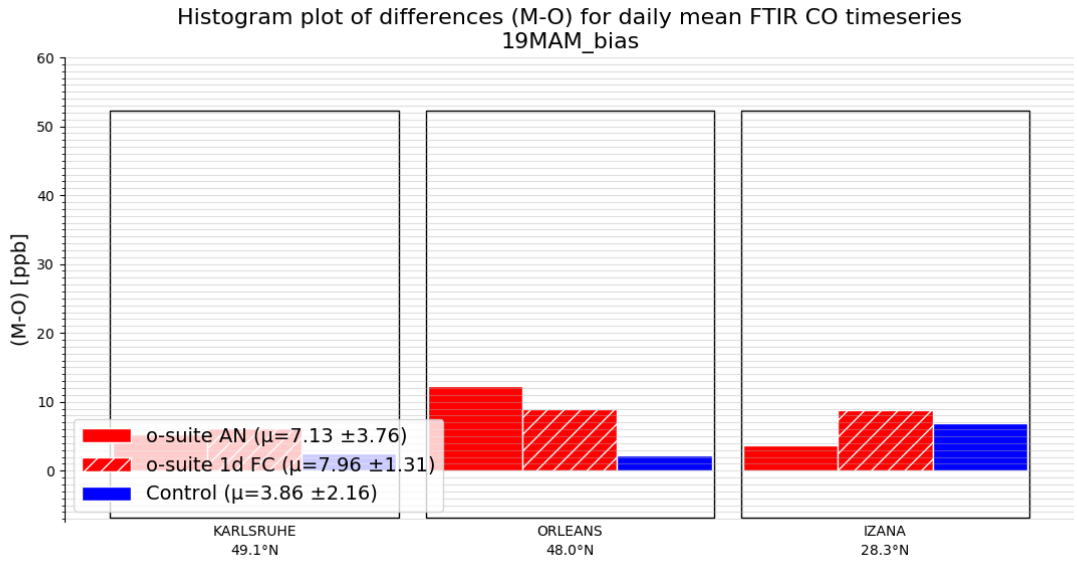

Figure 4.4.3: Differences during the reporting period. Orleans data covers March, April and May. Karlsruhe and Izana data cover only March.

4.5 Evaluation with MOPITT and IASI data

In this section, modeled CO total columns are compared to MOPITT version 8 (thermal infrared radiances) (Emmons et. al., 2009, Deeter et al., 2010) and IASI satellite retrievals (Clerbaux et al., 2009). Figure 4.5.1 shows the global distribution of CO total columns retrieved from MOPITT V8 (top left) and IASI (top right) and the relative biases of the model runs with respect to MOPITT V8 for April 2019.

Both, MOPITT and IASI show high CO values over the biomass burning areas in Central Africa, and over the Northern parts of South America and China. IASI observations show somewhat higher values than MOPITT especially over the above-mentioned regions with high CO emissions. Interestingly over Europe, the MOPITT values are higher compared to IASI. The modeled CO geographical distribution and magnitude of values show that the model performs reasonably well. The relative difference between the model runs and MOPITT shows that the o-suite performs better than the control run without data assimilation with biases within ±10%, with some regional exceptions where biases reached 20%, e.g. Australia. The control run overestimates the satellite observations over the Southern Hemisphere by about 20% and underestimates observations over the Northern Hemisphere by about 10%, over Europe and North Africa by about 20%. Both runs show a slightly growing positive bias on the 4th forecast day over the fire active areas in North America and Africa and over China.

Figure 4.5.2 shows time series of CO total column for MOPITT V8, IASI and the model runs over the eight selected regions. For the comparison with MOPITT, the modelled CO concentrations were transformed using MOPITT V8 averaging kernels (Deeter, 2004). Both, MOPITT and IASI CO total columns are assimilated in the o-suite run, while a bias correction scheme is applied to IASI data to bring it in line with MOPITT. MOPITT and IASI CO total columns show a relatively similar variability over different regions. IASI CO values are lower than MOPITT over most regions with some seasonal exceptions till the year 2016. Since then IASI and MOPITT are more consistent with each other over Europe, the US and East Asia. Significant difference between MOPITT and IASI are observed over the Alaskan and Siberian fire regions in winter seasons, with IASI CO total column values being lower up to 30%. In North and South Africa, deviations become larger since 2016 with IASI values being higher than MOPITT by up to 20%. The modelled seasonality of CO total columns is in relatively good agreement with the retrievals. In general, the comparison between the o-suite and control run shows that the assimilation of satellite CO has a more positive, pronounced impact on model results over East and South Asia, South Africa, and since the end of 2016, over the US in winter and spring seasons, and smaller impact over the other regions. Since June 2016, the o-suite shows very good agreement with the satellite retrievals over Europe and the US with biases less than 5%. In late summer and early autumn of 2018 over Europe, the control run has larger negative biases compared to the satellite data then early in 2018 and the two previous autumn seasons.

A general reduction of CO values from the year 2015 to the year 2018 can be seen over Europe, the US and East Asian regions. The South African region shows a slight increase of the seasonal minimum compared to previous springs.

The modified normalized mean bias (MNMB) of the model runs compared to MOPITT V8 (Fig. 4.5.3) allows quantifying the impact of the assimilation on the model performance. The o-suite model run shows negative biases over Europe, the US and Alaskan fire regions with some seasonal exceptions.

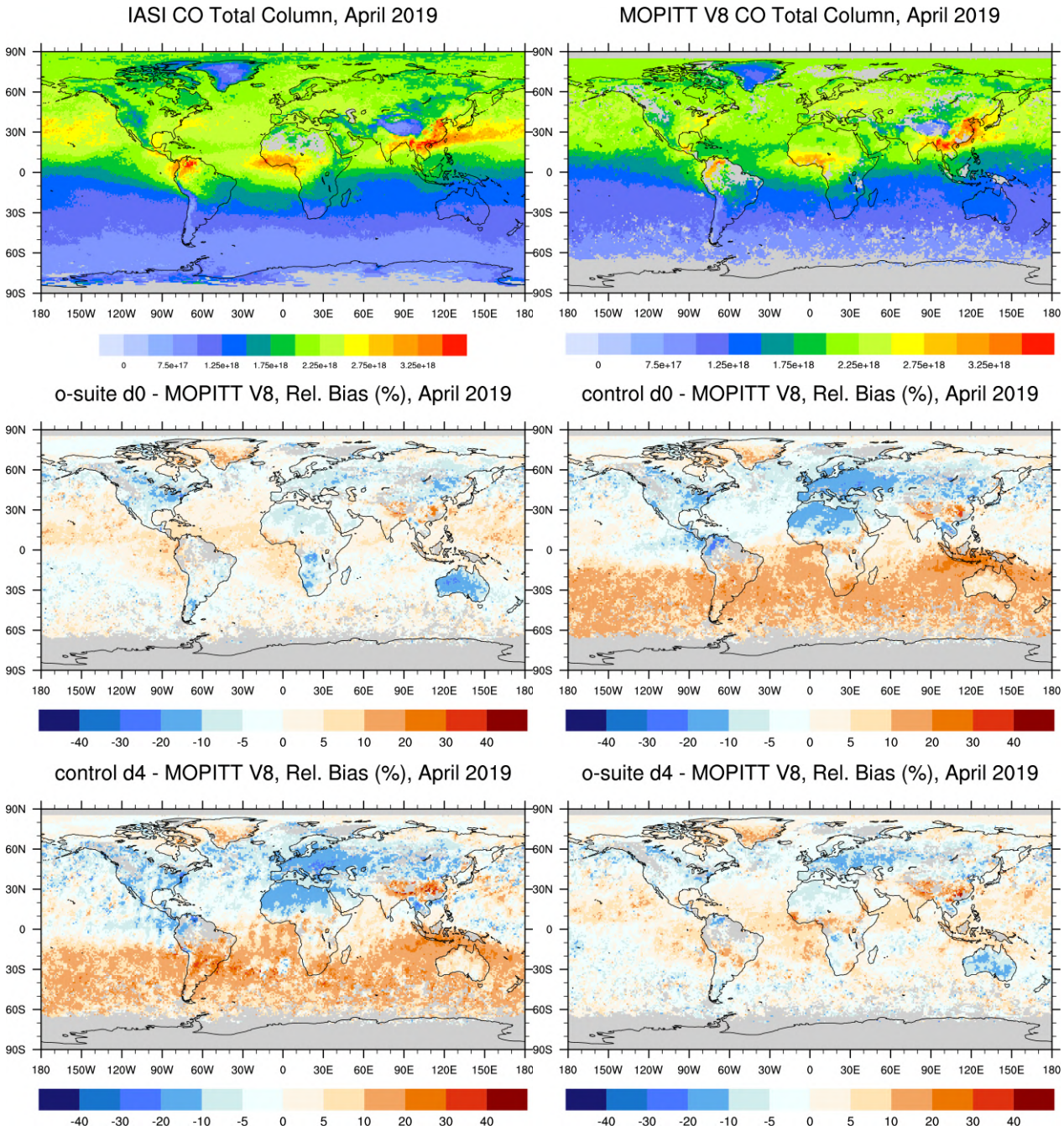

Fig. 4.5.1: CO total columns for MOPITT V8 (top left) and IASI (top right) satellite retrievals and relative difference between the model runs and MOPITT for April 2019: o-suite (middle left), control run (middle right), o-suite 4th forecast day (bottom left), o-suite 4th forecast day (bottom right). Grey colour indicates missing values.

The control run shows a systematic positive bias up to 20% over South Asia in November-December 2014, 2015, 2016, and 2017. Over southern Africa the control run overestimates satellite retrieved values by up to 25% in winter and spring 2015, 2016, and 2017. In general, the o-suite is within +/- 10% in all regions, while the control run shows larger biases over East and South Asia and North and South Africa, as well as stronger seasonal cycles.

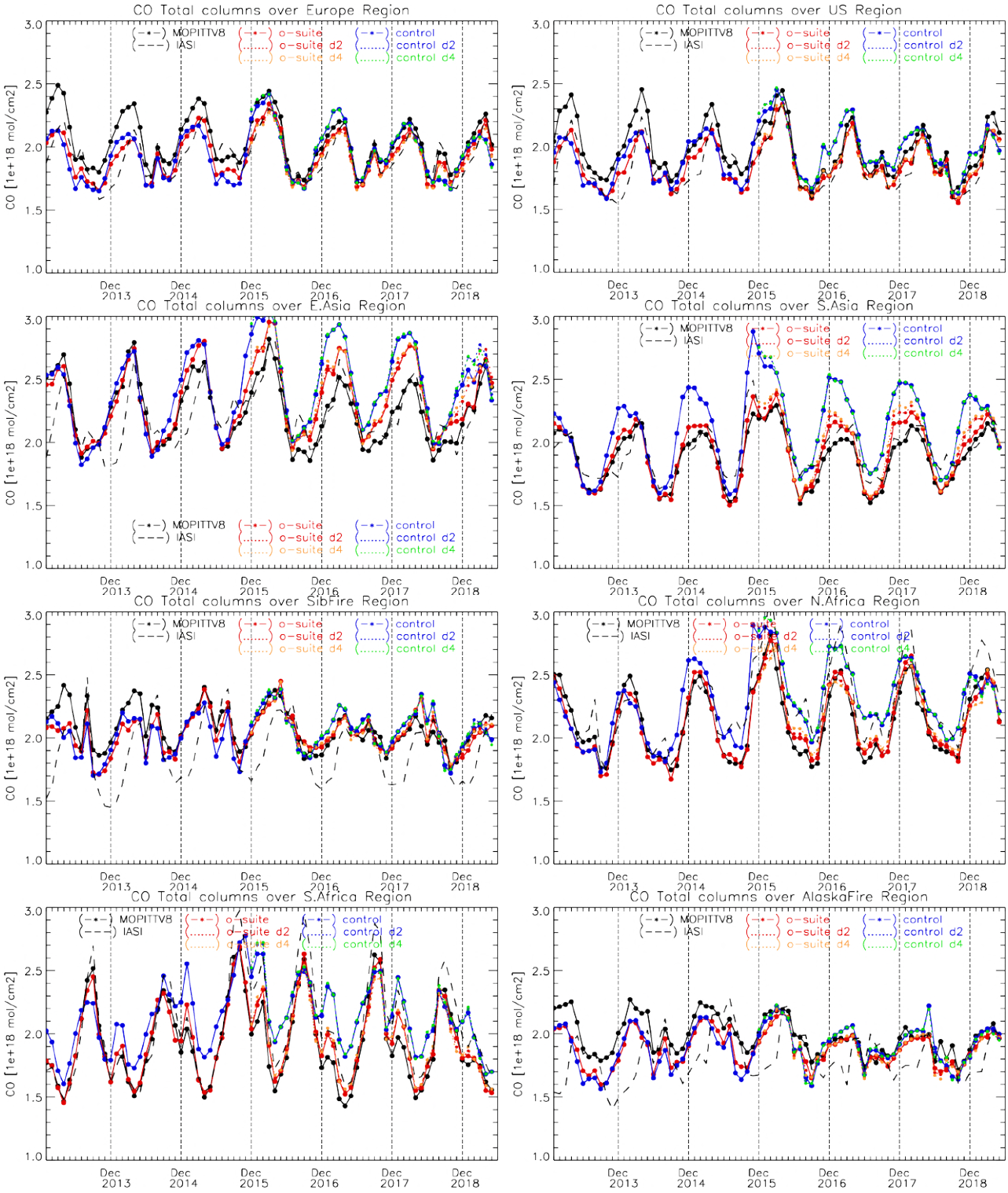

Fig. 4.5.2: Time series of CO total columns for satellite retrievals MOPITT V8, IASI (black) and the model runs over the selected regions: o-suite (red, solid), control (blue, solid), o-suite 2nd forecast day (red, dotted), o-suite 4th forecast day (orange, dotted), control 2nd forecast day (blue, dotted), control 4th forecast day (green, dotted). Period: January 2013 to May 2019.

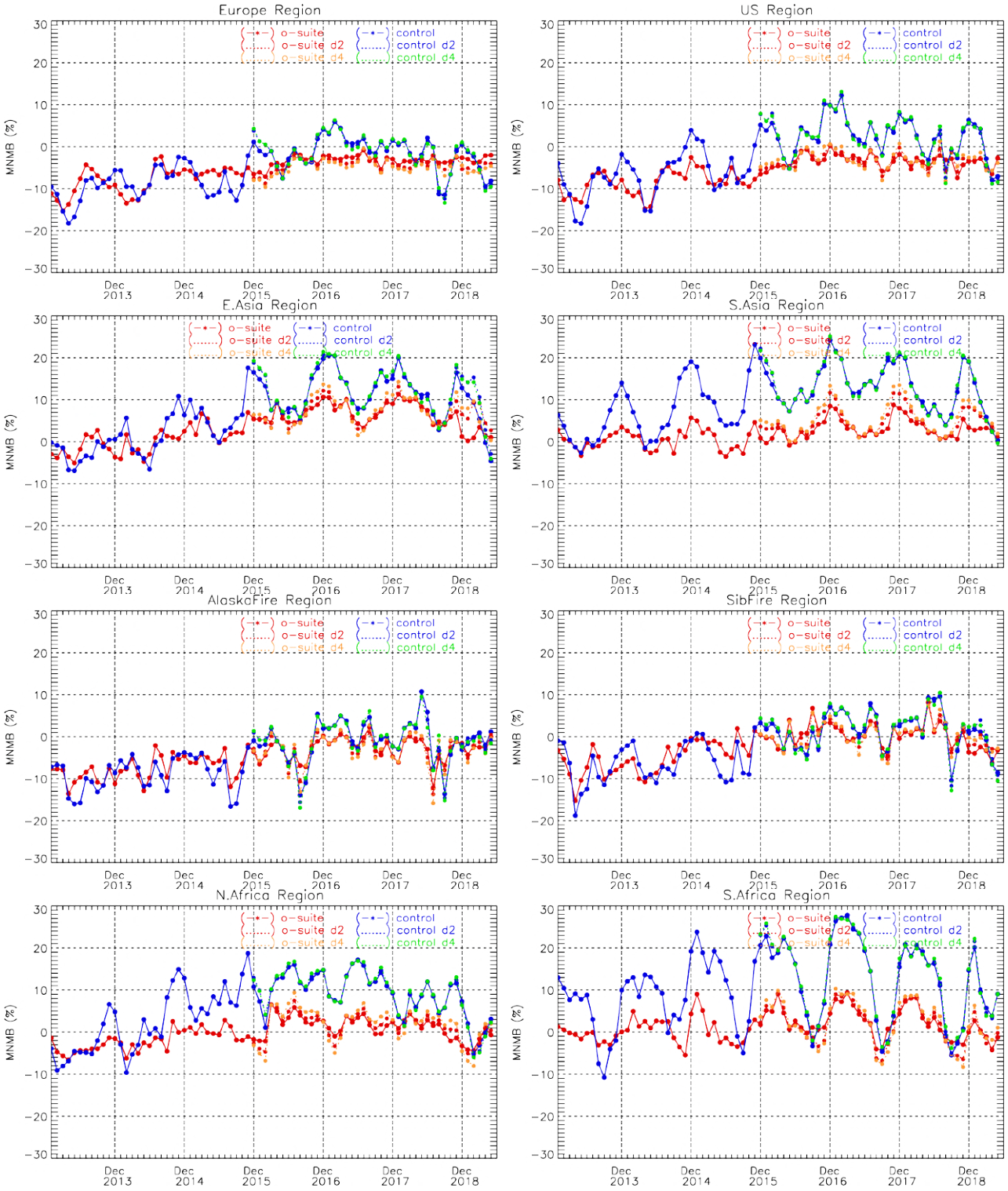

Fig. 4.5.3: Timeseries of modified normalized mean bias (%) for CO total columns from the model simulations vs MOPITT V8 retrievals over selected regions. O-suite (red, solid), control run (blue, solid), o-suite 2nd forecast day (red, dotted), o-suite 4th forecast day (orange, dotted), control 2nd forecast day (blue, dotted), control 4th forecast day (green, dotted). Period: January 2013 to May 2019.

The region East Asia shows good improvements indicating high agreement with the satellite data in the first half of 2019. The o-suite bias in MAM is within 5%, whereas it is about 10% during similar season in the last two years. The control run has an untypical negative bias for this area, though it is small, within 5%. In South Asian and North African regions, the control run's biases are reduced and account of about 5% which are almost similar to the o-suite run in contrast to previous years with biases of about 15%. Over the South African region both runs show good improvements reflecting in reduced, almost by half, biases. Over Europe the o-suite bias is within 5%, whereas the control run underestimates the observations by up to 10% in contrast to previous years. Both runs show good agreement with the satellite data for the Alaskan fire region in the first half of 2019, with biases within 5%. The observations for the Siberian fire region are underestimated by the o-suite by about 5% and by control run by up to 10%.

5. Tropospheric nitrogen dioxide

5.1 Evaluation against GOME-2 retrievals

In this section, model columns of tropospheric NO_2 are compared to SCIAMACHY/Envisat NO_2 satellite retrievals (IUP-UB v0.7) [Richter et al., 2005] for model data before April 2012, and to GOME-2/MetOp-A NO_2 satellite retrievals (IUP-UB v1.0) [Richter et al., 2011] for more recent simulations. This satellite data provides excellent coverage in space and time and very good statistics. However, only integrated tropospheric columns are available, and the satellite data is always taken at the same local time, roughly 10:00 LT for SCIAMACHY and 09:30 LT for GOME-2, and at clear sky only. Therefore, model data are vertically integrated, interpolated in time and then sampled to match the satellite data. GOME-2 data were gridded to model resolution (i.e. 0.4° deg x 0.4° deg). Model data were treated with the same reference sector subtraction approach as the satellite data. Uncertainties in NO_2 satellite retrievals are large and depend on the region and season. Winter values in mid and high latitudes are usually associated with larger error margins. As a rough estimate, systematic uncertainties in regions with significant pollution are on the order of 20% – 30%.

Figure 5.1.1 shows global maps of GOME-2 and model monthly mean tropospheric NO_2 columns as well as differences between retrievals and simulations for May 2019 as an example of the maps for spring 2019. The overall spatial distribution and magnitude of tropospheric NO_2 is well reproduced by both model runs, indicating that emission patterns and NO_x photochemistry are reasonably represented. Some differences are apparent between observations and simulations, with generally larger shipping signals simulated by the models. For example, shipping signals are much more pronounced in model simulations to the south of India. Emissions over Europe and especially the pollution hotspots around the Benelux countries are underestimated. However, other local maxima of values observed over anthropogenic emission hotspots in East Asia (e.g. over the heavily populated Sichuan Basin; 30°N, 105°E), India and others such as Teheran, Mecca, around Lebanon/Israel and Moscow are regularly overestimated. Values over boreal forest fires in Alaska and Canada and for fires around Sierra Leone are overestimated.

Closer inspection of the seasonal variation of tropospheric NO_2 in some selected regions (Fig. 5.1.2) reveals significant differences between the models and points to some simulation problems. Over regions where anthropogenic emissions are major contributors to NO_x emissions, models catch the shape of the satellite time series rather well. However, over East-Asia absolute values and seasonality were strongly underestimated before 2014 by all model runs (most likely due to an underestimation of anthropogenic emissions) for all seasons apart from summertime minima, with the o-suite showing the best results since an upgrade in July 2012. As wintertime NO_2 column retrievals decreased significantly in 2014, model simulated wintertime maxima are in better agreement with the satellite retrieved ones for recent years. However, the observed NO_2 decrease is not reproduced by the simulations and therefore the better agreement for more recent years cannot be attributed to model improvements. Moreover, summertime model minima increased in 2015 compared to previous years, which is in contrast to the satellite retrievals, so that the simulated values for the summers since 2015 are about 50% larger than satellite retrieved ones.

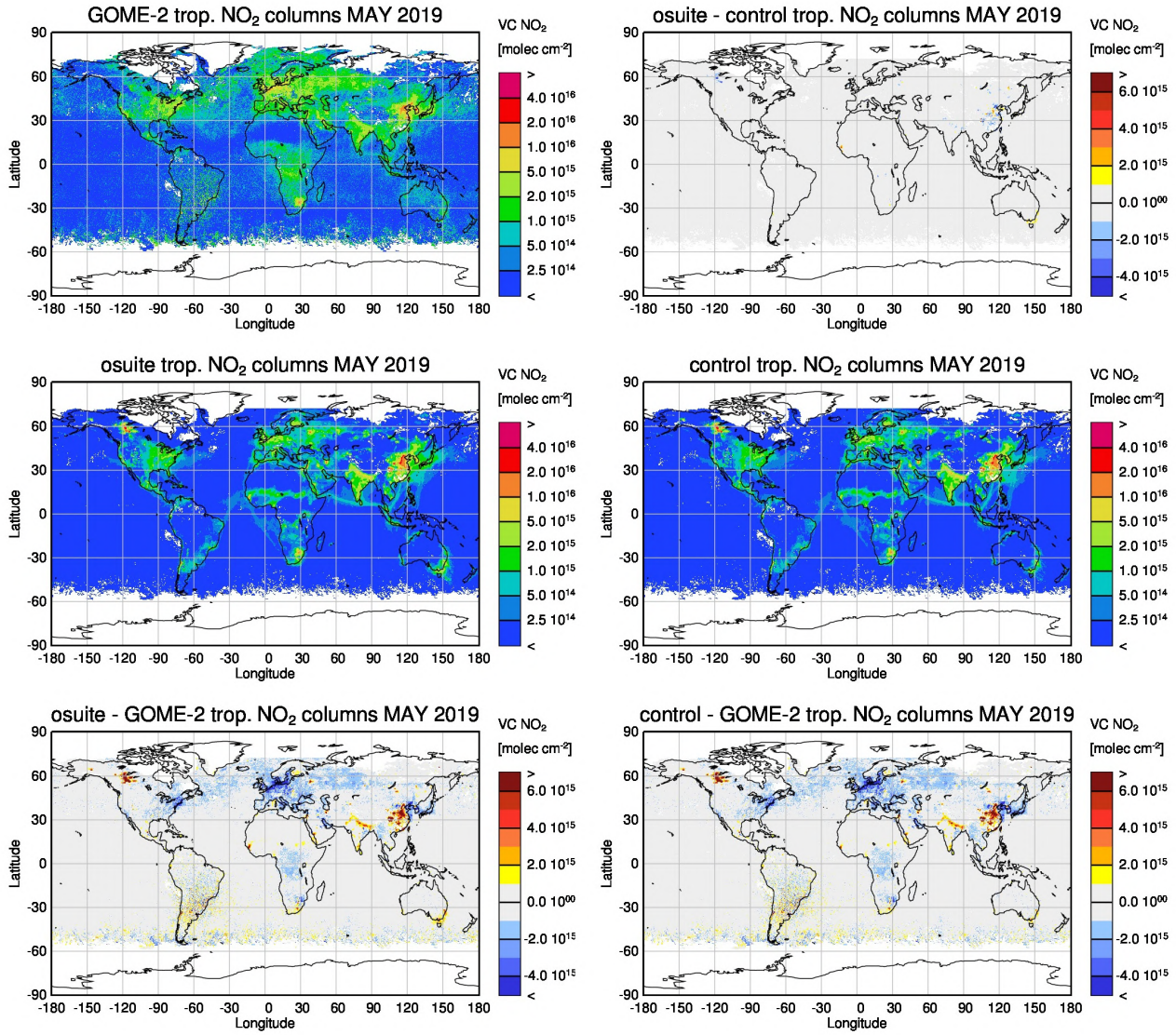

Figure 5.1.1: Global map comparisons of satellite retrieved, and model simulated tropospheric NO_2 columns [molec cm-2] for May 2019. The top row shows monthly mean tropospheric NO_2 columns retrieved by GOME-2 as well as the difference between o-suite and control, the second row shows the corresponding tropospheric NO_2 columns for model simulated averages. The third row shows differences of monthly means between models and GOME-2. GOME-2 data were gridded to model resolution (i.e. 0.4° deg x 0.4° deg). Model data were treated with the same reference sector subtraction approach as the satellite data.

The sharp decrease observed by GOME-2 for February 2019 over East-Asia is not reproduced by the simulations. As for East-Asia, a decrease in satellite retrieved values also occurred in 2015 over Europe where a peak is usually found around January, which was, as a result, only slightly underestimated by the models for January 2015. The underestimation of tropospheric NO_2 columns over Europe may be caused to some extent by a change of emission inventories in 2012. However, the situation changed for the three winter periods between 2015 and 2017, for which GOME-2 shows (compared to previous years) a strong increase in January peak values, combined with a decrease in values for December and February that is not reproduced by the models. It is not clear if

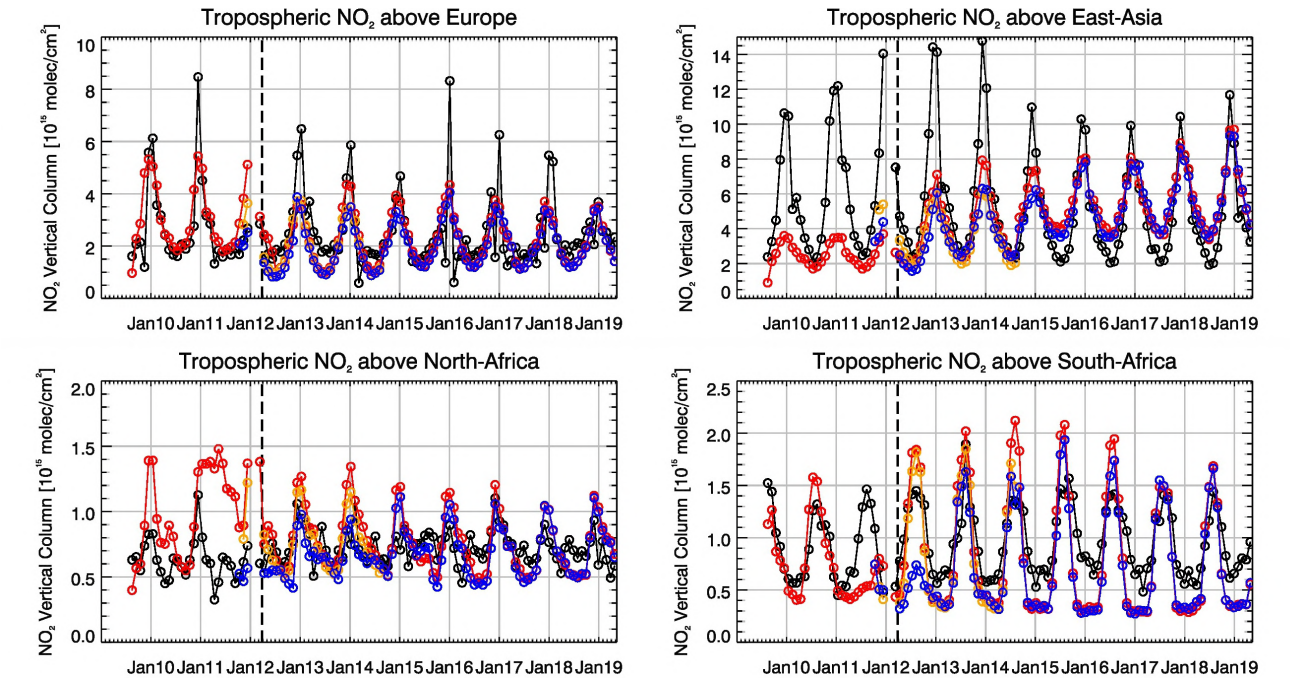

Figure 5.1.2: Time series of average tropospheric NO_2 columns [10^{15} molec cm^{-2}] from SCIAMACHY (up to March 2012, black) and GOME-2 (from April 2012 onwards, black) compared to model results (red: o-suite, blue: MACC_fncrt_TM5/MACC_CIFS_TM5/control, orange - MACC_fcnrt_MOZ) for different regions (see Annex 2 for definition of regions). The upper panels represent regions dominated by anthropogenic emissions, and the lower panels represent those dominated by biomass burning. Vertical dashed black lines mark the change from SCIAMACHY to GOME-2 based comparisons in April 2012.

the GOME-2 observations are realistic here, although a first inspection of daily GOME-2 satellite images did not point to problems regarding the retrieval. The retrievals show the same pattern as the simulations however for winter 2018/2019.

Over regions where biomass burning is the major contributor to NO_x emissions, seasonality and amplitude of model columns are determined by fire emissions. The seasonality for the two regions in Africa was simulated reasonably well for 2010 and after October 2011. In the time period in between, a bug in reading fire emissions lead to simulation errors for all MOZART runs. Over North-Africa, the o-suite shows improved results since an update in July 2012 and the change to IFS-CB05 in September 2014. However, tropospheric NO_2 columns around December are still overestimated by the models. Summertime NO_2 columns over North-Africa are underestimated compared to the satellite data from 2015 onwards. The models (especially the o-suite) generally overestimate the seasonal cycle for South-Africa, particularly for 2014-2016 with an overestimation of the seasonal maximum which usually occurs around August (e.g. by a factor of 1.4 larger compared to GOME-2 retrievals in 2016). However, August maxima are in better agreement since the upgrade of the o-suite in 2017, but minima during SH summer remain underestimated.

More NO_2 evaluation plots can be found on the CAMS website, see table 1.2.

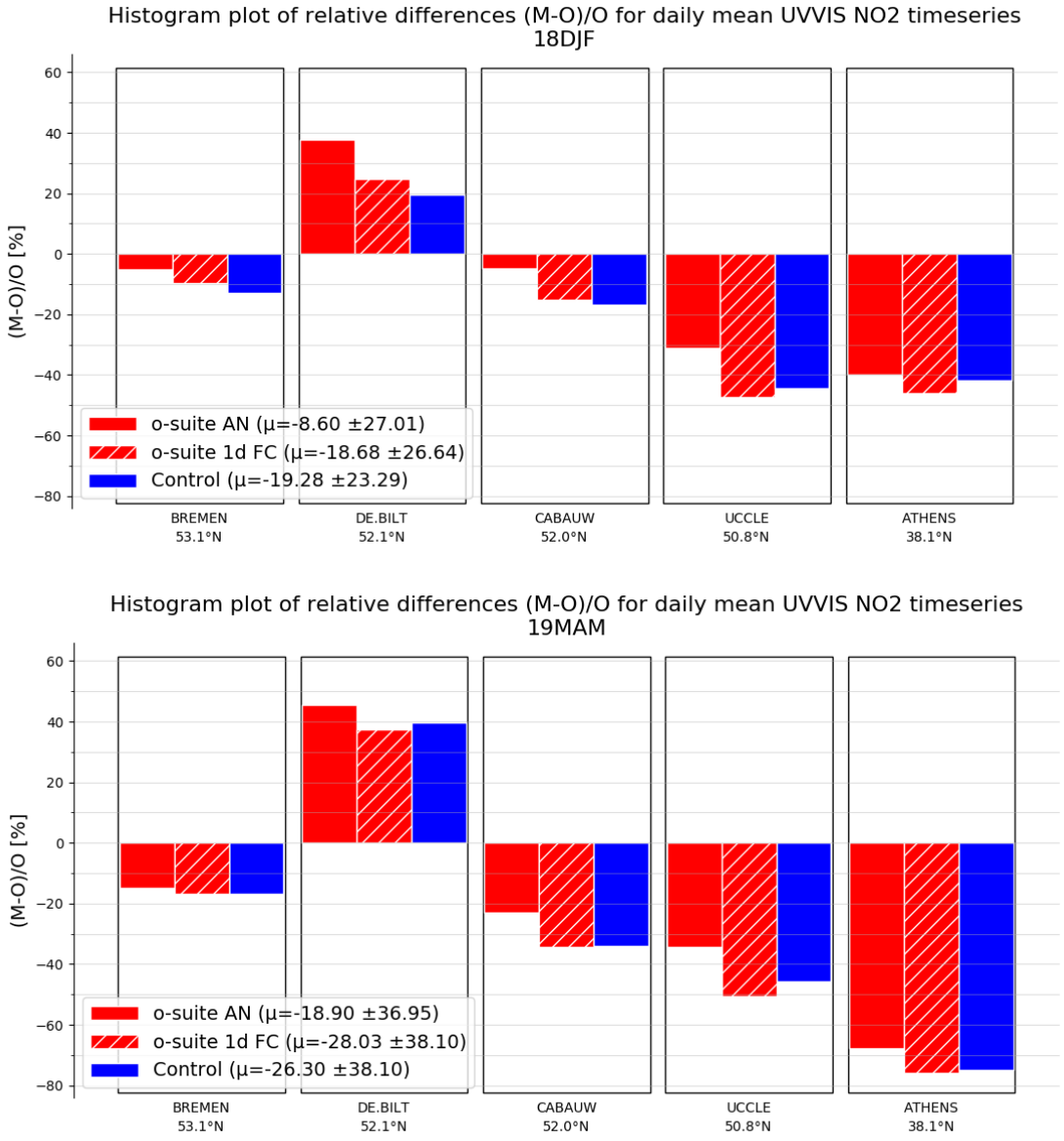

Figure 5.2.1: Table diagram showing the seasonal bias Dec-Feb 2019 (top) and March-May 2019 (bottom) for five stations, sorted by latitude. Compared to the previous validation period DJF, the relative biases in SON have increased.

5.2 Evaluation against ground-based DOAS observations

In this section, we compare the NO_2 columns of the CAMS products with UVVIS DOAS profile measurements at Uccle and column data from the other stations.[1] This ground-based, remote-sensing instrument is sensitive to the NO_2 abundance in the lower troposphere, up to 1km altitude with an estimated uncertainty of 8%. Tropospheric NO_2 profiles and columns are validated (up to 3.5km or 10km). A description of the instruments and applied methodologies is the same for all DOAS OFFAXIS measurements, see http://nors.aeronomie.be.

[1] No contribution from Xianghe, Reunion and OHP due to instrument failure.

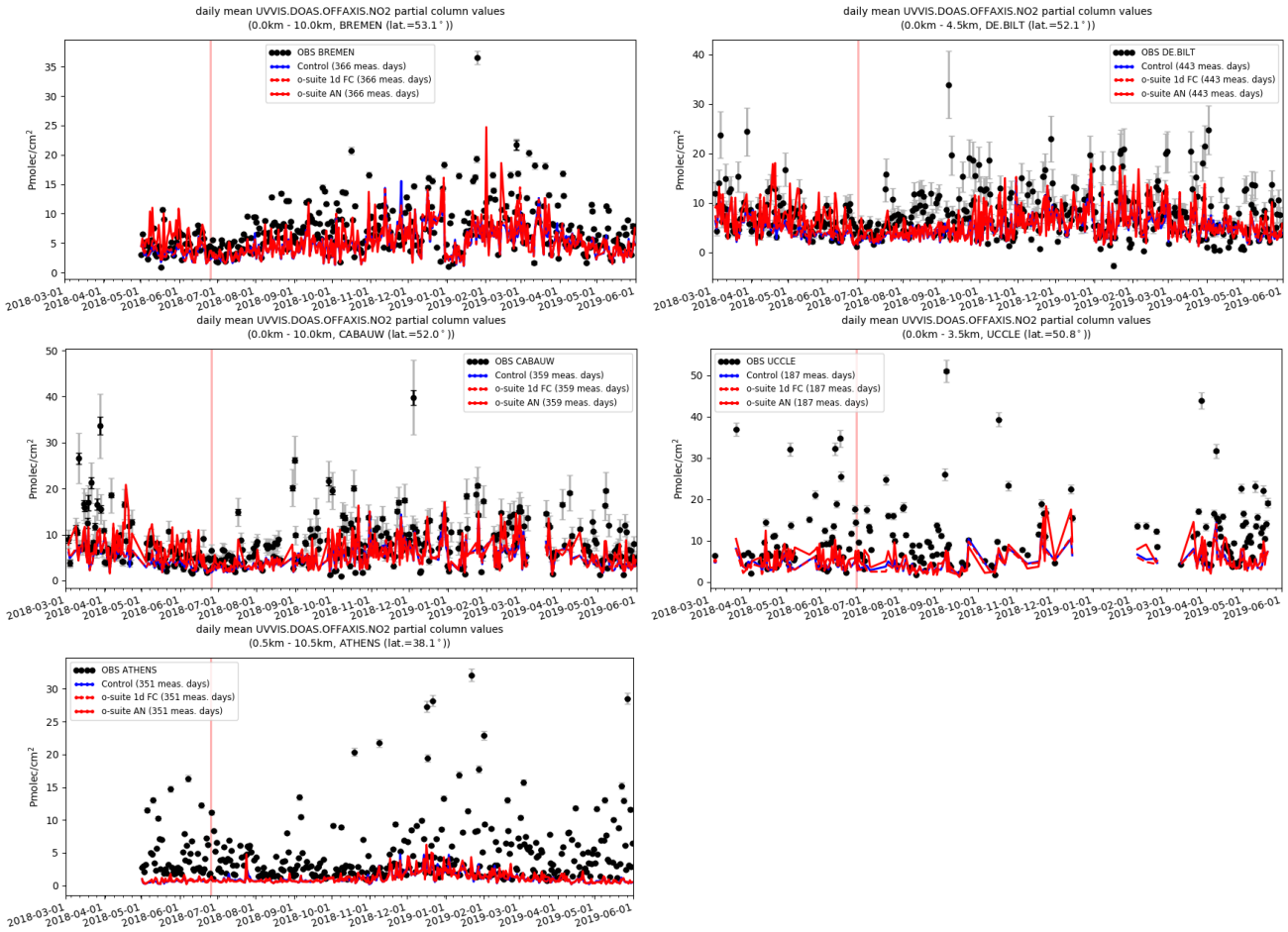

Figure 5.2.2: Time series of NO_2 partial columns at the five different sites. For all sites except Athens, background concentrations are well captured by the CAMS products. The o-suite and control product show little difference.

It is important to mention here that the model partial column values are calculated from the smoothed model profiles. This guarantees that the model levels where the measurement is not sensitive do not contribute to the observed bias. We should mention that the measurement data is still catalogued as rapid delivery and not in the consolidated NDACC database.

Fig. 5.2.1 shows the biases for the latest validation periods Dec-Feb 2019 and March-May 2019 at the different sites. The biases have all increased. At the urban sites at Uccle and Athens a strong underestimation is observed. For the other sites (Bremen, De Bilt and Cabauw) the o-suite AN is able to capture only few of the high pollution events.

6. Formaldehyde

6.1 Validation against satellite data

In this section, simulations of tropospheric formaldehyde are compared to SCIAMACHY/Envisat HCHO satellite retrievals (IUP-UB v1.0) [Wittrock et al., 2006] for model data before April 2012 and to GOME-2/MetOp-A HCHO data (IUP-UB v1.0) [Vrekoussis et al., 2010] afterwards. As the retrieval is performed in the UV part of the spectrum where less light is available and the HCHO absorption signal is smaller than that of NO_2, the uncertainty of monthly mean HCHO columns is relatively large (20% – 40%) and both noise and systematic offsets have an influence on the results. However, absolute values and seasonality are retrieved more accurately over HCHO hotspots.

In Figure 6.1.1, monthly mean satellite HCHO columns are compared to model results for May 2019. The magnitude of oceanic and continental background values and the overall spatial distribution are well represented by the o-suite and control. The models overestimate values over regions in Central Africa which could be due to fire or biogenic emissions.

Time series in Fig. 6.1.2 highlight three cases:

- East-Asia and the Eastern US, where HCHO is dominated by biogenic emissions. Model results and measurements generally agree rather well. However, all model runs underestimate the yearly cycle over East-Asia since 2012. In contrast to MOZART runs, MACC_CIFS_TM5 overestimated satellite values for the Eastern US since the middle of 2013. However, the newer IFS-CB05 runs perform well for Eastern US since 2015. For recent years and both regions, there is virtually no difference between the most recent o-suite run with IFS-CB05 chemistry and the corresponding control run without data assimilation. The variability or “ups and downs” in HCHO columns observed by GOME-2 since December 2014 is due to the lack of data (caused by instrument degradation) for these regions during winter in the Northern Hemisphere, leading to e.g. the negative values in the GOME-2 time series for Eastern US since December 2015. Summertime maxima are still underestimated over East-Asia despite of the higher resolution of the model runs since 2016.

- North-Africa, where biomass burning as well as biogenic sources largely contribute to HCHO and its precursors. Satellite observations over North-Africa tend to be slightly overestimated by IFS-CB05 chemistry model runs since 2014 and also the latest higher resolution model versions since July 2016.

- Indonesia, where HCHO is also dominated by biogenic sources and biomass burning. Old MOZART based model versions generally overestimated satellite values here (by a factor of 3 – 4 in the second half of 2010) and failed to reproduce the observed seasonality. This may be due to the use of fire emissions including El Nino years, which experience much larger fire activities. MOZART simulations and observations agreed much better since late 2012. IFS-CB05 runs agree very well with satellite retrieved ones for December 2014 to August 2015. For September and October 2015, satellite retrieved HCHO columns show a pronounced maximum. 2015 was a strong El Nino year, which caused droughts and higher fire activity in

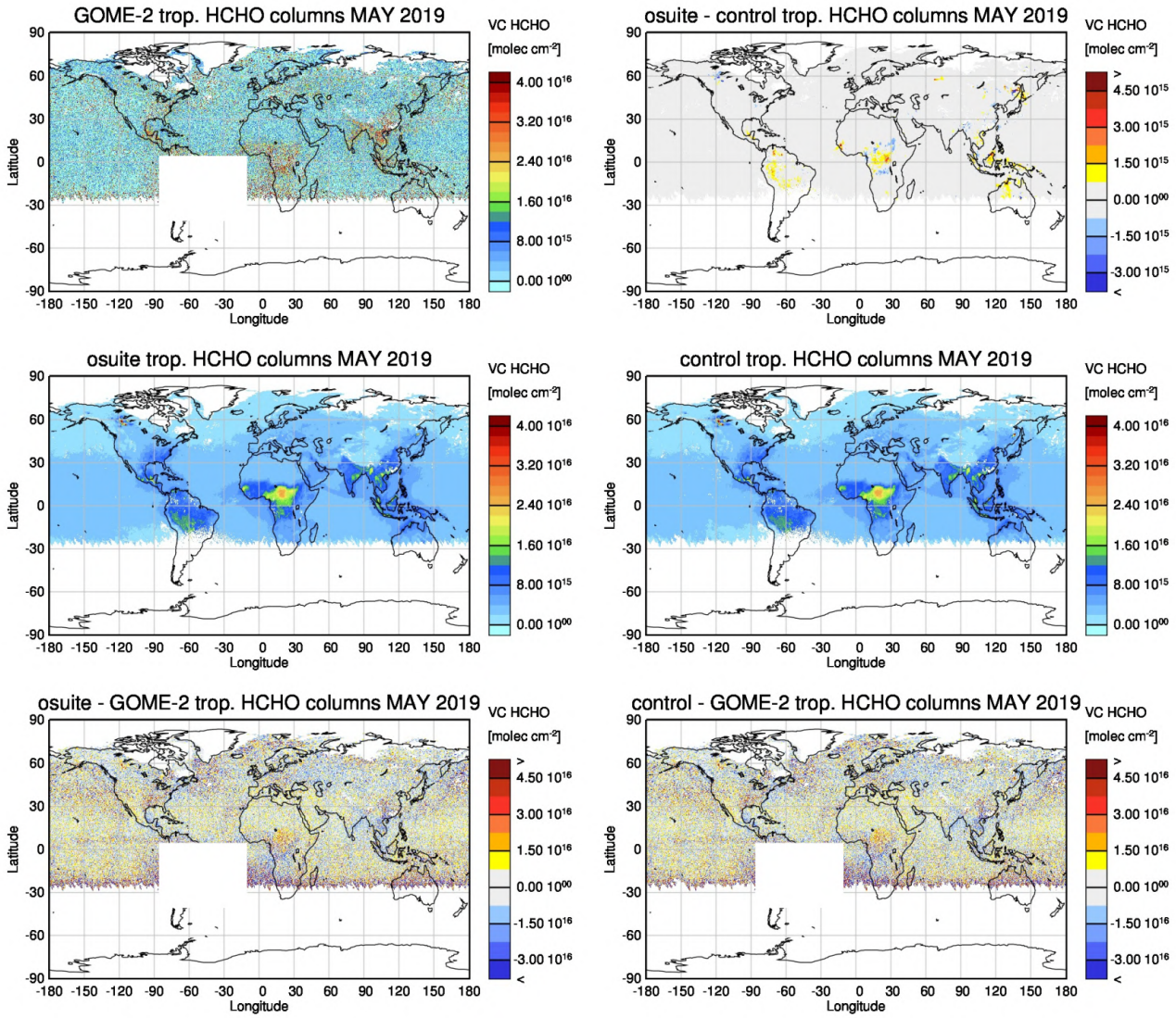

Figure 6.1.1: Global map comparisons of satellite retrieved and model simulated tropospheric HCHO columns [molec cm-2] for May 2019. The top row shows monthly mean tropospheric HCHO columns retrieved by GOME-2, the second row shows the same but for model simulated averages. The third row shows differences of monthly means between models and GOME-2. GOME-2 data were gridded to model resolution (i.e. 0.4° deg x 0.4° deg). Model data were treated with the same reference sector subtraction approach as the satellite data. Satellite retrieved values in the region of the South Atlantic anomaly are not valid and therefore masked out (white boxes in all images except those which show model results only).

Indonesia. As for previous El Nino years, fire emissions used by IFS-CB05 seem to be largely overestimated, resulting in model-simulated HCHO columns which are almost twice as large as those retrieved by GOME-2. Further investigations (see previous reports) show that this is not caused by cloud flagging applied to the satellite and model data. There is mainly little variation from one month to another in both, satellite observations and model simulations since middle of 2016 and the magnitude of model and satellite values agrees overall well, the decrease in retrieved HCHO columns for Dec 17/ Jan 18 and an increase in May 2018 are not reproduced by the simulations.

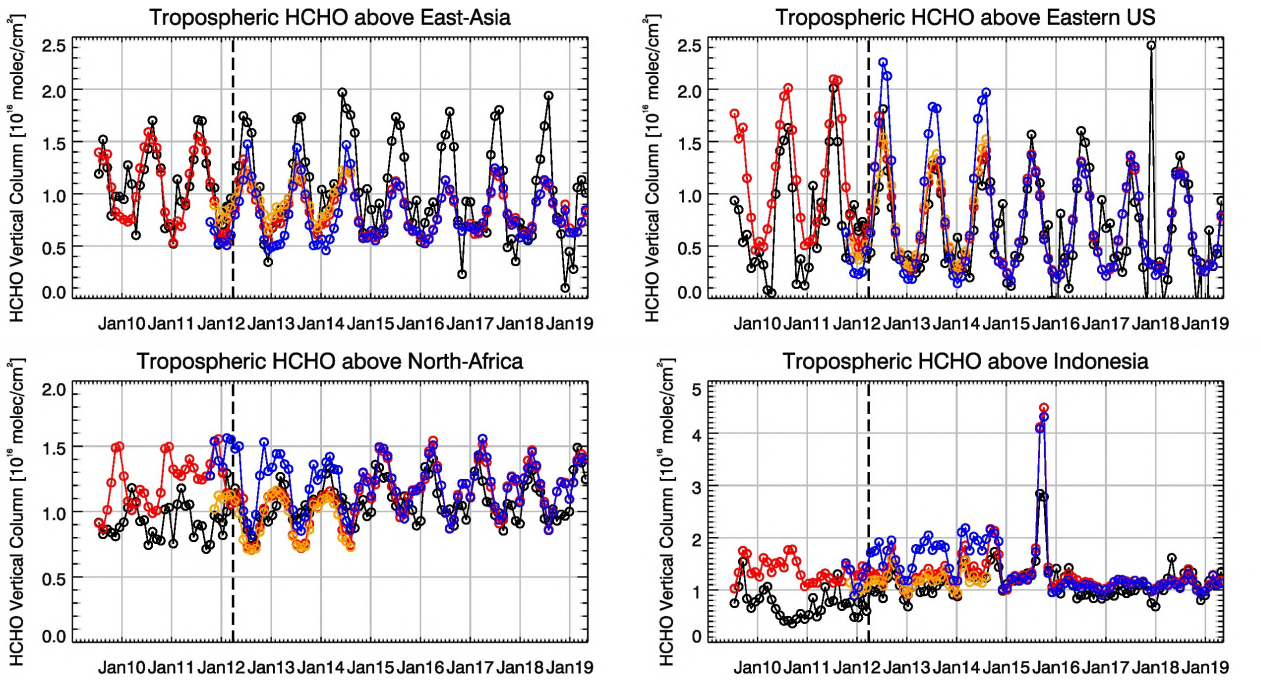

Figure 6.1.2: Time series of average tropospheric HCHO columns [1016 molec cm-2] from SCIAMACHY (up to March 2012, black) and GOME-2 (from April 2012 onwards, black) compared to model results (red - osuite, blue - MACC_fncrt_TM5/MACC_CIFS_TM5/control, orange - MACC_fcnrt_MOZ) for different regions. The blue line shows MACC_fcnrt_TM5 from November 2011 to November 2012, MACC_CIFS_TM5 results from December 2012 to August 2014 and control results from September 2014 onwards (the model run without data assimilation is termed control since Sep 2014). The regions differ from those used for NO2 to better focus on HCHO hotspots: East-Asia (25-40°N, 110-125°E), Eastern US (30-40°N, 75-90°W), Northern Africa (0-15°N, 15°W-25°E) and Indonesia (5°S-5°N, 100-120°E). Negative satellite retrieved values over Eastern US are due to a lack of data (caused by instrument degradation) during Northern Hemisphere winter months for this region. Vertical dashed black lines mark the change from SCIAMACHY to GOME-2 based comparisons in April 2012.

For details on the HCHO evaluation: http://www.doas-bremen.de/macc/macc_veri_iup_home.html

6.2 Evaluation against ground-based DOAS observations

In this section, we compare the HCHO columns of the CAMS products with UVVIS DOAS measurements at Uccle, Cabauw and De Bilt.[2] These ground-based, remote-sensing instruments are sensitive to the HCHO abundance in the lower troposphere. Tropospheric HCHO profiles and columns are validated (up to 3.5km (Uccle) or 10km (Cabauw and De Bilt)). A description of the instruments and applied methodologies is the same as for the MWR O_3 and FTIR O_3 and CO validations see http://nors.aeronomie.be. It is important to mention here that the model partial column values are calculated for the smoothed model profiles. This guarantees that the model levels where the measurement is not sensitive do not contribute to the observed bias. We should mention that the measurement data is catalogued as rapid delivery and not in the consolidated NDACC database.

[2] No contribution from Reunion, Xianghe and OHP due to instrument failure.

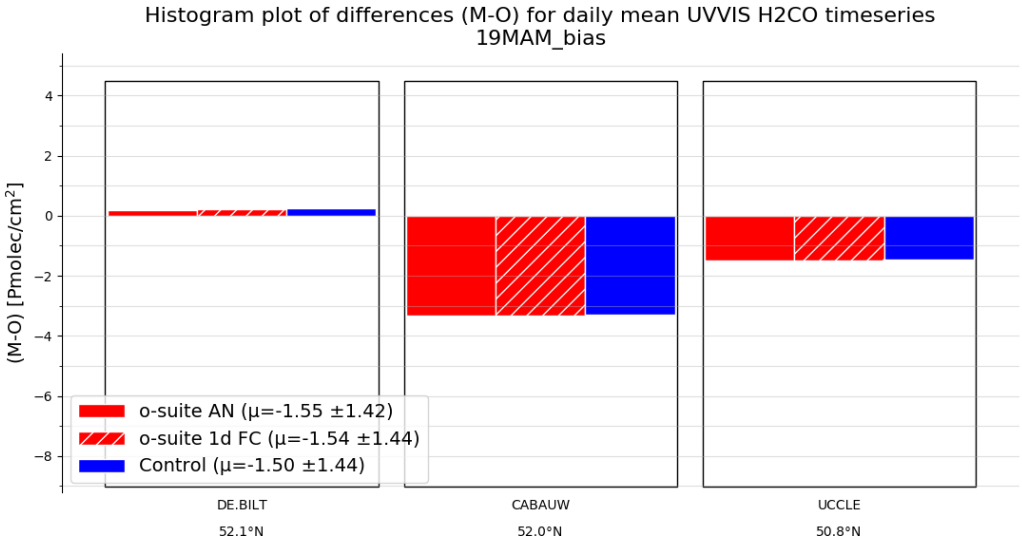

Figure 6.2.1: Table diagram showing the seasonal absolute bias in MAM 2019 for three stations, sorted by latitude. Fig. 6.2.1 shows the absolute biases March - May 2019 at the different sites and indicates nearly vanishing bias for the different sites. At Cabauw and De Bilt the underestimation has decreased during the SON 2018 period and in November 2018 the bias has changed sign (Fig 6.2.2): the HCHO abundance decreased due to less production and this seasonal variation is not fully captured by the model. From Fig. 6.2.1 and 6.2.2 we see little difference between the o-suite and the control run. Although the background column values are well captured by the products, the high emission events are not.

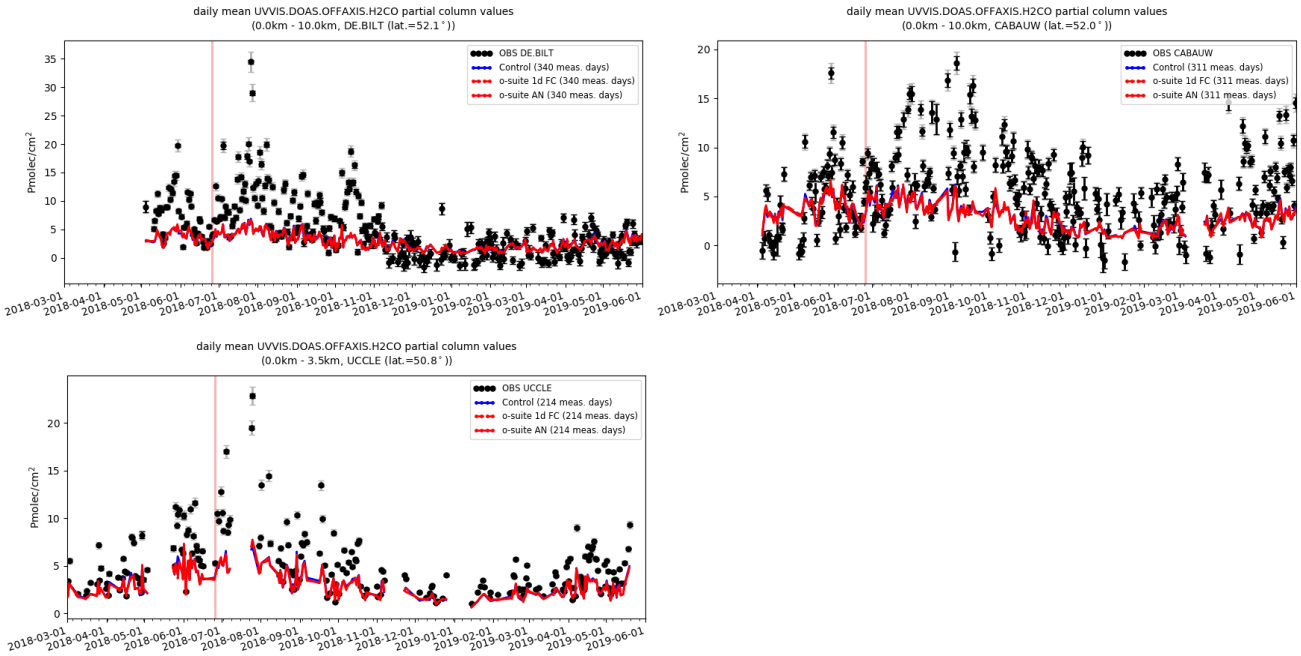

Figure 6.2.2: Time series of H2CO partial columns at the five different sites. All CAMS products underestimate the H2CO concentrations, except at De Bilt, where the model overestimates during the winter months.

7. Aerosol

7.1 Global comparisons with Aeronet and EMEP

The comparison of the CAMS simulation of time series of aerosol optical depth can be found for all Aeronet stations at: http://aerocom.met.no/cams-aerocom-evaluation/

More detailed evaluation including scores, maps, scatterplots, bias maps and histograms illustrating the performance of the aerosol simulation in the IFS system are made available through the AeroCom web interface. The model run can be compared here to e.g. the CAMS interim reanalysis and other models, such as the AeroCom Median model.

Correlation, based on daily aerosol optical depth and NRT Aeronet observations, has been rather stable recently. The o-suite forecast at +3 days shows only slightly lower correlation. See figure S3.

Part of the month-to-month variation in correlation is due to the varying quality and coverage of the Aeronet network. This has been improved by the version 3 from Aeronet. We use therefore version 3 level 1.5 for all global comparison to Aeronet.

The performance of the o-suite model exhibits some seasonal variation in AOD depending on region (Fig. 7.1.1). Noteworthy is the persistent AOD overestimation over North America (Fig. 7.1.1-bottom), but also a long-term trend to overestimation in East Asia. The latitudinal display of model and Aeronet AOD in the period investigated here (Fig. 7.1.2) shows a specific positive bias against Aeronet in the Southern Hemisphere.

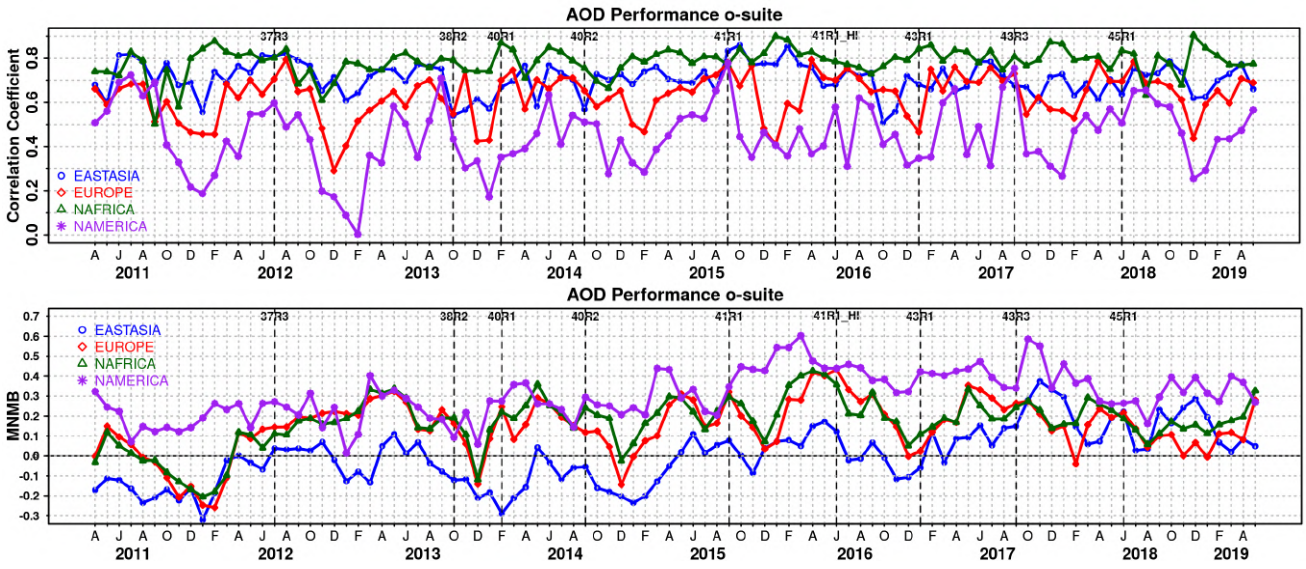

Figure 7.1.1. (top) Correlation coefficient and (bottom) modified normalized mean bias (MNMB) in AOD, since 2011, based on daily AOD comparison (Aeronet V3 level 1.5 data) in four world regions [East-Asia (blue); Europe (red); North Africa (green); North America (purple)] for the o-suite.

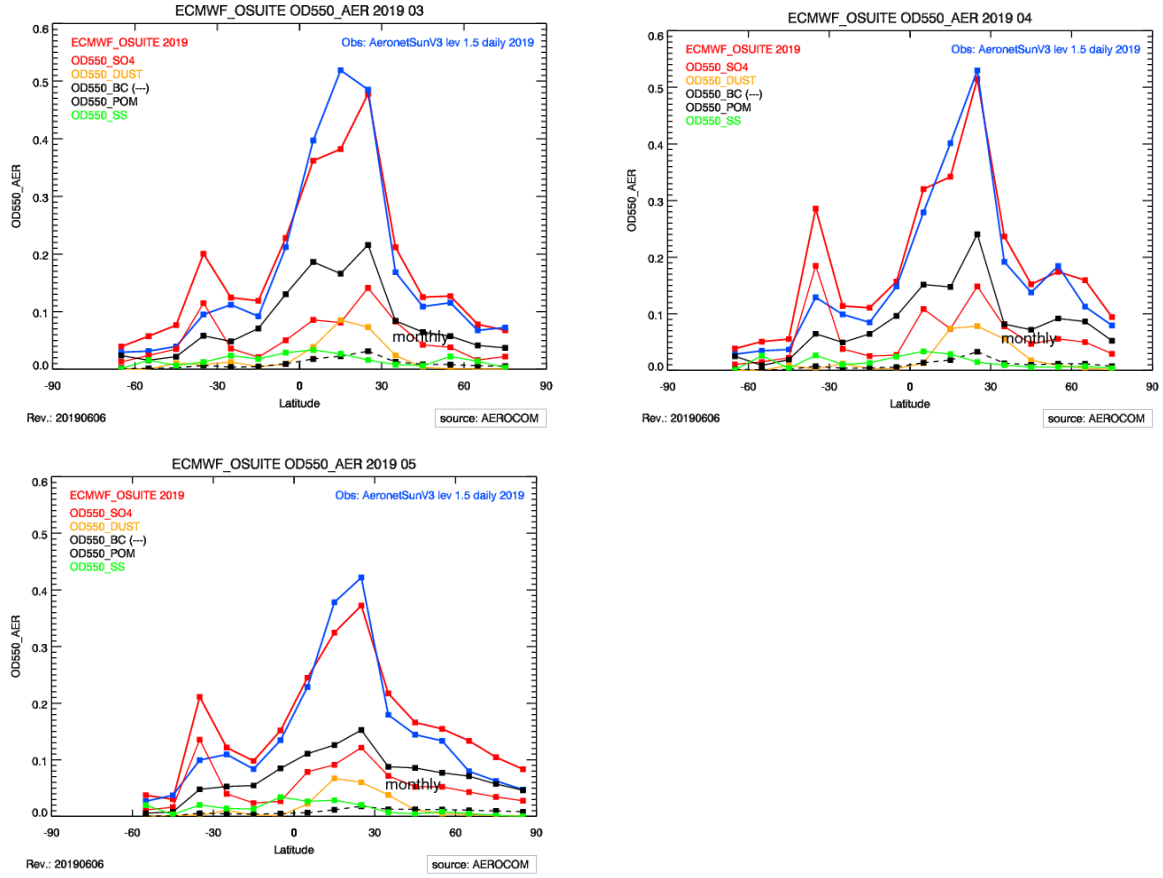

Figure 7.1.2. Aerosol optical depth of o-suite (red) compared to latitudinally aggregated Aeronet V3 level 1.5 data (blue) for the three months covered by this report.

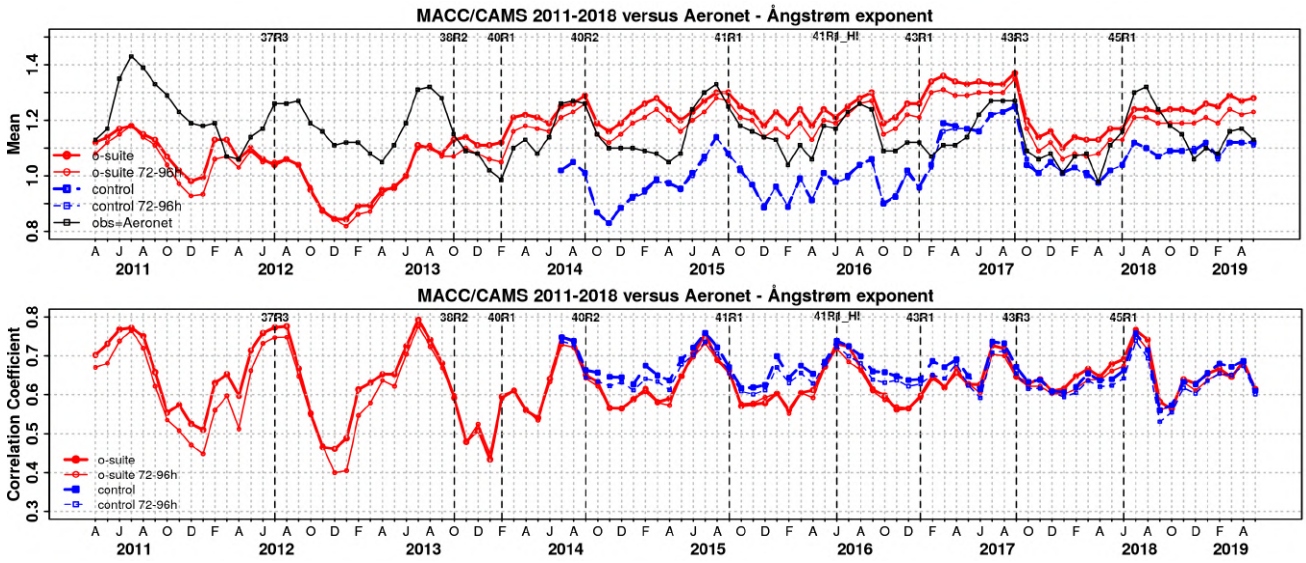

Figure 7.1.3. a) (top) Evolution of mean Ångström exponent in o-suite and control at Aeronet sites (Aeronet V3 level 1.5 data), based on matching monthly mean values. o-suite (thick red curve); o-suite at last forecast day (light red curve); control (blue dashed curve); control at last forecast day (light blue dashed curve). b) (bottom) Correlation using daily matching Ångström exponent.

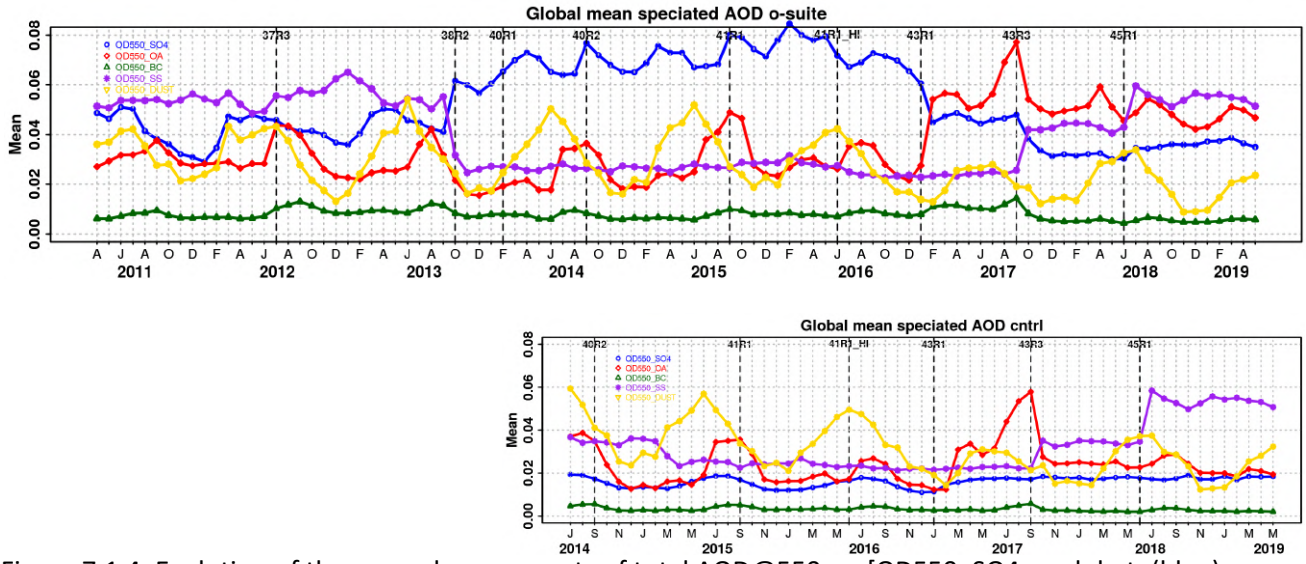

Figure 7.1.4. Evolution of the aerosol components of total AOD@550nm [OD550_SO4 = sulphate(blue); OD550_OA = organics(red); OD550_BC = black carbon(green); OD550_SS = sea salt(purple); OD550_DUST = dust(yellow)] in o-suite and control simulation.

o-suite				
	Mean DJF 2018/19 0-24h	Change wrt to first day on day 4	Mean MAM 2019 0-24h	Change wrt to first day on day 4
AOD@550	0.153	-15%	0.160	-19%
BC-OD@550	0.005	-24%	0.005	-29%
Dust-OD@550	0.011	13%	0.026	2%
OA-OD@550	0.044	-28%	0.054	-29%
SO4-OD@550	0.037	-23%	0.032	-24%
SS-OD@550	0.056	-6%	0.043	-14%

Table 7.1.1. Mean global total and speciated AOD in the o-suite for the last two periods covered by the VAL report and change after 3 forecast days.

The simulated aerosol size distribution may be validated to first order using the wavelength dependent variation in AOD, computed as Ångström exponent, with higher Ångström exponents indicative of smaller particles. We find in MAM 2019 a small bias (Figure 7.1.3-a). Temporal and spatial variability is difficult to capture, but correlation from all daily data is lower than for AOD (Figure 7.1.3-b and S3). Figure 7.1.4 shows that the Sep 2017 and Jun 2018 model changes are responsible for a shift in Ångström exponent. More organic matter seems to shift the size distribution to smaller sizes. The model upgrade in Feb 2017 with a bugfix for sea salt and improved parameterisations for SO4 lead to sea salt increased with 45% while sulphate further decreased a bit. Sea salt has increased further due to a new sea salt emission scheme implemented in the latest model upgrade and is back to earlier 2011-2013 levels.

The o-suite uses data assimilation to obtain an analysis of the aerosol field. In the forecast period, however, a-priori model parameterisations and emissions (except fire emissions, which are kept in

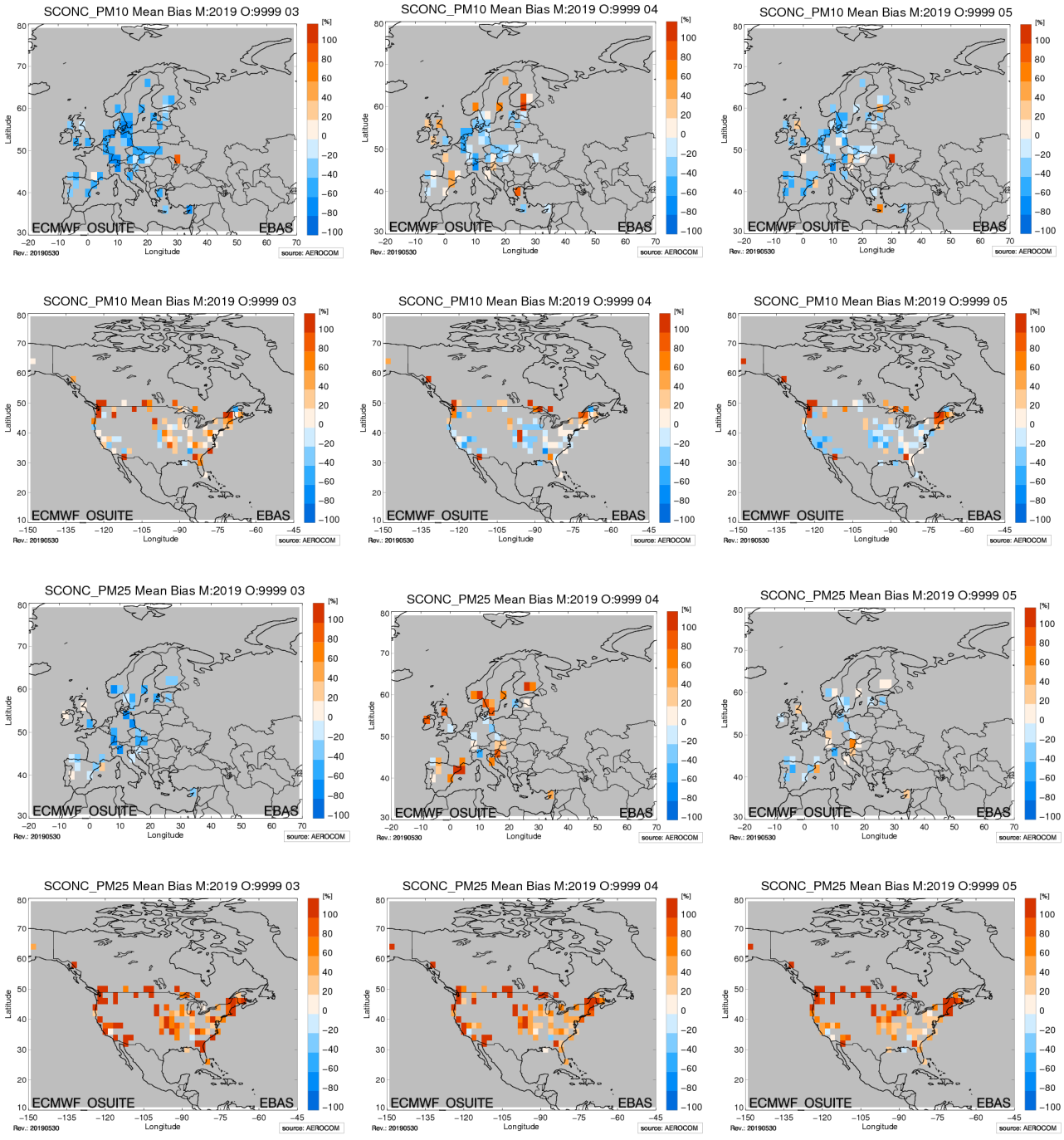

Figure 7.1.5. Bias [%] map of monthly mean PM10 and PM2.5 concentrations at EMEP (Europe, first and third row) and IMPROVE sites (North America, second and fourth row) for March (left column), April (middle) and May 2019 (right); simulated o-suite versus EMEP/IMPROVE derived climatological average (2000-2009).

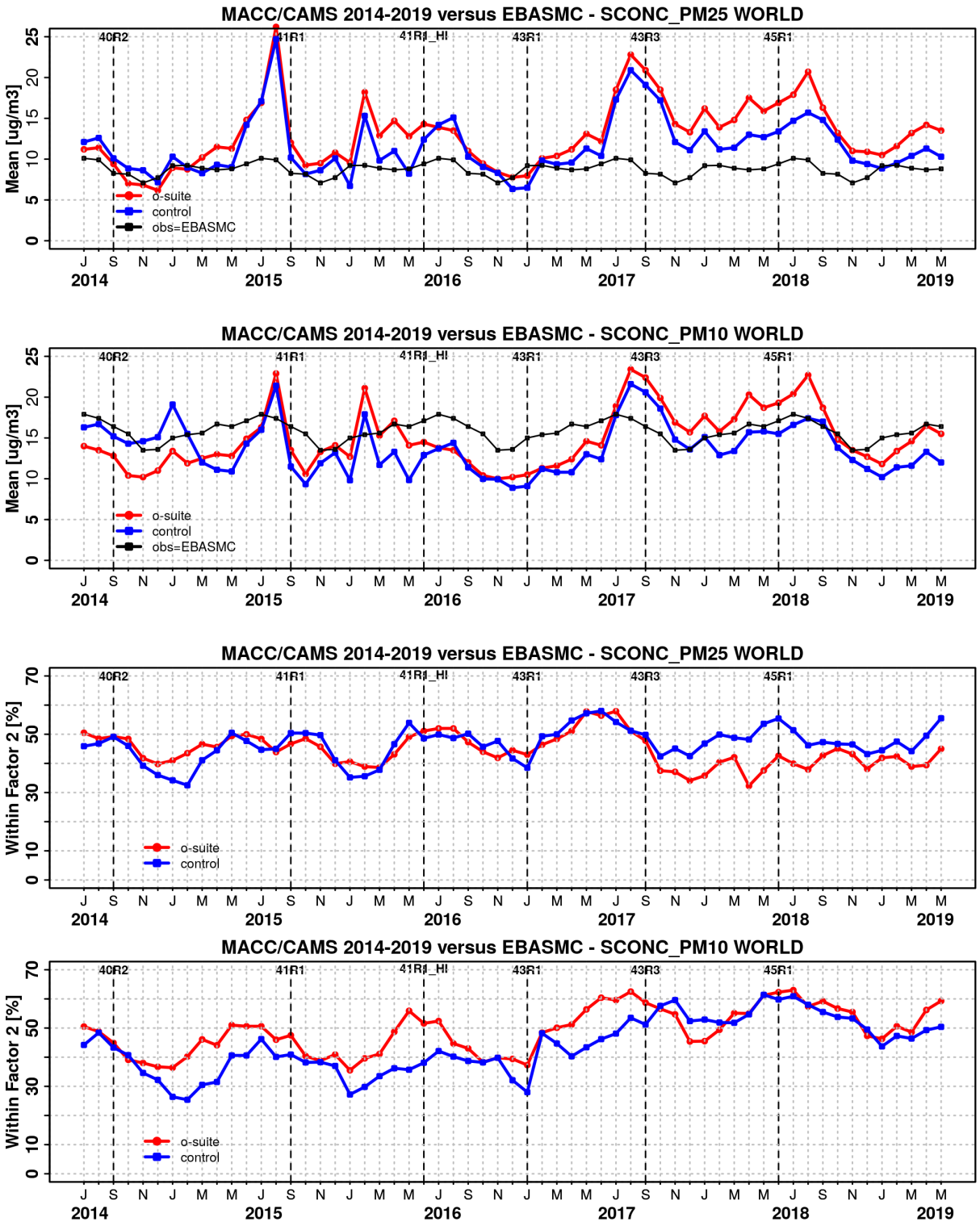

Figure 7.1.6. Temporal evolution of monthly mean average PM25 and PM 10 concentrations at EMEP (Europe) and IMPROVE sites (North America) and data fraction within a factor 2 of observed; ca 160 sites, observed data averaged from data available in EBAS from 2000-2009.

the forecast equal to the latest GFAS emission values) determine increasingly the aerosol fields. The performance of the day three forecasted AOD fields as compared to the first guess is shown in Figure S3 in the summary of this report. Table 7.1.1 shows an average global decrease in total aerosol optical depth during the first four forecast days, dominated by sulphate and organics. The control run with no assimilation shows significant less AOD (-19% compared to o-suite, see figure S3). All this supports the conclusion that either a-priori IFS aerosol and aerosol precursor sources are too small, or sinks are too effective in the IFS model.

Surface concentration of particulate matter below 10 µm (PM10) and below 2.5 µm (PM25) from the o-suite experiment have been validated against data from 160 background IMPROVE and EMEP stations. A climatological average has been constructed from data in the period 2000-2009 as available in the EBAS database hold at NILU. The data availability is not the same at all stations, and sometimes covers only a few years.

A negative MNMB bias of PM10 in Europe and an overestimate in North America PM2.5 appears (Fig. 7.1.5), consistent with the AOD bias in the two regions. Figure 7.1.6 shows the evolution of mean observed and simulated PM10 and PM2.5. The biggest change appeared in July 2017 with the bias of o-suite now becoming positive overall. Shown is also the statistics of being within factor 2, a more robust metrics for a comparison to climatological data. This statistical indicator has clearly improved over time, indicating best PM10 and PM25 performance in summer months for the o-suite. O-suite is also better most of the times than the control simulation for PM10. For PM25 the difference is less clear, but since September 2017 (upgrade to 43R3) the control is performing better than the o-suite.

7.2 Dust forecast model inter-comparison: Validation of DOD against AERONET, and comparisons with Multi-model Median from SDS-WAS

The 72-hour forecasts (on a 3-hourly basis) dust aerosol optical depth (DOD) from CAMS o-suite and control have been validated for the period 1 March – 31 May 2019 against AERONET cloud-screened observations, MODIS/Terra and Aqua Collection 6.1 Level 3 (1º x 1º) and SDS-WAS Multi-model Median DOD. The SDS-WAS Multi-model Median DOD is obtained from (currently) twelve dust prediction models participating in the Sand and Dust Storm Warning Advisory and Assessment System (SDS-WAS) Regional Center for Northern Africa, Middle East and Europe (http://sds-was.aemet.es/). As a first time, we are including the AERONET Spectral Deconvolution Algorithm (SDA) product in the comparison. At those sites where the SDA products are available, the dust optical depth (DOD) evaluation considers AODcoarse for the comparison. Coarse fractions of the AOD is fundamentally associated with maritime/oceanic aerosols and desert dust. Since sea-salt is related to low AOD (< 0.03; Dubovik et al., 2002) and mainly affects coastal stations, high AODcoarse values are mostly related to mineral dust.

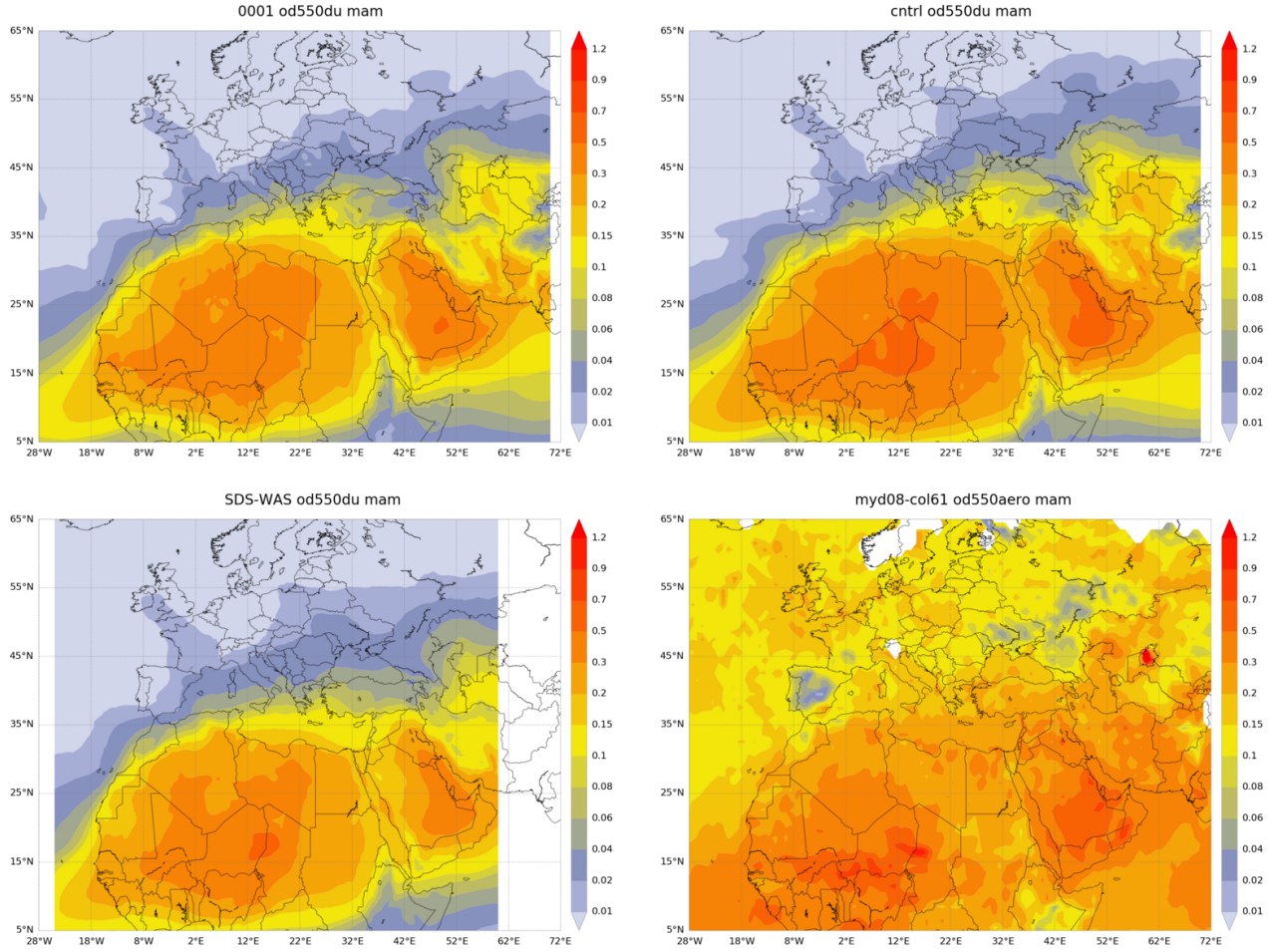

Figure 7.2.1: Averaged DOD 24h forecast from o-suite (top left) and control (top right), DOD of the multi-model SDS-WAS Median product (bottom left) as well as AOD from MODIS/Terra Collection 6.1 Level 3 combined Dark Target and Deep Blue product (bottom right) for the study period.

During this season, satellites (see MODIS in Figure 7.2.1) show that major dust activity in Northern Africa (seasonal AOD up to 0.3) is concentrated in latitudes southern of 27ºN with maximum seasonal values (seasonal AOD over 0.7) over the Sahara in the Bodélé Basin, Algeria and the Mali/Mauritania border and in Iraq and south-eastern Arabia Peninsula. In North Africa, both CAMS experiments can simulate the main areas of dust activity in the North Africa in comparison with MODIS (see Figure 7.2.1) although both CAMS experiments overestimates AOD seasonal values in the Eastern Sahara and northern Arabian Peninsula. CAMS o-suite presents lower season values (seasonal DOD up to 0.5) than control (seasonal DOD up to 0.7) which are in general higher than the SDS-WAS multi-median product. Otherwise, dust transport over the North Atlantic region and the Red Sea appears underestimated in comparison with the satellites (particularly in o-suite). Neither the CAMS experiments nor the SDS-WAS multi-model are capturing the maximum AOD seasonal values observed over Cape Verde (up to 0.3).

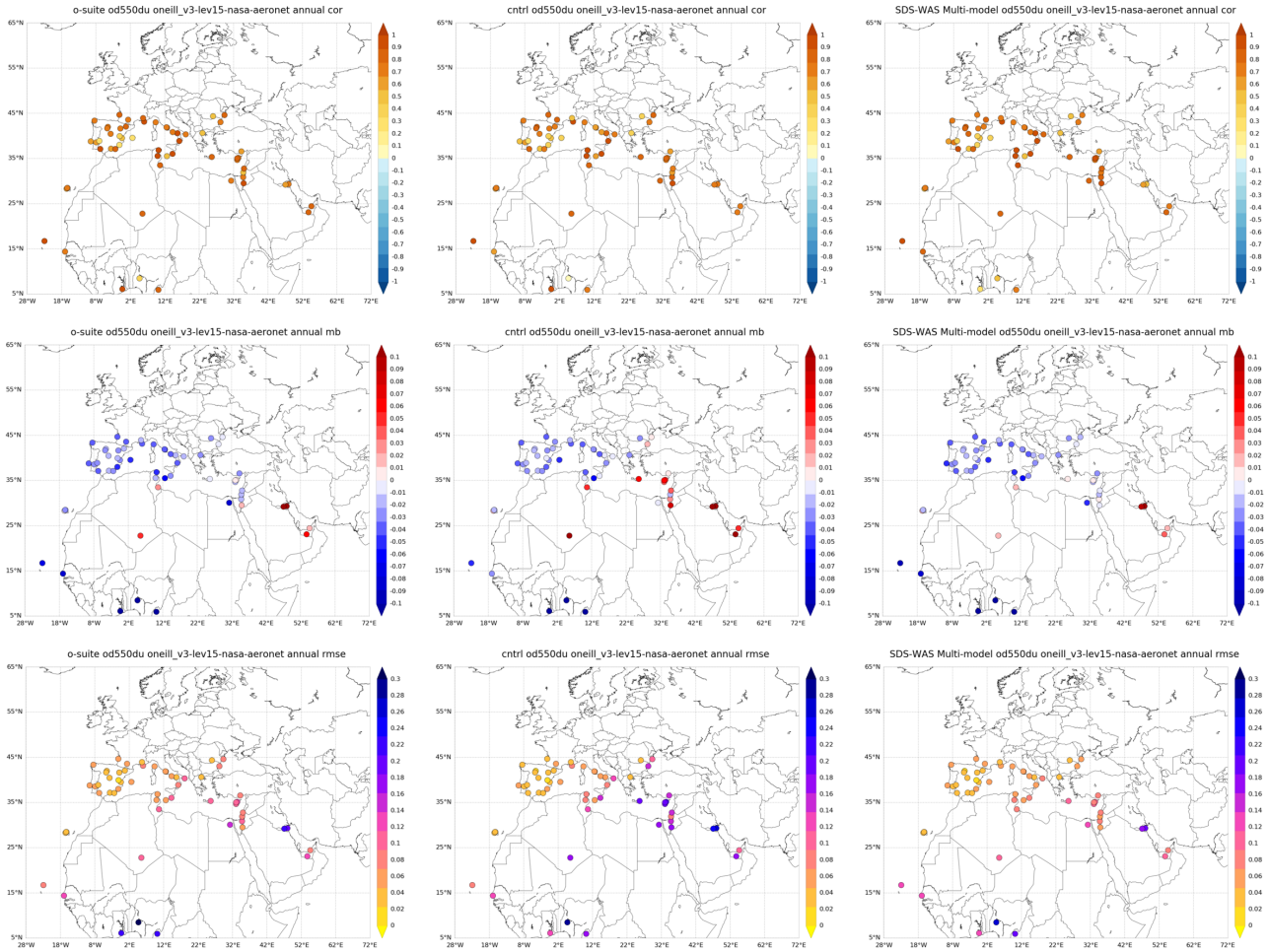

Figure 7.2.2: Skill scores (correlation coefficient, MB and RMSE) for 24-hour forecasts of CAMS o-suite (left column), control (central column) and DOD Multimodel SDS-WAS Median (right column) for the study period. AODcoarse from AERONET SDA is the reference.

For March to May, the o-suite reproduces the daily variability of AERONET observations (see Figure 7.2.2) with a correlation coefficient of 0.84, averaged over all the AERONET sites (as in the case of the SDS-WAS multi-model that achieves values of 0.85), this is close to the control experiment that shows a correlation coefficient of 0.82. Regarding mean bias (MB), both CAMS experiments (o-suite and control), as well as the SDS-WAS Multi-model, underestimate the AERONET observations resulting in an MB of 0 for control, -0.02 for o-suite and the SDS-WAS multi-model. The Tropical North Atlantic (see Capo Verde in Figure 7.2.3) and Central Mediterranean (see Tunis Carthage in Figure 7.2.3) are region has the best results in the AERONET comparison in terms of correlation. Both experiments can reproduce the daily variability with a correlation coefficient of with values of 0.94 and 0.90, respectively Tropical North Atlantic and Central Mediterranean for o-suite and with values of 0.91 and 0.89, respectively for control.

Over the Sahara (see Tamanrasset INM in Figure 7.2.3) both CAMS experiments show closer results with a correlation coefficient of 0.82 for control and 0.84 for o-suite although o-suite shows slightly higher overestimation (MB of 0.05) than the control experiment which tends to overestimate the

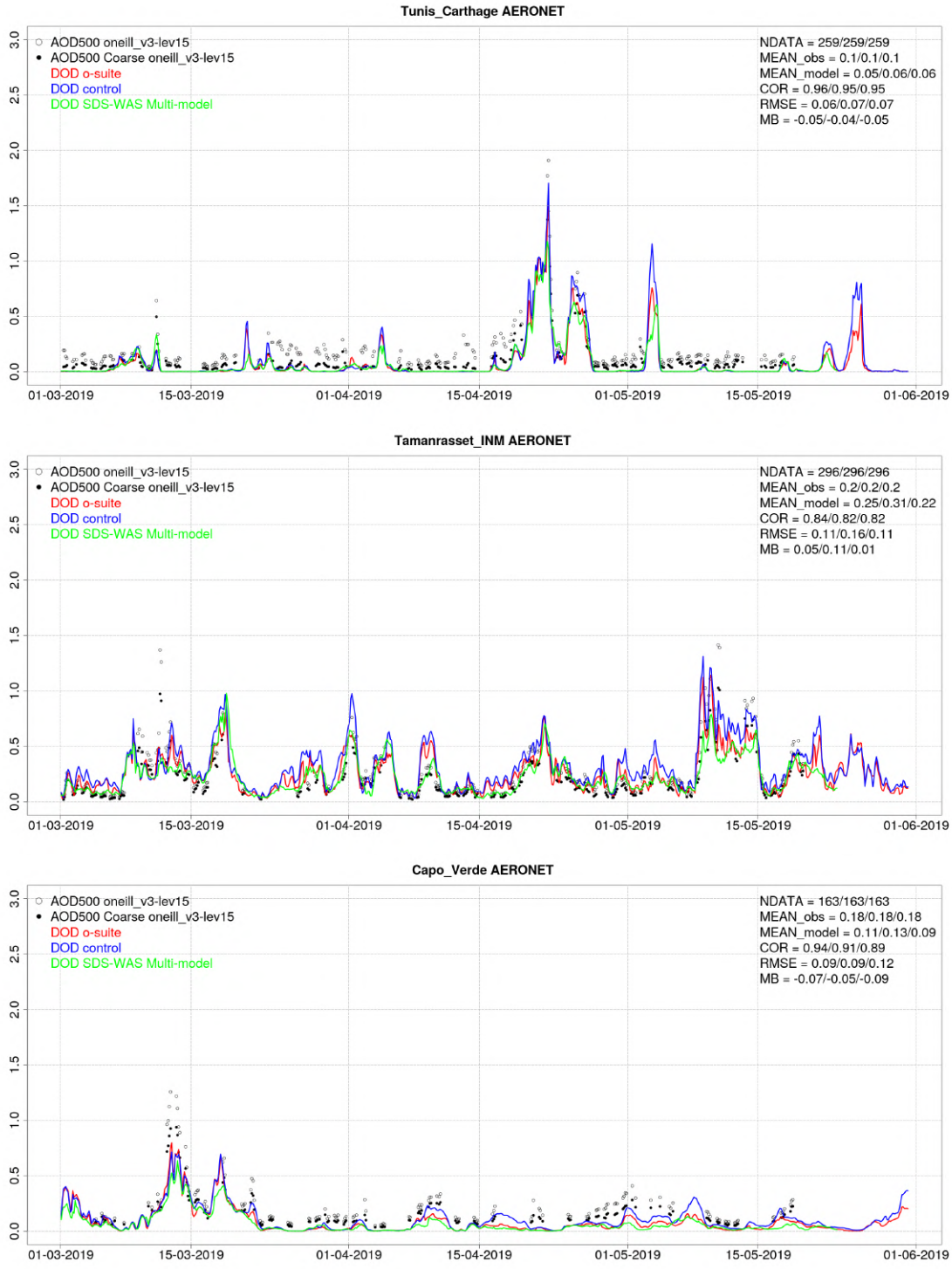

Figure 7.2.3a: AOD and AODcoarse from AERONET (black dots), DOD o-suite (red line), DOD control (blue line) and DOD Multimodel SDS-WAS Median (green line) for the study period over Tunis Carthage (North Western Magrebh), Tamanrasset_INM (Sahara) and Capo Verde (Tropical North Atlantic). Skill scores per each individual site and model (o—suite/control/SDS-WAS Multi-model) are shown in the upper right corner (NDATA: available 3-hourly values used for the calculations, MEAN observations, MEAN_model, COR, RMSE, MB).

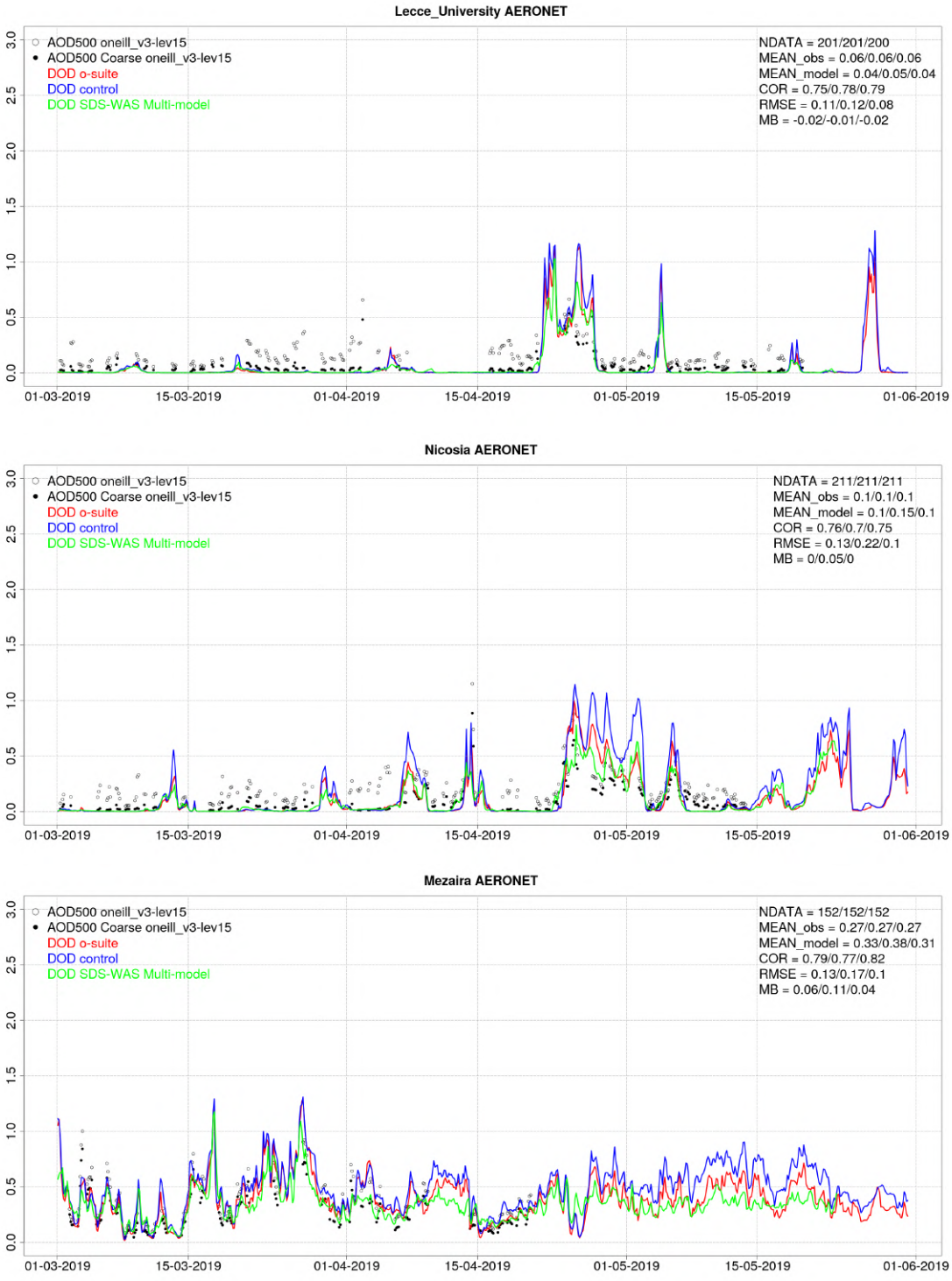

S

Figure 7.2.3b: AOD and AODcoarse from AERONET (black dots), DOD o-suite (red line), DOD control (blue line) and DOD Multimodel SDS-WAS Median (green line) for the study period over Lecce University (Central Mediterranean), Nicosia (Eastern Mediterranean) and Mezaira (Middle East). Skill scores per each individual site and model (o—suite/control/ SDS-WAS Multi-model) are shown in the upper right corner (NDATA: available 3-hourly values used for the calculations, MEAN observations, MEAN_model, COR, RMSE, MB).

AERONET observations (MB of 0.11). o-suite presents slightly lower skills scores than the SDS-WAS Median Multi-model that shows a correlation coefficient of 0.82 for the Sahara, although it underestimates the observations with an MB of 0.01. In the Sahel (see Figure 7.2.2), the o-suite shows strong underestimations (MB of -0.12, slightly higher than control with MB of -0.06) although the o-suite better reproduces the observed daily variability (with a correlation value of 0.53 for o-suite in comparison of for control that has a correlation of 0.45). The underestimations observed in o-suite in the Sahel are also spread to the Tropical North Atlantic (MB of -0.07 for o-suite) in agreement with the underestimation also observed in comparison with MODIS (Figure 7.2.1).

In the Middle East (see Figure 7.2.2 and the Mezaira AERONET site in Figure 7.2.2), o-suite better reproduces the daily variability than control (with a correlation coefficient of 0.73 for o-suite and 0.71 for control) and the SDS-WAS Multi-model presents lower correlations (0.63). Overestimations are observed in both CAMS experiments (MB of 0.14 for control and 0.17 for o-suite). Spring is the season with maximum dust activity in the Middle East.

Both CAMS models present high correlations between 0.75 and 0.90 over the Iberian Peninsula and the Mediterranean (except in the Western Iberian Peninsula in which correlation drops up to 0.50 for o-suite (see Figure 7.2.2). This is related to the low aerosol concentration levels during this season in this region. Otherwise, slight underestimations (MB between -0.03 and -0.01) are observed over these regions except in the Eastern Mediterranean region where slightly overestimations are observed in o-suite (MB of 0.03). In this region, both CAMS experiments tend to overestimate the maximum DOD peaks observed (see Nicosia in Figure 7.2.3).

The comparison of 1 to 3-day forecasts shows that the prediction is stable during the 3-days forecasts with correlation coefficients of 0.84 (0.82), 0.82 (0.81), and 0.79 (0.79) respectively for 24, 48 and 72h forecasts for all the sites for o-suite (control) and MB of -0.02 (0), -0.02 (0) and -0.01 (0) respectively for 24, 48 and 72h forecasts for all the sites for o-suite (control).

7.3 Backscatter profiles

The technical specifications of the data sources, the evaluated parameters and the methods are described in Eskes et al. (2018). In this section, the temporal and vertical variation of the backscatter coefficient (BSC) profiles are evaluated, showing the statistics including bias, correlation, and standard deviation of the o-suite and control run versus ceilometers. These scores are summarized in Taylor plots.

Period Overview

The model aerosol optical depth (AOD) and ceilometer overviews exhibit periods with significant aerosol plumes over Germany. Figure 7.3.1 shows the maximum AOD over Germany, separately for contributions of mineral dust (SD), sea salt (SS), carbonaceous matter (CM), black (BC) and organic carbon (OC), as well as sulfate (SU). Weak SD events, e.g. 20 April 2019 and several days with elevated sulfate and sea salt stick out. All components follow their usual seasonality.

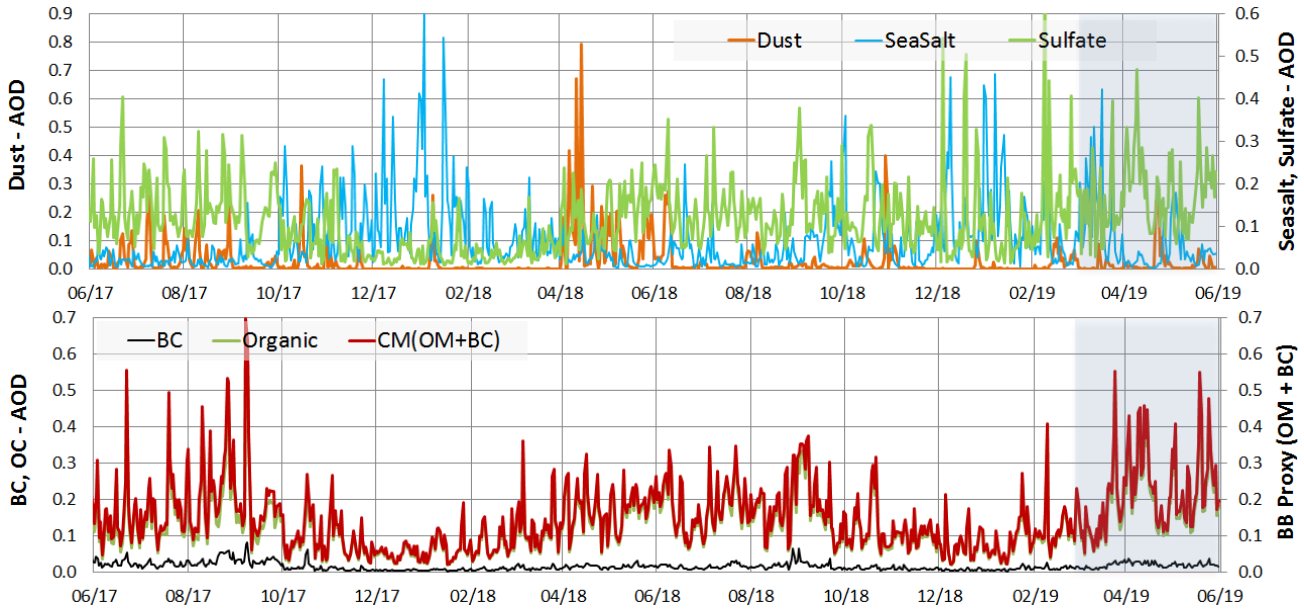

Figure 7.3.1: Maximum daily AOD over Germany for aerosols included in the IFS model from 06/2017 - 05/2019: sea salt (blue), dust (orange), sulfate (light green), black carbon (BC, black), organic matter (green), proxy for 'biomass burning' (as OC+BC - red). Note the different y-axes for the aerosol species.

Mean profiles

Model BSC in the PBL are on average lower than observed. The annual variation of the PBL height is rudimentary reproduced but is strongly smoothed. While enhanced emissions of organic matter (OM) have been introduced in Jan 2017, and parametrizations of SO_2/SO_4 conversion/deposition were improved, nitrate and ammonia are still missing in the current model version, which contribute roughly 10-30% of aerosol mass (as NO_3NH_4 or $(NH_4)_2SO_4$) in the rural central European PBL. (According to pers. communication - S. Remy/Z. Kipling - nitrates and ammonium are ready in the current model and possibly get activated in the next cycle). Technically, this could be compensated by assimilating observational data for run 0001, but without profile information this results in a vertical redistribution with a positive bias in the free troposphere, a too smooth transition at the PBL top (Fig. 7.3.2 and Fig. 7.3.3) and a negative bias in the PBL. Thus the assimilation increases aerosol loads in run 0001 relative to the control run (gsyg, gzhy), but does not introduce a realistic step at the top of the PBL to lower values in the free troposphere (FT) evident in the ceilometer profiles. Therefore, the amplitude of the vertical profile of the model compared to observations (reference), coded in the standard deviation in the Taylor plots, is too low.

Secondly, our forward operator (including mass→volume conversion) presently uses particle densities of the pure materials, not taking into account that dry aged atmospheric particles are often porous (sponge-like, even fractal) with entrapped air owing to coagulation and variable internal mixing, and thus exhibit reduced bulk density. A high-biased particle density results in low-biased equivalent particle volume, and a corresponding underestimation of optical properties, because these depend strongly on the particle size. Density reductions for accumulation mode particles, composed of hydrophilic and hydrophobic materials may be as high as a factor 1.5 (~1.3 for surface). Thirdly, the capping transport barrier at the PBL top is less effective in the model,

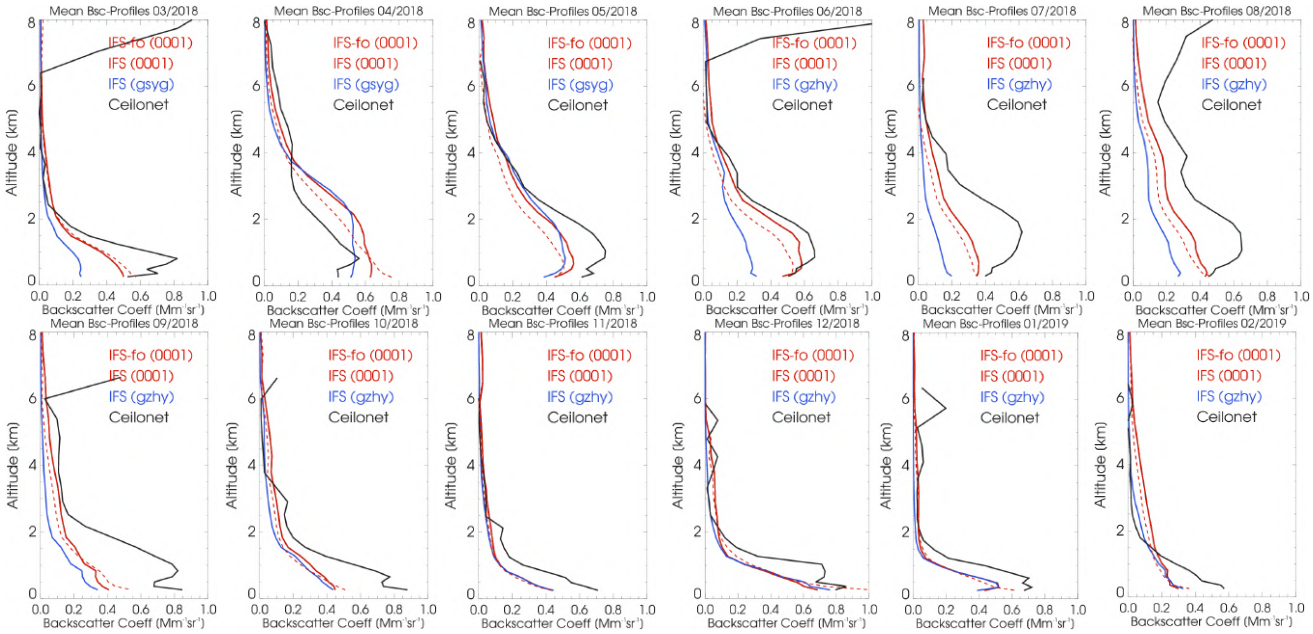

Figure 7.3.2: Monthly mean profiles of backscatter coefficients from o-suite (red), control run (blue), and ceilometers (black) combined from 21 German stations in Jun 2018 to May 2019. The profiles are partly contaminated by remaining cloud artefacts.

diluting high PBL concentrations with clean FT air and vice-versa. On average, however, the PBL height seems reasonable (this has been discussed in an earlier report).

The reason for the difference between mean model profiles calculated from DWD's forward operator DWD-FO and those retrieved from the MARS archive (IFS-FO implemented in the IFS) is still investigated. The look-up table of conversion coefficients (rho, mass-specific extinction, lidar ratio, humidity growth) used by DWD and IFS are nearly the same. However, up to 0.12 Mm-1sr-1 higher monthly mean backscatter is calculated by the DWD-FO in summer - not so in autumn and winter - seemly rather an offset than a factor. Median differences are much smaller (Figs. 3.5.15 vs 3.5.16) indicating that single events cause most deviation, and that the effect is not symmetric to the median state. Changes between summer and winter months hint to temperature, seasonal aerosol (more organics, less sea-salt in summer). In dust-dominated periods (e.g. 07-13 Apr 18), profiles from both FO are consistent. IFS- FO often, but not always, yields higher bsc during sea-salt/organic cases which could point to humidity-dependent hygroscopic growth as a possible source for discrepancy. But humidity and air-density profiles calculated by both FO are about consistent. The clean FT is equally affected like the PBL, and calculating the profiles with overall high (90%) relative humidity by the DWD- FO has little effect. Thus, it seems neither an aerosol nor a humidity effect. Often shallow layers are smoothed in the IFS-FO profiles (~1-3 km in April 2018). For sea-salt the relative behaviour of both FO seems not systematic. This issue remains under investigation.

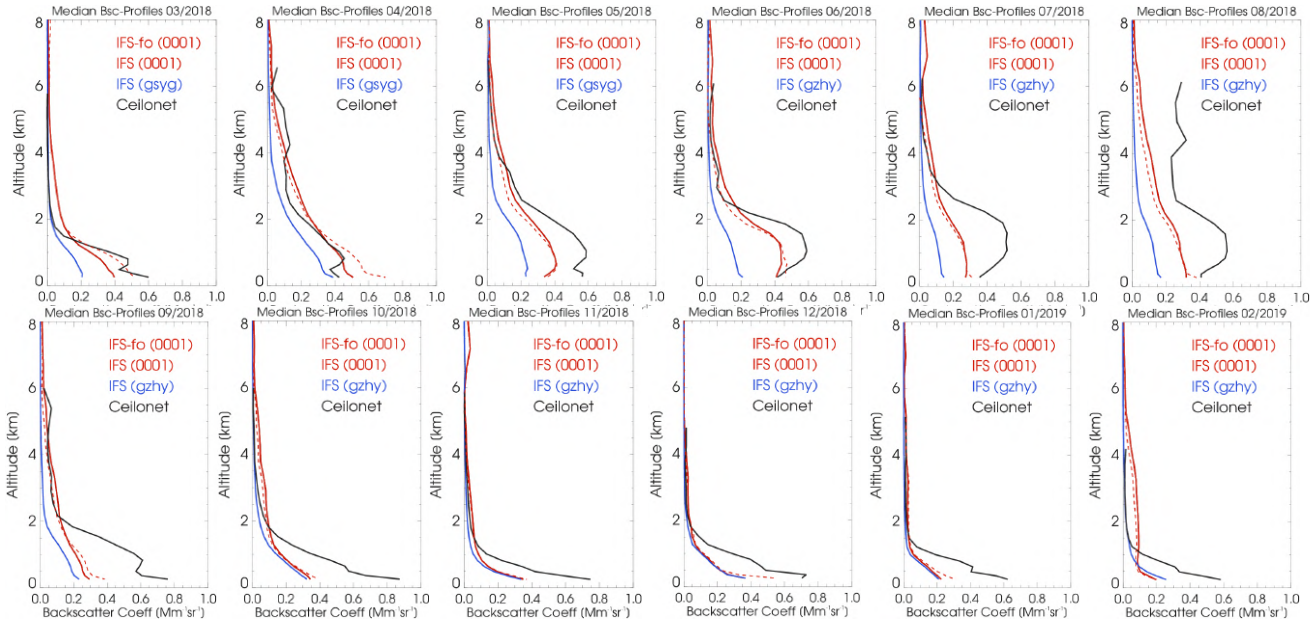

Figure 7.3.3: Monthly median profiles of backscatter coefficients from o-suite (red), control run (blue), and ceilometers (black) combined from 21 German stations in Jun 2018 to May 2019. The profiles are partly contaminated by remaining cloud artefacts.

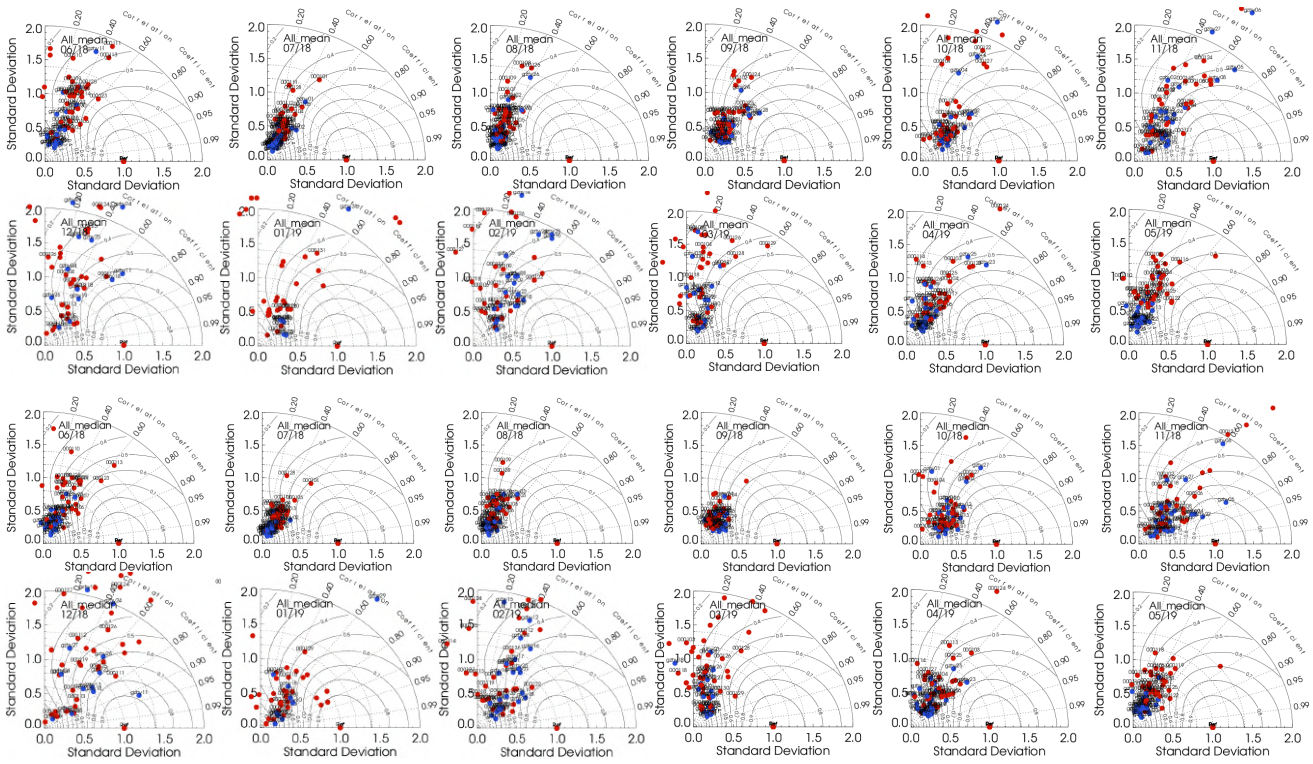

Fig. 7.3.4: Taylor polar plots with daily average standard deviation of vertical profiles vs correlation coefficient, averaged over 21 German ceilometer sites for Jun 2018 – May 2019. O-suite red, control blue. Top: mean values, Bottom: median values.

Taylor Plots

The average coefficient of correlation between modelled and observed vertical backscatter profiles clusters around r = 0.4-0.6. The absolute standard deviation (SD) are normalized to the SD of observations per day, as reference value at SD ≡ 1.0. In summer 2018, the o-suite (red dots) performs better than the control run (blue dots) in terms of SD (profile amplitude), which becomes less marked during autumn and winter but re-appears in summer 2019. There is a large day-to-day and also a seasonal variation of the performance. Individual cases suggest that the large spread and the high bias, observed on many days in winter (Dec, Jan) is due to layers with high sea-salt concentrations.

7.4 Aerosol validation over the Mediterranean

Three-hourly aerosol optical depth (AOD) and surface concentration (PM10 and PM2.5) from o-suite experiment and control experiment have been validated for the period 1 March 2019 – 31 May 2019 against AERONET direct-sun cloud-screened observations.

Aerosol optical depth

CAMS o-suite can reproduce the daily variability of AERONET observations. In Western, Central and Eastern Mediterranean, the correlation coefficient moves from 0.66, 0.85 and 0.76, to 0.53, 0.83 and 0.72, respectively for control and o-suite during spring (see the correlation coefficient by sites in Figure 7.4.1). Overestimations observed in the Mediterranean Basin in control (MB of 0.03, 0.06 and 0.12 for Western, Central and Eastern Mediterranean regions respectively) are slightly corrected in o-suite for Eastern Mediterranean (0.09 for Eastern Mediterranean) although introduce higher overestimations in Central-Western Mediterranean (MB of 0.08 and 0.11 for Western and Central Mediterranean regions respectively) as it is shown in Figure 7.4.1. The highest peaks on CAMS AOD simulations are linked to desert dust intrusions that both CAMS experiments reproduce the timing of the arrival of the dust plume correctly although o-suite better captures the intensity of the most intense events, reducing the overestimations observed in control (see Palma de Mallorca, Messina and IMS-METU-ERDEMLI AERONET sites in Figure 7.4.2). Otherwise, o-suite tends to increase the background aerosol levels during non-dust dominated days.

Surface aerosol concentrations

For spring, PM10 and PM2.5 results of CAMS o-suite and control show similar skill scores in comparison with EIONET-Airbase observations on 3-hourly basis (see Figure 7.4.3, Figure 7.4.4 and Figure 7.4.5) with PM10 and PM2.5 close to the observations with an annual MB in average for all the sites of 27.01 (26.31) and 11.47 (13.43) $\mu g/m^3$, respectively for PM10 and PM2.5 for o-suite (control). Aerosol events (PM > 50 $\mu g/m^3$) in the Mediterranean sites observed in control are corrected in o-suite reducing the observed PM peaks around 50% (see Sa Pobla, Bastia Giraud, Venaco in Figure 7.4.5). The only exception is the event during 18-23 April in which o-suite predicts higher PM values than control achieving PM10 values over 220$\mu g/m^3$.

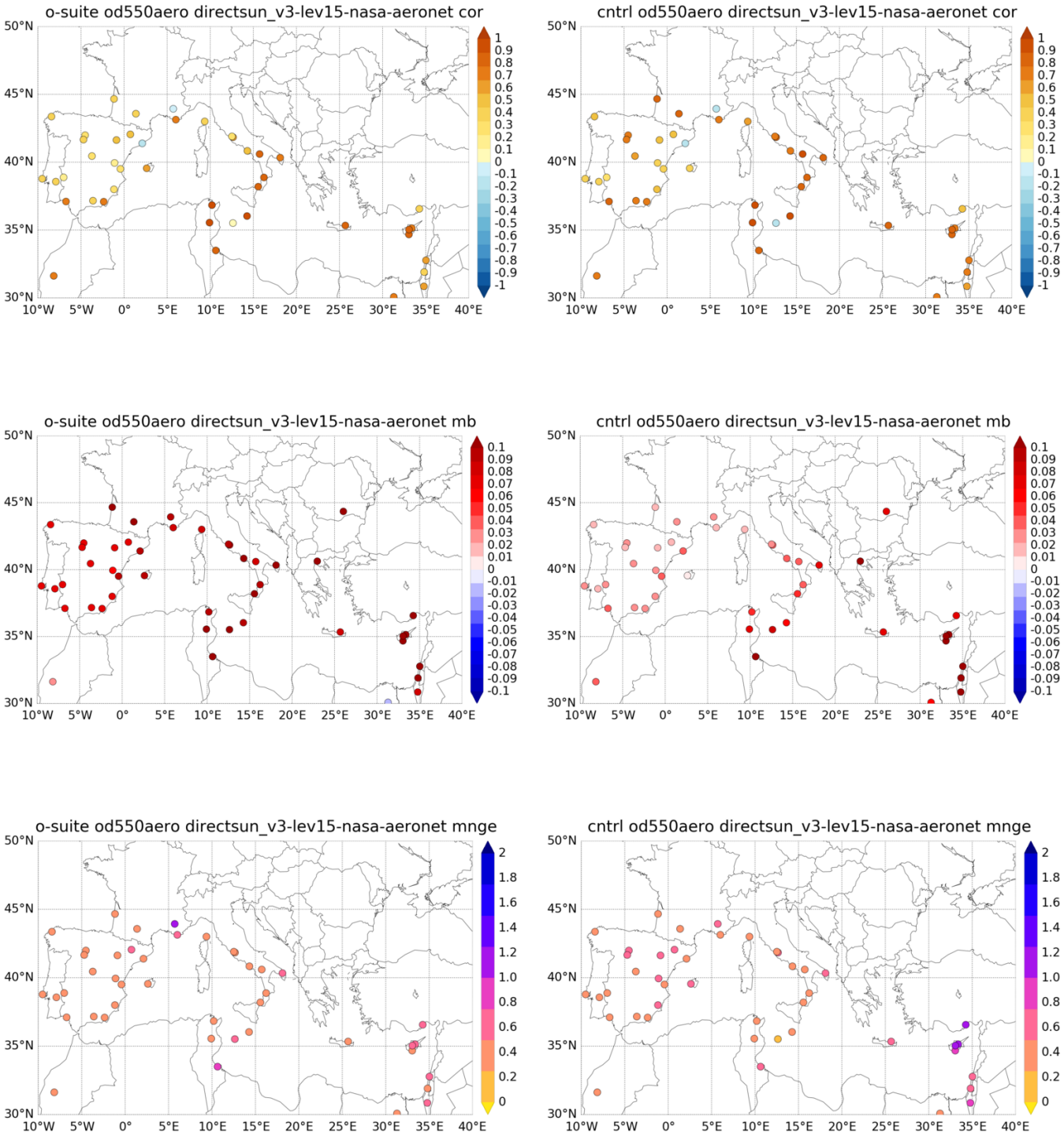

Figure 7.4.1: Skill scores (correlation coefficient, MB and FGE) for 24-hour forecasts of CAMS o-suite and control for the study period. AOD from AERONET is the reference.

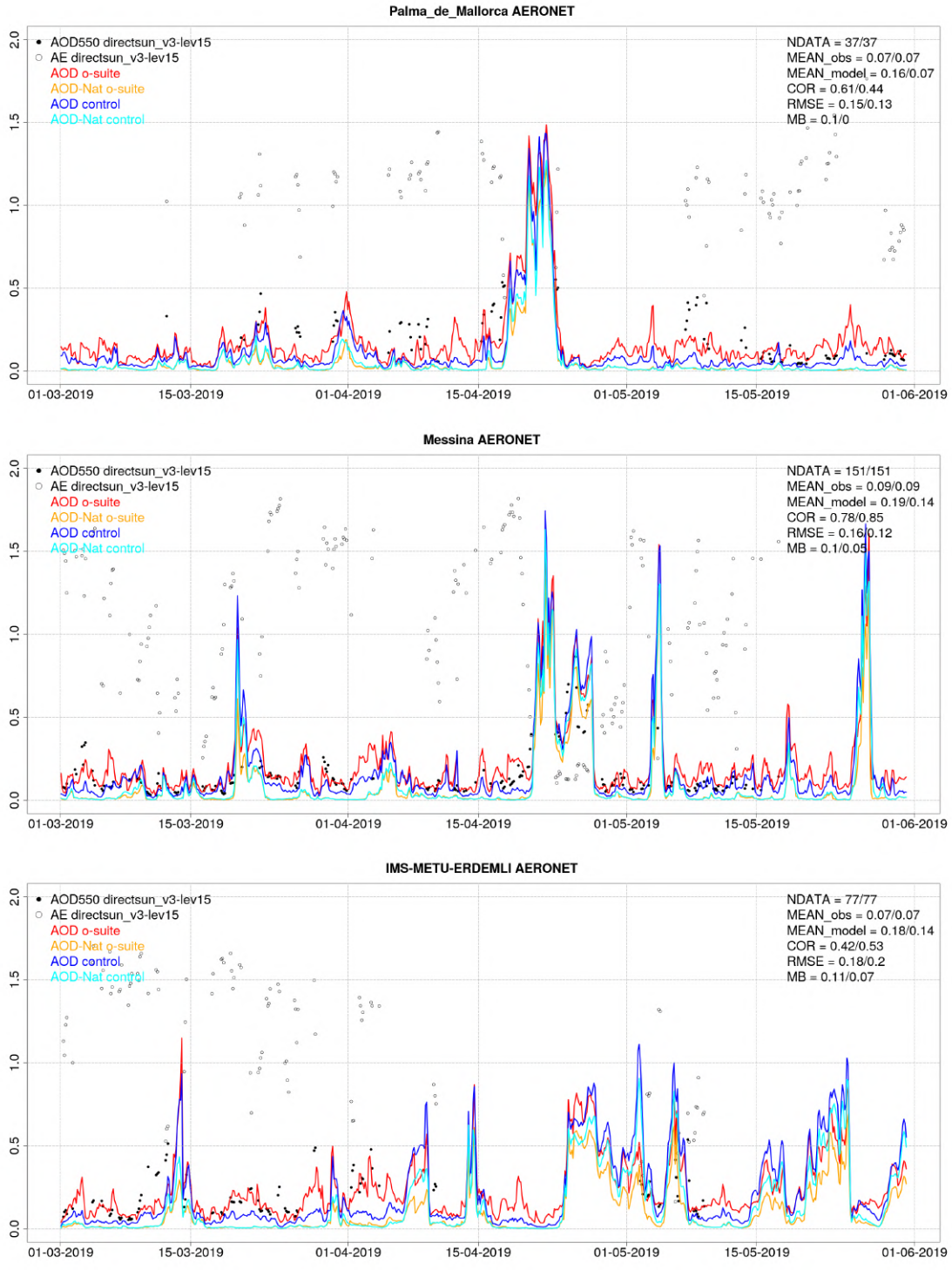

Figure 7.4.2: AOD from AERONET (black dot), AOD o-suite (red line), AOD control (blue line), AOD-Nat o-suite (orange line), AOD-Nat control (cyan line), for the study period over Palma de Mallorca (Balearic Islands, Spain), Messina (Italy) and IMS-METU-ERDEMLI (Israel). AOD-Nat corresponds to the natural aerosol optical depth that includes dust and sea-salt. Skill scores per each individual site and model (o—suite/control) are shown in the upper right corner (NDATA: available 3-hourly values used for the calculations, MEAN observations, MEAN_model, COR, RMSE, MB).

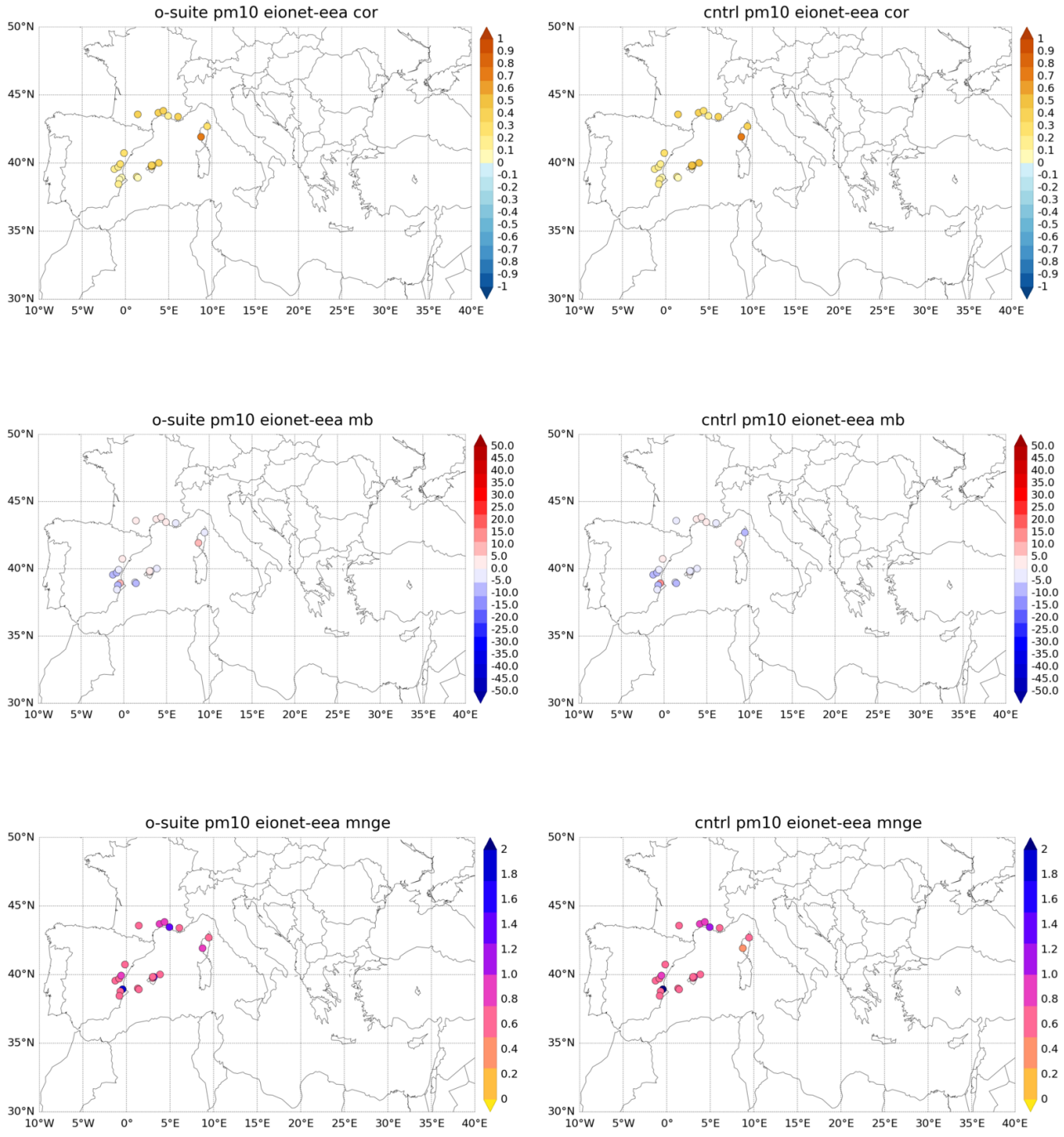

Figure 7.4.3: Skill scores (correlation coefficient, MB and FGE) for 24-hour forecasts of CAMS o-suite and control for the study period. PM10 from EIONET are the reference. Only background suburban and rural available stations are displayed.

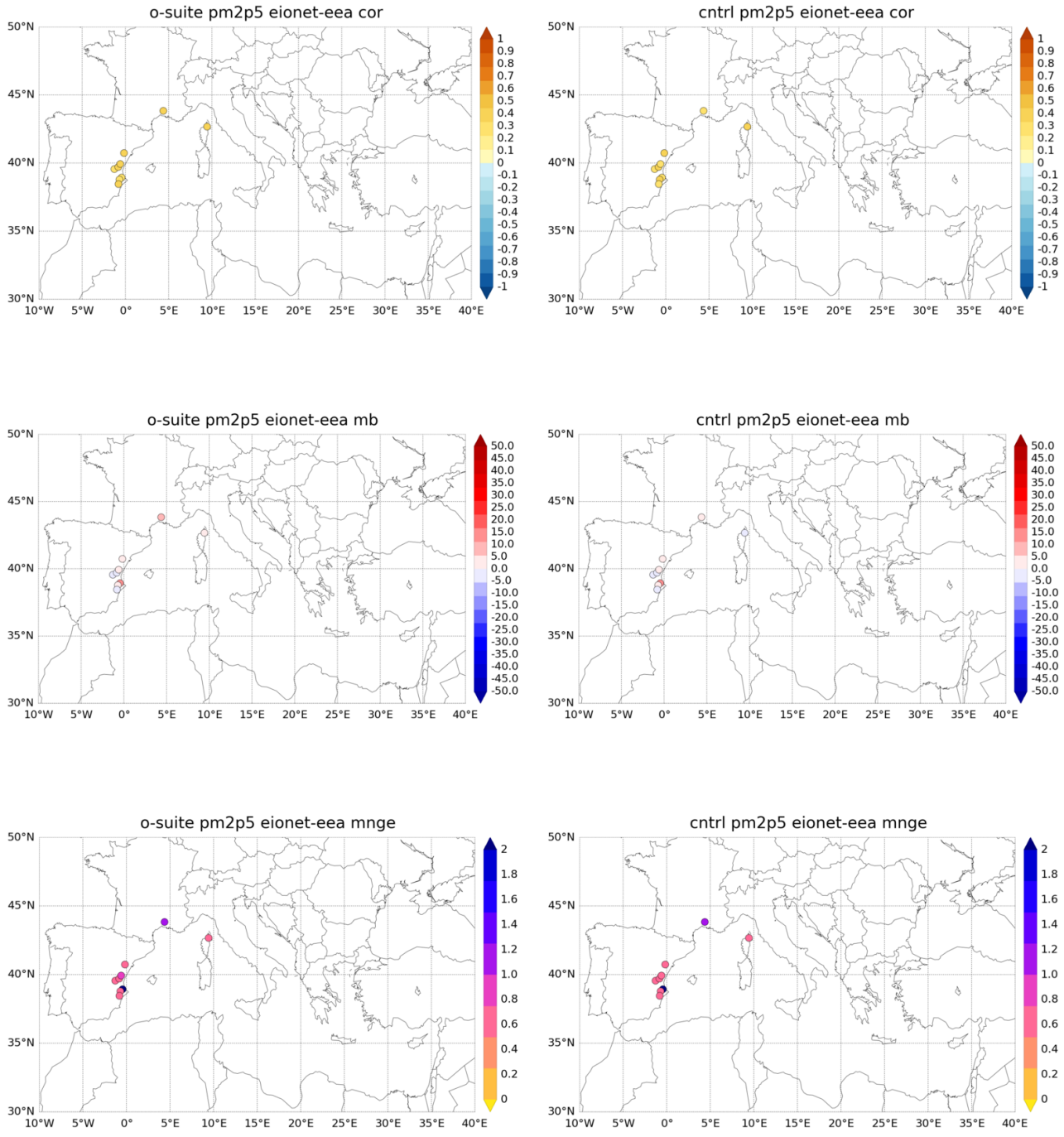

Figure 7.4.4: Skill scores (top to bottom: correlation coefficient, mean bias and FGE) for 24-hour forecasts of CAMS o-suite (left) and control (right), for the study period. PM2.5 from EIONET are the reference. Only background suburban and rural available stations are displayed.

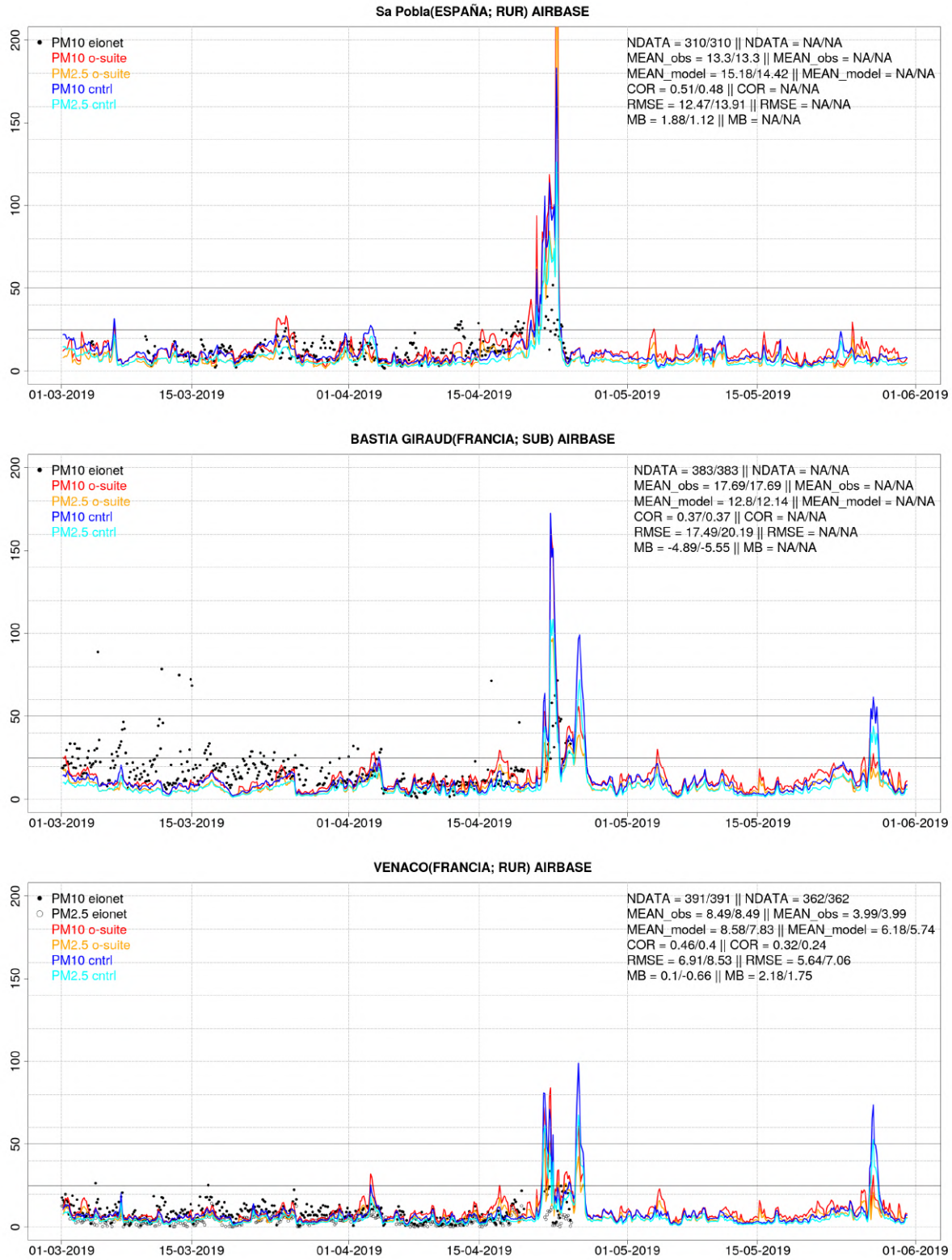

Figure 7.4.5: PM10 and PM2.5 Airbase observations (black and grey dots, respectively), PM10 and PM2.5 o-suite (red and orange lines, respectively) and PM10 and PM2.5 control (blue and cyan lines, respectively) for the study period over Sa Pobla (Balearic Islands, Spain), Bastia Giraud (France) and Venaco (Corse, France).

8. Stratosphere

8.1 Validation against ozone sondes

In this section, we present the results of the stratospheric ozone evaluation against ozone soundings from the NDACC, WOUDC, NILU and SHADOZ databases. The sondes have a precision of 3-5% (~10% in the troposphere for Brewer Mast) and an uncertainty of 5-10%. For further details see Cammas et al. (2009), Deshler et al. (2008) and Smit et al (2007). Model profiles of the o-suite are compared to balloon sondes measurement data of 44 stations for the period January 2013 to May 2019 (please note that towards the end of the validation period fewer soundings are available). As C-IFS-CB05 stratospheric composition products beyond O_3 in the o-suite is not useful we provide only a very limited evaluation of the control experiment. A description of the applied methodologies and a map with the sounding stations can be found in Eskes et al. (2016). The o-suite shows MNMBs within the range ±12%, for all regions and months (some exceptions with MNMBs of up to ±18% for single months in the high latitude regions). Figure 8.1.1. shows the results for the past year, and Fig 8.1.2 for the past 6 years.

Fig. 8.1.3 compares the averaged profiles in each region during April 2019. The vertical distribution of stratospheric ozone is quite well represented for all regions by the o-suite, with little overestimation in all latitude bands (MNMBs between -4 to +2% for MAM 2019).

The control run shows a strong overestimation of stratospheric ozone in the upper stratosphere, and an underestimation between 50hPa and 300 hPa in the Antarctic and the Northern Midlatitudes, for the Arctic between 100 and 300 hPa.

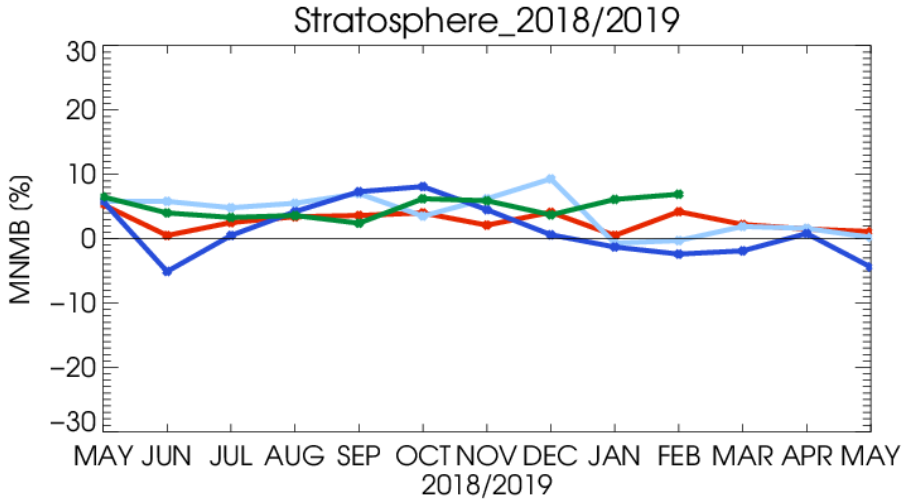

Figure 8.1.1: MNMBs (%) of ozone in the stratosphere from the o-suite against aggregated sonde data in the Arctic (light blue), Antarctic (dark blue) northern midlatitudes (red) and tropics (green). Period May 2018 to May 2019. The stratosphere is defined as the altitude region between 60 and 10 hPa in the tropics and between 90 and 10 hPa elsewhere.

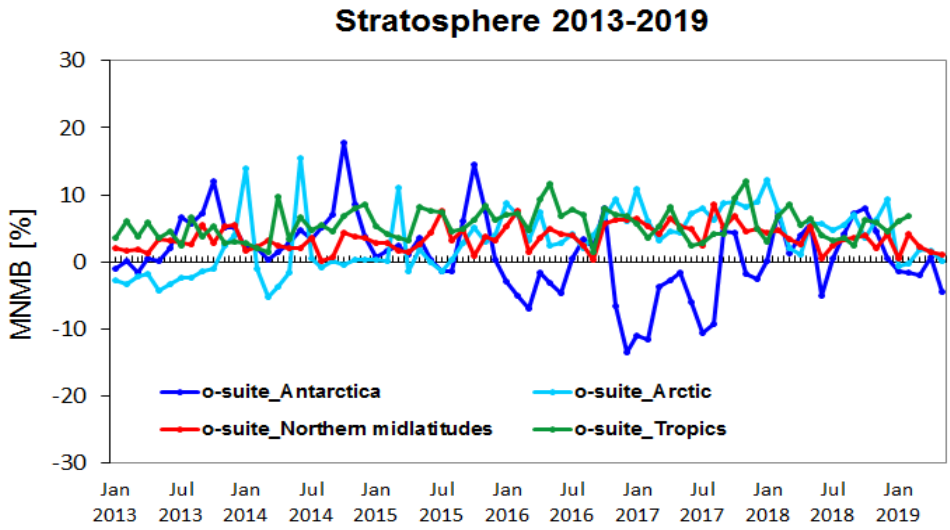

Figure 8.1.2: MNMBs (%) of ozone in the stratosphere from the o-suite against aggregated sonde data in the Arctic (light blue), Antarctic (dark blue) northern midlatitudes (red) and tropics (green) from 2013 to May 2019.

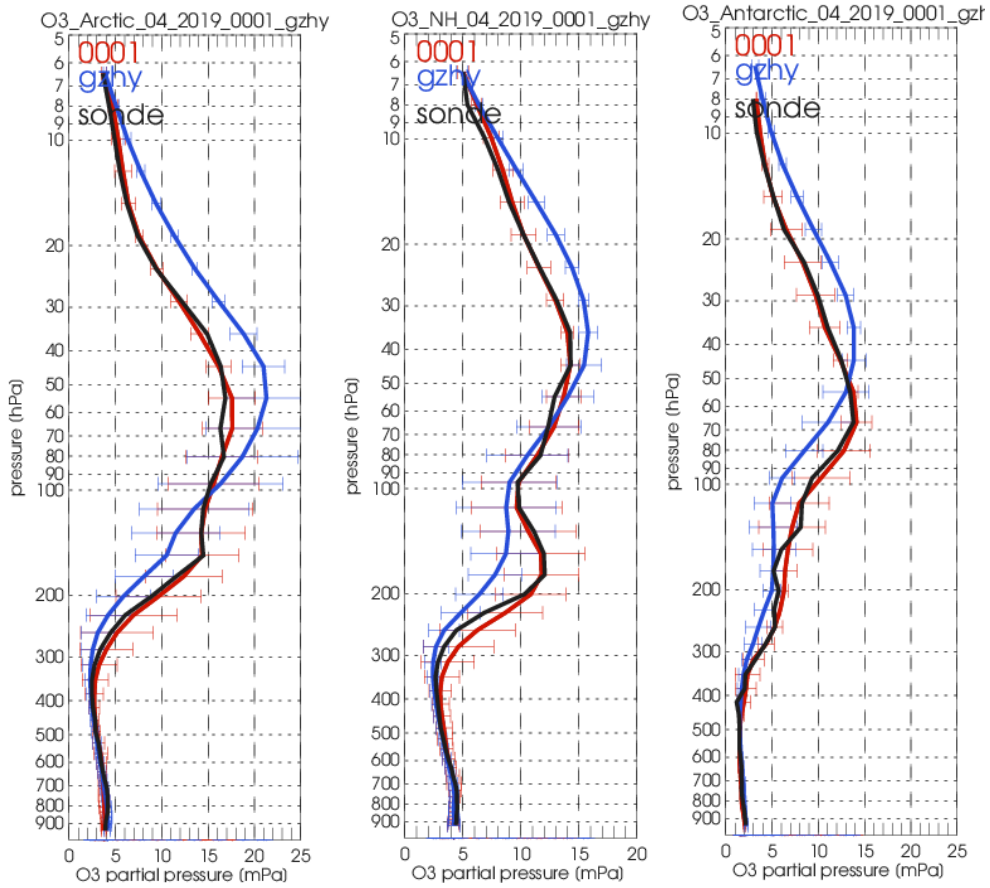

Figure 8.1.3: Comparison between mean O_3 profiles (units: mPa) of o-suite (red), and control (blue) in comparison with observed O_3 sonde profiles (black) for April 2019 for the various latitude bands: Arctic, NH-mid latitudes and Antarctic.

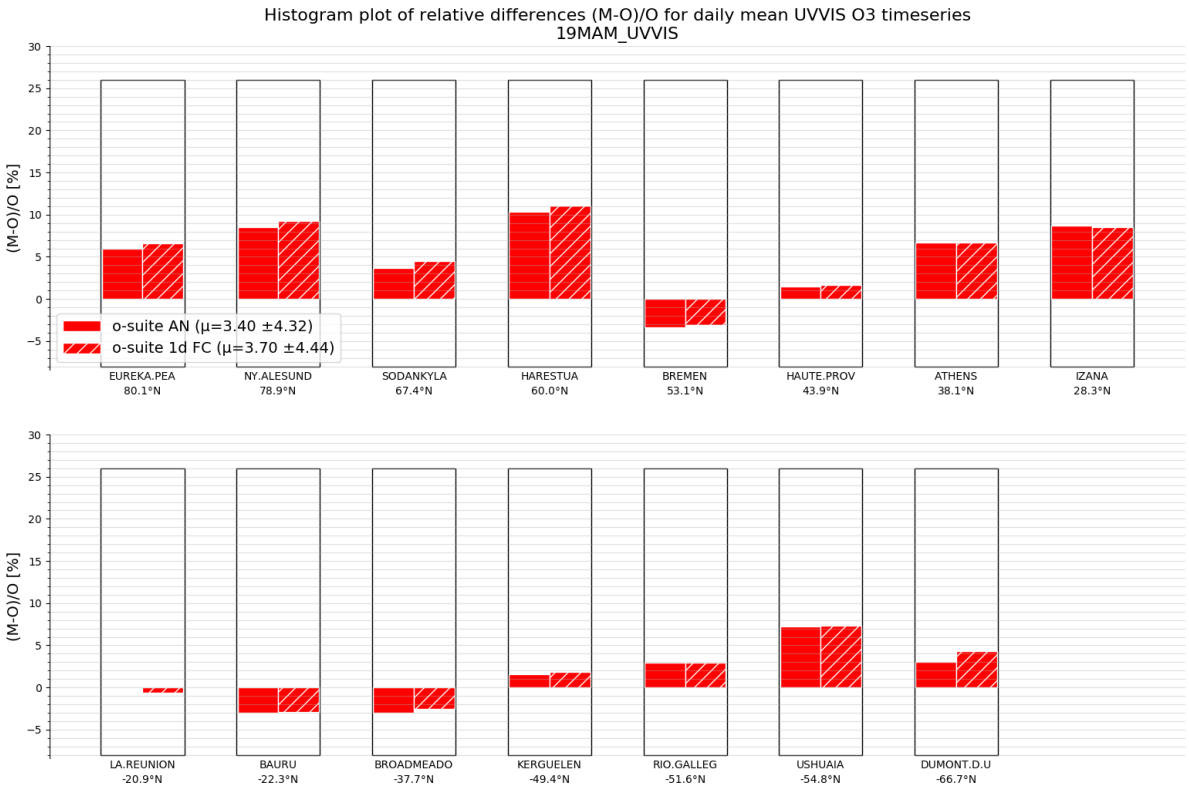

Figure 8.2.1 Relative biases during quarter MAM 2019 for 15 UVVIS stations measuring stratospheric ozone columns with ZENITH measurement geometry (stations sorted with decreasing latitude). The overall relative bias is positive for all latitudes and within the typical measurement uncertainty of 5% for most of the sites. The strong overestimation during Feb 2019 at Eureka is reduced to 5%.

8.2 Validation against observations from the NDACC network

UVVIS and FTIR stratospheric columns

Since the start of the CAMS27 project, the number of UVVIS Zenith ozone measurements have increased on NDACC. Currently fifteen sites provided data in the recent quarter allowing for a representative picture on the latitude dependence of the model data.

The systematic uncertainty of the UVVIS measurements is typically 5%, hence the relative biases for most sites for both the AN and 1d FC of the o-suite are very close to each other and within the uncertainty ranges, see Figure 8.2.1. The averaged bias for the 15 UVVIS sites is 4% and the averaged correlation is 0.92.

The correlations between the sites and the model are presented in the Taylor diagrams in Figure 8.2.2. Again, the o-suite AN and 1d FC perform very similarly in correlation coefficients.

Figure 8.2.3 depicts the FTIR stratospheric columns showing a discontinuity in the o-suite 1d FC model for the tropical sites (Mauna Loa, Altzomoni and Reunion) in the June 2016 model update.

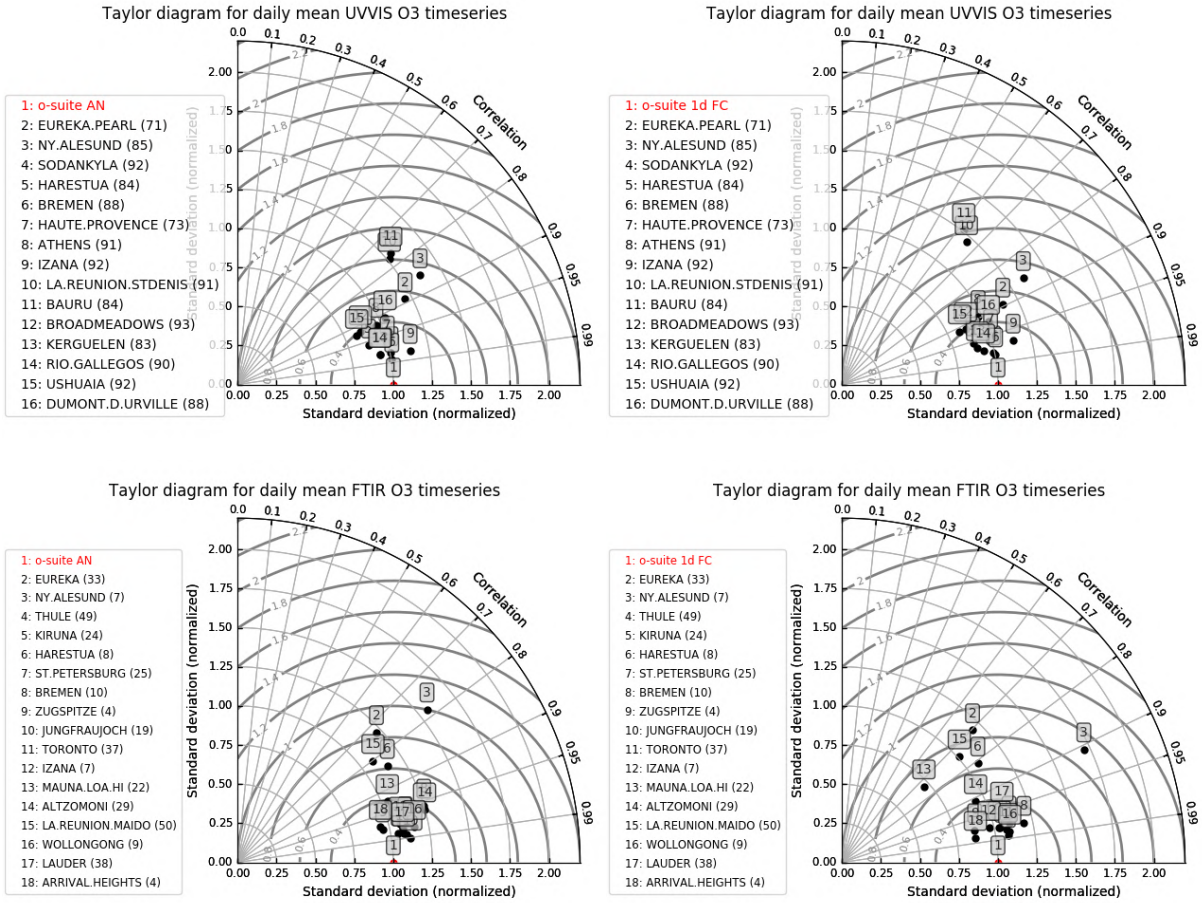

Figure 8.2.2 Taylor diagrams relating the standard deviations for the model and GB stratospheric column time series and their correlation for the time period MAM 2019. All time series are normalized such that the std of the model is 1. The performance for the osuiteAN is slightly better (averaged correlation is 0.95 for FTIR and 0.86 for UVVIS) compared to the 1d FC (averaged correlation is 0.88 for FTIR and 0.85 for UVVIS).

Profile comparison using LIDAR and MWR

In this section we present a comparison between the CAMS o-suite and control products against MWR and LIDAR observations from the NDACC network. A detailed description of the instruments and applied methodologies for all NDACC instruments can be found at http://nors.aeronomie.be. MWR (microwave) at Ny Alesund (79°N, 12°E, Arctic station) and Bern (47°N, 7°E, northern midlatitude station). LIDAR at Observatoire Haute Provence (OHP), France (43°N, 5.7°E, altitude 650m) and Hohenpeissenberg, Germany (47°N, 11°E, altitude 1km).

Figure 8.2.3 shows that at Ny Alesund the o-suite overestimates the mesospheric ozone concentration with more than 10% during SON/DJF/MAM and the bias vanishes during summer months JJA (the IUP instrument at Ny Alesund went down in July 2018-April 2019, and the UBern instrument at Ny Alesund is now part of CAMS27 and is shown in Fig 8.2.4). Between the model upgrades from September 2015 and January 2017 the relative bias at Bern vanishes (i.e. is comparable to the measurement uncertainty).

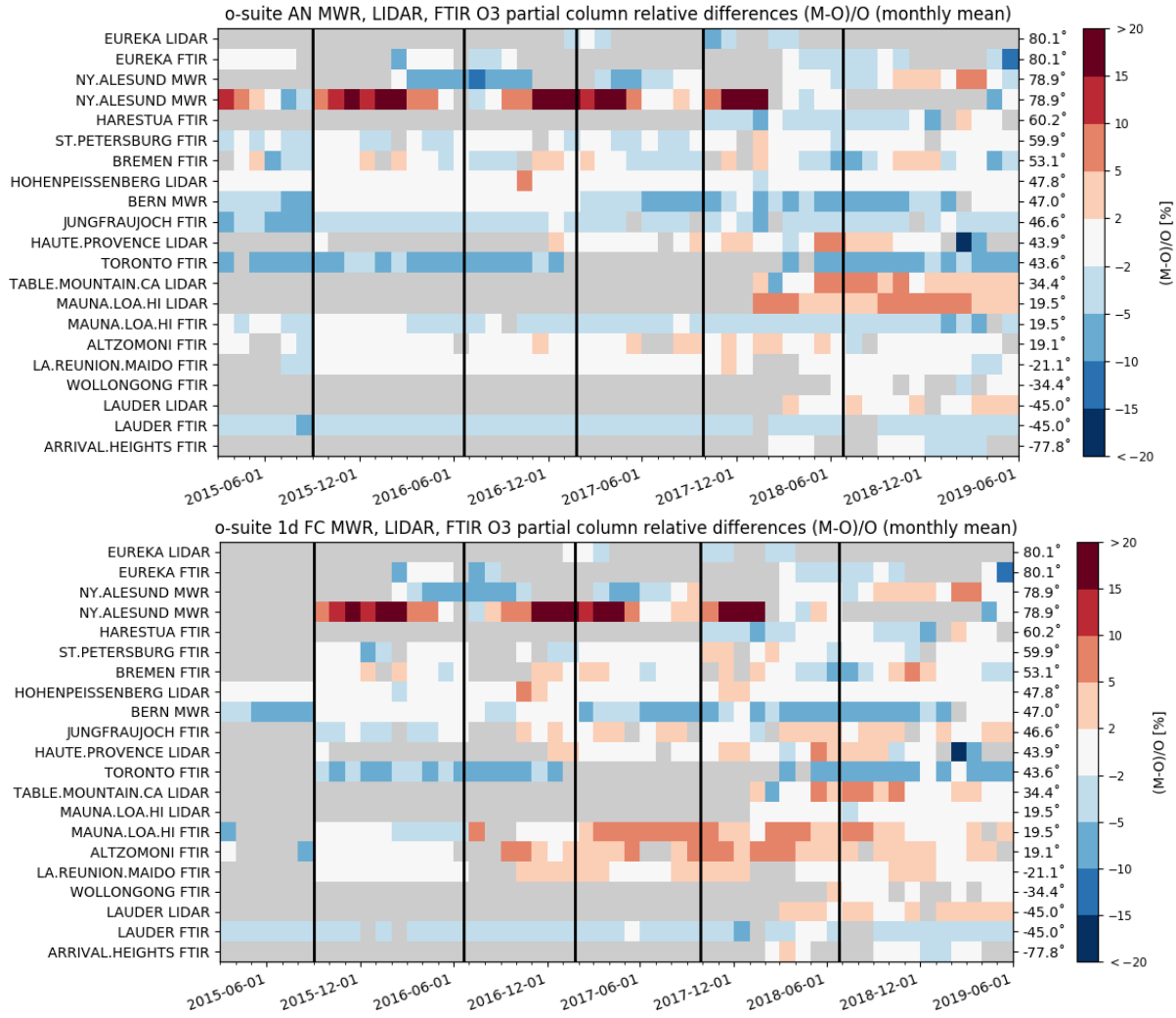

Figure 8.2.3 Time series of monthly mean relative differences for stratospheric columns (FTIR and LIDAR) and mesospheric (MWR) columns along with model cycle updates (black vertical lines) (o-suite AN top, o-suite 1d FC bottom). The stratospheric FTIR columns at St Petersburg, Jungfraujoch, Altzomoni and La Reunion show a slight positive trend in the relative differences, which is probably introduced by model updates.

At OHP and Hohenpeissenberg (LIDAR), the o-suite slightly overestimates the observed ozone (<10%) between 25km and 35km. The uncertainty on the LIDAR concentration increases with altitude and above 35km the observed differences are comparable to the measurement uncertainty (>10%, see http://nors.aeronomie.be/projectdir/PDF/NORS_D4.2_DUG.pdf).

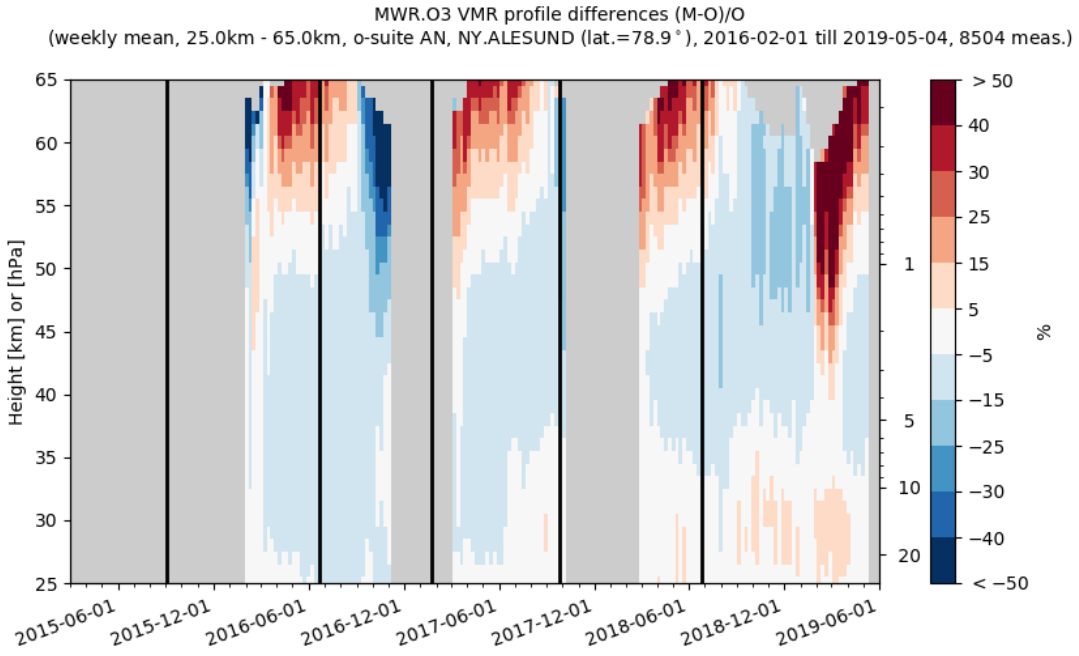
MWR.O3 VMR profile differences (M-O)/O
(weekly mean, 25.0km - 65.0km, o-suite AN, NY.ALESUND (lat.=78.9°), 2016-02-01 till 2019-05-04, 8504 meas.)
Height [km] or [hPa]
65
60
55
50
45
40
35
30
25
1
5
10
20
2015-06-01
2015-12-01
2016-06-01
2016-12-01
2017-06-01
2017-12-01
2018-06-01
2018-12-01
2019-06-01
> 50
40
30
25
15
5
−5
−15
−25
−30
−40
< −50
%

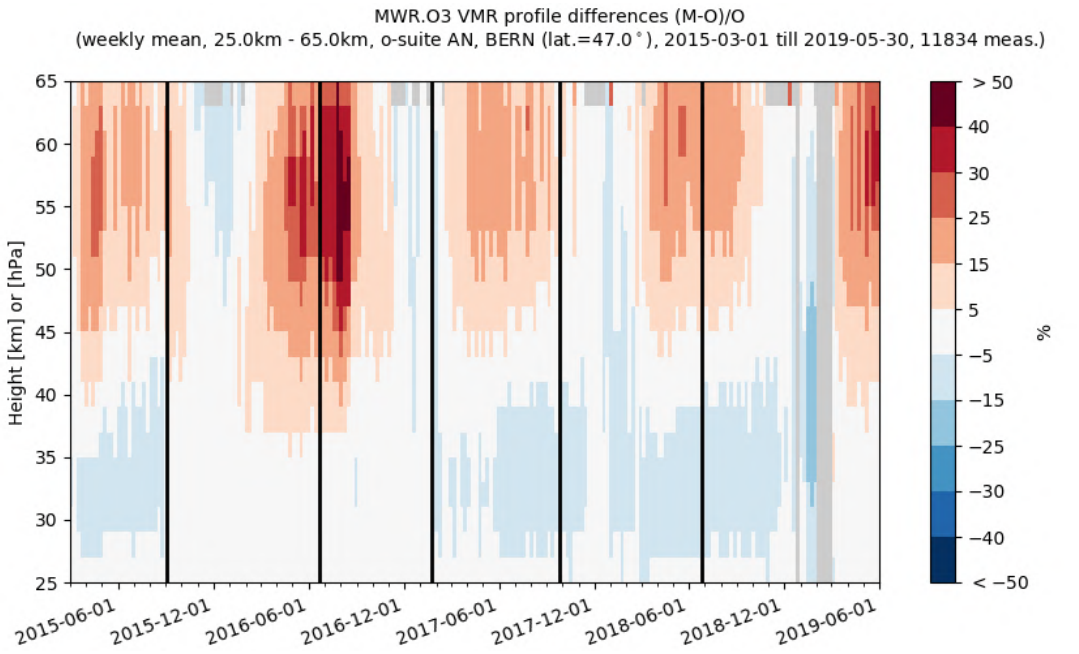
MWR.O3 VMR profile differences (M-O)/O
(weekly mean, 25.0km - 65.0km, o-suite AN, BERN (lat.=47.0°), 2015-03-01 till 2019-05-30, 11834 meas.)
Height [km] or [hPa]
65
60
55
50
45
40
35
30
25
2015-06-01
2015-12-01
2016-06-01
2016-12-01
2017-06-01
2017-12-01
2018-06-01
2018-12-01
2019-06-01
> 50
40
30
25
15
5
−5
−15
−25
−30
−40
< −50
%

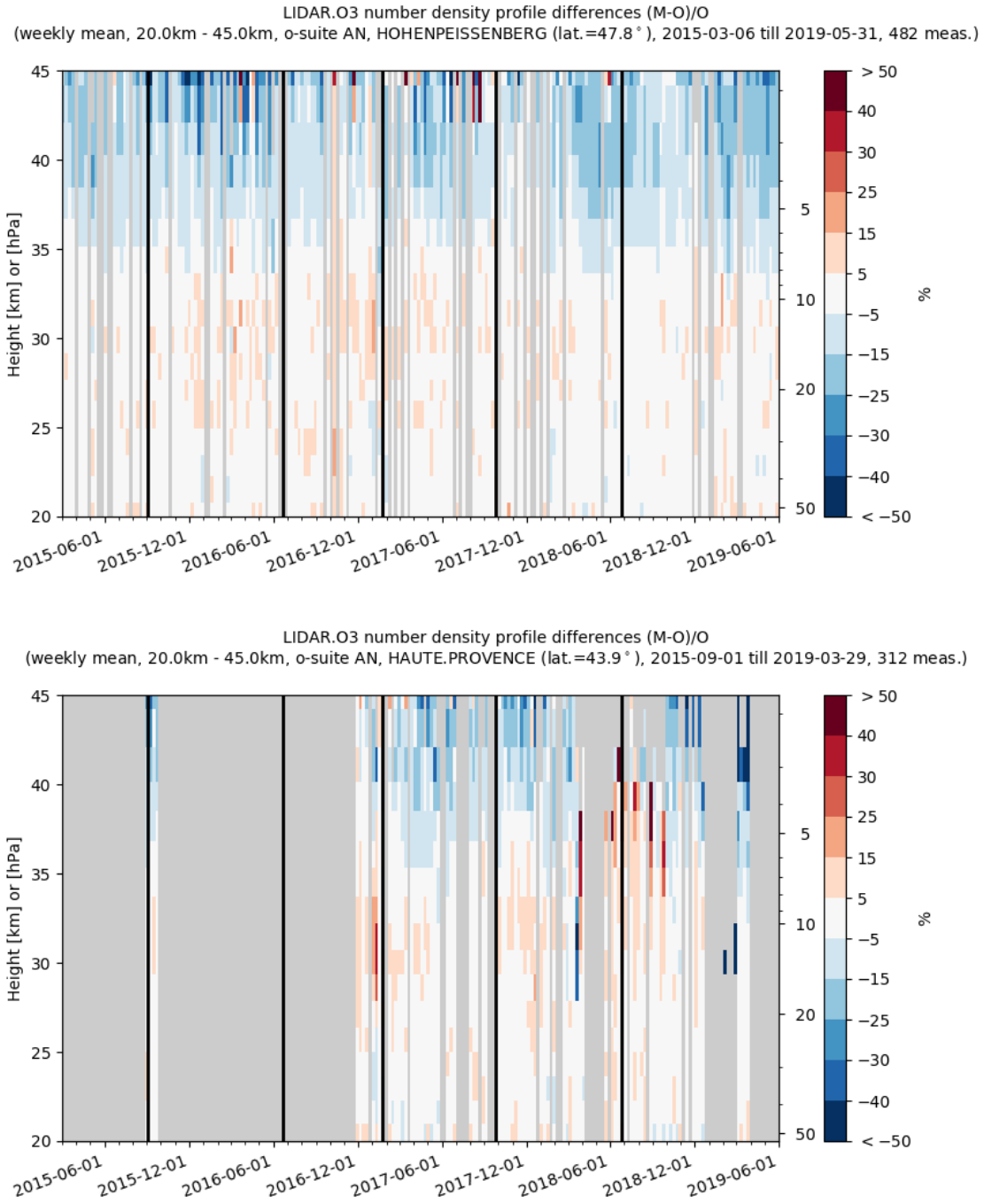

Figure 8.2.4: Comparison of the weekly mean profile bias between the O_3 mixing ratios of o-suite and the NDACC station at Ny Alesund, Bern, Hohenpeissenberg and OHP. For the LIDAR stations, the measurement uncertainty above 35km is comparable to the observed profile bias.

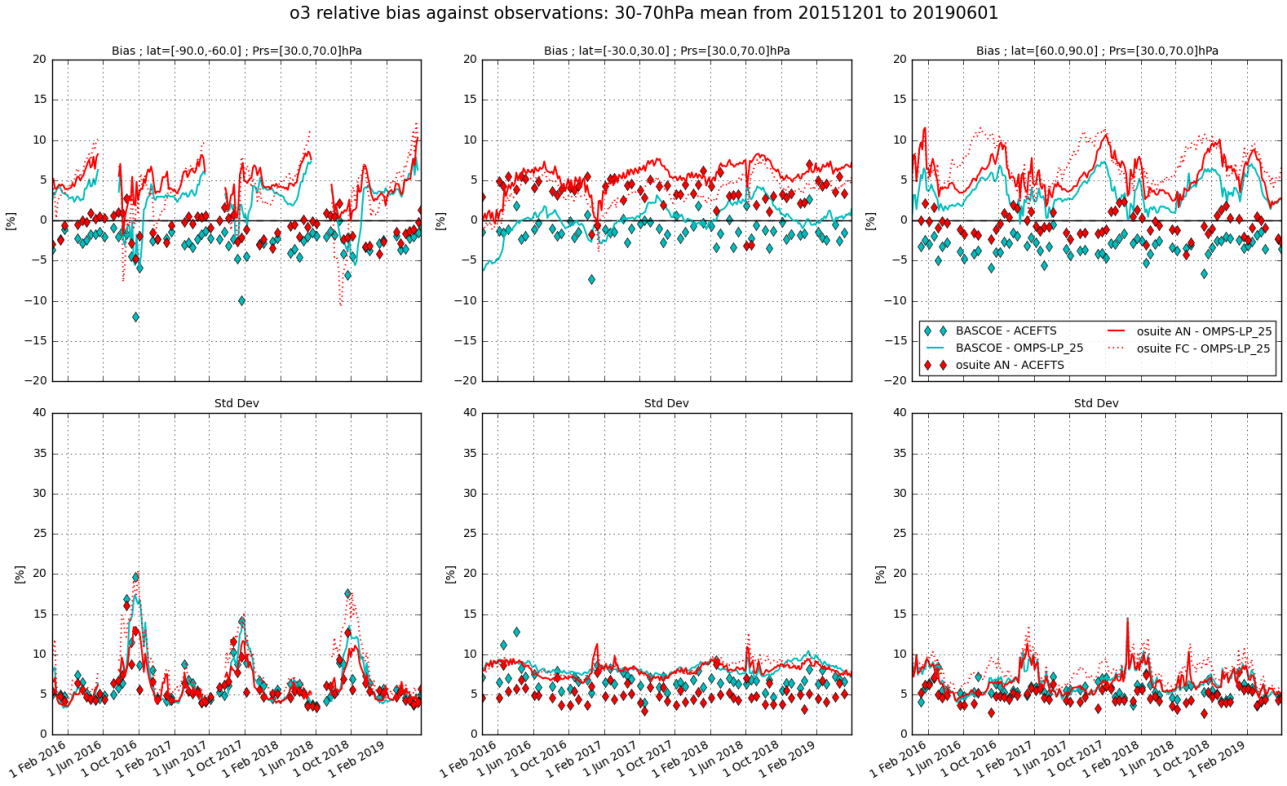

Figure 8.3.1: Time series comparing models to observations for the period 2015-12-01 to 2019-06-01 in the middle stratosphere (30-70hPa averages): o-suite analyses vs OMPS-LP (red, solid), o-suite forecasts 4th day vs OMPS-LP (red, dotted), o-suite analyses vs ACE-FTS (red markers), BASCOE vs OMPS-LP (cyan, solid) and BASCOE vs ACE-FTS(cyan markers). Top row, normalized mean bias (model-obs)/obs (%); bottom row, standard deviation of relative differences (%).

8.3 Comparison with dedicated systems and with observations by limb-scanning satellites

This section compares the output of the o-suite for the last period with observations by limb-scanning satellite instruments, using the methodology described by Lefever et al. (2015). We also include the comparisons for the o-suite 4th day forecasts (96h to 120h) of stratospheric ozone. These forecasts are represented by dotted lines in the figures.

All datasets are averaged over all longitudes and over the three most interesting latitude bands for stratospheric ozone: Antarctic (90°S-60°S), Tropics (30°S-30°N) and Arctic (60°N-90°N). In order to provide global coverage, the two mid-latitude bands (60°S-90°S and 60°N-90°N) are also included in some comparisons with satellite observations.

In this section, we use on one hand the version 2.5 of OMPS-LP (i.e. the Limb Profiler) and the version 3.6 of ACE-FTS. For reference, we include also the BASCOE analyses which are very constrained by the AURA MLS offline profiles.

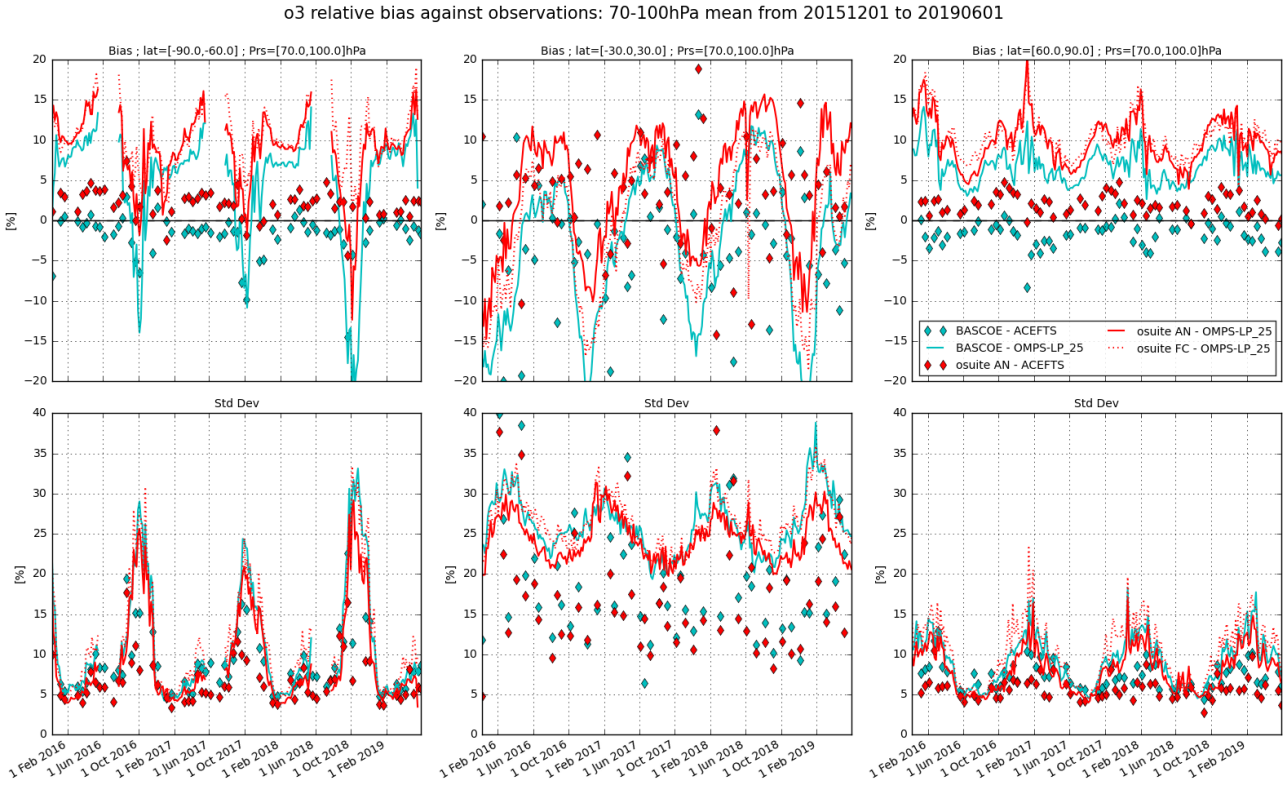

Figure 8.3.2: Time series comparing models to observations for the period 2015-09-01 to 2019-03-01 in the lower stratosphere (70-100hPa averages): o-suite analyses vs OMPS-LP (red, solid), o-suite forecasts 4th day vs OMPS-LP (red, dotted), o-suite analyses vs ACE-FTS (red markers), BASCOE vs OMPS-LP (cyan,solid) and BASCOE vs ACE-FTS(cyan markers). Top row, normalized mean bias (model-obs)/obs (%);bottom row, standard deviation of relative differences (%).

Figure 8.3.1 and Figure 8.3.2 present, in the upper row, the timeseries over the last 42 months of the bias of the o-suite against the two satellite measurements for respectively two regions of the lower stratosphere and UTLS (30-70hPa and 70-100hPa); the bottom row of the figures shows the standard deviation of the differences and can be used to evaluate the random error in the analyses.

Compared to OMPS-LP in the 30hPa to 70hPa region, there is a systematic overestimation by the o-suite: up to 8% in the tropics and and up to 12% in the polar regions. Compared to OMPS-LP in the 70hPa to 100hPa region, the North polar bias increases up to 20% at various periods, while the variability of the bias is much stronger in the South polar region; the tropics exhibits a strong seasonal variation for the bias, with a high variability indicated by the standard deviation.

The agreement with ACE-FTS is much better: the bias is generally within ±5%, except in the tropics for 70hPa to 100hPa region, where the standard deviations indicate less reliable results.

The bias of BASCOE against the satellite observations for the considered regions is systematically lower, but follows a similar evolution as the o-suite.

Figure 8.3.3 and Figure 8.3.4 display vertical profiles of the relative biases between the o-suite or BASCOE and the satellite measurements. The difference is averaged over the most recent 3-month period considered in this validation report, i.e. March to May 2019.

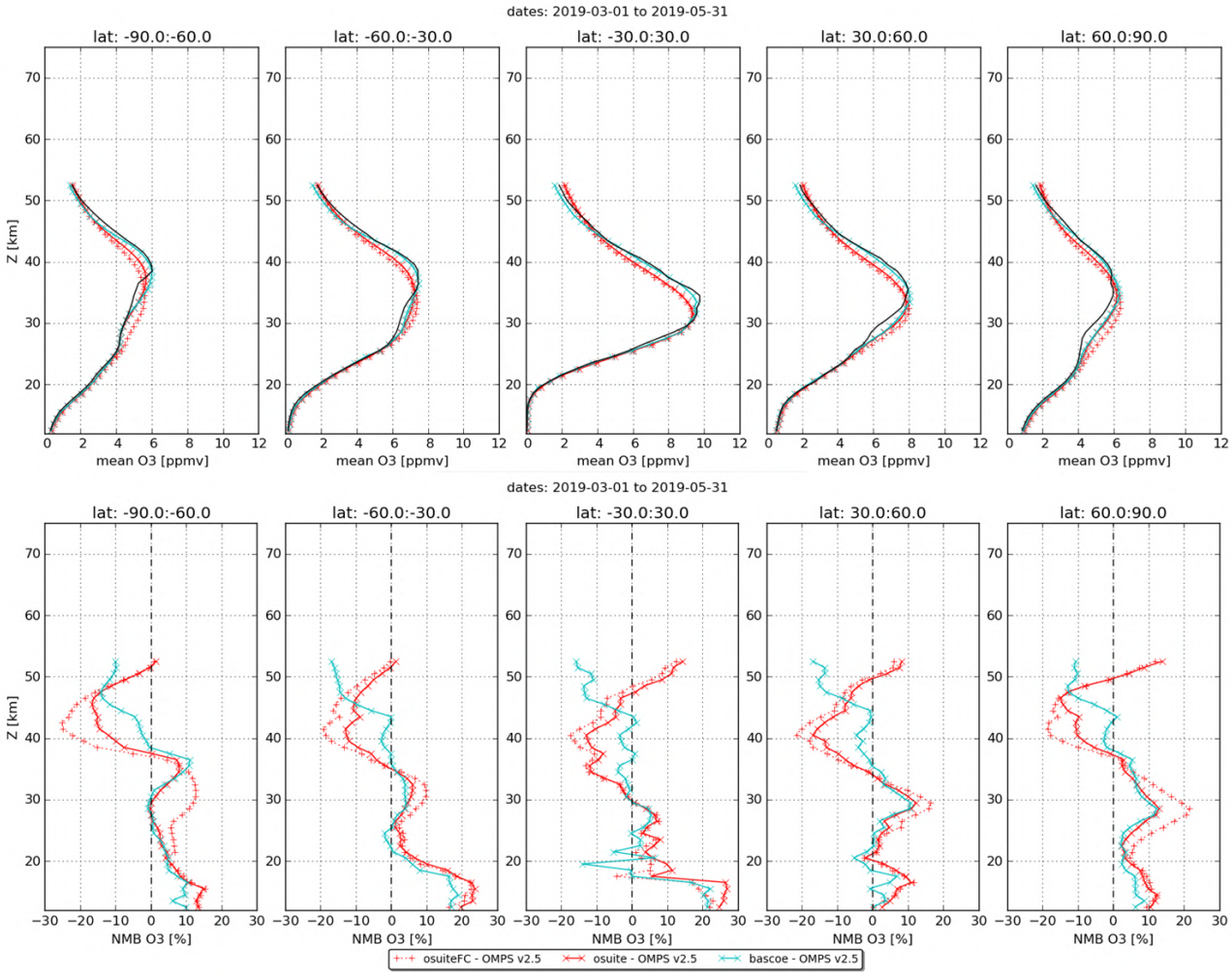

Figure 8.3.3: Mean value (top) and normalized mean bias (bottom) of the ozone profile between o-suite analyses (red, solid), o-suite forecasts 4th day (red, dotted) and BASCOE (cyan line) with OMPS-LP v2.5 observations for the period March 2019 to May 2019.

The OMPS-LP profiles are much more irregular than the ACEFTS or MLS profiles, but the relative bias between o-suite and OMPS-LP is mostly within ±10% between 20km and 35km.

The negative bias above 35km is confirmed by the ACEFTS profiles, otherwise there is a good agreement in the middle and lower stratosphere.

It must be noted that the different instruments have a variety of spatial and temporal coverage: for a 3 month period and over the latitude bands considered, OMPS and Aura MLS (not shown) provide daily data with more than 40000 valid profiles, while ACE-FTS provides around 700 profiles in the polar region and 200 profiles in the tropics.

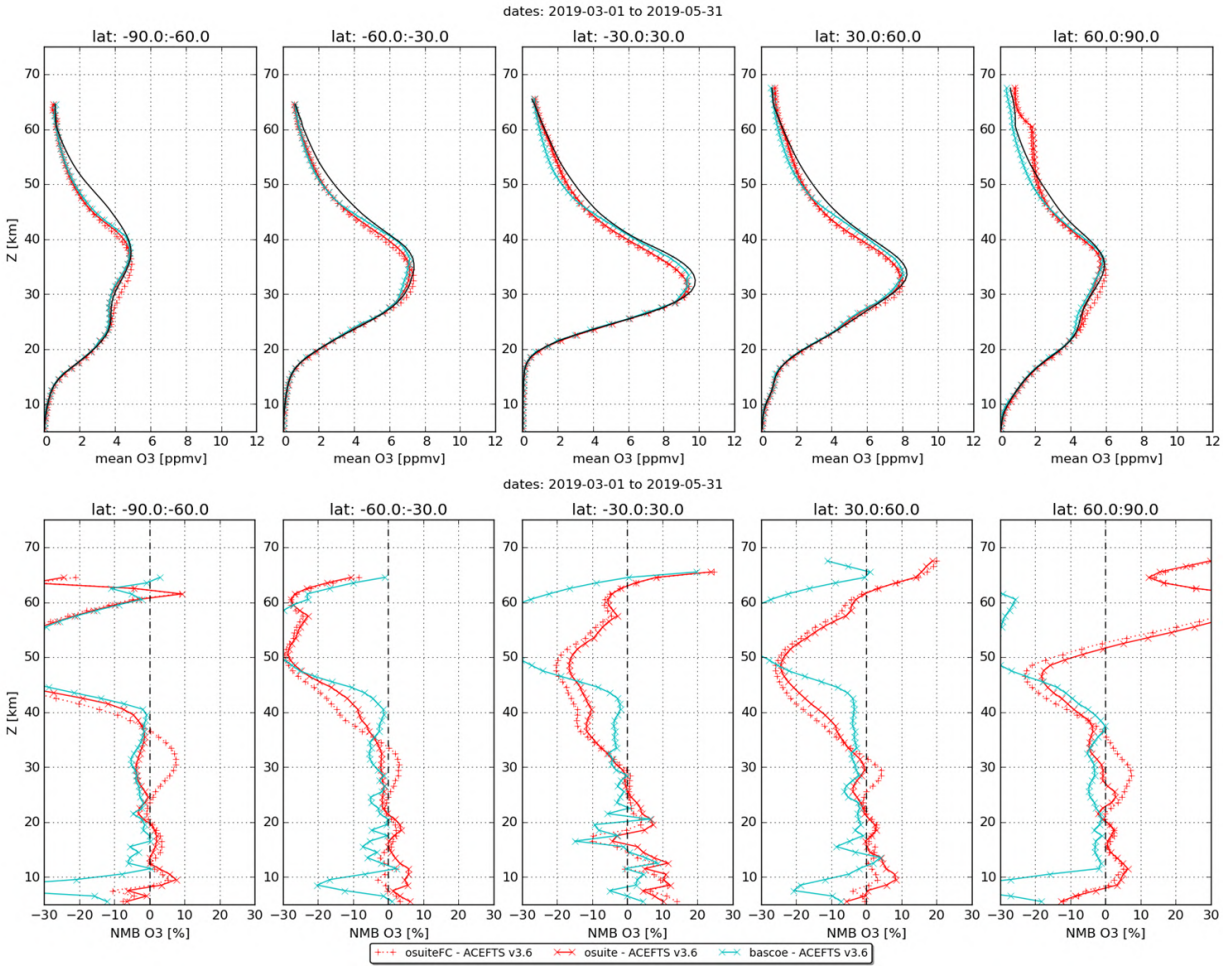

Figure 8.3.4: Mean value (top) and normalized mean bias (bottom) of the ozone profile between o-suite analyses (red, solid), o-suite forecasts 4th day (red, dotted) and BASCOE (cyan line) with ACE-FTS observations for the period March 2019 to May 2019.

8.4 Stratospheric NO_2

The CAMS model uses a tropospheric chemistry scheme in combination with a parameterization for stratospheric ozone. Stratospheric ozone is also well constrained by satellite observations. Therefore, the only useful product in the stratosphere is ozone, and all other compounds, including NO_2, should not be used, as demonstrated by the validation results presented here.

In this section, nitrogen dioxide from SCIAMACHY/Envisat satellite retrievals (IUP-UB v0.7) and GOME-2/MetOp-A satellite retrievals (IUP-UB v1.0) are compared to modelled stratospheric NO_2 columns. Monthly mean stratospheric NO_2 columns from SCIAMACHY and GOME-2 have relatively small errors on the order of 20% in the tropics and in mid-latitudes in summer and even lower errors at mid-latitudes in winter. As the time resolution of the saved model files is rather coarse and NO_x photochemistry in the stratosphere has a large impact on the NO_2 columns at low sun, some uncertainty is introduced by the time interpolation at high latitudes in winter.

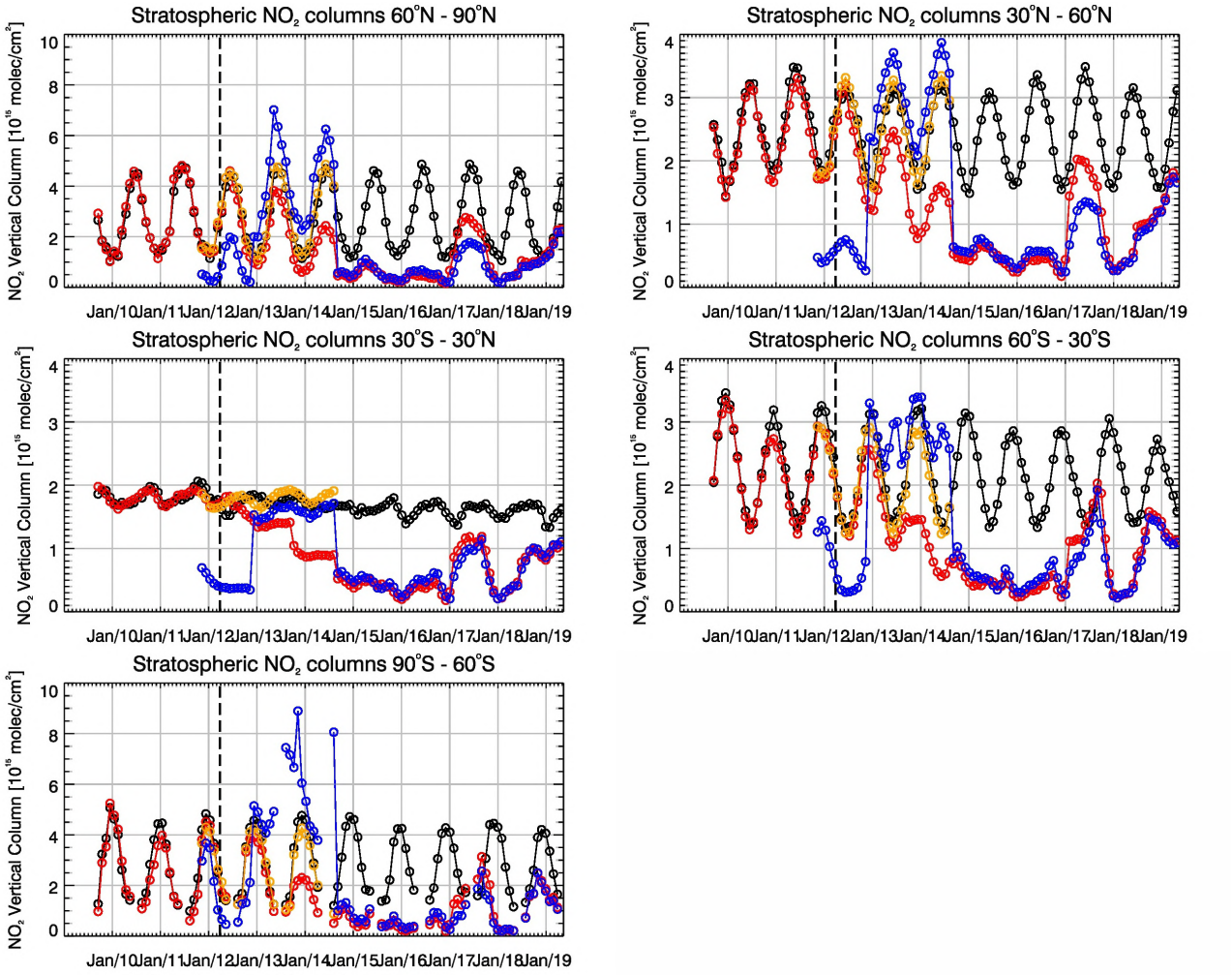

Figure 8.4.1: Time series of average stratospheric NO2 columns [10^{15} molec cm-2] from SCIAMACHY (up to March 2012) and GOME-2 (from April 2012, black) compared to model results (red: osuite, blue: MACC fcnrt TM5/MACC CIFS TM5/control, orange: MACC fcnrt MOZ) for different latitude bands. See text for details. The blue line shows MACC_fcnrt_TM5 from November 2011 to November 2012, MACC_CIFS_TM5 results from December 2012 until August 2014 and control results from September 2014 onwards (the model run without data assimilation is termed control since Sep 2014). The vertical dashed black lines mark the change from SCIAMACHY to GOME-2 based comparisons in April 2012.

As shown in Figure 8.4.1, amplitude and seasonality of satellite stratospheric NO_2 columns are poorly modelled with CB05-based chemistry runs including the more recent versions of the o-suite. The significant differences between observations and CB05 chemistry runs, i.e. a strong underestimation of satellite retrievals by models, can be explained by the missing stratospheric chemistry for these model versions. The only constraint on stratospheric NO_x is implicitly made by fixing the HNO_3/O_3 ratio at the 10 hPa level. This assumption, in combination with the changing model settings for stratospheric O_3 for control compared to MACC_CIFS_TM5, may explain some of the jumps we see in stratospheric NO_2. In any of these runs the stratospheric NO_2 is poorly constrained. It clearly indicates that stratospheric NO_2 in the latest versions of the o-suite is not a useful product and should be disregarded. However, model simulated values increased with an upgrade of the o-suite in February 2017, so that simulations are closer to the satellite observations for 2017, especially for northern hemisphere latitude bands where seasonality seems to have been reproduced (in contrast to the Southern Hemisphere) by the o-suite apart from the pronounced

underestimation. O-suite values are larger than the control in 2017 at all latitude bands. The better agreement found for 2017 did not continue in the beginning of 2018 and values decreased to the magnitude of 2015-2016 runs at all latitude bands, followed however by a similar increase as in 2017 in late 2018 (development to be seen with the next reports).

Comparison of the o-suite from July 2012 until August 2014 with the other model runs and satellite observations shows that the previous version of the o-suite stratospheric NO_2 columns had a systematic low bias relative to those from MACC_fcnrt_MOZ and satellite observations for all latitude bands. For example, o-suite values are a factor of 2 smaller than satellite values between 60°S to 90°S for October 2013. Best performance was achieved with the MOZART chemistry experiments without data assimilation (MACC_fcnrt_MOZ, running until September 2014), especially northwards of 30°S. Details on the NO_2 evaluation can be found at: http://www.doas-bremen.de/macc/macc_veri_iup_home.html.

9. Validation results for greenhouse gases

This section describes the NRT validation of the pre-operational, high resolution forecast of CO_2 and CH_4 from 1st June 2018 to 1st June 2019 based on observations from 17 surface stations, located in Western Europe; 15 TCCON stations measuring XCO_2 and XCH_4 total columns, and 13 NDACC stations measuring partial and total CH_4 columns. We compare the observations to the high-resolution forecast experiments (*gqpe/gznv, Tco1279L137; 9x9 km*), coupled to the analysis experiment (*gqiq/gwx3, Tco399L137, 25x25 km*). The *gqpe* forecast experiment is using the IFS model cycle CY43R1 and has been officially implemented on 1st Nov. 2017. The *gznv*/*gwx3* experiments, based on IFS CY45R1, are used from 1st December 2018 on. This new experiment benefits from a couple of bugs fixed in the modelled biogenic fluxes which should result in an improved seasonal cycle in the northern hemisphere and some degradation in the tropics.

9.1 CH4 and CO2 validation against ICOS observations

The CO_2 and CH_4 simulations from the analysis and high-resolution forecast have been compared to the 17 ICOS stations. The near–real time data processing of the in-situ measurements is ensured by the Atmospheric Thematic Center (Hazan et al., 2016). Among the 17 stations we can distinguish three sites located on top of mountains (PUY, JFJ, CMN), two background sites (PAL, ZEP) and 12 tall towers. For the later we consider only in this report the highest sampling level which is at least at 100m above the ground.

For CO_2 the correlation coefficients are higher than 0.8 for all sites except one at Ispra, located in the Po valley, and poorly represented by the model due to the complex orography (Figure 9.1.1). The synoptic scale variability is overestimated at almost all stations except one (CMN). The best correlation coefficients are obtained for the background stations PAL, ZEP and JFJ. For CH_4, there is not much difference in the correlation coefficients between the background sites and the tall towers, which are close to 0.8 with two exceptions at Monte Cimone and Ispra where correlations are below 0.5. Overall, we notice a small degradation of the CH_4 correlations with the high-resolution forecast experiment compared to the analysis (Figure 9.1.1). This is particularly true at the Trainou tall tower. In this case several spikes are wrongly simulated by the models in summer, and their amplitude is getting worse with the high-resolution forecast. This is probably due to the vicinity of hot spot emissions in Paris area, either mis-located or overestimated in the emission inventory, whose influence is amplified when using higher resolution.

Figure 9.1.2 shows the time varying biases (observations minus model), averaged on a weekly basis, for all ICOS stations. There is not much difference between the high-resolution forecast and the analysis runs. The CO_2 biases display clear seasonal cycles (±10 ppm) at most sites with negative biases in Summer/Autumn, and positive biases in Winter/Spring. One example is detailed on Figure 9.1.3 for the Norunda tall tower located in Sweden. At this stage it is too early to evaluate the improvement expected from the new experiments, used since December 2018. For CH_4 we observe a clear latitudinal gradient in the biases. At the Scandinavian sites the model overestimates (up to 50 ppb) the observations all along the year. The example of Norunda (Figure 9.1.3) clearly shows that the CH_4 spikes are systematically too high in the model runs, which could indicate that the

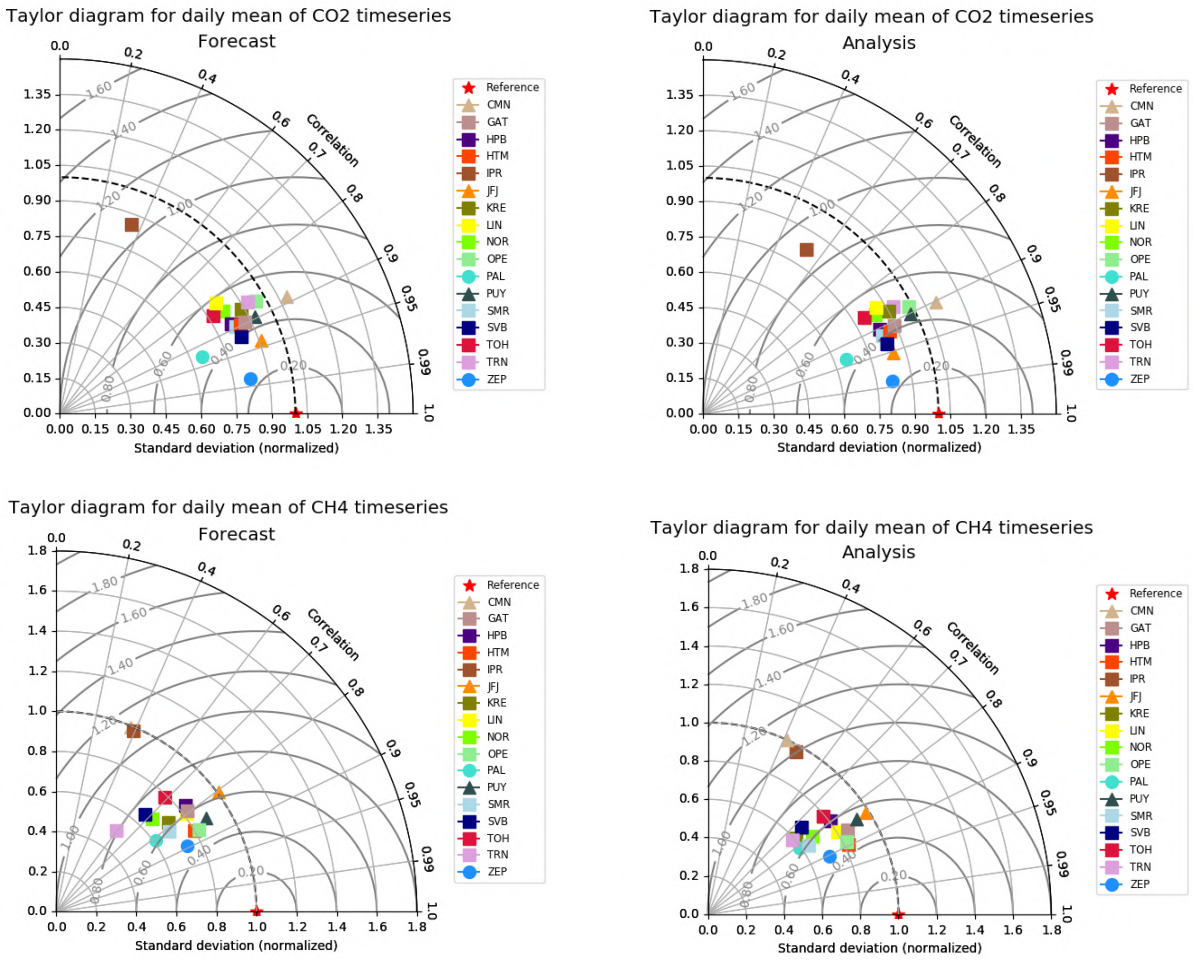

Figure 9.1.1: Taylor diagrams relating the standard deviations for the model and time series of CO2 (above) and CH4 (below) mole fractions and their correlation. The normalized standard deviation is calculated as the ratio observed SD / modelled SD (SD values lower than one mean an overestimation of the variability by the model). The left panels shows the high resolution forecast, and the right panels the analysis.

wetland emissions are overestimated. For sites located at lower latitudes, the bias is generally lower, and is getting negative in Summer/Autumn. It is even systematically negative at the mountain sites PUY and JFJ.

We have done an evaluation of the model performance based on a composite of all European stations (Figure 9.1.4). Overall this composite comparison highlights the seasonal cycle of the CO_2 bias, and an overestimation of CH_4 concentrations. For CO_2, the model overestimation is maximal in Spring 2018 (May-June). For several sites, like Norunda (Figure 9.1.3), this maximum corresponds to a high mismatch resulting from the heatwave that hit North Europe in 2018. It should also be noted that the coefficient correlations are significantly lower from April to September, during the growing season of the vegetation when the biospheric fluxes are maximum. The overestimation of the CO_2 seasonal amplitude by ±1% was already described in previous reports and is expected to decrease with the new experiments. For CH_4 we observe positive biases between 10 and 20 ppb for most of the year, getting closer to zero in summertime.

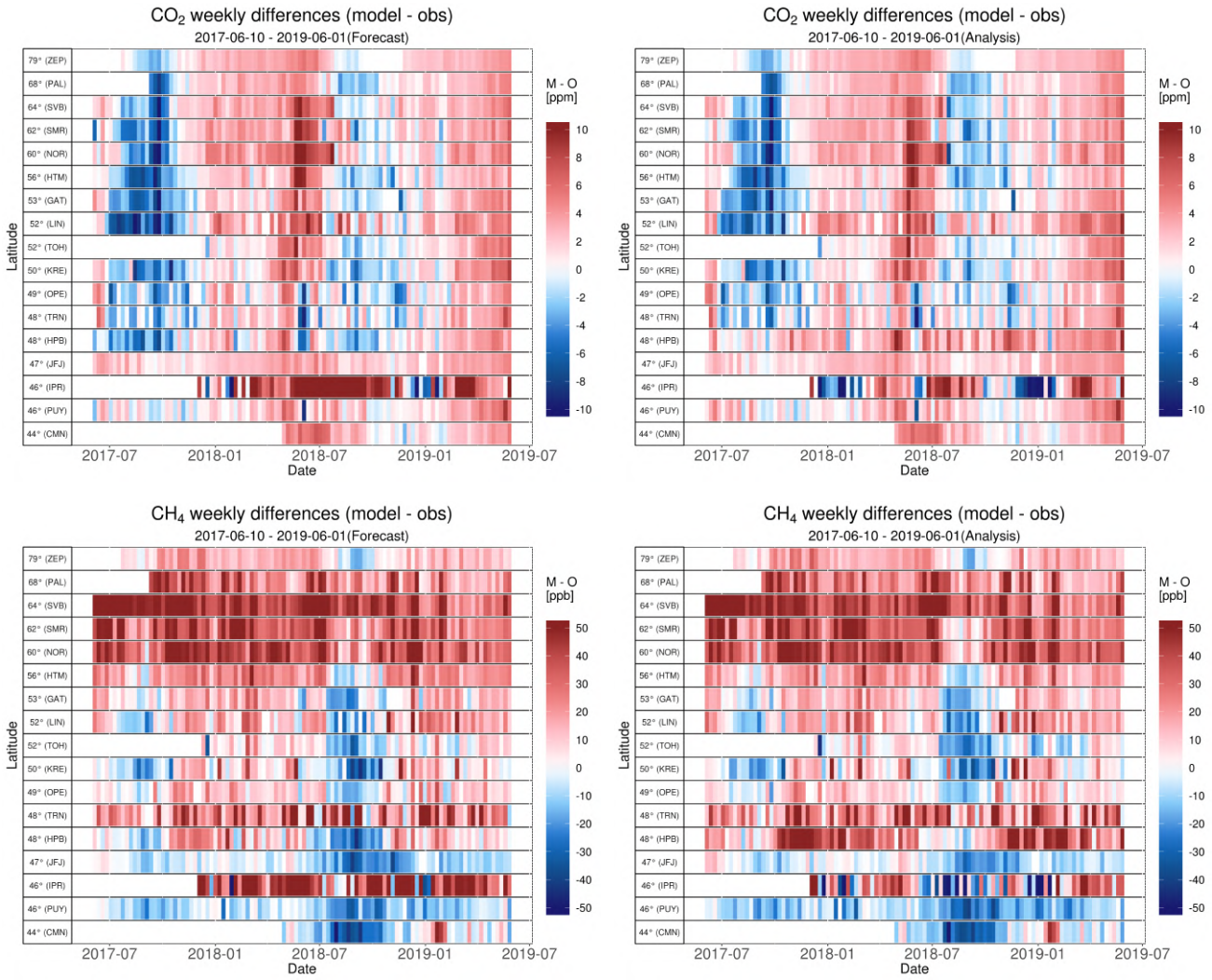

Figure 9.1.2: Mosaic plot of CO2 (above, in ppm) and CH4 (below, in ppb) biases of the CAMS products (left: high resolution forecast, right: analysis run) compared to surface station observations. Each vertical coloured line represents a weekly mean.

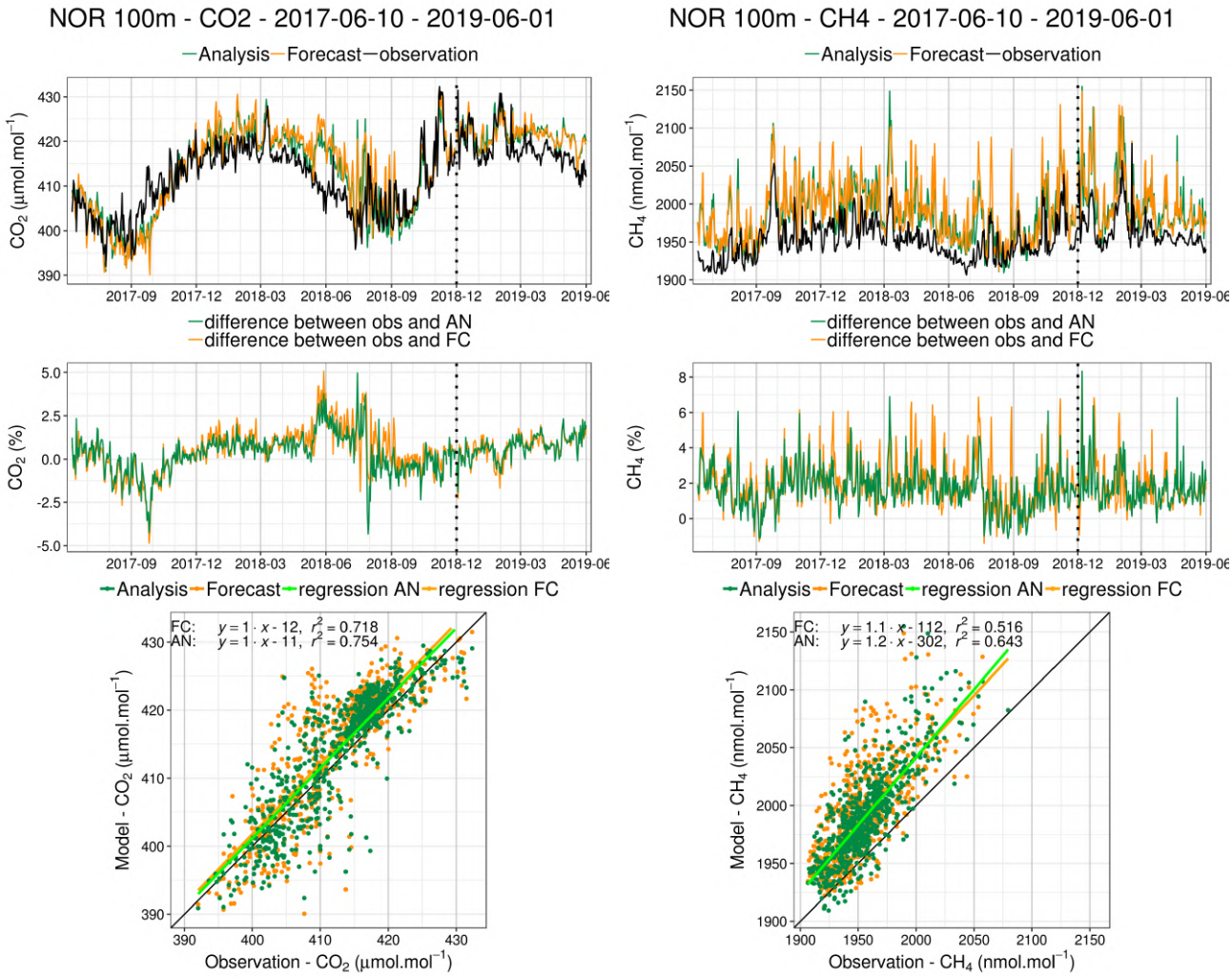

Figure 9.1.3: Comparison of CO2 (left) and CH4 (right) daily means observed (black) with the analysis run (green) and the high-resolution forecast (orange) at the Norunda tall tower. Middle: differences of the observations minus the simulations. Below: Linear fit between observations and simulations.

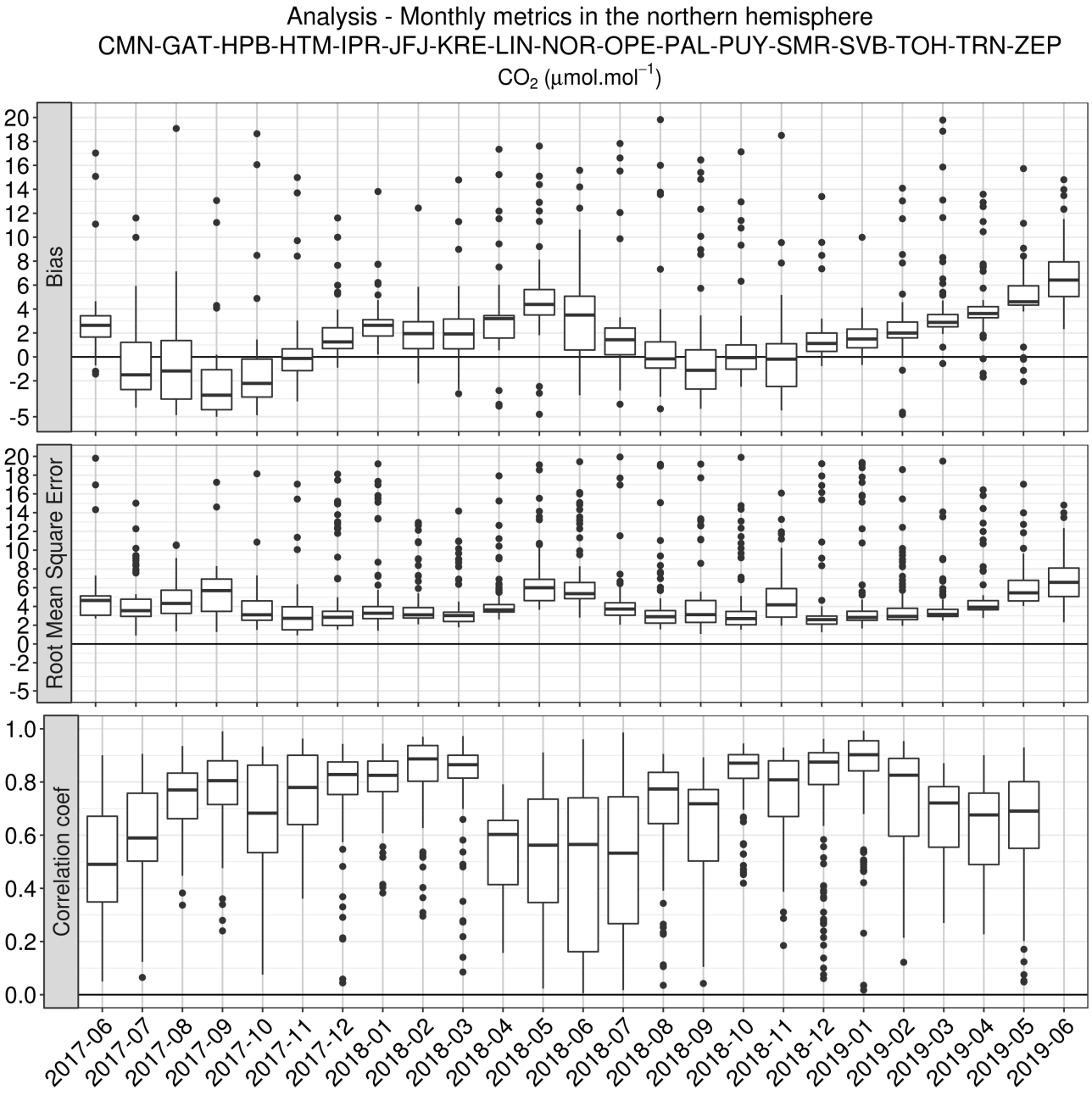

Figure 9.1.4a: Monthly statistics (bias, RMSE, correlation coefficients) of the analysis experiment compared to CO2 surface measurements at ICOS sites. The results obtained for all European sites (see the list of sites in the title) are averaged.

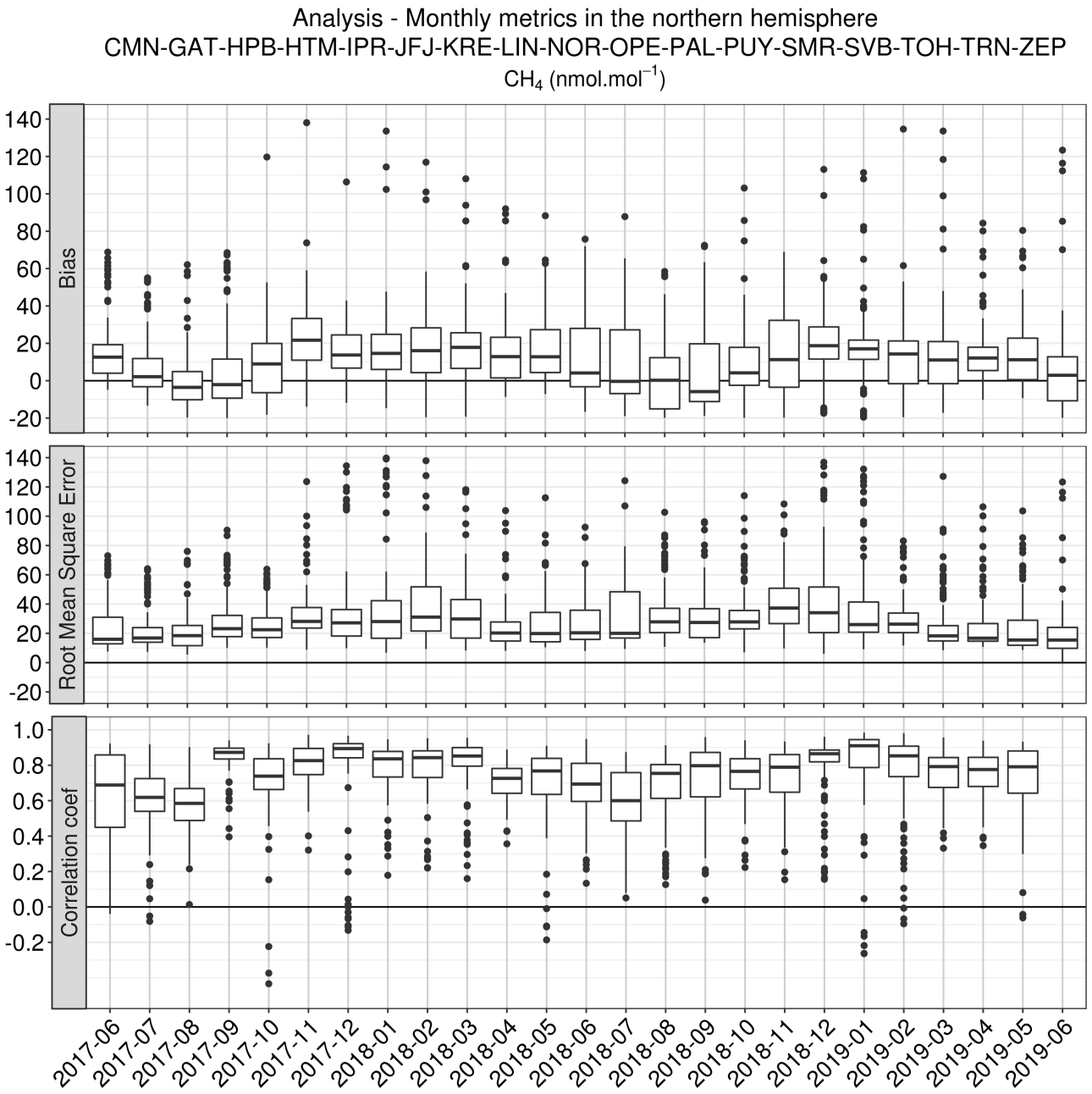

Figure 9.1.4b: Same as Figure 9.1.3a for CH4.

9.2 CH_4 and CO_2 validation against TCCON observations

For the validation column averaged mole fractions of CO_2 and CH_4 (denoted as XCO_2 and XCH_4) from the Total Carbon Column Observing Network (TCCON) are used. Column averaged mole fractions provide different information than the in-situ measurements and are therefore complementary to the in-situ data.

The validation routines used for TCCON data are the same as used for the NDACC network and are documented in Langerock et al. (2015). The routines have been adapted to use the TCCON data format. In this section, we compare column averaged mole fractions of CO of the CAMS models with TCCON retrievals. Data from the following TCCON sites has been used:

Izana (Blumenstock et al., 2017), Reunion (De Mazière et al., 2017), Bialystok (Deutscher et al., 2017), Manaus (Dubey et al., 2017), Four Corners (Dubey et al., 2017), Ascension (Feist et al., 2017), Anmeyondo (Goo et al., 2017), Darwin (Griffith et al., 2017), Wollongong (Griffith et al., 2017), Karlsruhe (Hase et al., 2017), Edwards (Iraci et al., 2017), Indianapolis (Iraci et al., 2017), Saga (Kawakami et al., 2017), Sodankyla (Kivi et al., 2017), Hefei (Liu et al., 2018), Tsukuba (Morino et al., 2017), Burgos (Morino et al., 2018), Rikubetsu (Morino et al., 2017), Bremen (Notholt et al., 2017), Spitsbergen (Notholt et al., 2017), Lauder (Sherlock et al., 2017, Pollard et al., 2019), Eureka (Strong et al., 2018), Garmisch (Sussmann et al., 2017), Zugspitze (Sussmann et al., 2018), Paris (Te et al., 2017), Orleans (Warneke et al., 2017), Park Falls (Wennberg et al., 2017), Caltech (Wennberg et al., 2017), Lamont (Wennberg et al., 2017), Jet Propulsion Laboratory (Wennberg et al., 2017), East Trout Lake (Wunch et al., 2017).

For the validation of the models in March, April, May only the TCCON site Orleans provides data over the whole 3 months. For the month of March data are also available from Karlsruhe, Izana and East Trout Lake.

The reason for the low availability of TCCON data is the following: The requirement for TCCON data to become public is 1 year after the measurement. Some TCCON groups make their data earlier available. In the previous CAMS84 project only data from Bialystok, Orleans and Reunion was timely available for the validation of the CAMS models. The Bialystok site has stopped operation and the instrument is currently being installed in Cyprus. Data from Cyprus will become available soon. Reunion had technical problems and is therefore not operational. It is likely that for future reports fast data will become available again for Orleans, Cyprus and Reunion. During the first year of the current CAMS84 project data was timely available from several TCCON sites. The reason was that during the first year after the launch of the Sentinel 5 precursor (S5p) several sites received funding to make TCCON data timely available for the validation of the S5p CH_4 and CO retrievals. Several non-European TCCON partners contributed to this effort.

Methane (CH_4)

Figure 9.2.1 shows the data for the last 4 years. The only data for the reporting period is from Orleans, East Trout Lake, Karlsruhe and Izana. Due to the low number of measurements for East Trout Lake during the reporting period only data from Orleans, Karlsruhe and Izana is used for the model evaluation. The data from these two stations show that the model data continues to underestimate the CH_4 for these stations by 5-15 ppb.

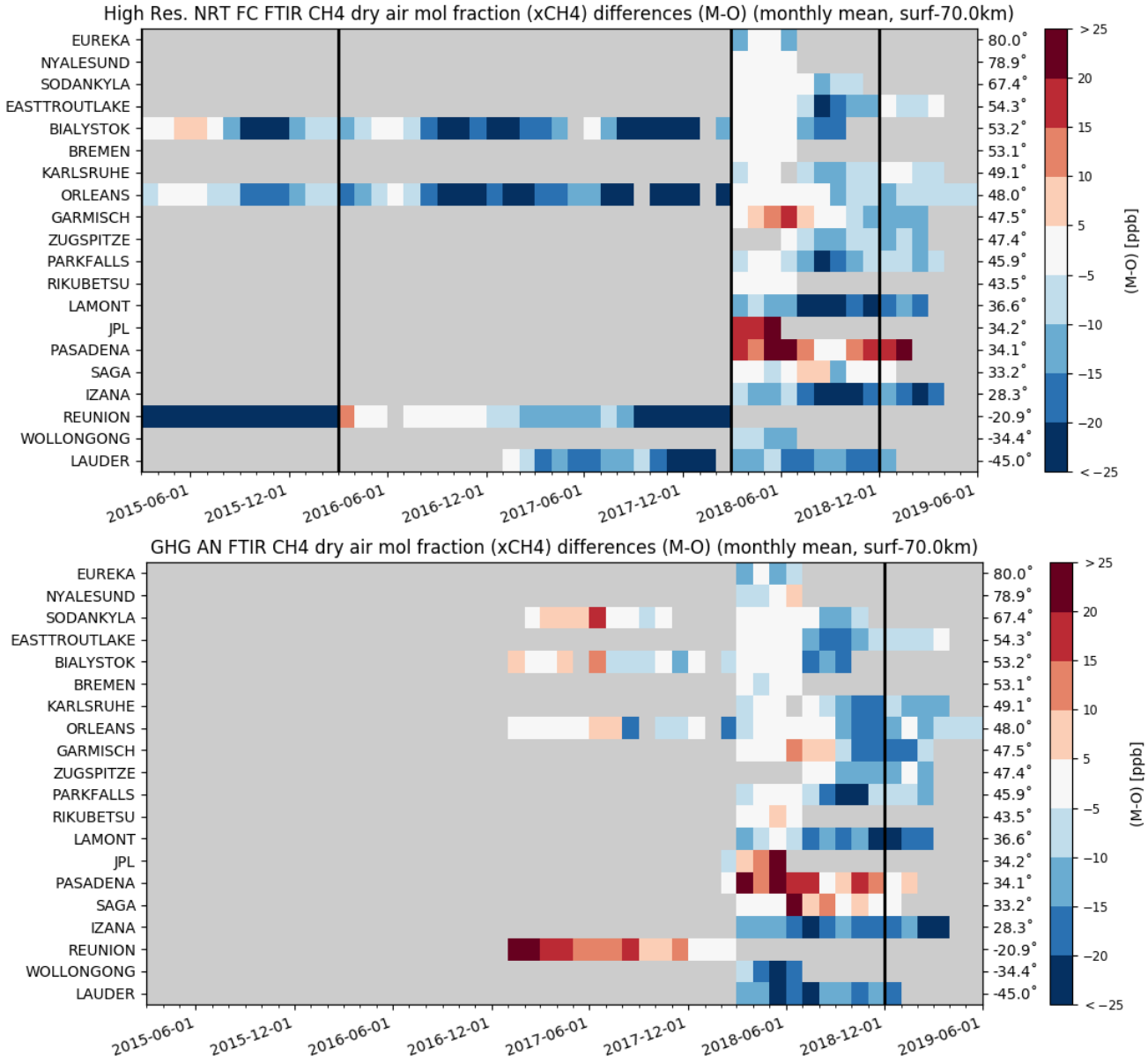

Figure 9.2.1: Monthly differences for the last 4 years (upper plot: high res NRT, lower plot: GHG AN). The stations are sorted by latitude (northern to southern hemisphere).

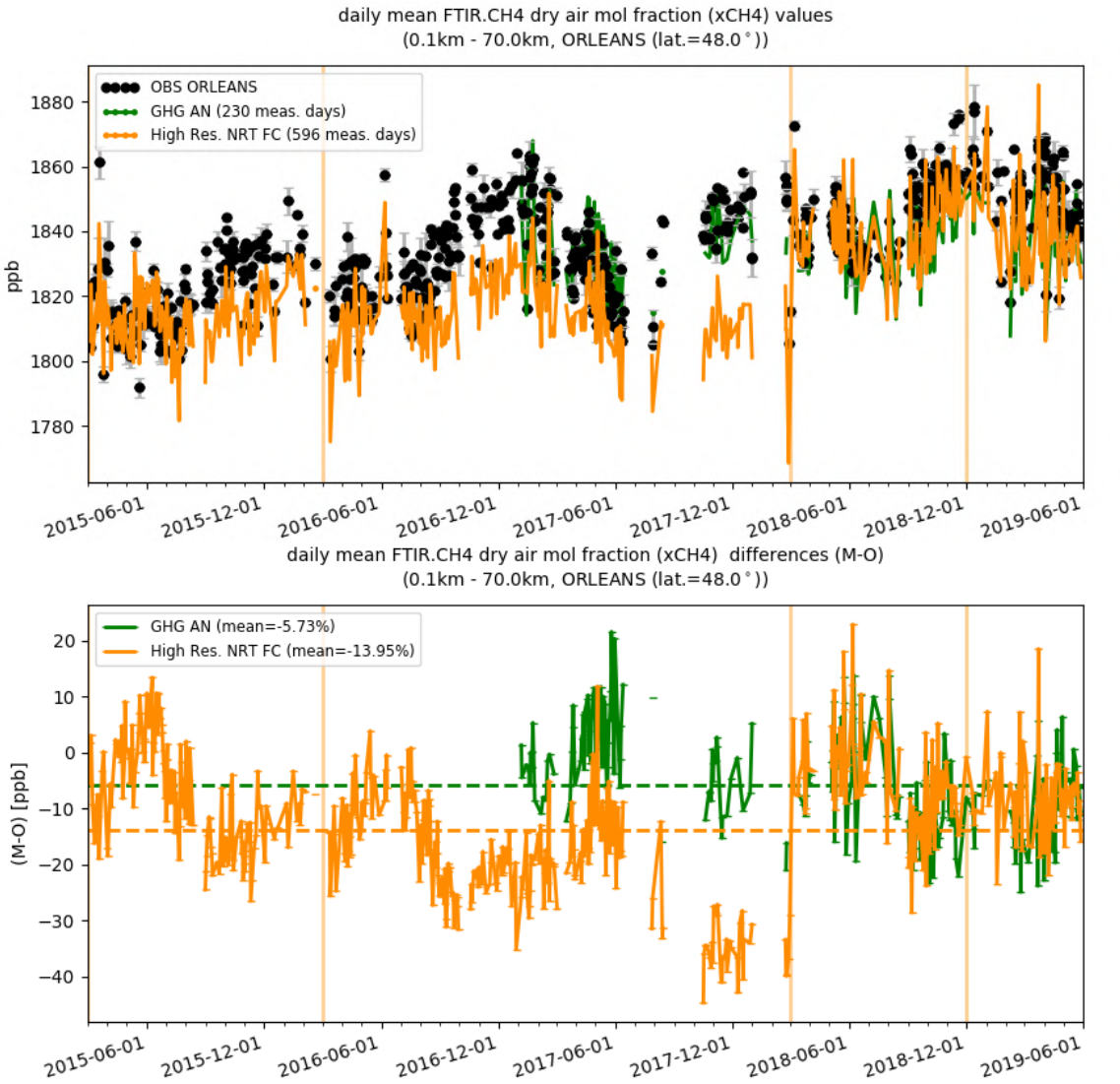

Figure 9.2.2: Comparison of the CO2 model data with TCCON CH4 at Orleans.

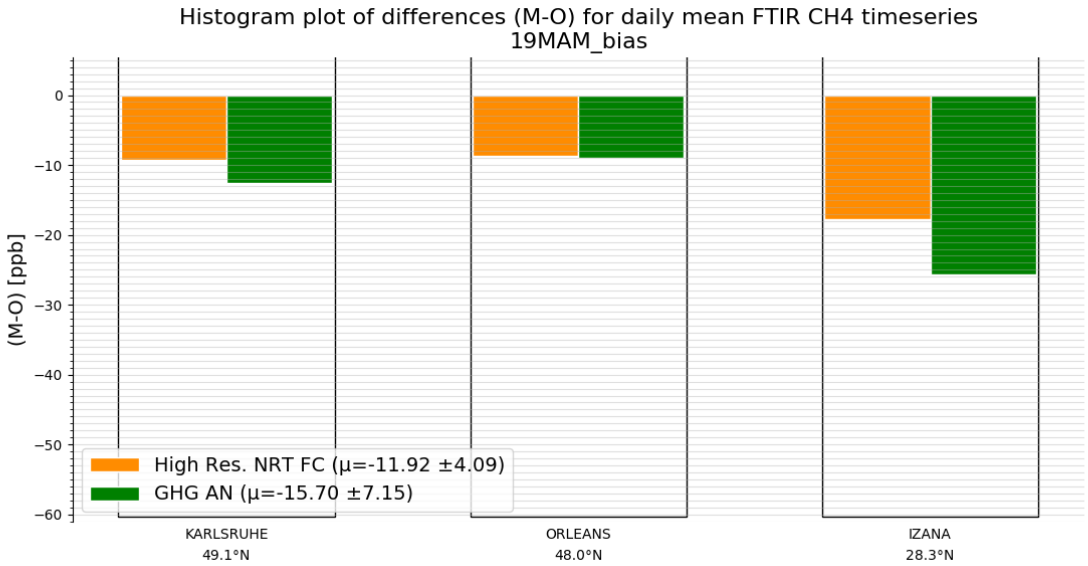

Figure 9.2.3: Differences during the reporting period

Carbon dioxide (CO_2)

Figure 9.2.4 shows the data for the last 4 years. The only data for the reporting is from Orleans, East Trout Lake, Karlsruhe and Izana. Due to the low number of measurements for East Trout Lake during the reporting period only data from Orleans, Karlsruhe and Izana is used for the model evaluation. While the Orleans data cover the whole 3 months of the reporting period, Karlsruhe and Izana data only cover 1 month (March).

The data from these stations show that the model data continues to overestimate the CO_2. The comparison at Orleans shows that the overestimation is significantly higher than in previous years and reached up to 5-6 ppm.

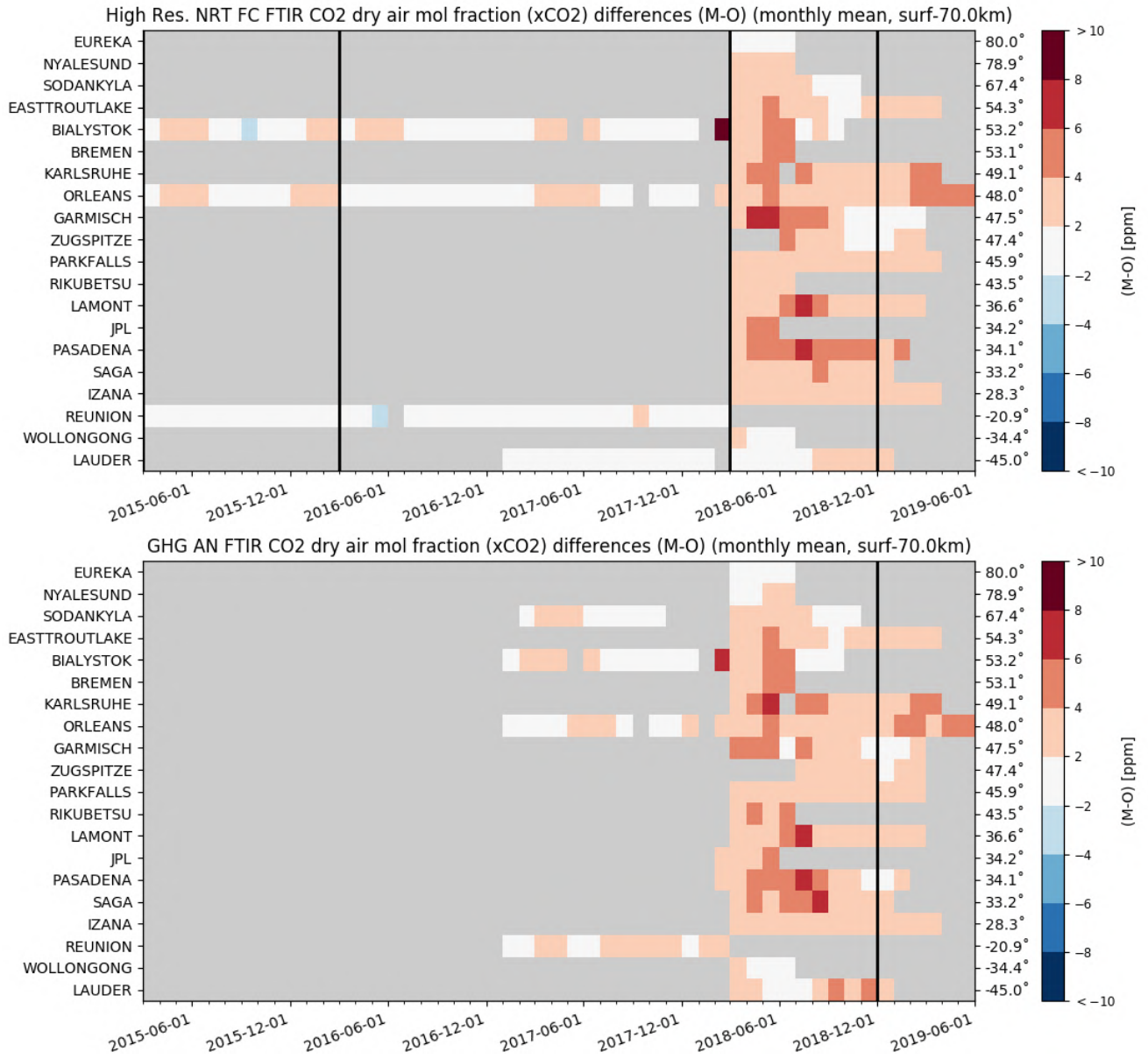

Figure 9.2.4: Monthly differences for the last 4 years (upper plot: high res NRT, lower plot: GHG AN). The stations are sorted by latitude (northern to southern hemisphere).

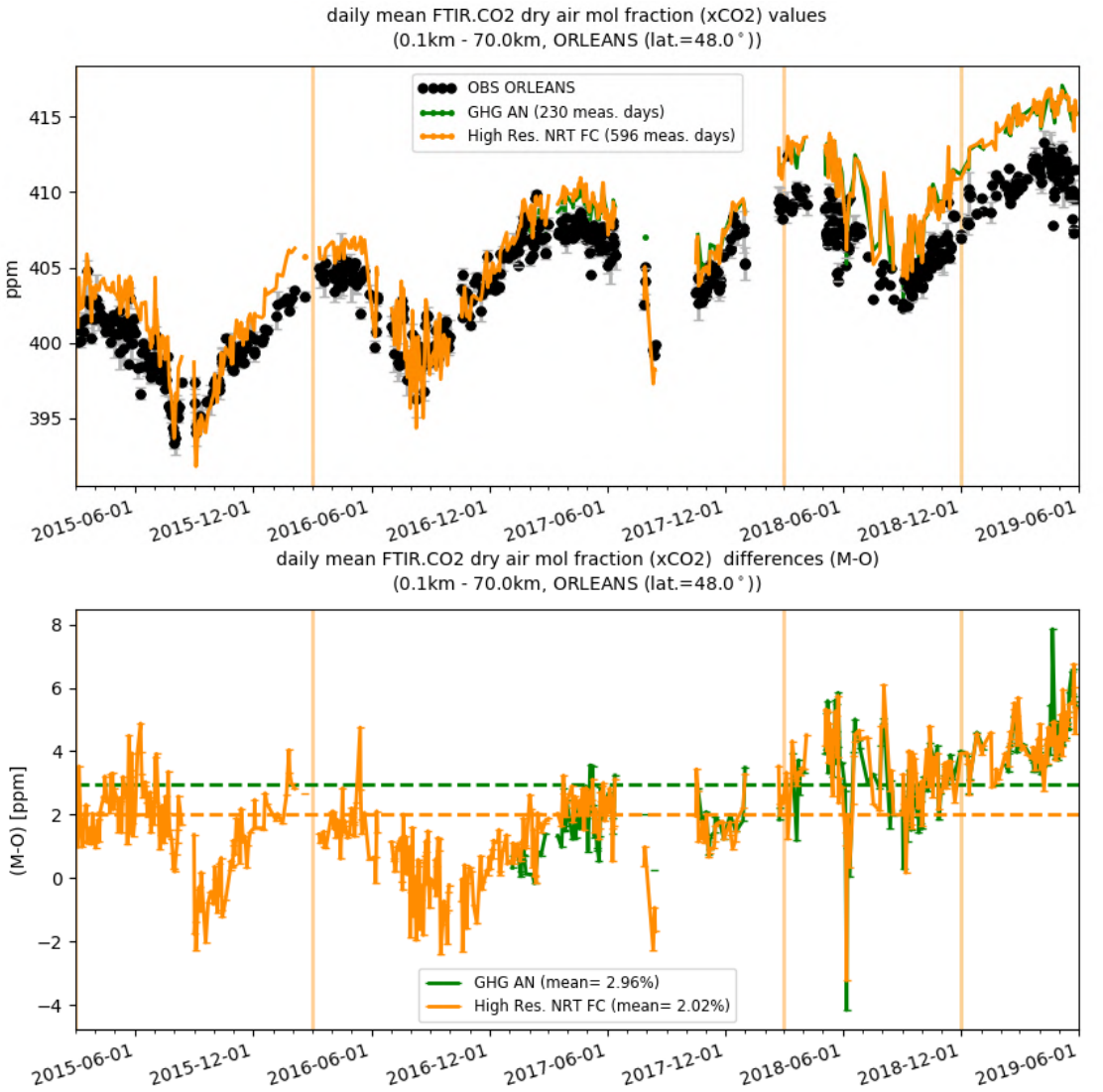

Figure 9.2.5: Comparison of the CO2 model data with TCCON CO2 at Orleans.

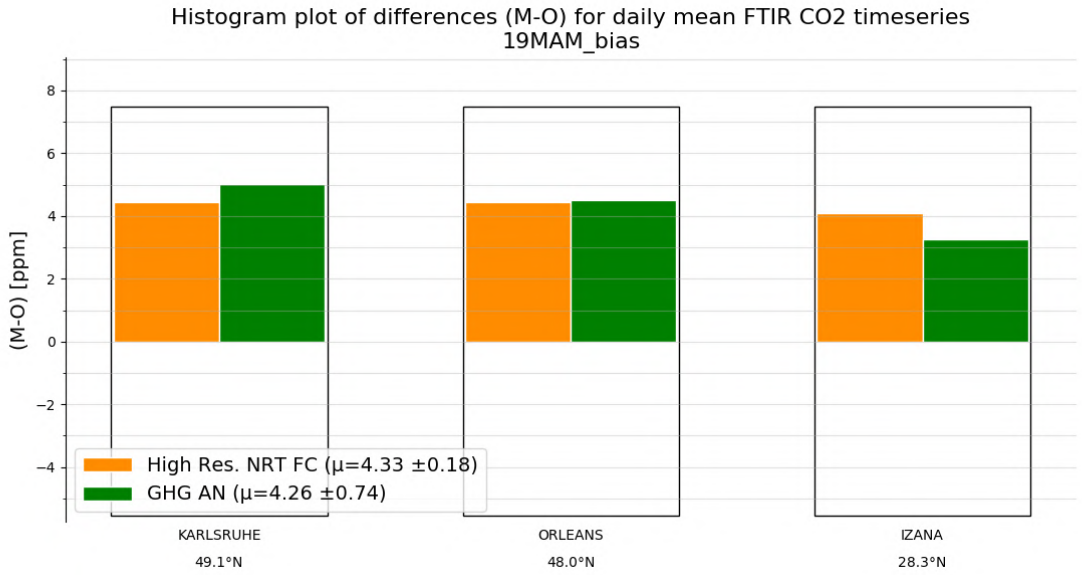

Figure 9.2.6: Differences during the reporting period

9.3 Validation against FTIR observations from the NDACC network

In this section, we compare the CH_4 profiles of the CAMS GHG products with FTIR measurements at different FTIR stations within the NDACC network. These ground-based, remote-sensing instruments are sensitive to the CH4 abundance in the troposphere and lower stratosphere, i.e. between the surface and up to 25 km altitude. Tropospheric and stratospheric CH4 columns are calculated from the FTIR profile data and used to validate corresponding columns obtained from the model data. A description of the instruments and applied methodologies can be found at http://nors.aeronomie.be. The typical uncertainty on the FTIR tropospheric column is 2%, while the uncertainty on the stratospheric column is 7.5%, adding together to a 3% uncertainty on the total column. The systematic uncertainty is large for the NDACC methane product mostly due to higher spectroscopic uncertainties.

Figure 9.3.1 (middle row) shows that the tropospheric columns of CH_4 agree well and only small differences appear between the analysis and the high-resolution model. In comparison with the measurement uncertainty, a slight underestimation is observed in the tropospheric columns which is in agreement with the TCCON results. At Paramaribo the results deviate strongly and this is related to the fact that the Paramaribo measurements have a reduced sensitivity and the tropospheric/stratospheric split is not valid in this case.

The stratospheric columns (Figure 9.3.1, bottom row) show a slight overestimation compared to the measurement uncertainty.

At some sites a seasonal change is observed in either the tropospheric or stratospheric concentrations. Due to the short time period, it is unclear if this is a recurring seasonal dependent model performance. In Figure 9.3.2 the tropospheric and stratospheric relative difference time series are plotted at Thule and St. Petersburg.

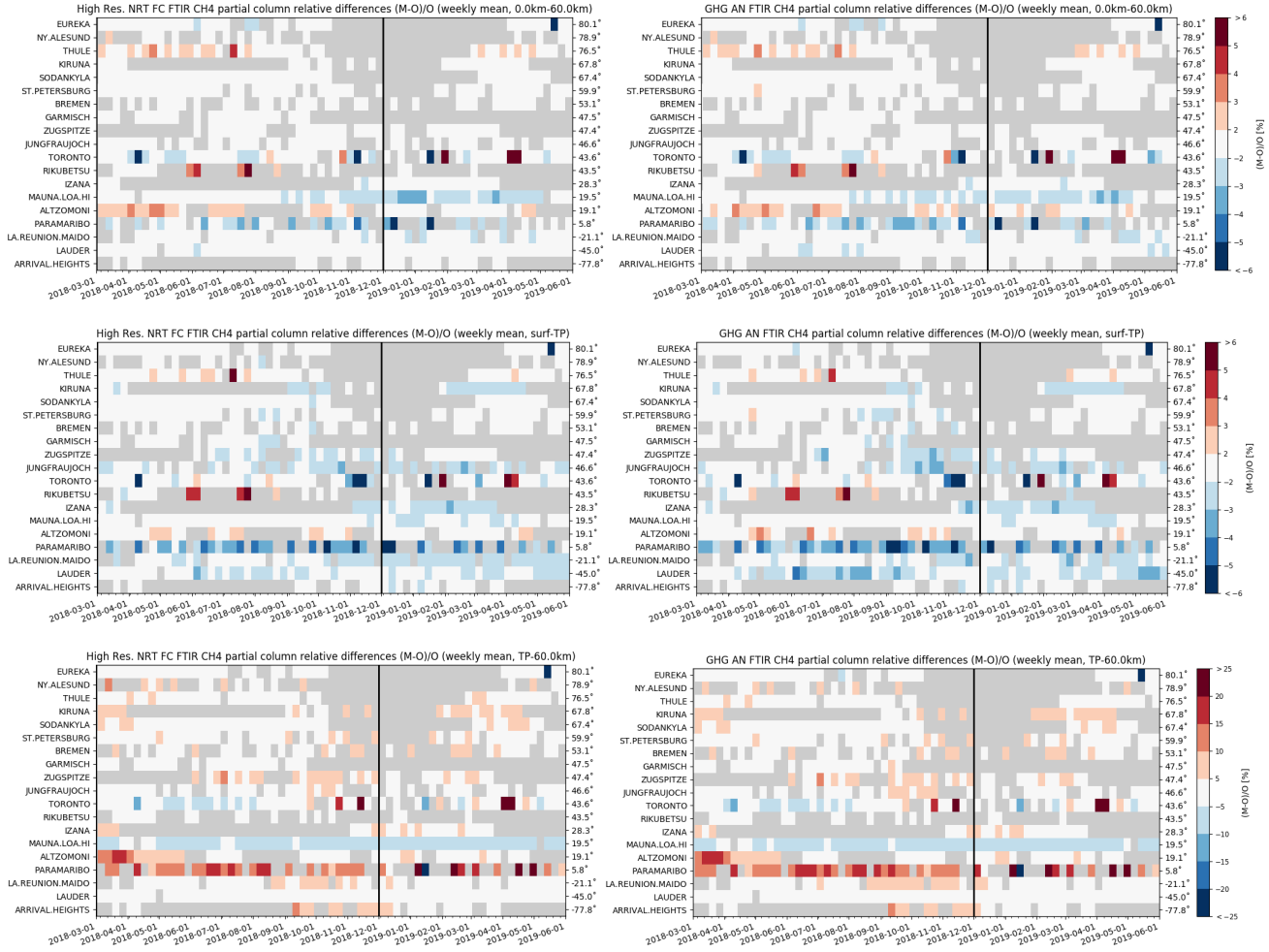

Figure 9.3.1: Weekly mean relative bias for total (top row), tropospheric (middel row) and stratospheric CH4 columns (bottom row) for the period March 2018 – May 2019 for high resolution forecast (left) and the analysis (right). The mid latitude stations at Rikubetsu and Altzomoni show a strong overestimation for both products of the CH4 column. The overall uncertainty for the CH4 total column measurements is approximately 4%. The overall uncertainty for the CH4 total/tropospheric column measurements is approximately 2%, while the stratospheric uncertainty is 7.5% (color scale for the mosaic plots follows uncertainty scale)

Figure 9.3.3 shows Taylor diagrams for the DJF time period and for a selected number of sites (many high latitude stations are not measuring during DJF): some stations have limited observations and should be treated with care. Assimilation has a small effect on the correlation coefficients for most sites; at Reunion and Altzomoni, the analysis has worse correlation.

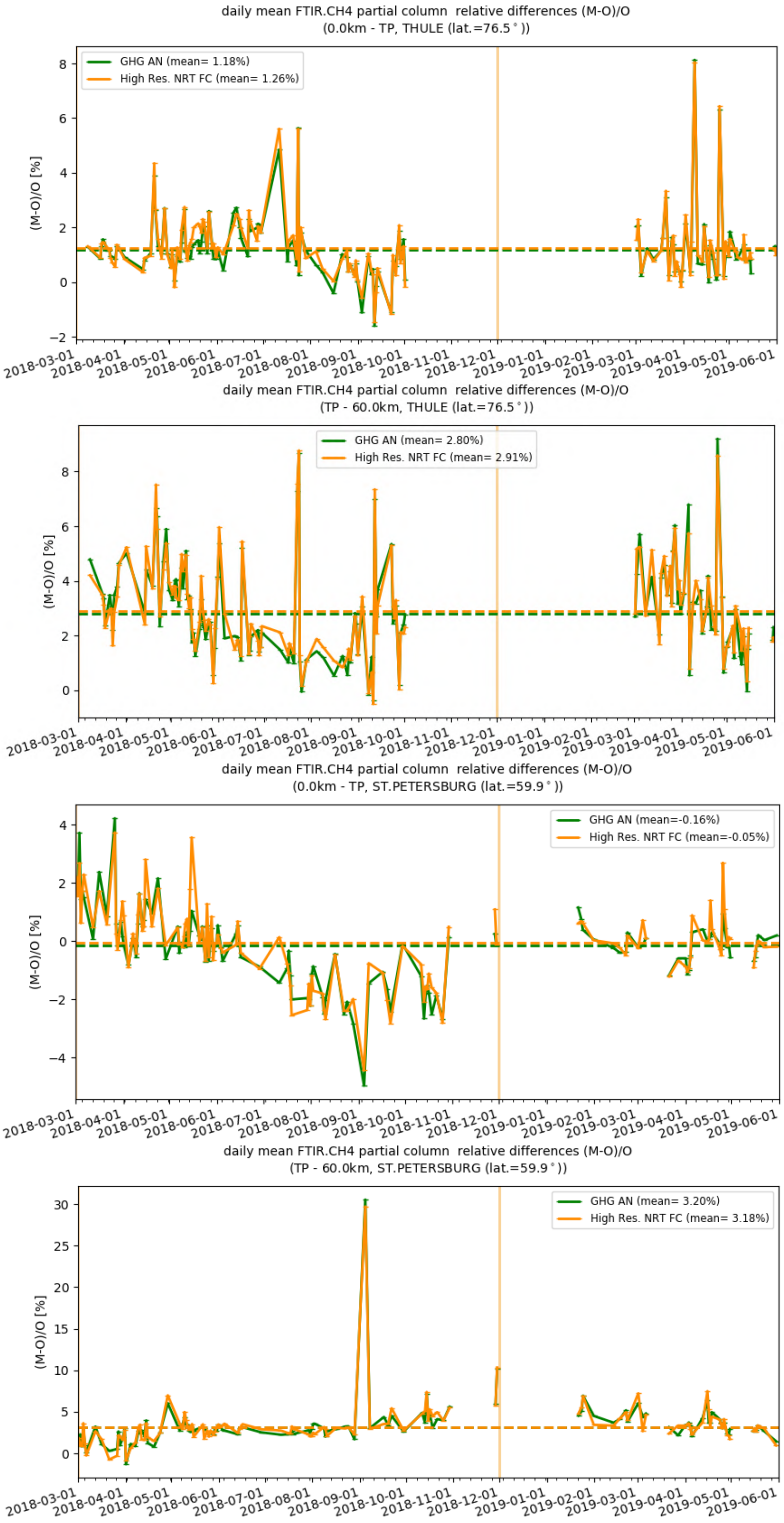

Figure 9.3.2: Daily mean of relative differences for tropospheric CH4 columns (left) and stratospheric CH4 columns (right) at Thule (top) and St Petersburg (bottom). At Thule the stratospheric column shows a reduced bias during the summer, while at St Petersburg the tropospheric column performs worse during June-October.

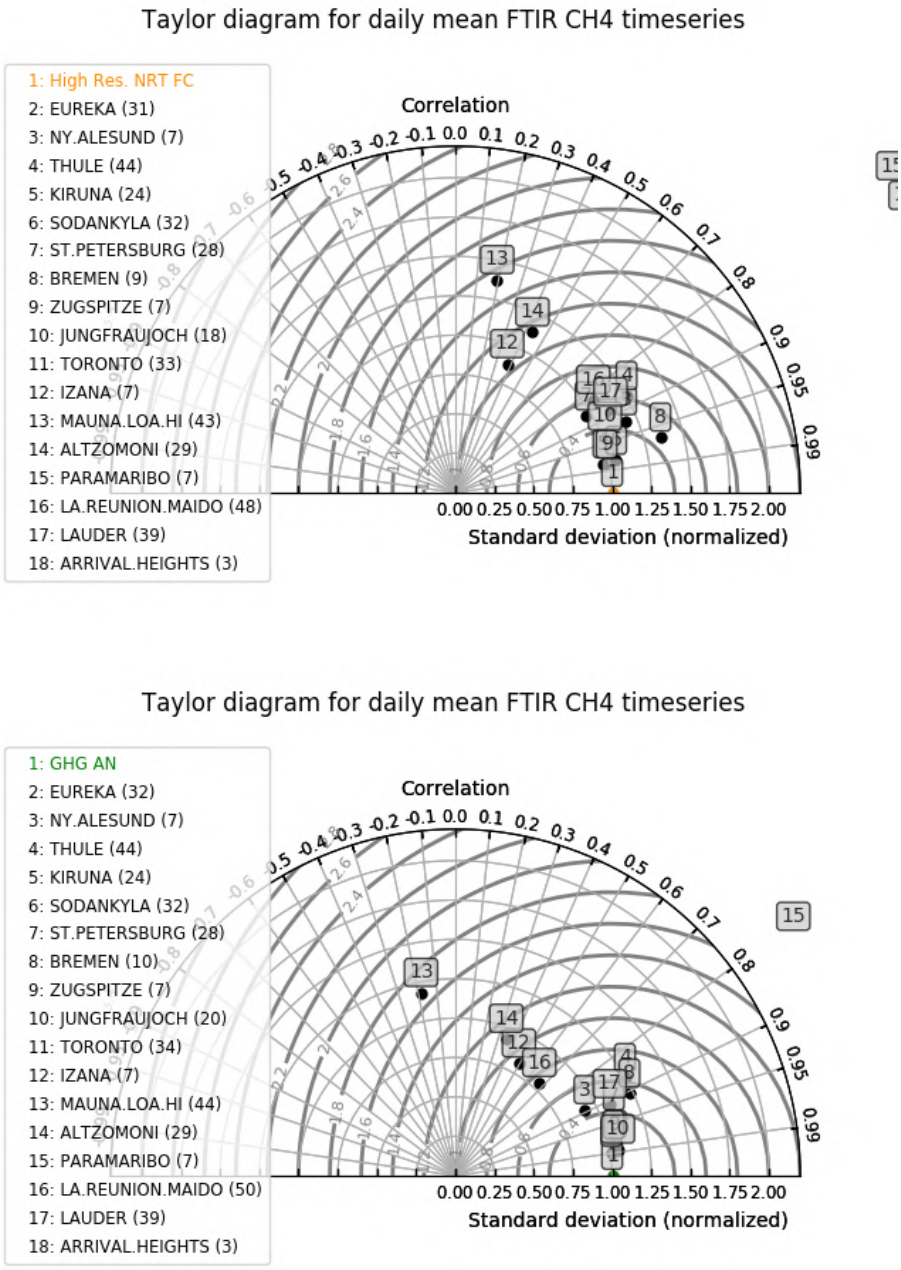

Figure 9.3.3: Taylor diagrams relating the standard deviations for the model /GB time series of total CH4 column data and their correlation for the period 2019 MAM (the stations with a limited number of measurements should be ignored). All time series are normalized such that the std of the model column time series is 1. For the tropical sites Altzomoni, Izana, Mauna Loa and Reunion (Maido) the assimilation decreases the ratio of the standard deviations of both time series significantly: the analysis methane columns are more variable compared to the high-resolution forecast.

10. Event studies

10.1 Fire event in China in April 2019

There was a fire case in the south-west of China in the beginning of April 2019. IASI data does not show the exact location of the fire due to missing data pixels, but it clearly shows an eastward transportation plume on April 2nd. Both model runs captured the geographical location and extent of the plume. There is a clear underestimation of the CO values in the plume up to 40% in the o-suite run and up to 50% in the control run. The values located close to the source of the fire seems to be overestimated.

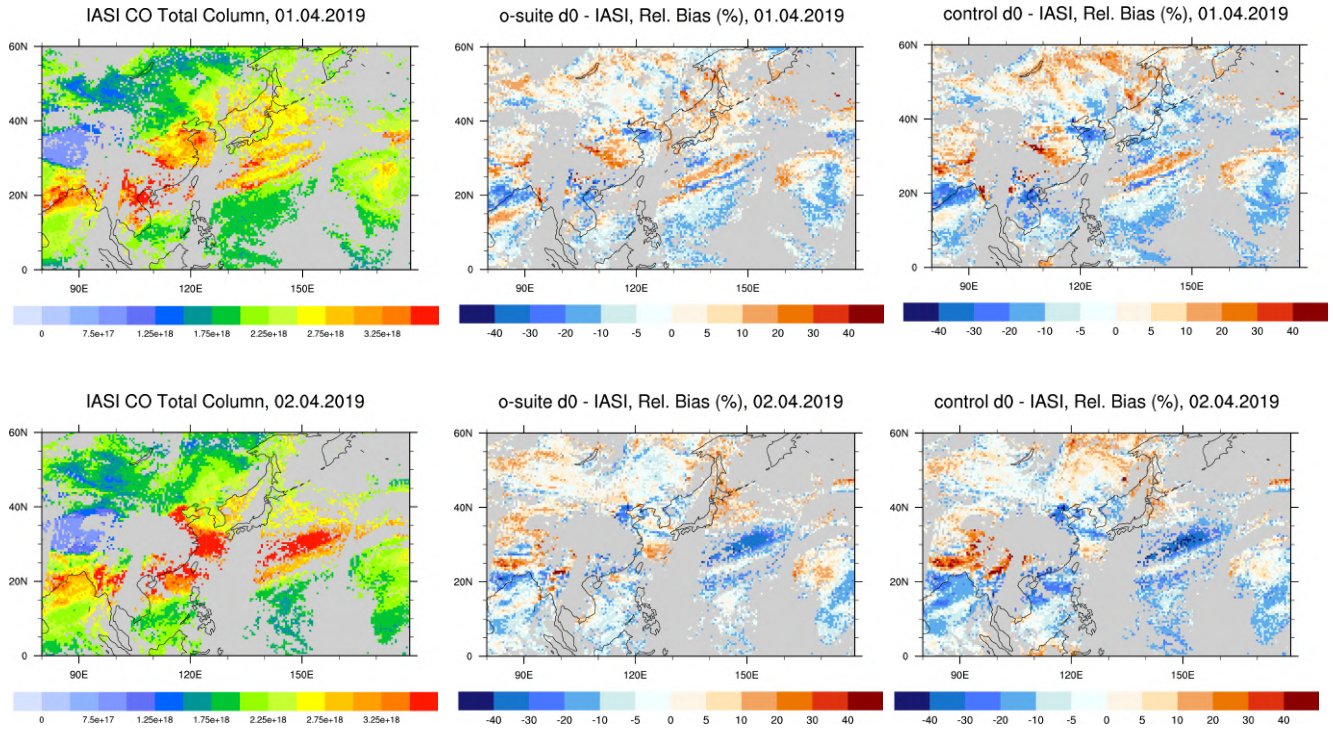

Fig. 10.1: CO total columns from IASI satellite retrievals (left) and relative difference between the model runs and IASI: o-suite (middle) and control (right) for 01.04.19 (top) and 02.04.19 (bottom).

10.2 Dust outbreak over the Mediterranean during April 2019

In second half of April 2019, the MODIS satellite detected an intense outbreak of dust over the Mediterranean Basin (see Figure 10.1.1). The event started on 18th April associated with a low-pressure system in North of Algeria that caused the dust emission in the region of North Algeria and Syria. Dust was transported towards the Western Mediterranean (see Palma de Mallorca in Figure 7.2.3 and Sa Pobla in Figure 7.4.5) and during the following days the dust plume crossed the Central Mediterranean (see Lecce in Figure 7.2.3, Messina in Figure 7.4.2 and Venaco in Figure 7.4.3), arriving in the Eastern Mediterranean on 23rd April (see Nicosia in Figure 7.2.3 and IMS-METU-ERDEMLI in Figure 7.4.2).

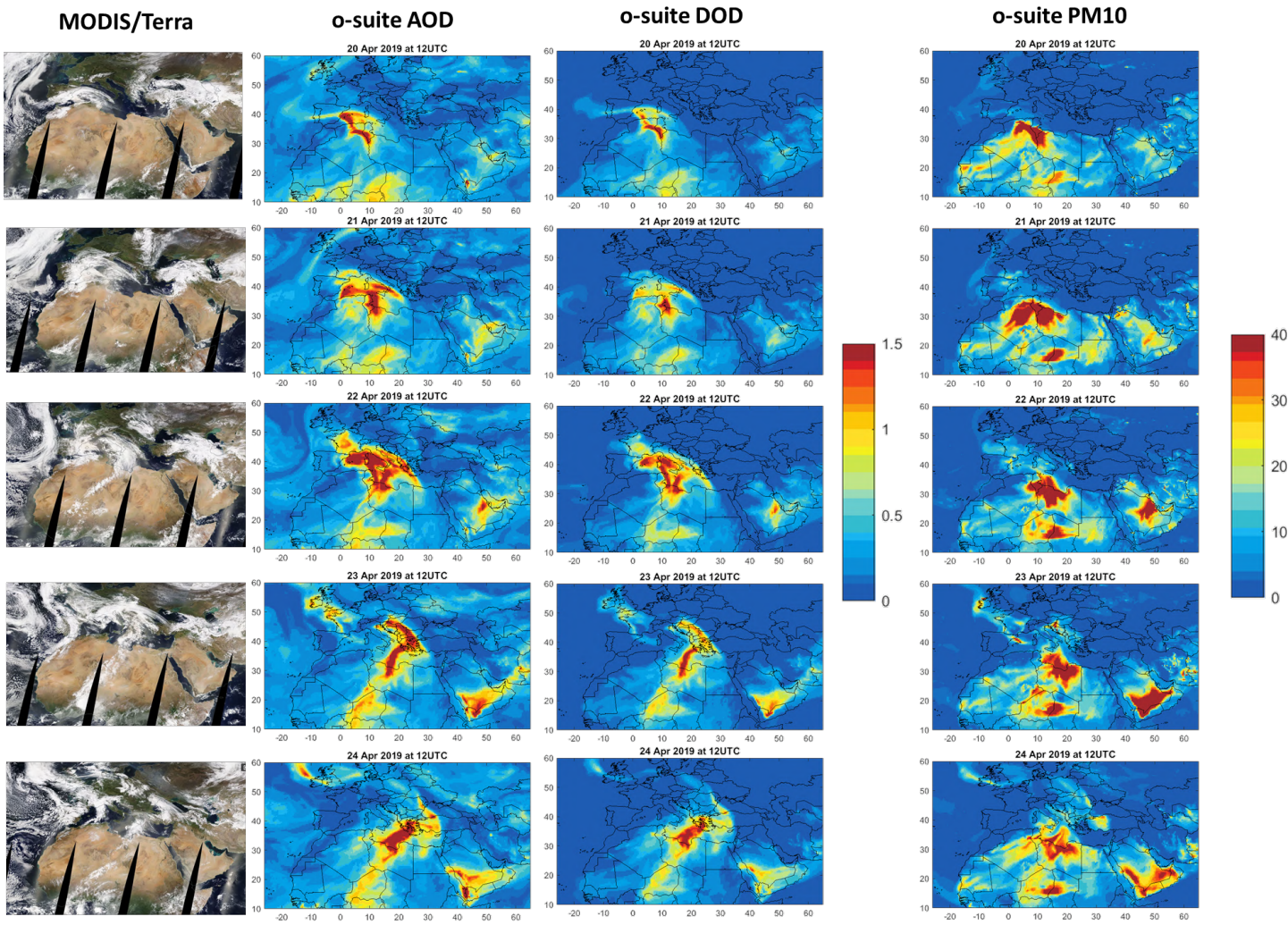

Figure 10.1.1: Daily composite of NASA MODIS/Terra well as AOD, DOD and PM10 at 12UTC from o-suite) for 20-24 April 2019.

The event was associated with the presence of clouds as shown in Figure 10.1.1. Because of this, the quantitative comparison with the MODIS AOD products is limited. The CAMS o-suite AOD did reproduce the spatial distribution and timing of the two dust plumes as shown by the comparison with MODIS/Terra (see Figure 10.1.1). However, the comparison with AERONET (Section 7.2 and 7.4) and EIONET (Section 7.4) shows that CAMS o-suite overestimated the aerosol concentrations during this event, reaching AOD values over 1.5 over the Mediterranean and PM10 over 300 μg/m^3 in some European sites.

11. References

Agusti-Panareda, A., Monitoring upgrades of analysis/forecast system, MACC-III Deliverable D44.04, June 2015.

Bergamaschi, P., Frankenberg, C., Meirink, J. F., Krol, M., Villani, M. G., Houweling, S., Dentener, F., Dlugokencky, E. J., Miller, J. B., Gatti, L. V., Engel, A., and Levin, I.: Inverse modeling of global and regional CH4 emissions using SCIAMACHY satellite retrievals, J. Geophys. Res., 114, D22301, doi:10.1029/2009JD012287, 2009.

Benedetti, A., J.-J. Morcrette, O. Boucher, A. Dethof, R. J. Engelen, M. Fisher, H. Flentjes, N. Huneeus, L. Jones, J. W. Kaiser, S. Kinne, A. Mangold, M. Razinger, A. J. Simmons, M. Suttie, and the GEMS-AER team: Aerosol analysis and forecast in the ECMWF Integrated Forecast System. Part II : Data assimilation, J. Geophys. Res., 114, D13205, doi:10.1029/2008JD011115, 2009.

Boussetta, S., Balsamo, G., Beljaars, A., Agusti-Panareda, A., Calvet, J.-C., Jacobs, C., van den Hurk, B., Viterbo, P., Lafont, S., Dutra, E., Jarlan, L., Balzarolo, M., Papale, D., and van der Werf, G.: Natural carbon dioxide exchanges in the ECMWF Integrated Forecasting System: implementation and offline validation, J. Geophys. Res.-Atmos., 118, 1–24, doi: 10.1002/jgrd.50488, 2013.

Braathen, WMO Arctic Ozone Bulletin No 1/2016, DOI:10.13140/RG.2.1.4929.6403, 2016.

Cammas, J.P., Brioude J., Chaboureau J.-P., Duron J., Mari C., Mascart P., Nédélec P., Smit H., Pätz H.-W., Volz-Thomas A., Stohl A., and Fromm M., Injection in the lower stratosphere of biomass fire emissions followed by long-range transport: a MOZAIC case study. Atmos. Chem. Phys., 9, 5829-5846, 2009

Cariolle, D. and Teyssèdre, H.: A revised linear ozone photochemistry parameterization for use in transport and general circulation models: multi-annual simulations, Atmos. Chem. Phys., 7, 2183-2196, doi:10.5194/acp-7-2183-2007, 2007.

Dee, D. P. and S. Uppala, Variational bias correction of satellite radiance data in the ERA-Interim reanalysis. Quart. J. Roy. Meteor. Soc.,135, 1830-1841, 2009.

Deeter, M. N., Emmons, L. K., Edwards, D. P., Gille, J. C., and Drummond, J. R.: Vertical resolution and information content of CO profiles retrieved by MOPITT, Geophys. Res. Lett., 31, L15112, doi:10.1029/2004GL020235, 2004.

Deeter, M. N., et al. (2010), The MOPITT version 4 CO product: Algorithm enhancements, validation, and long-term stability, J. Geophys. Res., 115, D07306, doi:10.1029/2009JD013005.

Dentener, F., et al., 2006: Emissions of primary aerosol and precursor gases in the years 2000 and 1750 prescribed data-sets for AeroCom, Atmos. Chem. Phys., 6, 4321 – 4344.

Deshler, T., J.L. Mercer, H.G.J. Smit, R. Stubi, G. Levrat, B.J. Johnson, S.J. Oltmans, R. Kivi, A.M. Thompson, J. Witte, J. Davies, F.J. Schmidlin, G. Brothers, T. Sasaki (2008) Atmospheric comparison of electrochemical cell ozonesondes from different maufacturers, and with different cathode solution strengths: The Balloon Experiment on Standards for Ozonsondes. J. Geophys. Res.113, D04307, doi:10.1029/2007JD008975

Dupuy, E., et al.: Validation of ozone measurements from the Atmospheric Chemistry Experiment (ACE), Atmos. Chem. Phys., 9, 287-343, doi:10.5194/acp-9-287-2009, 2009.

Elbern, H., Schwinger, J., Botchorishvili, R.: Chemical state estimation for the middle atmosphere by four-dimensional variational data assimilation: System configuration. Journal of Geophysical Research (Atmospheres) 115, 6302, 2010.

Emmons, L. K., D. P. Edwards, M. N. Deeter, J. C. Gille, T. Campos, P. Nédélec, P. Novelli, and G. Sachse, Measurements of Pollution In The Troposphere (MOPITT) validation through 2006 Atmos. Chem. Phys., 9, 1795-1803, 2009

Errera, Q., Daerden, F., Chabrillat, S., Lambert, J. C., Lahoz, W. A., Viscardy, S., Bonjean, S., and Fonteyn, D., 4D-Var Assimilation of MIPAS chemical observations: ozone and nitrogen dioxide analyses, Atmos. Chem. Phys., 8, 6169-6187, 2008.

Errera, Q. and Ménard, R.: Technical Note: Spectral representation of spatial correlations in variational assimilation with grid point models and application to the belgian assimilation system for chemical observations (BASCOE), Atmos. Chem. Phys. Discuss., 12, 16763-16809, doi:10.5194/acpd-12-16763-2012, 2012.

Eskes, H.J., S. Basart, A. Benedictow, Y. Bennouna, A.-M. Blechschmidt, S. Chabrillat, Y. Christophe, E. Cuevas, J. Douros, H. Flentje, K. M. Hansen, J. Kapsomenakis, B. Langerock, M. Ramonet, A. Richter, M. Schulz, N. Sudarchikova, A. Wagner, T. Warneke, C. Zerefos, Observations characterisation and validation methods document, Copernicus Atmosphere Monitoring Service (CAMS) report, CAMS84_2015SC3_D.84.8.1.1-2018_observations_v3.pdf, October 2018 (2018a). Available from: http://atmosphere.copernicus.eu/user-support/validation/verification-global-services

Eskes, H. J., S. Basart, A. Benedictow, Y. Bennouna, A.-M. Blechschmidt, S. Chabrillat, Y. Christophe, H. Clark, E. Cuevas, K. M. Hansen, U. Im, J. Kapsomenakis, B. Langerock, K. Petersen, M. Schulz, A. Wagner, C. Zerefos, Upgrade verification note for the CAMS near-real time global atmospheric composition service, Copernicus Atmosphere Monitoring Service (CAMS) report, CAMS84_2015SC3_D84.3.1.5_201802_esuite_v1.pdf, February 2018 (2018b)

Eskes et al., Upgrade verification note for the CAMS near-real time global atmospheric composition service, Addendum July 2018, CAMS84_2015SC3_D84.3.1.5_201802_esuite_v1.pdf (2018c).

Flemming, J., Huijnen, V., Arteta, J., Bechtold, P., Beljaars, A., Blechschmidt, A.-M., Diamantakis, M., Engelen, R. J., Gaudel, A., Inness, A., Jones, L., Josse, B., Katragkou, E., Marecal, V., Peuch, V.-H., Richter, A., Schultz, M. G., Stein, O., and Tsikerdekis, A.: Tropospheric chemistry in the Integrated Forecasting System of ECMWF, Geosci. Model Dev., 8, 975-1003, doi:10.5194/gmd-8-975-2015, 2015.

Flemming, J., Benedetti, A., Inness, A., Engelen, R. J., Jones, L., Huijnen, V., Remy, S., Parrington, M., Suttie, M., Bozzo, A., Peuch, V.-H., Akritidis, D., and Katragkou, E.: The CAMS interim Reanalysis of Carbon Monoxide, Ozone and Aerosol for 2003–2015, Atmos. Chem. Phys., 17, 1945-1983, doi:10.5194/acp-17-1945-2017, 2017.

Franco, B., et al., Retrievals of formaldehyde from ground-based FTIR and MAX-DOAS observations at the Jungfraujoch station and comparisons with GEOS-Chem and IMAGES model simulations, Atmos. Meas. Tech., 8, 1733-1756, 2015

Gielen, C., Van Roozendael, M., Hendrick, F., Pinardi, G., Vlemmix, T., De Bock, V., De Backer, H., Fayt, C., Hermans, C., Gillotay, D., and Wang, P.: A simple and versatile cloud-screening method for MAX-DOAS retrievals, Atmos. Meas. Tech., 7, 3509-3527, doi:10.5194/amt-7-3509-2014, 2014.

Granier, C. et al.: Evolution of anthropogenic and biomass burning emissions of air pollutants at global and regional scales during the 1980–2010 period. Climatic Change (109), 2011

Holben, B. N., Eck, T. F., Slutsker, I., Tanré, D., Buis, J. P., Setzer, A., Vermote, E., Reagan, J. A., Kaufman, Y. J., Nakajima, T., Lavenu, F., Jankowiak, I., and Smirnov A.: AERONET – a federated instrument network and data archive for aerosol characterization, Remote Sens. Environ., 66, 1–16, 5529, 5533, 5537, 5544, 1998.

Hommel, R., Eichmann, K.-U., Aschmann, J., Bramstedt, K., Weber, M., von Savigny, C., Richter, A., Rozanov, A., Wittrock, F., Khosrawi, F., Bauer, R., and Burrows, J. P.: Chemical ozone loss and ozone mini-hole event

during the Arctic winter 2010/2011 as observed by SCIAMACHY and GOME-2, Atmos. Chem. Phys., 14, 3247-3276, doi:10.5194/acp-14-3247-2014, 2014.

Huijnen, V., et al.: The global chemistry transport model TM5: description and evaluation of the tropospheric chemistry version 3.0, Geosci. Model Dev., 3, 445-473, doi:10.5194/gmd-3-445-2010, 2010.

Inness, A., Blechschmidt, A.-M., Bouarar, I., Chabrillat, S., Crepulja, M., Engelen, R. J., Eskes, H., Flemming, J., Gaudel, A., Hendrick, F., Huijnen, V., Jones, L., Kapsomenakis, J., Katragkou, E., Keppens, A., Langerock, B., de Mazière, M., Melas, D., Parrington, M., Peuch, V. H., Razinger, M., Richter, A., Schultz, M. G., Suttie, M., Thouret, V., Vrekoussis, M., Wagner, A., and Zerefos, C.: Data assimilation of satellite-retrieved ozone, carbon monoxide and nitrogen dioxide with ECMWF's Composition-IFS, Atmos. Chem. Phys., 15, 5275-5303, doi:10.5194/acp-15-5275-2015, 2015.

Janssens-Maenhout, G., Dentener, F., Aardenne, J. V., Monni, S., Pagliari, V., Orlandini, L., Klimont, Z., Kurokawa, J., Akimoto, H., Ohara, T., Wankmueller, R., Battye, B., Grano, D., Zuber, A., and Keating, T.: EDGAR-HTAP: a Harmonized Gridded Air Pollution Emission Dataset Based on National Inventories, JRC68434, EUR report No EUR 25 299–2012, ISBN 978-92-79- 23122-0, ISSN 1831-9424, European Commission Publications Office, Ispra (Italy), 2012.

Jaross, G., Bhartia, P.K., Chen, G., Kowitt, M., Haken, M., Chen, Z., Xu, Ph., Warner, J., Kelly, T. : OMPS Limb Profiler instrument performance assessment, J. Geophys. Res. Atmos 119, 2169-8996, 2014.

Kaiser, J. W., Heil, A., Andreae, M. O., Benedetti, A., Chubarova, N., Jones, L., Morcrette, J.-J., Razinger, M., Schultz, M. G., Suttie, M., and van der Werf, G. R.: Biomass burning emissions estimated with a global fire assimilation system based on observed fire radiative power, Biogeosciences, 9, 527-554, doi:10.5194/bg-9-527-2012, 2012.

Kramarova, N. A., Nash, E. R., Newman, P. A., Bhartia, P. K., McPeters, R. D., Rault, D. F., Seftor, C. J., Xu, P. Q., and Labow, G. J.: Measuring the Antarctic ozone hole with the new Ozone Mapping and Profiler Suite (OMPS), Atmos. Chem. Phys., 14, 2353-2361, doi:10.5194/acp-14-2353-2014, 2014.

Lahoz, W. A., Errera, Q., Viscardy, S., and Manney G. L., The 2009 stratospheric major warming described from synergistic use of BASCOE water vapour analyses and MLS observations, Atmos. Chem. Phys. 11, 4689-4703, 2011

Lambert, A, et al., Aura Microwave Limb Sounder Version 3.4 Level-2 near real-time data user guide, http://disc.sci.gsfc.nasa.gov/Aura/data-holdings/MLS/documents/NRT-user-guide-v34.pdf

Langerock, B., De Mazière, M., Hendrick, F., Vigouroux, C., Desmet, F., Dils, B., and Niemeijer, S.: Description of algorithms for co-locating and comparing gridded model data with remote-sensing observations, Geosci. Model Dev., 8, 911-921, doi:10.5194/gmd-8-911-2015, 2015.

Lefever, K., van der A, R., Baier, F., Christophe, Y., Errera, Q., Eskes, H., Flemming, J., Inness, A., Jones, L., Lambert, J.-C., Langerock, B., Schultz, M. G., Stein, O., Wagner, A., and Chabrillat, S.: Copernicus stratospheric ozone service, 2009–2012: validation, system intercomparison and roles of input data sets, Atmos. Chem. Phys., 15, 2269-2293, doi:10.5194/acp-15-2269-2015, 2015.

Liu, Z., et al., Exploring the missing source of glyoxal (CHOCHO) over China, Geophys. Res. Lett., 39, L10812, doi: 10.1029/2012GL051645, 2012

Massart, S., Flemming, J., Cariolle, D., Jones, L., High resolution CO tracer forecasts, MACC-III Deliverable D22.04, May 2015, available from http://www.gmes-atmosphere.eu/documents/macciii/deliverables/grg

Morcrette, J.-J., O. Boucher, L. Jones, D. Salmond, P. Bechtold, A. Beljaars, A. Benedetti, A. Bonet, J. W. Kaiser, M. Razinger, M. Schulz, S. Serrar, A. J. Simmons, M. Sofiev, M. Suttie, A. M. Tompkins, and A. Untch: Aerosol

analysis and forecast in the ECMWF Integrated Forecast System. Part I: Forward modelling, J. Geophys. Res., 114, D06206, doi:10.1029/2008JD011235, 2009.

Richter, A., Burrows, J. P., Nüß, H., Granier, C, Niemeier, U.: Increase in tropospheric nitrogen dioxide over China observed from space, Nature, 437, 129-132, doi: 10.1038/nature04092, 2005

*Richter, A., Begoin, M., Hilboll, A., and Burrows, J. P.: An improved NO2 retrieval for the GOME-2 satellite instrument, Atmos. Meas. Tech. , **4**, 1147-1159, doi:10.5194/amt-4-1147-2011, 2011*

Schulz, M., Y. Christophe, M. Ramonet, Wagner, A., H.J. Eskes, S. Basart, A. Benedictow, Y. Bennouna, A.-M. Blechschmidt, S. Chabrillat, E. Cuevas, A. El- Yazidi, H. Flentje, K.M. Hansen, U. Im, J. Kapsomenakis, B. Langerock, A. Richter, N. Sudarchikova, V. Thouret, T. Warneke, C. Zerefos, Validation report of the CAMS near-real-time global atmospheric composition service: Period December 2018 -February 2019, Copernicus Atmosphere Monitoring Service (CAMS) report, CAMS84_2018SC1_D1.1.1_DJF2019_v1.pdf, June 2019, doi:10.24380/7th6-tk72.

Sindelarova, K., Granier, C., Bouarar, I., Guenther, A., Tilmes, S., Stavrakou, T., Müller, J.-F., Kuhn, U., Stefani, P., and Knorr, W.: Global data set of biogenic VOC emissions calculated by the MEGAN model over the last 30 years, Atmos. Chem. Phys., 14, 9317-9341, doi:10.5194/acp-14-9317-2014, 2014.

Smit, H.G.J., W. Straeter, B.J. Johnson, S.J. Oltmans, J. Davies, D.W. Tarasick, B. Hoegger, R. Stubi, F.J. Schmidlin, T. Northam, A.M. Thompson, J.C. Witte, I. Boyd: Assessment of the performance of ECC-ozonesondes under quasi-flight conditions in the environmental simulation chamber: Insights from the Juelich Ozone Sonde Intercomparison Experiment (JOSIE), J. Geophys. Res. 112, D19306, doi:10.1029/2006JD007308, 2007.

Solomon, S., Haskins, J., Ivy, D. J. and Min, F.: Fundamental differences between Arctic and Antarctic ozone depletion, PNAS 2014 111 (17) 6220-6225, doi:10.1073/pnas.1319307111, 2014.

Stavrakou,T., First space-based derivation of the global atmospheric methanol fluxes, Atm. Chem. Phys., 11, 4873-4898, 2013.

Strahan, S.E., A.R. Douglass, and P.A. Newman, The contributions of chemistry and transport to low arctic ozone in March 2011 derived from Aura MLS observations, J. Geophys. Res. Atmos., 118, 1563–1576, doi:10.1002/jgrd.50181, 2013.

Taha, G.; Jaross, G. R.; Bhartia, P. K.: Validation of OMPS LP Ozone Profiles Version 2.0 with MLS, Ozone Sondes and Lidar Measurements, American Geophysical Union, Fall Meeting 2014, abstract #A33J-3322, 2014.

Taylor, K.E.: Summarizing multiple aspects of model performance in a single diagram. J.Geophys. Res., 106, 7183-7192, 2001.

van der A, R. J. , M. A. F. Allaart, and H. J. Eskes, Multi sensor reanalysis of total ozone, Atmos. Chem. Phys., 10, 11277–11294, doi:10.5194/acp-10-11277-2010, www.atmos- chem-phys.net/10/11277/2010/, 2010

van der A, R., M. Allaart, H. Eskes, K. Lefever, Validation report of the MACC 30-year multi-sensor reanalysis of ozone columns Period 1979-2008, MACC-II report, Jan 2013, MACCII_VAL_DEL_D_83.3_OzoneMSRv1_20130130.docx/pdf.

van der A, R. J., Allaart, M. A. F., and Eskes, H. J.: Extended and refined multi sensor reanalysis of total ozone for the period 1970–2012, Atmos. Meas. Tech., 8, 3021-3035, doi:10.5194/amt-8-3021-2015, 2015.

*Vrekoussis, M., Wittrock, F., Richter, A., and Burrows, J. P.: GOME-2 observations of oxygenated VOCs: what can we learn from the ratio glyoxal to formaldehyde on a global scale?, Atmos. Chem. Phys., **10**, 10145-10160, doi:10.5194/acp-10-10145-2010, 2010*

Wennberg, P. O., Mui, W., Wunch, D., Kort, E. A., Blake, D. R., Atlas, E. L., Santoni, G. W., Wofsy, S. C., Diskin, G. S., Jeong, S., and Fischer, M. L.: On the sources of methane to the Los Angeles atmosphere, Environ. Sci. Technol., 46, 9282–9289, https://doi.org/10.1021/es301138y, 2012

Wittrock, F., A. Richter, H. Oetjen, J. P. Burrows, M. Kanakidou, S. Myriokefalitakis, R. Volkamer, S. Beirle, U. Platt, and T. Wagner, Simultaneous global observations of glyoxal and formaldehyde from space, Geophys. Res. Lett., 33, L16804, doi:10.1029/2006GL026310, 2006

WMO (2010), Guidelines for the Measurement of Atmospheric Carbon Monoxide, GAW Report No. 192, World Meteorological Organization, Geneva, Switzerland, 2010.

WMO (2013), Guidelines for the Continuous Measurements of Ozone in the Troposphere, GAW Report No. 209, World Meteorological Organization, Geneva, Switzerland, 2013.

Wunch, D., Wennberg, P. O., Toon, G. C., Keppel-Aleks, G., and Yavin, Y. G.: Emissions of greenhouse gases from a North American megacity, Geophys. Res. Lett., 36, 1–5, https://doi.org/10.1029/2009GL039825, 2009.

Annex 1: Acknowledgements

Listed below are the authors contributing to the sections in this report. The authors contributing to the model description are also provided, as well as acknowledgements to the validation datasets.

Tropospheric reactive gases reactive gases

Annette Wagner, MPG (editor, O3 sondes, GAW data)
Yasmine Bennouna, Valerie Thouret, CNRS-LA (IAGOS)
Harald Flentje, DWD (O3 sondes, GAW data)
Anne Blechschmidt and Andreas Richter, IUB Bremen (GOME-2 NO2, HCHO)
John Kapsomenakis, Christos Zerefos, AA (ESRL)
Natalia Sudarchikova, satellite IR observations (MPG)
Kaj Hansen, Ulas Im, AU (Arctic theme)
Bavo Langerock, BIRA (NDACC)

Tropospheric aerosol

Michael Schulz, MetNo (editor, Aerocom, Aeronet)
Anna Benedictow, Jan Griesfeller, MetNo (Aerocom, Aeronet)
Sara Basart, MTeresa Pay, Oriol Jorba, BSC-CNS (Aeronet, MODIS, AirBase, SDS-WAS NAMEE RC)
Emilio Cuevas, AEMET (Aeronet, MODIS, AirBase, SDS-WAS NAMEE RC)
Harald Flentje, DWD (Backscatter profiles)

Stratospheric reactive gases

Yves Christophe, BIRA (editor, model-satellite intercomparisons)
Simon Chabrillat, BIRA (model intercomparisons)
Annette Wagner, MPI-M (O_3 sondes)
Bavo Langerock, BIRA (NDACC FTIR, MWR, UVVIS DOAS, LIDAR)
Anne Blechschmidt and Andreas Richter, IUB-UB Bremen (SCIAMACHY/GOME-2 NO_2)

Greenhouse gases

Michel Ramonet, IPSL (ICOS)
Abdelhadi El-Yazidi and Leonard Rivier, LSCE (ICOS)
Thorsten Warneke, UBC (TCCON)
Bavo Langerock, BIRA (TCCON)

Reactive gases and aerosol modeling

Johannes Flemming (ECMWF), Antje Inness (ECMWF), Angela Benedetti (ECMWF), Sebastien Massart (ECMWF), Anna Agusti-Panareda (ECMWF), Johannes Kaiser (KCL/MPIC/ECMWF), Samuel Remy (LMD), Olivier Boucher (LMD), Vincent Huijnen (KNMI), Richard Engelen (ECMWF)

Acknowledgements for the validation datasets used

We wish to acknowledge the provision of NRT GAW observational data by: Institute of Atmospheric Sciences and Climate (ISAC) of the Italian National Research Council (CNR), South African Weather Service, National Centre for Atmospheric Science (NCAS, Cape Verde), National Air Pollution Monitoring Network (NABEL) (Federal Office for the Environment FOEN and Swiss Federal Laboratories for Materials Testing and Research EMPA), Atmospheric Environment Division Global Environment and Marine Department Japan Meteorological Agency, Chinese Academy of Meteorological Sciences (CAMS), Alfred Wegener Institut, Umweltbundesamt (Austria), National Meteorological Service (Argentina), Umweltbundesamt (UBA, Germany)

We are grateful to the numerous operators of the Aeronet network and to the central data processing facility at NASA Goddard Space Flight Center for providing the NRT sun photometer data, especially Ilya Slutker and Brent Holben for sending the data.

The authors thank to all researchers, data providers and collaborators of the World Meteorological Organization's Sand and Dust Storm Warning Advisory and Assessment System (WMO SDS-WAS) for Northern Africa, Middle East and Europe (NAMEE) Regional Node. Also special thank to Canary Government as well as AERONET, MODIS, U.K. Met Office MSG, MSG Eumetsat and EOSDIS World Viewer principal investigators and scientists for establishing and maintaining data used in the activities of the WMO SDS-WAS NAMEE Regional Center (http://sds-was.aemet.es/).

We wish to acknowledge the provision of ozone sonde data by the World Ozone and Ultraviolet Radiation Data Centre established at EC in Toronto (http://woudc.org), by the Data Host Facility of the Network for the Detection of Atmospheric Composition Change established at NOAA (http://ndacc.org), by the Norwegian Institute for Air Research and by the National Aeronautics and Space Administration (NASA).

We wish to thank the NDACC investigators for the provision of observations at Ny Alesund, Bern, Jungfraujoch, Izaña, Xianghe, Harestua, Reunion Maido, Uccle, Hohenpeissen, Mauna Loa, Lauder and Haute Provence.

The authors acknowledge the NOAA Earth System Research Laboratory (ESRL) Global Monitoring Division (GMD) for the provision of ground-based ozone concentrations.

The MOPITT CO data were obtained from the NASA Langley Research Center ASDC. We acknowledge the LATMOS IASI group for providing IASI CO data.

SCIAMACHY lv1 radiances were provided to IUP-UB by ESA through DLR/DFD.

GOME-2 lv1 radiances were provided to IUP-UB by EUMETSAT.

The authors acknowledge Environment and Climate Change Canada for the provision of Alert ozone data and Sara Crepinsek – NOAA for the provision of Tiksi ozone data. Surface ozone data from the Zeppelin Mountain, Svalbard are from www.luftkvalitet.info. Surface ozone data from the Villum Research Station, Station Nord (VRS) were financially supported by "The Danish Environmental Protection Agency" with means from the MIKA/DANCEA funds for Environmental Support to the Arctic Region. The Villum Foundation is acknowledged for the large grant making it possible to build VRS in North Greenland.

We acknowledge the National Aeronautics and Space Administration (NASA), USA for providing the OMPS limb sounder data (http://npp.gsfc.nasa.gov/omps.html) and the Aura-MLS offline data (http://mls.jpl.nasa.gov/index-eos-mls.php).

We thank the Canadian Space Agency and ACE science team for providing level 2 data retrieved from ACE-FTS on the Canadian satellite SCISAT-1.

The European Environment Information and Observation Network (Eionet) Air Quality portal provides details relevant for the reporting of air quality information from EU Member States and other EEA member and co-operating countries. This information is submitted according to Directives 2004/107/EC and 2008/50/EC of the European Parliament and of the Council.

We are grateful to the IAGOS operators from the various institutes which are members of IAGOS-AISBL (http://www.iagos.org). The authors also acknowledge the strong support of the European Commission, Airbus, and the airlines (Lufthansa, Air France, Austrian, Air Namibia, Cathay Pacific, Iberia, China Airlines and Hawaiian Airlines so far) which have carried the MOZAIC or IAGOS equipment and undertaken maintenance since 1994. In the last 10 years of operation, MOZAIC has been funded by INSU-CNRS (France), Météo-France, Université Paul Sabatier (Toulouse, France) and Research Center Jülich (FZJ, Jülich, Germany). IAGOS has been additionally funded by the EU projects IAGOS-DS and IAGOS-ERI. The MOZAIC–IAGOS database (http://www.iagos-data.fr) is supported by AERIS (CNES and INSU-CNRS). Data are also available via AERIS web site www.aeris-data.fr.

We acknowledge the contribution of the ICOS Atmospheric Thematic Center (Lynn Hazan, Amara Abbaris, and Leonard Rivier) for the near real time data processing of surface CO_2 and CH_4 concentrations. The ICOS monitoring sites are maintained by the national networks: ICOS-Czech Rep. (Michal Marek, Katerina Komínková, Gabriela Vítková), ICOS-Finland (Olli Peltola, Janne Levula, Tuomas Laurila), ICOS-France (Michel Ramonet, Marc Delmotte, Sebastien Conil, Morgan Lopez, Victor Kazan, Aurélie Colomb, Jean Marc Pichon, Roxanne Jacob, Julie Helle, Olivier Laurent), ICOS-Germany (Matthias Lindauer, Dagmar Kubistin, Christian Plass-Duelmer, Dietmar Weyrauch, Marcus Schumacher), ICOS-Italy (Paolo Cristofanelli, Michela Maione, Francesco Apadula), ICOS-Norway (Cathrine Lund Myhre, Ove Hermansen), ICOS-Sweden (Jutta Holst, Michal Heliasz, Meelis Molder, Mikaell Ottosson Lofvenius, Anders Lindroth, Per Marklund), ICOS-Switzerland (Martin Steinbacher, Simon Wyss), European Commission, Joint Research Centre, Directorate for Energy, Transport and Climate (Peter Bergamaschi, Giovanni Manca).

The TCCON site at Orleans is operated by the University of Bremen and the RAMCES team at LSCE (Gif-sur-Yvette, France). The TCCON site at Bialystok is operated by the University of Bremen. Funding for the two sites was provided by the EU-project ICOS-INWIRE and the University of Bremen. The TCCON site at Réunion is operated by BIRA-IASB, in cooperation with UReunion and is funded by BELSPO in the framework of the Belgian ICOS program.

TCCON references:

Hazan, L., J. Tarniewicz, M. Ramonet, O. Laurent and A. Abbaris **(2016)**. *Automatic processing of atmospheric CO_2 and CH_4 mole fractions at the ICOS Atmosphere Thematic Centre*. Atmospheric Measurement Techniques 9(9): 4719-4736.

Blumenstock, T., F. Hase, M. Schneider, O. E. García, and E. Sepúlveda. 2017. "TCCON data from Izana (ES), Release GGG2014.R1." CaltechDATA. doi:10.14291/tccon.ggg2014.izana01.r1.

De Mazière, M., M. K. Sha, F. Desmet, C. Hermans, F. Scolas, N. Kumps, J.-M. Metzger, V. Duflot, and J.-P. Cammas. 2017. "TCCON data from Réunion Island (RE), Release GGG2014.R1." CaltechDATA. doi:10.14291/tccon.ggg2014.reunion01.r1.

Deutscher, N. M., J. Notholt, J. Messerschmidt, C. Weinzierl, T. Warneke, C. Petri, and P. Grupe. 2017. "TCCON data from Bialystok (PL), Release GGG2014.R1." CaltechDATA. doi:10.14291/tccon.ggg2014.bialystok01.r1/1183984.

Dubey, M. K., B. G. Henderson, D. Green, Z. T. Butterfield, G. Keppel-Aleks, N. T. Allen, J.-F. Blavier, C. M. Roehl, D. Wunch, and R. Lindenmaier. 2017. "TCCON data from Manaus (BR), Release GGG2014.R0." CaltechDATA. doi:10.14291/tccon.ggg2014.manaus01.r0/1149274.

Dubey, M. K., R. Lindenmaier, B. G. Henderson, D. Green, N. T. Allen, C. M. Roehl, J.-F. Blavier, et al. 2017. "TCCON data from Four Corners (US), Release GGG2014.R0." CaltechDATA. doi:10.14291/tccon.ggg2014.fourcorners01.r0/1149272.

Feist, D. G., S. G. Arnold, N. John, and M. C. Geibel. 2017. "TCCON data from Ascension Island (SH), Release GGG2014.R0." CaltechDATA. doi:10.14291/tccon.ggg2014.ascension01.r0/1149285.

Goo, T.-Y., Y.-S. Oh, and V. A. Velazco. 2017. "TCCON data from Anmeyondo (KR), Release GGG2014.R0." CaltechDATA. doi:10.14291/tccon.ggg2014.anmeyondo01.r0/1149284.

Griffith, D. W. T., N. M. Deutscher, V. A. Velazco, P. O. Wennberg, Y. Yavin, G. Keppel-Aleks, R. A. Washenfelder, et al. 2017. "TCCON data from Darwin (AU), Release GGG2014.R0." CaltechDATA. doi:10.14291/tccon.ggg2014.darwin01.r0/1149290.

Griffith, D. W. T., V. A. Velazco, N. M. Deutscher, C. Paton-Walsh, N. B. Jones, S. R. Wilson, R. C. Macatangay, G. C. Kettlewell, R. R. Buchholz, and M. O. Riggenbach. 2017. "TCCON data from Wollongong (AU), Release GGG2014.R0." CaltechDATA. doi:10.14291/tccon.ggg2014.wollongong01.r0/1149291.

Hase, F., T. Blumenstock, S. Dohe, J. Groß, and M.ä. Kiel. 2017. "TCCON data from Karlsruhe (DE), Release GGG2014.R1." CaltechDATA. doi:10.14291/tccon.ggg2014.karlsruhe01.r1/1182416.

Iraci, L. T., J. R. Podolske, P. W. Hillyard, C. Roehl, P. O. Wennberg, J.-F. Blavier, J. Landeros, et al. 2017. "TCCON data from Edwards (US), Release GGG2014.R1." CaltechDATA. doi:10.14291/tccon.ggg2014.edwards01.r1/1255068.

—. 2017. "TCCON data from Indianapolis (US), Release GGG2014.R1." CaltechDATA. doi:10.14291/tccon.ggg2014.indianapolis01.r1/1330094.

Kawakami, S., H. Ohyama, K. Arai, H. Okumura, C. Taura, T. Fukamachi, and M. Sakashita. 2017. "TCCON data from Saga (JP), Release GGG2014.R0." CaltechDATA. doi:10.14291/tccon.ggg2014.saga01.r0/1149283.

Kivi, R., P. Heikkinen, and E. Kyrö. 2017. "TCCON data from Sodankylä (FI), Release GGG2014.R0." CaltechDATA. doi:10.14291/tccon.ggg2014.sodankyla01.r0/1149280.

Liu, Cheng, Wei Wang, and Youwen Sun. 2018. "TCCON data from Hefei (PRC), Release GGG2014.R0." CaltechDATA. doi:10.14291/tccon.ggg2014.hefei01.r0.

Morino, I., N. Yokozeki, T. Matsuzaki, and M. Horikawa. 2017. "TCCON data from Rikubetsu (JP), Release GGG2014.R2." CaltechDATA. doi:10.14291/tccon.ggg2014.rikubetsu01.r2.

Morino, I., T. Matsuzaki, and M. Horikawa. 2017. "TCCON data from Tsukuba (JP), 125HR, Release GGG2014.R2." CaltechDATA. doi:10.14291/tccon.ggg2014.tsukuba02.r2.

Morino, Isamu, Voltaire A. Velazco, Akihiro Hori, Osamu Uchino, and David W. T. Griffith. 2018. "TCCON data from Burgos, Ilocos Norte (PH), Release GGG2014.R0." CaltechDATA. doi:10.14291/tccon.ggg2014.burgos01.r0.

Notholt, J., C. Petri, T. Warneke, N. M. Deutscher, M. Palm, M. Buschmann, C. Weinzierl, R. C. Macatangay, and P. Grupe. 2017. "TCCON data from Bremen (DE), Release GGG2014.R0." CaltechDATA. doi:10.14291/tccon.ggg2014.bremen01.r0/1149275.

Notholt, J., T. Warneke, C. Petri, N. M. Deutscher, C. Weinzierl, M. Palm, and M. Buschmann. 2017. "TCCON data from Ny Ålesund, Spitsbergen (NO), Release GGG2014.R0." CaltechDATA. doi:10.14291/tccon.ggg2014.nyalesund01.r0/1149278.

Pollard, David Frank, John Robinson, and Hisako Shiona. 2019. "TCCON data from Lauder (NZ), Release GGG2014.R0." CaltechDATA. doi:10.14291/tccon.ggg2014.lauder03.r0.

Sherlock, V., B. Connor, J. Robinson, H. Shiona, D. Smale, and D. F. Pollard. 2017. "TCCON data from Lauder (NZ), 120HR, Release GGG2014.R0." CaltechDATA. doi:10.14291/tccon.ggg2014.lauder01.r0/1149293.

—. 2017. "TCCON data from Lauder (NZ), 125HR, Release GGG2014.R0." CaltechDATA. doi:10.14291/tccon.ggg2014.lauder02.r0/1149298.

Strong, K., S. Roche, J. E. Franklin, J. Mendonca, E. Lutsch, D. Weaver, P. F. Fogal, J. R. Drummond, R. Batchelor, and R. Lindenmaier. 2018. "TCCON data from Eureka (CA), Release GGG2014.R3." CaltechDATA. doi:10.14291/tccon.ggg2014.eureka01.r3.

Sussmann, R., and M. Rettinger. 2017. "TCCON data from Garmisch (DE), Release GGG2014.R2." CaltechDATA. doi:10.14291/tccon.ggg2014.garmisch01.r2.

—. 2018. "TCCON data from Zugspitze (DE), Release GGG2014.R1." CaltechDATA. doi:10.14291/tccon.ggg2014.zugspitze01.r1.

Té, Y., P. Jeseck, and C. Janssen. 2017. "TCCON data from Paris (FR), Release GGG2014.R0." CaltechDATA. doi:10.14291/tccon.ggg2014.paris01.r0/1149279.

Warneke, T., J. Messerschmidt, J. Notholt, C. Weinzierl, N. M. Deutscher, C. Petri, and P. Grupe. 2017. "TCCON data from Orléans (FR), Release GGG2014.R0." CaltechDATA. doi:10.14291/tccon.ggg2014.orleans01.r0/1149276.

Wennberg, P. O., C. M. Roehl, D. Wunch, G. C. Toon, J.-F. Blavier, R. Washenfelder, G. Keppel-Aleks, N. T. Allen, and J. Ayers. 2017. "TCCON data from Park Falls (US), Release GGG2014.R1." CaltechDATA. doi:10.14291/tccon.ggg2014.parkfalls01.r1.

Wennberg, P. O., C. M. Roehl, J.-F. Blavier, D. Wunch, and N. T. Allen. 2017. "TCCON data from Jet Propulsion Laboratory (US), 2011, Release GGG2014.R1." CaltechDATA. doi:10.14291/tccon.ggg2014.jpl02.r1/1330096.

Wennberg, P. O., D. Wunch, C. M. Roehl, J.-F. Blavier, G. C. Toon, and N. T. Allen. 2017. "TCCON data from Caltech (US), Release GGG2014.R1." CaltechDATA. doi:10.14291/tccon.ggg2014.pasadena01.r1/1182415.

—. 2017. "TCCON data from Lamont (US), Release GGG2014.R1." CaltechDATA. doi:10.14291/tccon.ggg2014.lamont01.r1/1255070.

Wennberg, P. O., D. Wunch, Y. Yavin, G. C. Toon, J.-F. Blavier, N. T. Allen, and G. Keppel-Aleks. 2017. "TCCON data from Jet Propulsion Laboratory (US), 2007, Release GGG2014.R0." CaltechDATA. doi:10.14291/tccon.ggg2014.jpl01.r0/1149163.

Wunch, D., J. Mendonca, O. Colebatch, N. T. Allen, J.-F. Blavier, S. Roche, J. Hedelius, et al. 2017. "TCCON data from East Trout Lake, SK (CA), Release GGG2014.R1." CaltechDATA. doi:10.14291/tccon.ggg2014.easttroutlake01.r1.

Wunch, D., Toon, G. C., Sherlock, V., Deutscher, N. M., Liu, C., Feist, D. G., & Wennberg, P. O. (2015). The Total Carbon Column Observing Network's GGG2014 Data Version. Tech. rep., California Institute of Technology, Pasadena. doi:10.14291/tccon.ggg2014.documentation.R0/1221662

Copernicus Atmosphere Monitoring Service

ECMWF - Shinfield Park, Reading RG2 9AX, UK

Contact: info@copernicus-atmosphere.eu